STUDIES ON REGENERATED NONMULBERRY SILK FILMS AND FIBERS

THESIS SUBMITTED TO

DELHI TECHNOLOGICAL UNIVERSITY

FOR THE AWARD OF THE DEGREE OF

DOCTOR OF PHILOSOPHY

Submitted By

CHANDRA MOHAN SRIVASTAVA

(Reg. No. 2k12/Ph.D./AC/11)

Under the Supervision of

Dr. ROLI PURWAR

DEPARTMENT OF APPLIED CHEMISTRY

DELHI TECHNOLOGICAL UNIVERSITY

SHAHBAD, DAULATPUR, BAWANA ROAD, DELHI - 110042 (INDIA)

APRIL 2017

DELHI TECHNOLOGICAL UNIVERSITY

(Formerly Delhi College of Engineering)
Department of Applied Chemistry
Shahbad Daulatpur, Bawana Road, Delhi – 110042, India

DECLARATION

This is to certify that the work presented in this thesis entitled **"Studies on regenerated nonmulberry silk films and fibers"** is original and has been carried out by me for the degree of **Doctor of Philosophy** under the supervision of Dr. Roli Purwar, Assistant Professor, Department of Applied Chemistry. This thesis is a contribution of my original research work. Wherever research contributions of others are involved, every effort has been made to clearly indicate the same. To the best of my knowledge, this research work has not been submitted in part or full for the award of any degree or dipolma of Delhi Technological University or any other University/Intitutions.

<div align="right">

Chandra Mohan Srivastava
Research Scholar
(Reg. No. 2K12/Ph.D./AC/11)

</div>

Date:

Time:

DELHI TECHNOLOGICAL UNIVERSITY
(Formerly Delhi College of Engineering)
Department of Applied Chemistry
Shahbad Daulatpur, Bawana Road, Delhi – 110042, India

CERTIFICATE

This is to certify that the PhD thesis entitled **"Studies on regenerated nonmulberry silk films and fibers"** submitted to the Delhi Technological University, Delhi-110042, in fulfilment of the requirement for the award of the degree of **Doctor of Philosophy** by the candidate **Mr. Chandra Mohan Srivastava** (Reg. No. 2K12/Ph.D./AC/11) under the supervision of **Dr. Roli Purwar, Assistant Professor,** Department of Applied Chemistry. It is further certified that the work embodied in this thesis has neither partially nor fully submitted to any other university or institution for the award of any degree or diploma.

(Dr. Roli Purwar)
Supervisor
Department of Applied Chemistry
Delhi Technological University
Delhi

(Dr. Archna Rani)
Head of Department
Department of Applied Chemistry
Delhi Technological University
Delhi

Dedicated
To
My Family

ACKNOWLEDGEMENT

Date:

Time:

(Chandra Mohan Srivastava)

ABSTRACT

The whole thesis is summarized in the following eight chapters. The scientific information as well as past and current scenario related to this work that explains the importance of work is summarized as introduction and objectives of thesis sectioned as Chapter 1. The detailed scientific status of work in the particular field is given as Literature Review in the Chapter 2. Chapter 3 deals with the experimental techniques, methodology and tools that have been utilized to complete the objectives of the work. This chapter explains source of different materials, methodology, scheme of work and name and parameters of different characterization techniques. Chapter 4 deals with the preparation and characterization of nonwoven composite dressing of different muga and tasar fibroin films. These nonwoven films are further modified by chitosan in order to prepare composite structure to improve the mechanical, physical as well as biological properties. Chapter 5 gives insight about the preparation and characterization of regenerated nonmulberry muga and tasar silk fibroin based nanofibrous nonwoven mats for wound dressing and skin tissue regeneration. Chapter 6 explains about preparation and characterization of flexible muga and tasar silk fibroin films using dextrose as plasticizer. Chapter 7 deals with preparation and characterization of flexible silk fibroin films by incorporating hydrogel particles. These hydrogel particles are doped with muga and tasar silk fibroin in order to increase the fluid uptake capacity and flexibility of these regenerated silk fibroin films. Chapter 8 concludes the major finding of the thesis with the future prospective of the given work.

TABLE OF CONTENTS

Contents	*Page No.*

Contents	*Page No.*

LIST OF FIGURES

LIST OF TABLES

LIST OF SCHEMES

LIST OF ABBREVIATIONS

TFF	Tasar nonwoven mat
0.75% CMTFF	0.75% w/v chitosan solution modified tasar nonwoven composite mats
1% CMTFF	1% w/v chitosan solution modified tasar nonwoven composite mats
1.5% CMTFF	1.5% w/v chitosan solution modified tasar nonwoven composite mats
2%CMTFF	2% w/v chitosan solution modified tasar nonwoven composite mats
MFF	Muga nonwoven mat
0.75% CMMFF	0.75% w/v chitosan solution modified muga nonwoven composite mats
1% CMMFF	1% w/v chitosan solution modified muga nonwoven composite mats
1.5% CMMFF	1.5% w/v chitosan solution modified muga nonwoven composite mats
2%CMMFF	2% w/v chitosan solution modified muga nonwoven composite mats
MNF	Muga nanofibrous mat
MNF-20	Muga nanofibrous mat prepared at 20 kV applied voltage
TNF	Tasar nanofibrous mat
TNF-25	Tasar nanofibrous mat prepared at 25 kV applied voltage
TCP	Tissue culture plate
MCF	Muga cast film
DAPI	4',6-Diamidino-2-Phenylindole
FITC	Fluorescein isothiocyanate
SDS-PAGE	Sodium dodecyl sulphate gel electrophoresis
BMIMAc	1-butyl-3-methylimidazolium acetate
RMS	Root mean square deviation
Ra	Arithmetic average height deviation

MF	Muga cast film
DMMF	Dextrose modified muga fibroin film
TF	Tasar fibroin films
DMTF	Dextrose modified tasar fibroin films
MTT	3-(4,5-dimethylthiazol-2-yl)-2,5-diphenyltetrazolium bromide
ECM	Extra cellular matrix
kDa	Kilo Dalton
PBS	Phosphate buffer saline
DMEM	Dulbecco's modified Eagle's medium
FBS	Fetal bovine serum
ASTM	American society for testing and materials
WVTR	Water vapor transmission rate
AATCC	American Association of Textile Chemists and Colorists
SD	Standard deviation
RGD	Arginylglycylaspartic acid
APS	Ammonium persulphate
MBA	N,N′-Methylenebis(acrylamide)
AAm	Acrylamide
HDMFF	Hydrogel particle doped muga fibroin film
HDTFF	Hydrogel particles doped tasar fibroin film
DMSO	Dimethyl sulfoxide
AgNP	Silver nanoparticle
AgNP-TNF-25	Silver nanoparticle coated tasar nanofibrous mat

CHAPTER 1

INTRODUCTION AND OBJECTIVES

1.1 Introduction

Natural silk fiber, known as queen fiber of textile, is obtained from wide variety of insects during their life cycle. Major insects which produce silk fiber are *Bombyx mor*i, *Antheraea mylitta*, *Antheraea assama* and *Antheraea ricini* [1] and the varieties of silk fibers produced by these insects are known as mulberry, tasar, muga and eri, respectively [2-9].

The silk fibers obtained from silkworm cocoon have two major protein constituents, fibroin and sericin. Fibroin protein is made up of two protein chains known as heavy chain and light chain, mainly constitute of alanine, tyrosine and glycine. Sericin, which surrounds the fibroin, is a globular gummy protein, soluble in hot water, mainly consists of serine, alanine and glycine [10-12]. The mechanical strength of silk fiber is in the range of 1.9-5.2 g/den.

The use of silk fibroin fibers in the field of textile and medical suture is known from centuries [13]. Recently, the applications of silk fibroin fibers are expanding day by day as biomaterials due to its excellent biocompatibility, controlled biodegradability, non-inflammatory characteristic and tuned mechanical properties. The properties of silk fibers can be tailor made for its suitable use in biomedical either by surface modification or by its regeneration. Most of the biomedical applications are centered on the fibroin protein, which is found to be potential substrate for adherence and growth of large varieties of human cells.

The regenerated silk fibroin protein has various capabilities such as controlling the molecular structure for biodegradation, easy enzyme immobilization and blending with other polymers. The regeneration of silk fibroin proteins is carried out in three steps, degumming which involves boiling of cocoon in water to remove glue sericin protein, dissolution of fibroin fibers in suitable solvents to prepare silk fibroin solution and processing of silk fibroin solution to form films, fibers, nonwoven scaffolds, nanofibers, aerogels and cryogels. The sericin protein present on the outer surface of fiber creates problem in regeneration process, therefore, it should be removed prior to regeneration process. The presence of sericin affects the solubility of fibroin in various solvents [14]. In addition to that sericin is detected as antigenic factor by T cells and has reported to cause immunogenic reactions *in vivo* [15,16].

A wound results due to break in integrity of normal anatomical structure of skin [17,18]. The basic mechanism of wound healing is nearly same for all types of wound but rate of wound healing is affected by the types of wound, age, immune response of human body as well as the condition or environment of wound. Proper healing of wound not only depends upon medication but also requires suitable wound dressing. Open wounds are highly susceptible to microbial infection so it is very important to use wound dressing materials that shield the wound site from microbial attacks and provide favorable environment in order to boost the healing mechanism [19]. The ideal wound dressing should perform the following functions: it should absorb excess exudates of the wound, provide thermal insulation and mechanical protection, prevent bacterial contamination, allow gases and fluid exchange, be non-adherent to the wound, be easily removable without irritation, provide some debridement action, and be nontoxic, non-allergic, and non-scarring [14].

Different types of wound dressings in the form of films, gels, nonwoven and woven fabrics, foam and hydrocolloids are present in the market. Wound dressings must be selected on the basis of types of wound. Hydrocolloid wound dressings are most commonly used wound dressing, which are generally made up of carboxymethyl cellulose with gelatin and pectin, are suitable for light or moderately exudating wounds such as pressure sore, minor burns and burn injuries. Hydrocolloid dressings are available in market in the name of Aquacel (Conva Tec, Hounslow, UK) and Tegasorb (3M Healthcare, Loughborough, UK). Hydrogel dressings are non-adherent, cool the surface of wound and provide moist healing, so causes less pain during change of dressing. These wound dressings have wide acceptability by the patients. Some examples of hydrogel dressings are Nu-gel[TM] (Johnson & Johnson, Ascot, UK) and Purilon[TM] (Coloplast) [20]. Semi permeable wound dressings made of nylon derivative mesh supported on adhesive polyethylene gauge have less exudates absorption ability, so exudates accumulate beneath the wound dressing which results in maceration and proliferation of infectious microorganisms [21]. Foam dressings generally consist of porous polyurethane foam, have high water absorbance ability, provide the moist environment and very good water vapor transmission rate, which make them suitable for partial or full thickness wounds having moderate to high exudation. Some commercial foam dressings are marketed in the name of Lyofoam (Conva Tec) and Allevyn (Smith and Nephew) [21–23]. These types of wound dressings are only suitable for superficial wounds.

Unfortunately, the body cannot heal deep dermal injuries adequately. With burn injuries arising from fire, accidents, terrorist attacks and an aging population (for chronic wound), there will always be a continual demand for skin regeneration

products [15,24,25]. Dermal wound healing is a complex process that requires interaction between cells, extracellular matrix components, cytokines, and growth factors [16]. Many skin substitutes such as xenografts, allografts and autografts have been employed for wound healing. However, these approaches have many disadvantages such as higher cost, limited availability of skin grafts in severely burned patients, problems of disease transmission and immune response [26–28]. One strategy for dealing with serious skin damage is to develop tissue engineered skin substitute. Various synthetic and natural polymers such as chitosan, silk, collagen, poly (glycolic) acid, poly (L-Lactic) acid and poly (lactic-co-glycolic) acid are currently being employed as tissue engineered scaffolds for skin reconstruction [29,30]. Various type of tissue engineered skin substitutes have been successfully prepared and commercialized such as collagen/chondroitin-6 sulphate deposited silicon sheet (Integra) and human fibroblast cultured poly (glycolic) acid (Dermagraft) etc.

Nonwoven wound dressing materials are highly advantageous over the conventional sheet and foam based wound dressing due to improved absorbency, bacterial barrier, high water vapor permeability, air permeability and porosity. The high surface area and porosity of wound dressing results in ease transport of nutrients and other materials as well as exchange of gases which is very essential for growth and regeneration of neo-tissues. As further advancements in medical technologies and material science are taking place, the interest of scientist is shifted towards development of advanced nanofibrous nonwoven mats. Electrospun nanofibrous mats have been successfully utilized as an alternative to skin grafts in the field of tissue

engineering and regenerative medicine due to high surface area and porosity that stimulates adherence, growth and proliferation of seeded cells [31–33].

Bombyx mori silk fibroin has been extensively utilized as biomaterial for skin tissue engineering and wound dressing applications. Liu *et* al. [34] have explored the feasibility of using regenerated mulberry silk fibroin membrane to construct artificial skin substitute for wound healing. They observed that silk fibroin films do not have an adverse effect on the growth and biofunction of fibroblast and vascular endothelial cells. It also does not interfere with the secretion of angiogenesis growth factors such as VEGF, Ang-1, FGF2 and PDGF. Inpanya *et* al. [35] have studied the *Aloe vera* gel blended mulberry silk fibroin films and compared to *Aloe* free fibroin films; the blended film enhanced the attachment and proliferation of skin fibroblasts. Vasconcelos *et* al. [36] have developed the mulberry silk fibroin and elastin scaffolds for treatment of burn wounds. Mulberry silk fibroin/keratin films having a synthetic inhibitor of elastase is used to control the high level expression of this enzyme produced in chronic wound environment [37]. Mulberry silk fibroin/alginate sponge demonstrates a higher healing effect than both the components acting alone [38]. Karahaliloglu *et* al. [39] have modified the surface of mulberry silk fibroin film to obtain a biologically inspired nano-featured surface morphology, which enhanced the adhesion and proliferation of human epidermal keratinocytes and dermal fibroblasts.

It is reported that biocompatibility of nonmulberry silk fibroin protein such as tasar is more as compared to mulberry silk fibroin due to presence of R(arg)-G(gly)-D(asp) (AY136274) sequences which is responsible for adherence of cells [40]. Recently,

tasar and muga fibroin have been engineered in the form of films [41], nanofibers [42–44], cryogels [45], aerogels [46], freeze dried scaffolds [47–49] and have emerged as promising materials in the field of tissue engineering due to their excellent biocompatibility, controlled biodegradability and higher mechanical property [50-61]. Tasar silk fibroin obtained from silkworm gland have been utilized for cornea [50], cardiac [51], skin [41] and cartilage [54] tissue engineering.

Although a good amount of work has been carried out on the muga and tasar silk fibroin extracted from silkworm gland in the field of tissue engineering, but only little work has been reported on the applications of muga & tasar silk fibroin extracted and regenerated from cocoon due to its insolubility in the most of catastrophic solvents [37,41,45]. Another drawback with regenerated fibroin films is their brittleness which makes them non-suitable to be use as wound dressing [46,47,48].

1.2   Motivation of research

Nonmulberry silk fibroin proteins are found to be potential biomaterials; however the utility of these materials has not been fully explored in the field of wound dressing and skin tissue engineering. India is the largest producer of nonmulberry silk fibroin protein and most of present studies are confined to nonmulberry silk fibroin proteins extracted from silkworm gland. It is very difficult to develop the biomedical products for commercial use from the protein obtained from silkworm gland. Therefore, there is a need to explore utility of regenerated nonmulberry silk fibroin extracted from cocoon in order to develop various substrates for biomedical applications.

1.3   Objective

Design and development of regenerated nonmulberry silk fibroin films and fibers for wound dressing applications

1.4   Specific Objectives

In order to achieve the above objective, the specific objectives are:

- Preparation and characterization of nonwoven composite films

- Preparation and characterization of nanofibrous nonwoven mats using electrospinning

- Preparation and characterization of flexible films

CHAPTER 2

LITERATURE REVIEW

Silk is a protein material obtained from silkworm in the form of continuous filament. India is rich with four different varieties of silk, namely, *Bombyx mori* (mulberry), *Antheraea mylitta* (tasar), *Antheraea assama* (muga) and *Phylisomia ricini* (eri) [11]. Tasar, muga and eri varieties of silk are also known as wild silk or nonmulberry silk. It consists of two types of proteins which are known as fibroin and sericin. Sericin is a globular protein which binds the two fibroin filaments together. These two proteins constitute up to 95% of the raw silk fibers and rest is made up of other proteins, waxes, salts, fats and ash. Table 2.1 shows the composition of sericin and fibroin present in different varieties of silk [10–12]. The composition of amino acids in different varieties of silk fibroin is present in Table 2.2 [10–12]. Fibroin is mainly constituted of glycine, alanine and serine. Composition of these three amino acids was found to be the highest in case of eri (84%), which is followed by mulberry (82%), tasar (72%) and muga (68%). Freddi *et* al. [60] found that eri has high alanine content (36%) which is followed by tasar (35%), muga (34%) and mulberry (28%). The crystalline portion of silk fibroin is mainly made up of three different amino acids namely, alanine, glycine and serine. The composition of these three amino acids was about 91% for mulberry, 81 to 82% for tasar and muga fibroin while it was about 77% for eri [61]. The polymer chains of silk fibroin form β-sheet structure. Silk fiber is highly crystalline in nature. The mechanical strength of silk fiber is in the range of 1.9-5.2 g/den [10,11].

Table 2.1: Comparison of silk proteins depending on the origin [10–12]

Protein	Silkworm types			
	Bombyx mori (mulberry silk)	*Antheraea pernyi* (tussah or wild silk)	*Antheraea assamensis* (muga silk)	*Philosamia ricini* (eri silk)
Fibroin	70-80%	80-90%	80-90%	80-90%
Sericin	20-30%	8-10%	8-10%	4-5%
Others	2-3%	3-5%	3-5%	3-5%

Table 2.2: Amino acid composition of different mulberry and nonmulberry silk fibers [10–12]

Amino acids	*Bombyx mori* (mulberry silk)	*Antheraea assamensis* (muga silk)	*Antheraea mylitta* (tasar silk)	*Philosamia ricini* (eri silk)
Alanine	28	35	34	36
Glycine	44	28	27	29
Serine	11	9	10	9
Tyrosine	5.7	5.1	6.8	5.8
Aspartic acid	1.5	4.9	6.1	3.8
Arginine	1.16	4.7	4.9	4.12
Glutamic acid	1.53	1.36	1.27	1.31
Hystidine	0.15	0.72	0.78	0.75
Lysine	0.25	0.24	0.17	0.23
Phenylalanine	0.18	0.28	0.34	0.23
Tryptophan	0.75	2.18	1.26	1.68
Leucine	0.75	0.71	0.78	0.69
Isoleusine	0.78	0.51	0.61	0.45
Cystine	0.12	0.12	0.15	0.11
Methionine	0.11	0.32	0.28	0.34
Valine	2.89	1.5	1.72	1.32
Threonine	0.76	0.21	0.26	0.18
Proline	0.76	2.18	2.21	2.07

2.1 Regeneration of silk fibroin

The silk fibers are known from the centuries in the field of textile as well as in the field of medical as suture.The range of applications of silk fiber is expanding day by day in the field of biomedical as biomaterials due to its thermal stability, tuned biodegradability and

biocompatibility. Silk proteins need to be engineered into useful forms for suitable applications in the field of biomedical such as suture, biosensors and scaffold for tissue engineering and wound dressing materials. The properties of silk fibroin proteins can be tailor-made to utilize it as medical textiles either by surface modification or by its regeneration in the form of scaffolds, films and fibers. The regeneration of silk fibroin proteins by casting, electrospinning and wet-spinning process have various capabilities, such as controlling the structure & properties of silk fibroin proteins, allowing silk proteins to be blended with other materials as well as immobilizing different biological materials etc. The regeneration of silk fibroin proteins can be carried out in three steps: degumming, dissolution and regeneration [13]. The process of the removal of sericin from fibroin filaments is called degumming. When the degummed fibroin filaments are dissolved in a suitable solvent to prepare solution, it is called dissolution. The process of conversion of this silk fibroin solution in the form of films, fibers and scaffolds is called as processing. Figure 2.1 shows the schematic line diagram of the steps involved in the regeneration process of silk fibroin proteins in the form of fibers and films. The presence of residual sericin on the surface of fibroin fibers can affect the solubility of fibroin in various solvents for dope preparation. Therefore, it should be completely removed from the fibroin surface. The sericin is removed from the surface of fibroin by boiling the silk cocoon in 0.02 M sodium carbonate solution for 30-40 min [14]. Another method to remove the sericin from the surface of fibroin is to pressure boil via autoclave. The complete removal of sericin can be achieved by boiling the cocoon at 130 °C for 1 hour [62].
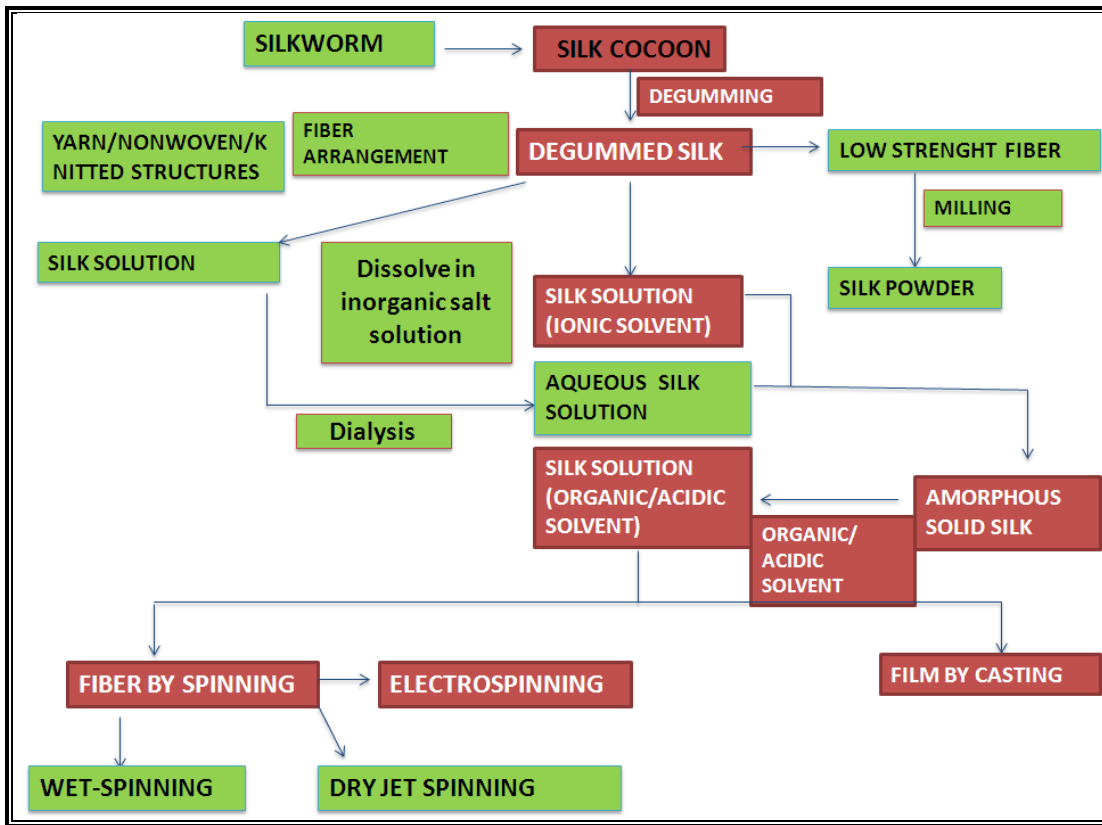
Figure 2.1: Schematic diagram for regeneration of silk fibroin proteins into different matrix form

Mulberry silk fibroin can be dissolved in wide range of protic and non-protic solvents. Major solvents which are used for regeneration process are summarized in Table 2.3. The solubilization of mulberry silk fibroin protein in $Ca(NO_3)_2$-MeOH-H_2O and LiBr–EtOH takes only 10 min while in Hexafluoro-isopropanol (HFIP) and hexafluoroacetone it takes 24 and 2 hours respectively. The $Ca(NO_3)_2$- MeOH-H_2O and LiBr-EtOH-H_2O have strongest solvation for the mulberry silk fibroin chains,with almost constant viscosity, while LiBr-H_2O (9.5M LiBr aqueous solution) have the weakest solvation with similar effects on the fibroin molecules to pure water. Recently mulberry silk fibers have shown its solubility in ecofriendly solvent N-methylmorpholine N-oxide. The molecular weight of regenerated fibroin in N-methylmorpholine N-oxide is 190 kDa [63–65].

Table 2.3: Solubility of silk fibroin in different types of solvents

Non Protic Solvents	Molar Ratio	Time for Solubilization	Silk fibroin	References
$Ca(NO_3)_2$-MeOH-H_2O	75:25	10 min	Mulberry	[64]
LiBr-EtOH-H_2O	45:44:11	10 min	Mulberry	[64]
LiBr-EtOH	40:60	30 min	Mulberry	[64]
$CaCl_2$-EtOH-H_2O	1:2:8	10 min	Mulberry	[64]
LiBr-H_2O	9.5 Molar	30 min	Mulberry	[63]
N-Methylmorpholine N-Oxide (NMMO)	Absolute	10 min	Mulberry	[63]
HFIP	Absolute	24 h	Mulberry	[65]
Hexafluoroacetone hydrate	Absolute	24 h	Mulberry	[65]
1-ethyl-3-methylimidazolium chloride	Absolute	1h	Mulberry	[66]
triethylammonium mesylate, (TeaMs)	Absolute	-	Mulberry	[67]
1-butyl-3-methylimidazolium acetate/chloride	Absolute	-	Muga	[55]
1-butyl-3-methylimidazolium chloride	Absolute	8h	*Bombyx mori*	[68]

2.1.1 Rheology of mulberry silk fibroin solution

Viscoelasticity of a polymer solution strongly affects its spinnability, which is related to the flow behavior of the polymer solution during the fiber spinning process. The rheology of the polymer solution depends on its concentration and its interaction with the solvent. The rheological properties of mulberry silk dope solutions are studied by several researchers [63,65,69]. Um *et* al. [69] have studied the rheological behavior of mulberry silk fibroin solution prepared in 98% formic acid and observed that the silk dope solution showed shear thinning behavior. The shear thinning behavior of a polymer solution is characteristic to the molecular entanglement. The entanglement of silk fibroin molecules induced by shear force may occur due to hydrophobic

interaction between molecules or hydrogen bonds between polar groups. Without any external shear force, silk fibroin chains entangled with each other. When the shear rate increases, some portion of entanglement is destroyed, resulting in a decrease of shear viscosity. Another important factor in the rheological properties of a dope solution for fiber spinning is the stability of the solution during storage. Viscosity of dope solution can increase or decrease due to the gelation or molecular degradation, respectively. It is observed that the shear viscosity of mulberry silk fibroin solution in formic acid remains constant for 5 days. The maximum viscosity of dope solution permitted for wet-spinning is 44 Pascal second at 75 °C [63,70].

2.1.2   Structural properties of regenerated silk fibroin

Native silk fibroin proteins have β-sheet conformation, which is changed to random coil structure after dissolution in solvents during regeneration. Regenerated silk fibroin film samples having random coil conformation are mechanically unstable and easily dissolve in aqueous environment; therefore regenerated samples are coagulated in organic solvents in order to induce β-sheet structure. During coagulation in organic solvents such as methanol its conformation reverts back to β-sheet. So it is very important to check the conformation of silk fibroin proteins before and after regeneration because most of the properties of regenerated silk fibroin proteins depend upon its conformation. Conformation of proteins is determined in terms of its structural properties [64]. FTIR, XRD and CD spectroscopy is a tool to analyze structural properties of regenerated silk fibroin proteins. Tasar silk fibroin proteins show a major peak at 23° and 9.4° which represent random coil conformation and is shifted to 23.33° and 9.3° after treatment with 70% ethanol representing β-sheet conformation [71]. Three different types of

structures are reported for silk fibroin proteins namely, Silk I for water soluble silk, existing within gland of silkworm before spinning, Silk II is the insoluble β-sheet structure which formed after spinning of silk fibers and Silk III is an unstable structure that formed at air water interface [1]. Kar *et* al. [72] reported that muga and eri silk fibroin films shows 2θ peak at 11.68 which is a characteristic of water soluble silk I structure (random coil). Regenerated muga and eri silk fibroin films showed 2θ peaks at 16.7 and 20.8° which is characteristic of crystalline β-sheet structure. Due to the presence of amide groups in the backbone of silk fibroin proteins, the peptide bonds show their characteristic absorption in amide I, II and III region due to (C=O) stretching, (N-H) bending and (C-N) stretching, respectively. The conformation of silk fibroin proteins is characterized by β-sheet having absorption bands at 1630, 1530 and 1240 cm^{-1}, random coil conformation having absorption bands at 1645, 1550 and 1230 cm^{-1}, whereas a band at 1655 cm^{-1} appears due to α-helix conformation [64,73].

Tasar silk fibroin protein aqueous solution showed a strong negative peak at 223 nm which corresponds to random coil conformation. Mandal *et* al. [74] reported that on addition of ethanol from 10 to 70% v/v, negative ellipticity of tasar silk fibroin shifted towards 220 nm, which is indication of conformation transition of fibroin protein from random coil to β-sheet.

2.1.3   Biological properties of silk

Silk fibroin are protein materials which contain positive charge amino acid residues and are responsible for adherence of animal cell that have negative surface charge. It is also reported that nonmulberry silk fibroin materials do not show significant inflammatory response [50]. Biocompatibility and biodegradability of regenerated silk

fibroin proteins may be tuned by processing it in different form such as cast films, nonwoven mats, nanofibrous mats and porous 3D scaffolds. Due to high surface area and porosity these different matrix architectures behave differently towards cells and active molecules such as proteolytic enzymes. Acharya *et* al. [75] reported that mulberry silk fibroin protein contains positively charged arginine residue near the C-terminus of the non-repetitive sequences may be responsible for cell adherence due to the fact that mammalian cells contain negative surface charge. It is also reported that nonmulberry silk fibroin proteins showed superior biocompatibility as compared to mulberry silk fibroin due to the presence of tripeptide sequences Arg(R)-Gly(G)-Asp(D), which is responsible for integrin mediated cell adhesion [75].

2.2 Regenerated silk fibroin as biological constructs

2.2.1 Silk fibroin based nonwoven microfibrous cast films

In tissue engineering fiber-bonding products such as nonwoven mats play very important role as scaffolds to guide tissue regeneration. High surface area and porosity of these nonwoven mats provide biomimetic environment similar to natural extracellular matrix which is responsible for improved adherence, proliferation and differentiation of cells that allows ease migration of cells, essential biomolecules as well as nutrients. These nonwoven mats are ideal candidates for wound healing due to its porosity, surface area, exudates absorbance capability, water vapor and gases exchange capability [44,76–81].

Kasoju *et* al. [79] successfully developed *Antheraea assama* silk fibroin based nonwoven mats using casting method and found that these 3D interconnected network structures exhibited very good porosity (90%) and water uptake ability (85%). These

mats are found to be effective as substrate for regeneration of skin tissue. Mandal *et al.* [82] developed 3D tasar silk fibroin nonwoven mats by winding the fibroin fibers at cover-slips in linear, mixed and random manner using biospinning.

2.2.2 Silk fibroin based nonwoven nanofibrous mats

Nanofibrous matrices fabricated by electrospinning have shown as promising alternative to allografts [83], autografts [32] and xenografts [84] due to their structural similarity to extracellular matrix (ECM). The electrospun scaffolds have a skeletal structure with individual fiber diameter in submicron to nano range that provides higher surface area which allows the seeded cells to proliferate and produce their own ECM [85]. Electrospun mats possess a very high surface area and porosity, which promote moisture retention, exudates absorption, tissue regeneration and hemostasis [86].

2.2.2.1 Processing of nanofibrous mat

Electrospinning is a dry spinning technique used for the fabrication of nano to submicron diameter fibers. Formhals was the first to file a patent for the fabrication of various nonwoven materials by electrospinning machine in 1934 [87]. Electrospinning machine essentially consists of three components; a high voltage power supplier, a grounded collector plate and a capillary needle. The electrospinning technique involves the application of a strong electric potential between a reservoir containing polymer solution such as a glass syringe with a capillary tip or needle, and a metallic collection plate. At the critical voltage, when applied voltage becomes higher than the surface tension of the droplet i.e. as the electric charge overcomes the surface tension of the deformed drop of suspended polymer solution formed on the capillary tip or needle, it results in the ejection of charged jet of the solution in the direction of

applied field. Under electro-hydrodynamic forces the diameter of electrically charged jet decreases and this jet undergoes a series of several electrically induced bending instabilities during passage to the collection plate, which results in extensive stretching [88].

During stretching process rapid evaporation of the solvent takes place, which results in reduction of the diameter of the jet. After stretching and drying, these fibers collect randomly or in an aligned manner on the surface of collecting plate. The diameter of electrospun nanofiber can be controlled by changing the processing parameters such as concentration of solution, viscosity and electric field; type of solvent employed, distance from tip to collector plate, flow rate, diameter and angle of the spinneret [89,90].

2.2.2.2 Process parameters for electrospinning of silk

There are many parameters that affect the electrospinning of silk fibroin solution and their blends such as the interaction between polymer and solvent, chemistry, molecular weight, molecular weight distribution of the polymer and the rheological behavior of the solution (concentration, viscosity, elasticity, conductivity and surface tension). The parameters such as hydrostatic pressure in syringe and needle, applied voltage, distance between tip and collector and flow rate of solution have great influence on processing of silk by electrospinning.

Recently, regenerated silk fibroin fiber with submicron diameter was prepared through electrospinning process [91–93]. The process parameters which affect the formation of electrospun fiber are summarized in Table 2.4

Table 2.4: Process parameter for regeneration of silk fibroin in the form of nanofibrous mat

Types of silk	Fibroin Conc. (%)	Solvent	Electric Field (kV/cm)	Spinning Distance (cm)	Av. Fiber Diameter (nm)	References
Bombyx mori	8	Formic acid	4	7	26.3	[94]
Bombyx mori	9	Formic acid	3	10	52.2	[95]
N. Clvipes (Dragline)	0.74	Hexafluoro-2-propanaol	24-30 kV	15	100	[96]
Bombyx mori	8, 9, 10, 11	Formic acid	12 kV	10	205, 235, 305, 320	[97]
Tussah	10	HFIP	12 kV	12	---	[98]
Bombyx mori	12	Formic acid	2 to 4	7	70 to 45	[94]
Bombyx mori	38	Aqueous	20 kV	20	2113	[99]
Antheraea mylitta/PVA(1:2 wt/wt)	4	Aqueous	15 kV	15	235	[42]
Eri	15	Trifluoroacetic acid	20 kV	15	400 to 500	[71]
Tasar	15	Trifluoroacetic acid	20 kV	15	800-1000	[71]
Eri	13	Chloroform/TFA (30:70)	20 kV	15	320	[100]
Eri/Tasar blend		Formic acid/Chloroform (70:30 v/v)	22 kV	15	200-800	[43]

Many researchers have investigated that there is a relationship between polymer concentration and fiber diameter [94,95]. It is studied that increasing the concentration of silk solution results in increased fiber diameter and decreased bead formation. If the solution concentration of *Bombyx mori* silk formic acid is too low (5%) then the fiber break into microsize droplets before reaching the collector so fiber will not be formed which results in phenomena of electrospray rather than electrospinning [95]. The phenomenon of electrospray is also observed when a solution of low molecular weight polymer is used. It is also noted that if the concentration of silk solution is too high, it will be difficult for the polymer solution

to flow through the capillary due to high viscosity; therefore no fiber will be formed [98]. The type of solvent also affects the electrospinnability of silk fiber. The effect of solvent on the diameter of electrospun *Bombyx mori* silk fiber has also been studied by Jeong *et* al. [101]. In this study it is found that mean diameter of electrospun nano-fibers from silk formic acid solution are smaller (80 nm) than those from HFIP silk solution (380 nm). This is only due to faster evaporation of HFIP than formic acid, which led to the formation of thicker fibers with less elongation. It is interesting to note that from 17% (w/v) aqueous *Bombyx mori* silk solution electrospun fiber is not formed, while at 28% (w/v) silk fiber with diameter from 400-800 nm is observed, with circular cross-sections and smooth exterior surfaces. At 39% (w/v) aqueous silk fiber solution an uneven and ribbon shaped silk fiber formed possibly due to slow rate of evaporation from fiber surface before the fiber reaches the collector. Zhu *et* al. (2007) found that from 30% (w/v) aqueous silk solution, electrospun fiber formed with diameter of 1749 nm but as the concentration increase from 33 to 38% the diameter of electrospun fibers reaches to 2275 and 2113 nm. The pH and concentration have a remarkable influence on the properties of regenerated silk fibroin aqueous solutions [102]. The lowering of pH could induce gel formation and decrease the electrospinnability of regenerated silk fibroin aqueous solutions. The uniform cylindrical fibers with a smaller average diameter of 265 nm obtained by using the solution of a pH of 4.8. At pH 6.0 and concentration of 33 wt%, a uniform cylindrical fiber with an average diameter of 718 nm is obtained. Applied electric potential is the one of the most important process parameter of electrospinning which has great influence on fiber diameter, jet formation and bead formation. Sukigara *et* al. [94] demonstrated that at an electric potential of 3 kV/cm, fiber did not form from

Bombyx mori silk-formic acid solution but when an electric field of 4 kV/cm was applied then fiber jet was induced and causes formation of fiber with diameter of 26.3 nm. This suggests that a sufficient electrostatic force can overcome solution surface tension and further extract silk fibroin chains [103].

The flow rate also has a great influence on the electrospinnability of silk fiber. The feed rate controls the volume of solution suspended at tip of the spinnerette that maintains the shape of Taylor cone. The maintenance of Taylor cone is very important for jet formation. Between 10 kV and 20 kV formation of stable jet is observed. The fiber diameter is narrowest at 10 kV (lowest electric field) for different concentrations [104].

2.2.3 Silk fibroin cast films

Mulberry and nonmulberry silk fibroin 2D films have been successfully prepared as shown in Table 2.5. Acharya *et* al. [75] successfully developed tasar silk fibroin gland protein based films by casting methods. Karahaliloglu *et* al. [39] developed mulberry silk fibroin films by casting techniques and found that these 2D films having nanophase roughness are very advantageous for skin tissue regeneration. Mandal *et* al. [74] have prepared 2D films using tasar fibroin extracted from silkworm gland. These films were further coagulated using methanol to induce β-sheet conformation. Goujan *et* al. [55] have successfully regenerated muga fibroin proteins film by using ionic liquid. Recently, it is reported that muga and tasar cocoon fibroins are dissolved in ionic liquids and can be regenerated in the form of films using alcohol as coagulating agent [47,51]. These regenerated fibroin films are brittle in nature and not suitable to be used as wound dressing [105]. The mechanical properties of different nonmulberry silk fibroin proteins regenerated from the cocoon have not been reported. Regenerated

silk fibroin films require flexibility to be used as wound dressing materials especially when they are used in load bearing area such as knee joints & elbow joints. To promote healing these films should have good biocompatibility, provide moist environment & protect against pathogens [36,85,106].

Table 2.5: Silk fibroin cast films

Silk Type	Solvent	Conc.	Coagulation	Type of film	Reference
Bombyx mori	9.3 M LiBr	8 wt%	Methanol	2D film	[107]
Bombyx mori	9.3 M LiBr	25% w/v	Methanol	2D film	[108]
Bombyx mori	9.3 M LiBr	2.5%	Methanol	2D film	[109]
Bombyx mori	$CaCl_2/H_2O/C_2H_5OH$ solution	140 mg/mL	---	2D film	[110]
Bombyx mori	9.3 M LiBr	80 mg/mL	Water vapor annealed	2D film	[111]
Bombyx mori	9.3 M LiBr/HFIP	6 wt%	Methanol/Ethanol /Water annealed	2D film	[112]
Bombyx mori	1-Butyl-3-methyl imidazolium chloride	10% wt/wt	Acetonitrile/meth anol	2D film	[66]
Bombyx mori	Calcium nitrate-methanol	10 % wt/wt	methanol	2D film	[113]
Tasar/ *Bombyx mori*	LiBr	0.8 mg/mL	---	2D film	[41]
Tasar fibroin extracted from silkworm gland	1% SDS	2% w/w	Freeze dried	3D scaffolds	[51]
Tasar fibroin extracted from silkworm gland	1% SDS	2% w/w	Freeze dried	3D scaffolds	[49]
Tasar fibroin extracted from silkworm gland	1% SDS	2% w/w	Methanol	Nanopart icles	[114]
Tasar fibroin extracted from silkworm gland	1% SDS	5% w/v	Ethanol	2D film	[74]
Tasar fibroin extracted from silkworm gland	1% SDS	2-8% w/v	Freeze dried	3D scaffolds	[48]
Muga fibroin	1-Butyl-3-methylimidazolium acetate/chloride	10% wt/v	Methanol	2D film	[55]

2.3   Applications of nonmulberry silk fibroin in biomedical field

Mulberry silk fibroin proteins are being used as textile and sutures for centuries. From last few decades mulberry silk fibroin protein has been exploited as biomaterial due to its impressive properties such as biocompatibility, biodegradability with good mechanical strength, ease to regenerate and can be chemically modified to address a wide range of biomedical and tissue engineering applications [79,115–117]. Silk fibroin obtained from *Bombyx mori* have been regenerated extensively in the form of films [105], electrospun mats [86], wet spun fibers [118] and hydrogels [119] due to its solubility in various catastrophic solvents. But utilization of nonmulberry silk fibroin proteins as biomaterials for tissue engineering and biomedical point of view is relatively new. Nonmulberry silk fibroin proteins have very high toughness and load bearing ability along with superior biocompatibility & controllable degradation which makes it an excellent candidate in the field of tissue engineering and regenerative medicine. *Antheraea assama*, a popularly known muga silk fibroin confined to north eastern state of India has been recently explored as a biomaterial for tissue engineering [79]. Nonmulberry silk fibroin obtained from glands have been successfully engineered in the form of films, nonwoven mats, cryogels and hydrogels for diverse biomedical applications for example bone, cartilage, adipose & skin tissue engineering. Due to high hydrophobic amino acid content, the nonmulberry fibroin proteins especially muga and tasar are not soluble in most of the solvents which are used for dissolution of *Bombyx mori* fibroin. Therefore, limited work has been carried out on muga and tasar fibroin and mainly confined to partial dissolution of cocoon fibroin fibers in formic acid or fibroin protein obtained from silkworm gland as shown in Table 2.5. Kasoju *et* al. [79,120] have prepared muga fibroin nonwoven scaffolds

by casting methods. These scaffolds show satisfactory blood compatibility and cytocompatibility with human A549, KB, HepG2 and HeLa cell line. Dutta *et* al. [117] have prepared muga fibroin films by extracting protein from glands of silkworm *Antheraea assama.* Kar *et* al. [72] have extracted muga fibroin protein from posterior gland of *Antheraea assama* silkworm and prepared 2D films. Muga gland fibroin proteins based 2D films are compatible to MG-63 human osteoblasts cells. Recently, muga fibroin protein extracted from gland is used for preparing 3D cryogels [45].

Tasar silk fibroin obtained from silkworm gland have been reported for cornea [50], cardiac [51], skin [41] and cartilage [54] tissue engineering. Acharya *et* al. [75] have found that adherence, growth and proliferation of dermal fibroblast cells seeded on tasar silk fibroin films are higher than mulberry silk fibroin films due to the presence of the tripeptide Arg(R)–Gly(G)–Asp(D). However, most of the studies have been carried out on tasar fibroin obtained from glands. Recently, 3D scaffolds have been prepared from tasar fibroin for alveolar bone [121], skin [74] and cartilage [54] regeneration. Mandal *et* al. [48] have regenerated tasar silk fibroin in the form of highly porous 3D scaffolds by using freeze drying technique. The 3D freeze dried scaffolds are biocompatible and having good biodegradability over the time. Eri and tasar silk fibroin based electrospun mats have been prepared for biomedical applications and it has been found that these fibroin electrospun mats show good biocompatibility and hemocompatibility. Hydroxyapatite coated eri-tasar silk fibroin nanofibrous mats show good physiological characteristics [122].

Although a good amount of work have been carried out on the muga and tasar silk fibroin extracted from silkworm gland, but only a little work has been reported on the

applications of muga & tasar silk fibroin extracted and regenerated from cocoon due to the its insolubility in most of the catastrophic solvents [11-12]. Recently, it is reported that muga and tasar cocoon fibroins can be dissolved in ionic liquids and regenerated in the form of films using alcohol as a coagulating agent [47,51]. Goujan *et* al. [123] have prepared regenerated muga fibroin films by dissolution of muga fibroin fibers obtained from cocoons in 1-butyl-3-methylimidazolium chloride and 1-butyl-3-methylimidazolium acetate ionic liquids and studied their structural & thermal properties. Tasar silk fibroin proteins fibers has been successfully dissolved in ionic liquid and regenerated in the form of hydrogels. These tasar fibroin protein based hydrogels are highly compatible to the human adipose stem cells. These regenerated silk fibroin protein based matrices are brittle in nature and are not suitable to be used as wound dressing [36,85,106]. It is pertinent to note that mechanical properties of different non-mulberry silk fibroin proteins regenerated from the cocoon have not been reported.

In order to further improve the biocompatibility and antimicrobial activity, recent research is focused on utilization of chitosan and mulberry fibroin based hybrid wound dressing. Chitosan being polycationic in nature favors cell proliferation and histoarchitectural tissue organization. Chitosan is also a natural hemostat, which helps in natural blood clotting [124–129]. Due to good biocompatibility and control biodegradability mulberry fibroin and chitosan blend based films [124–126], sponge [128] scaffolds [129] and hydrogels [127] have been prepared and utilized in the area of tissue engineering and regenerative medicine.

Regenerated nonmulberry silk fibroin proteins have been successfully utilized for different applications in the field of tissue engineering and regenerative medicine which is summarized in the Table 2.6.

Table 2.6: Different applications of nonmulberry silk fibroin proteins as biomaterials in the field of tissue engineering and regenerative medicine

S. No.	Fibroin source	Sample type	Application	
1	Muga silkworm gland	2 D film	-	[117]
2	Muga silkworm gland	2D film	Tissue engineering	[72]
3	Muga cocoons fibroin	Nonwoven mat prepared by casting method after dispersing cut muga fiber in formic acid	Tissue engineering	[79]
4	Muga cocoon fibroin	2D film prepared by dissolution in ionic liquid	Not specified	[130]
5	Muga silkworm gland	Cryogel scaffolds	Liver tissue engineering	[45]
6	Muga cocoon fibroin	Nonwoven mat prepared by casting method after dispersing cut muga fiber in formic acid followed by soaking in chlorosulphonic acid/pyridine (1:6) solution at 80 ˚C.	Hemo-and cytocompatible with lung carcinoma.	[120]
7	Tasar silkworm gland protein	3D scaffolds	Skin tissue engineering	[48]
8	Tasar silkworm gland protein	2D film	Corneal tissue engineering	[50]
9	Tasar silkworm gland protein	2D film	Cardiac tissue regeneration	[131]
10	Tasar silkworm gland protein	3D scaffolds	Skin tissue engineering	[47]
11	Tasar silkworm gland protein	3D scaffolds	Articular tissue engineering	[54]
12	Eri/Tasar fibroin blend	Nanofibers	Bone tissue engineering	[43]
13	Tasar silkworm gland protein	Nanoparticles	Drug delivery	[114]
14	Tasar silkworm gland protein	3D micro fibrous matrices	Skin tissue engineering	[82]
15	Tasar silkworm gland protein /Chitosan blend	Freeze dried 3D scaffolds	Cartilage repair	[132]
16	Oak tasar silkworm gland protein	Nanoparticles	Anticancer drug delivery	[133]
17	Tasar silkworm gland protein	2D film	Skin tissue engineering	[74]
18	Tasar gland fibroin/PVA blend	Nanofibers	Bone tissue engineering	[42]
19	*Bombyx mori* silk fibroin	Silk microfiber reinforced silk hydrogel composite	Cartilage tissue engineering	[134]
20	Tasar gland fibroin protein	Tasar fibroin coated titanium	Bone tissue engineering	[135]

2.4 Wound dressing

Wounds are any defect or break in the normal anatomical structure of integrated skin, resulting from any thermal or physical damage or due to the presence of an underlying physiological or medical condition [20,106]. The regeneration of damaged skin starts immediately after wounding via a complex process known as wound healing. The wound that heals normally is known as acute wound whereas the wound that is arrested in a phase of wound healing process is known as chronic wound. The body is able to heal the acute wounds such as superficial wounds but body is unable to heal deep injuries and chronic wound adequately without proper medication and wound dressing [136,137]. Open wounds are highly susceptible to microbial infection so proper wound dressing is required that assists many aspect of wound healing process. Different types of wound dressing are available commercially and the choice of particular wound dressing must be on the basic nature of wound. The ideal wound dressing should have following properties such as good exudates absorption ability, provide moist environment, biocompatible, biodegradable, porosity, water vapor and gas exchange ability and adequate mechanical properties [58]. There are four different kind of wound dressings namely dry dressing (gauze, bandage and foam), moist dressing (hydrogels, hydrocolloids, gels & ointment), active dressing (antimicrobial dressings & composite dressings) and tissue engineered skin substitutes (allografts, xenografts, autografts & tissue engineered skin substitutes) have been successfully commercialized [138]. For the burn wound there is requirement for skin regeneration products. To treat the burn wounds skin substitutes such as autografts, allografts and xenografts are available however, they have several disadvantages such as limit availability of skin cells in severally burn patients, high cost, risk of disease

transmission. An alternate approach to treat such type of severely damaged skin tissues is by tissue engineered skin substitutes. In this respect, skin substitutes such as true skin, tegaderm are commercially available in the market. Various types of natural and synthetic polymers have been successfully utilized as scaffolds for skin regeneration [26,27,103].

2.5   Application of silk fibroin materials for wound management

Regenerated silk fibroin materials in the form of films, nano-fibrous membrane and woven textile have been employed as wound dressing for skin regeneration. Liu *et* al. [139] have explored the feasibility of using regenerated mulberry silk fibroin membrane to construct artificial skin substitute for wound healing. They observed that silk fibroin film does not have any adverse influence on the growth and biofunction of fibroblast and vascular endothelial. It also does not interfere with the secretion of angiogenesis growth factors such as VEGF, Ang-1, FGF2 and PDGF. Inpanya *et* al. [35] have studied Aloe vera gel blended mulberry silk fibroin films and compared them to aloe free fibroin films; the blended films enhanced the attachment and proliferation of skin fibroblasts. Vasconcelos *et* al. [36] have developed silk fibroin and elastin scaffolds for treatment of burn wounds. Mulberry silk fibroin/keratin films incorporating a synthetic inhibitor of elastase control the higher levels of this enzyme produced in a chronic wound environment [140]. Mulberry silk fibroin/alginate sponge demonstrates a higher healing effect than both components acting alone [141]. Karahaliloglu *et* al. [39] have modified the surface of silk fibroin film to obtain a biologically inspired nano-featured surface morphology, which enhanced the adhesion and proliferation of human epidermal keratinocytes and dermal fibroblasts.

A good amount of work has been carried out on mulberry silk fibroin proteins in the field of biomedical and tissue regeneration, due to its easy solubility in most of the solvents. But as scientific advancements are taking place interest of scientific community is shifted towards nonmulberry proteins. It is found that nonmulberry silk fibroin proteins such as muga and tasar have superior biocompatibility over mulberry silk fibroin proteins. Due to insolubility of nonmulberry fibroin proteins extracted from cocoons in many different solvents, most of the work on nonmulberry silk fibroin proteins is focused on utilization of gland protein that is extracted from gland of silkworm. For easy availability and commercialization, we have to utilize the nonmulberry fibroin proteins from cocoons of insects. Recently, some scientific groups have successfully dissolved and regenerated the nonmulberry silk fibroin proteins by using ionic liquids. But after the regeneration these fibroin proteins become brittle in nature so are practically unsuitable to be utilized as wound dressing especially in the load bearing areas such as knee and joints. Nonmulberry silk fibroin proteins have been successfully utilized for tissue engineering and regenerative medicine but only limited work have been carried out in the field of wound dressing and skin regeneration. Recently, Chouhan *et* al. [56] prepared epidermal growth factor functionalized muga gland fibroin/PVA blend based nanofibrous mat for wound healing applications. These functionalized nanofibrous mats showed improved cellular compatibility with dermal fibroblast cells *in vitro* as well as accelerated wound healing, good re-epithialization and highly vascularized granular tissue formation *in vivo*.

Table 2.7: Applications of regenerated silk constructs for wound dressing

1	Muga fibroin from cocoon	Muga microfibrous mats	Hemo-compatible	[120]
2	*Bombyx mori* silk fibroin from cocoon	2D film	Skin tissue engineering	[39]
3	*Bombyx mori* silk fibroin fiber coated with silver nanoparticles and chitosan	Microfibers	Skin tissue engineering	[142]
4	*Bombyx mori* silk fibroin from cocoon	2D film functionalized with growth factor	Wound healing	[58]
5	*Bombyx mori* silk fibroin from cocoon/Gelatin blend	3D Scaffold	Skin tissue engineering	[143]
6	*Bombyx mori* silk fibroin from cocoon/Elastin blend	2 D film	Wound healing	[36]
7	*Bombyx mori* silk fibroin from cocoon	Patterned 2D film	Skin tissue regeneration	[144]
8	*Bombyx mori* silk fibroin from cocoon/PEO blend	2D film	Hemocompatibility	[145]
9	*Bombyx mori* silk fibroin from cocoon/ Clay	Composite film	Wound healing	[146]
10	Tasar silk from gland protein	3D scaffolds	Hemocompatibility	[147]
11	Tasar silk from gland protein	2D film	Skin tissue engineering	[41]
12	*Bombyx mori* silk fibroin from cocoon	Nanofiber mat	Skin tissue engineering	[14]
13	*Bombyx mori* silk fibroin from cocoon	Nanofiber mat	Skin tissue engineering	[148]
14	*Bombyx mori silk* fibroin from cocoon/ aloe blend	2D film	Wound healing	[35]
15	*Bombyx mori* silk fibroin from cocoon	Nanofiber mat	Wound healing	[149]
16	*Bombyx mori* silk fibroin from cocoon	Woven textile	Burn wound healing	[150]

CHAPTER 3

EXPERIMENTAL METHODS

3.1 Materials

Multivoltine silk cocoons of *Bombyx mori* silkworm were purchased from Silk Development Department, Kalpipara, Bahraich, India. Muga silk cocoon were obtained from Research Extension Centre, Central Silk Board, Uttar Pradesh and Stofa International, Delhi, India. Tasar silk cocoons were procured from Silk Development Department, Sonbhadra, Uttar Pradesh, India. Cell culture reagents and other chemicals were obtained from Sigma-Aldrich, India. 1-butyl-3-methylimidazolium acetate (BMIMAc) and gentamicin sulphate were purchased from Sigma-Aldrich, India. Chemical used for conducting SDS-PAGE were obtained from Merck, Mumbai, India. Reagent grade of acrylamide (AAm), ammonium persulphate (APS), and N,N'-methylenebis(acrylamide) were procured from Sigma Aldrich. L929 fibroblast cells were purchased from National center for cell science, Pune. Sodium bicarbonate was purchased from Sigma-Aldrich. Slide-A-Lyzer dialysis flasks were procured from Thermo-Scientific. Protease XIV (from Streptomyces griseus, Sigma, 3.5 unit/mg activity) was purchased from Sigma-Aldrich. All other chemical used in the study were purchased from Sigma-Aldrich, until specified. Distilled water was used throughout the study.

3.2 Sodium dodecyl sulphate polyacrylamide gel electrophoresis (SDS-PAGE)

Molecular weight of muga and tasar silk fibroin after dissolution in ionic liquid was analyzed by SDS-PAGE. Dope solution is solvent-exchanged with 8M Urea (in 20 mM Tris-HCl; pH 8.0) at room temperature using Thermo Scientific Slide-A-Lyzer

Dialysis Flasks, 10K MWCO in order to minimize the anomalous in-gel mobility of fibroin due to chaotropicity rendered by imidazolium ions and then concentrate to 100 μg/mL [151,152]. Solvent exchanged fibroin sample was denatured by mixing in 1:1 ratio with gel loading buffer (0.5% Coomassie Brilliant Blue, 5% β-mercaptoethanol, 50 % Glycerol and 10% SDS in 250 mM Tris HCl pH 6.8) at 90°C for 10 min and were loaded against prestained molecular weight ladder (HiMark, NuPAGE) and resolved on 12% acrylamide gel and 5% stacking gel. The resolved bands of protein were visualized by staining with 0.25% Coomassie Brilliant Blue R-250.

3.3   Rheological measurements

Rheological properties of muga and tasar silk fibroin ionic liquid solution were measured using Brooke Field viscometer (DV-II), equipped with S-63 spindle as the function of varying shear rate and time.

3.4   Circular dichroism

Circular dichroism spectroscopy of dissolved muga fibroin was performed on Jasco spectropolarimeter (715) with a quartz cell of 1 mm and 10 mm path length for far – UV and near UV, respectively. To record the CD spectra muga fibroin-BMIMAc solution was diluted to concentration of 0.1 mg/mL using ionic liquid. CD spectra was obtained by averaging atleast five scans at a scan speed of 100 nm/mm with a response time of 0.5 s. A blank solution measured under same condition was subtracted from the data [153].

3.5   Fourier transform infrared spectroscopy

Structural conformation of muga and tasar silk fibroin after dissolution in BMIMAc as well as different silk fibroin constructs and capped silver nanoparticles was

determined by Thermo Scientific Nicolet 380 Spectrometer, Japan, in reflection mode at 4 cm^{-1} resolution using 64 scans in the spectral range 2000 to 800 cm^{-1}.

3.6 Morphological and elemental characterization

Different silk fibroin samples were sputter coated with gold and analyzed by scanning electron microscope (Hitachi 3700 N) at an accelerating voltage of 15 kV. The diameter of fibers was calculated by measuring at least 30 fibers from 10 images randomly using Image J software. Mean particle size diameter and volume fraction of the nanoparticles as well as hydrogel particles were measured in the milliQ water and ethanol, respectively, using Particle Size Analyzer (Microtrac S 3500). For TEM, a drop of the sonicated aqueous suspension of AgNPs was drop cast on carbon coated copper HR-TEM grid (FEI Technai S Twin) & then analyzed at the voltage of 200 kV and magnification upto 10, 30,000x. The formation and deposition of silver nanoparticles on the surface of tasar nanofibrous mat was further validated through EDX and EDX mapping analysis using Hitachi S 3700N SEM machine equipped with EDX assembly.

3.7 Mechanical and dynamic mechanical thermal testing

The mechanical properties of samples were determined by using Universal Testing Machine (Instron-2700) in tension mode as per ASTM D 882-02. The samples were cut into strips with dimensions of 70x10 mm and then fixed at the jaw of tensile tester [105]. The strain rate and gauge length were 50 mm/min and 20 mm, respectively. At least five samples were tested and their stress-strain curves were recorded.

The dynamic mechanical thermal analysis of different silk fibroin constructs was carried out on a DM 8000 dynamic mechanical analyzer (Perkin Elmer) by using film

testing fixture. Specimens of 40×10 mm were run at tensile mode at a frequency of 1 Hz with 0.125% of strain and 3 °C/min of heating rate. The tan δ of specimens was determined as the function of temperature from 25-250 °C.

3.8   Thermal analysis

The thermogravimetry (TG) and differential thermal analysis (DTA) measurement of different silk fibroin samples were performed on a Perkin Elmer Diamond TG/DTA instrument. The amount of sample was approximately 5 mg. All the measurements were performed under nitrogen atmosphere from 30 to 800 °C at a heating rate of 10°C/min. The thermal analysis of silk films was performed by Differential Scanning Calorimetry (DSC) instrument (TA Instruments Q100 DSC) under a dry nitrogen gas flow of 50 ml/min. The silk film of approximately 5 mg was filled in aluminium pan and heated at 2 °C /min from 30 °C to 800 °C depending on types of samples.

3.9   Structural characterization of different regenerated silk fibroin constructs by XRD

The X-ray scans of different silk constructs as well as silver nanoparticles were performed with a Seimens type-F, X-ray diffractometer (Bruker D S Advanced, Germany). The X-ray source was Cu Kα radiation (40 kV, 30 mA and λ=1.5 A). The samples were mounted on aluminium frames and scanned from 5 to 50° (2θ) at a speed of 2°/min.

3.10 Porosity, pore size and surface roughness

Porosity of different silk fibroin samples was measured by liquid displacement method [154]. Hexane acts as non-solvent for silk fibroin, so it used as displacement liquid. It easily permeates through interconnected pores without causing any

shrinkage or swelling. For measurements, a rectangular piece of 20x20 mm from different silk fibroin samples was immersed in known volume (V_1) of hexane in graduated measuring cylinder for 10 min. The total volume of hexane after immersion of respective samples was recorded (V_2). The residual hexane volume (V_3) in cylinder after removal of hexane impregnated sample was also recorded. The porosity was calculated by the equation:

$$\varepsilon\ (\%) = [(V_1-V_3)/\ V_2-V_3)]\ x\ 100 \qquad\qquad ....(1)$$

The AFM analysis of different silk fibroin samples was performed on Park (XE-100) microscope equipped with V shape silicon nitride cantilever having spring constant 40 N/m in tapping mode. The morphology and surface roughness of samples were analyzed at room temperature by scanning the area of 2x2 μm. The roughness of samples was measured as root mean square (RMS) deviation and arithmetic average height (Ra). The RMS value attributed to standard deviation of the height values within scanned area and Ra represents the average deviation of roughness irregularities [155]. The average pore size was calculated by measuring at least 10 pore of 5 images using Image J software.

3.11 Water uptake

Water uptake of regenerated different silk fibroin samples was determined by the procedure as reported by Wharram *et* al. [86]. Briefly, the samples were cut in specific size (20x20 mm) and weighed. The samples were immersed in deionized water and incubate at 37 °C. After, definite time intervals, the samples were taken out and gently wiped with tissue paper until residual water was observed on the sample surface. Water

swollen sample was weighed at definite time interval till saturation has to be maintained. The percent water absorption was determined by the equation given below:

% Water absorption = (Wet Weight- Dry Weight)/Dry Weight x 100% ……..(2)

3.12 Contact angle measurement

Hydrophilicity of SF and DMSF films was determined by analyzing water droplet angle formed between liquid/solid interfaces of different films by Sessile drop method. The volume of water droplet was kept at 4 μl. Contact angle value for each sample was taken as the average of three readings obtained at five different places of the sample.

3.13 Water vapor transmission rate (WVTR)

WVTR of different silk fibroin samples was measured in accordance with standard ASTM D 1653 with some modifications [156]. Briefly, a plastic cup was filled with distilled water and then sealed by film samples of 9.5 cm^2. The assembly was weighed, kept in an environment of 36±0.5°C and 40±2% relative humidity for 24 h, and then weighed again. Water vapor transmission rate for different silk fibroin samples was calculated by the equation given below and expressed as g/m^2/day:

WVTR = [(W$_1$ − W$_2$) / A x 24] ……..(3)

Where W$_1$ and W$_2$ represent the weight of assembly before and after 24 h of water evaporation, respectively, and A represents the transmission area of the sealing samples.

3.14 Biocompatibility tests

3.14.1 Cell Culture

L929 fibroblast cells were obtained from National Center of Cell Science, Pune, India. These cells were cultured in DMEM supplemented with fetal bovine serum (10% v/v) and penicillin/streptomycin/amphotericin B antibiotic (1% v/v) solution. Fibroblast cells culture was maintained at 37 $^{\circ}$C in a humidified 5% CO_2 atmosphere. The media was changed every 3 days. DMEM and FBS were purchased from Sigma-Aldrich.

3.14.2 Cells seeding on different silk fibroin samples

For cytocompatibility study, all the samples were sterilized by treating with 70% ethanol for 15 min, which was followed by washing of samples with PBS and drying. Dried samples were again sterilized by exposing UV radiation under laminar air flow [157]. Sterile samples were cut in specific size and placed in 24 well plate. For cell proliferation and adherence study approximately $1x10^4$ cells were seeded per well on different silk fibroin samples at 37 $^{\circ}$C in a humidified atmosphere containing 5% CO_2. The cell seeded construct were monitored at different time interval (1, 3 and 5 days).

3.14.3 Cell adherence and spreading by SEM study

For SEM study, cell seeded constructs were washed twice with serum free PBS, then fixed in 2.5% gluteraldehyde in PBS (pH 7.4) for 2 h. After that constructs were dehydrated through series of gradient alcohol (50, 75 and 100%) for 30 min in each case and then incubated in iso-amyl alcohol for 5 min, dried in oven at 40 °C. Dried construct were sputter coated with gold and scanned using Hitachi 3700 N scanning electron microscope.

3.14.4 Cell adherence and morphology by fluorescence and phase contrast microscopy

Fluorescence microscopy was performed to elucidate the time dependent spreading of L929 cells on different silk fibroin samples. DAPI (4',6-Diamidino-2-phenylindole) fluorescent dye was used for visualization of the nucleus. After incubation for 1, 3 and 5 days, cell seeded construct were washed with PBS and fixed in 3% paraformaldehyde in PBS for 5 min and 0.5 mL of 0.2% Triton X-100 in PBS was added to permeabilize the cells. Cells were stained using DAPI (1μg/mL) for 30 min [75]. Cell seeded construct was washed with PBS twice; mounted between cover slip & glass slide. Stained cells seeded on films were imaged using fluorescence microscope (Zeiss, Axio Imager 2). The images of fluorescence were further analyzed using image J software to quantify the number of cells and statistical analysis was applied for three replicates at minimum four areas within the samples.

Growth and proliferation of L929 cells seeded on different silk fibroin samples were analyzed using phase contrast microscopy after 1, 3 and 5 days of incubation. The cell seeded silk fibroin constructs were washed with PBS and then observed under phase contrast microscope to study the morphology and time dependent spreading of L929 cells over different silk fibroin samples.

3.14.5 Cell viability and proliferation

MTT assay was carried out to check the mitochondrial activity. This provides direct indication about cell viability. An aliquot of 100 μL of MTT (5 mg ml^{-1}) was diluted in the ratio 1:10 in PBS and was added to each well, followed by incubation for 4 h at 37 $^{\circ}$C. At the end of the assay the blue formazan crystal was dissolved in 1 mL of dimethyl sulfoxide. Absorbance was measured at 595 nm in a Bio-Rad microplate reader.

Viability of cells grown on different silk fibroin samples were determined by using Trypan blue exclusion assay. This assay is also referred as dye exclusion assay which utilizes the concept that viable cells exclude the dye so have clear cytoplasm, whereas dead cells possess blue cytoplasm [75].

3.14.6 Hemolysis Assay

Hemolytic activity was assessed by determining hemoglobin release under static conditions (ASTM F 756-00, 2000). The materials with percentage of hemolysis over 5% are considered as hemolytic and materials having hemolysis below 2% are considered as non hemolytic. The materials show hemolysis percentage between 2 to 5% is classified as slight hemolytic. Porcine blood was collected in heparin-coated siliconized tube from the slaughterhouse according to the protocol reported by Kasoju *et* al. [79]. Different silk fibroin samples were placed in a siliconized tube containing 10 mL heparinized blood (1:10 diluted with PBS, pH 7.4). Heparinized blood (1 mL) diluted with PBS (9 mL) was taken as the negative control (0% hemolysis), and heparinized blood (1mL) diluted with distilled water (9 mL) was taken as the positive (100% hemolysis) control. The contents were gently mixed and incubated at 37 °C for 1 h without shaking. After incubation, each fluid was transferred to a suitable tube and centrifuged at 2000 rpm for 15 min. The hemoglobin released by hemolysis was measured by the optical densities (OD) of the supernatants at 540 nm using a spectrophotometer (Agilent Carry 300). The percentage of hemolysis was calculated as follows:

$$H\% = \{(OD_s - OD_{nc})/ (OD_{pc} - OD_{nc})\} \times 100 \qquad \ldots\ldots(4)$$

Where, ODs, ODnc and ODpc are optical density values of blood with sample,

negative control and positive control, respectively.

3.14.7 Platelets adhesion assay

Platelets adhesion is one of the important test to evaluate the hemocompatibility of biomaterials. The method used to carry out hemocompatibility test is as follows [120]. Five milliliter of porcine fresh blood was treated with 3.8% sodium citrate. This blood was spun at 1200 rpm for 5 min at 4 °C to obtain platelet rich plasma (PRP). The platelet concentration in PRP was adjusted to 1×10^5 platelets/mL. The sterilized silk fibroin samples were cut in specific size and placed in 96 well plates. Platelet rich plasma of 200 μL was poured on it, and allowed to incubate for 5 h. Platelets attached to pure silk fibroin samples were washed twice with PBS and immersed in PBS containing 2.5% gluteraldehyde (pH 7.4) for 5 h. These samples were subsequently dehydrated in gradient alcohol (20%, 40%, 60%, 80% and 100%) for 15 min and dried in vacuum. The morphology of platelets adhered tasar films was observed by the SEM (Hitachi S 3700 N).

3.15 Antimicrobial activity

The antimicrobial activity of gentamicin sulphate loaded different silk fibroin samples was investigated by agar diffusion assay (AATCC 30) against *E. coli* (gram -ve) and *S. aureus* (gram +ve) [158]. The gentamicin sulphate loaded different silk fibroin samples were cut in the form of circular disc of diameter 6 mm and sterilized under UV light in laminar air flow for 24 h. The sterile samples were placed on agar plates which had been cultured with *E. coli* and *S. aureus* and pressed lightly to ensure close contact with the surface. Plates were incubated at 37 °C for 24 h in an incubator. After incubation, the results were evaluated by determining the size of zone of inhibition

produced around the sample to assess the efficacy of antimicrobial loaded films. In all the cases duplicate specimens were tested.

3.16 Drug release

Different regenerated silk fibroin samples of 40x40 mm size were dipped in the freshly prepared gentamicin solution having a concentration of 2 mg/mL for 24 h at 36 °C. The amount of drug loaded on both samples was determined by using UV-Vis spectrophotometer at a wavelength of 333 nm. The amount of drug loaded on different silk fibroin samples was found in the range of 15 to 40 mg/mL, respectively. Antibiotic loaded different silk fibroin samples were immersed in 50 mL of PBS solution up to 7 days at 36 °C.

At determined time, 200 μL of aliquots were taken to determine the amount of gentamicin released using o-phthalaldehyde method at a wavelength of 333 nm [36,159]. After each measurement the sample were added back to experimental stock solution to maintain equilibrium condition. The amount of drug released was determined by gentamicin standard curve. All the release studies were performed for a period of 160 h. The release mechanism of gentamicin from MNF-20 and MCF were determined by fitting the experimental data to the semi empirical power law method given by Ritger-Peppas: [160]

$$M_t/M_\infty = kt^n \qquad\qquad ....(5)$$

3.17 *In vitro* biodegradation

In vitro biodegradation of different silk fibroin samples was determined by the protocol given by Kasoju *et* al. [79] with slight modifications. Pre-weighed samples of different

silk fibroin were immersed in 2 mL of PBS with and without trypsin (1 mg/mL, from bovine pancrease X3, activity 2500 NFU/mg) and incubated at 37 ^{o}C. The enzymatic solution was replaced every day with fresh solution in order to maintain the activity of enzyme. Every day, samples were removed from pure PBS and enzymatic solution, washed with distilled water, dried in oven at 50 ^{o}C & weight of each samples was determined. The extent of biodegradation was determined by the equation:

Weight loss (%) = $(W_o - W_t)/W_o$ x 100 ……… (6)

Where, W_0 and W_t are the weights of the nonwoven films before and after incubation in PBS.

3.18 Statistical analysis

All the data are presented as mean ± SD. One-way ANOVA was performed to assess the experimental data at the statistical significance levelof $p<0.05$.

CHAPTER 4

CHITOSAN FINISHED *ANTHERAEA MYLITTA* AND *ANTHERAEA ASSAMA* SILK FIBROIN NONWOVEN COMPOSITE FILMS FOR WOUND DRESSING

4.1 Introduction

Nonwoven fibrous mats have been known as promising materials for wound healing due to high surface area, porosity and gas permeability [44,81]. Recently, nonwoven fibrous mats have been prepared by casting techniques. The nonwoven fibrous mats prepared by casting technique have shown lower mechanical properties due to lack of adhesion between the fibers therefore these mats are not suitable for load bearing applications, for example wound dressing for knee and elbow joints [76–80]. The properties of these nonwoven fibrous films can be further improved by finishing with suitable binding agent.

Chitosan is a hemostat, which helps in natural blood clotting [124–129]. Due to good biocompatibility and control biodegradability mulberry fibroin and chitosan blends based films [124–126], sponge [128] scaffolds [129] and hydrogels [127] have been prepared and utilized in the area of tissue engineering and regenerative medicine. However, the major drawbacks associated with mulberry silk fibroin/chitosan blends are brittleness and poor mechanical properties due to degradation of silk fibroin protein during dissolution processes, which makes it unsuitable to be used as wound dressing in the load bearing areas.

The aim of this chapter is focused on the fabrication of muga and tasar fibroin fibers based nonwoven mats. These tasar and muga fibroin nonwoven mats were finished

with different concentrations of chitosan solution ranging from 0.75 to 2% w/v using dip coating method to fabricate nonwoven composite films. For tasar fibroin films the abbreviation used was TFF and for chitosan modified films the abbreviation used was CMTFF. In case of muga fibroin the abbreviation used was MFF and for chitosan modified muga fibroin film, it was CMMFF.

4.2   Experimental

4.2.1 Extraction of silk fibroin fibers from cocoon by degumming

Silk fibroin fibers was extracted from cocoons of mulberry, muga and tasar by the process as described earlier [79]. Silk cocoons were cut in small pieces and washed with distilled water. Raw silk fibers were degummed twice with 0.02 M $NaHCO_3$ solution at 100 °C for 30 minutes and then washed thoroughly with distilled water to remove glue-like sericin protein. The degummed fibroin fibers were then dried completely at room temperature.

4.2.2 Preparation of tasar fibroin nonwoven (TFF) and muga fibroin nonwoven (MFF) mats

Tasar fibroin nonwoven mat and muga silk fibroin nonwoven fibrous mats were prepared by casting method. Briefly, tasar and muga silk cocoons were cut in small pieces and degummed by boiling in 0.02 M Na_2CO_3 for 30 min. The degummed tasar and muga fibroin fibers were washed in running water to remove residual sericin and dried in oven at 60 °C [41]. 1g of tasar and muga degummed silk fibroin fibers were cut in small sizes (5 to 20 mm) and dispersed in 60 mL of formic acid by constantly stirring the mixture at 40 °C. The homogenized mixture was poured in petridishes and solvent was allowed to evaporate at 37 °C for 24 h. After drying, fibrous films were

washed thoroughly with distilled water in order to remove residual acid and salt and dried overnight under vacuum at 60 °C.
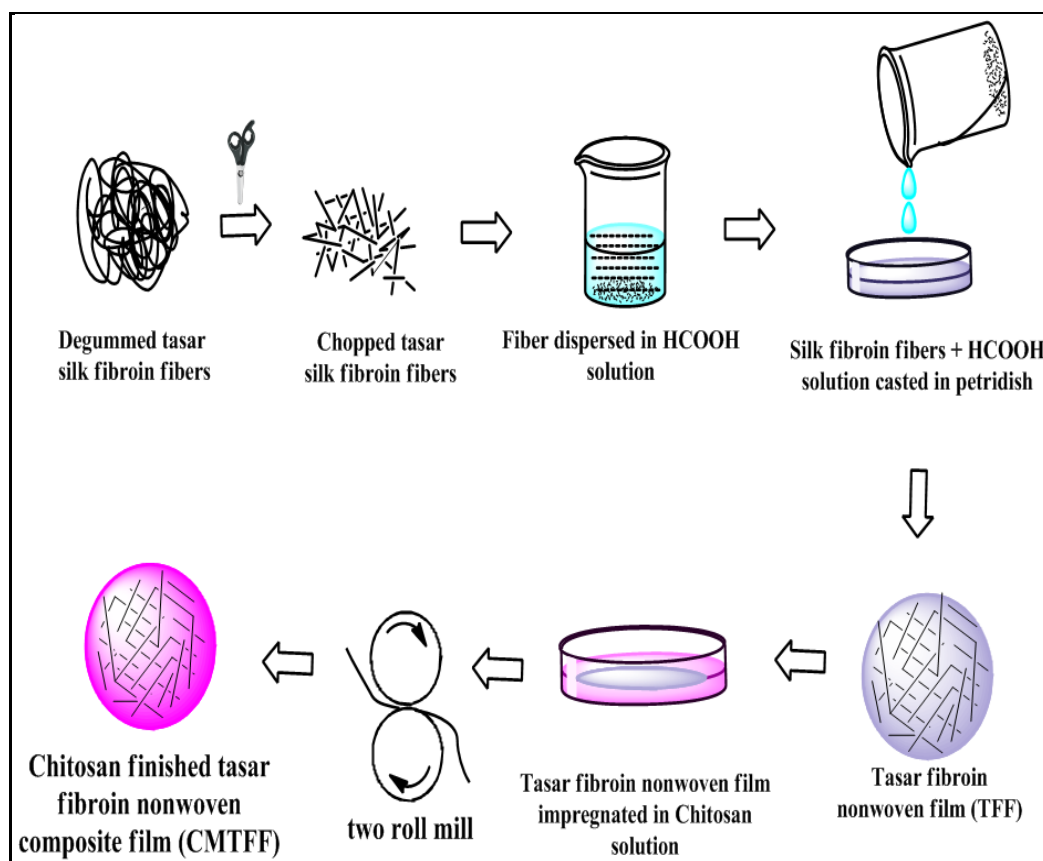
Scheme I: **Schematic representation for preparation of chitosan finished tasar nonwoven films**

4.2.3   Chitosan finishing of tasar and muga fibroin nonwoven films

Tasar fibroin nonwoven (TFF) and muga fibroin nonwoven (MFF) mats were finished by chitosan using pad-dry method [158]. Different chitosan solutions (0.75, 1, 1.5 and 2% w/v) were prepared in 1% (v/v) acetic acid aqueous solution. TFF and MFF films were dipped separately in different concentrations of chitosan solution (0.75, 1, 1.5 and 2% w/v) and passed through padding mangle to give 100% wet expression. After that these films were dried at 80 °C for 5 min. The schematic diagram of preparation of chitosan finished tasar nonwoven films are shown in the Scheme I and chitosan

finished muga nonwoven films in the Scheme II. The chitosan modified tasar fibroin nonwoven and muga fibroin nonwoven mats have been abbreviated as CMTFF and CMMFF, respectively. Based on the concentration of chitosan used for modification, these films have been designated as 0.75% CMTFF, 1% CMTFF, 1.5% CMTFF & 2% CMTFF and 0.75% CMMFF, 1% CMMFF, 1.5% CMMFF & 2% CMMFF.
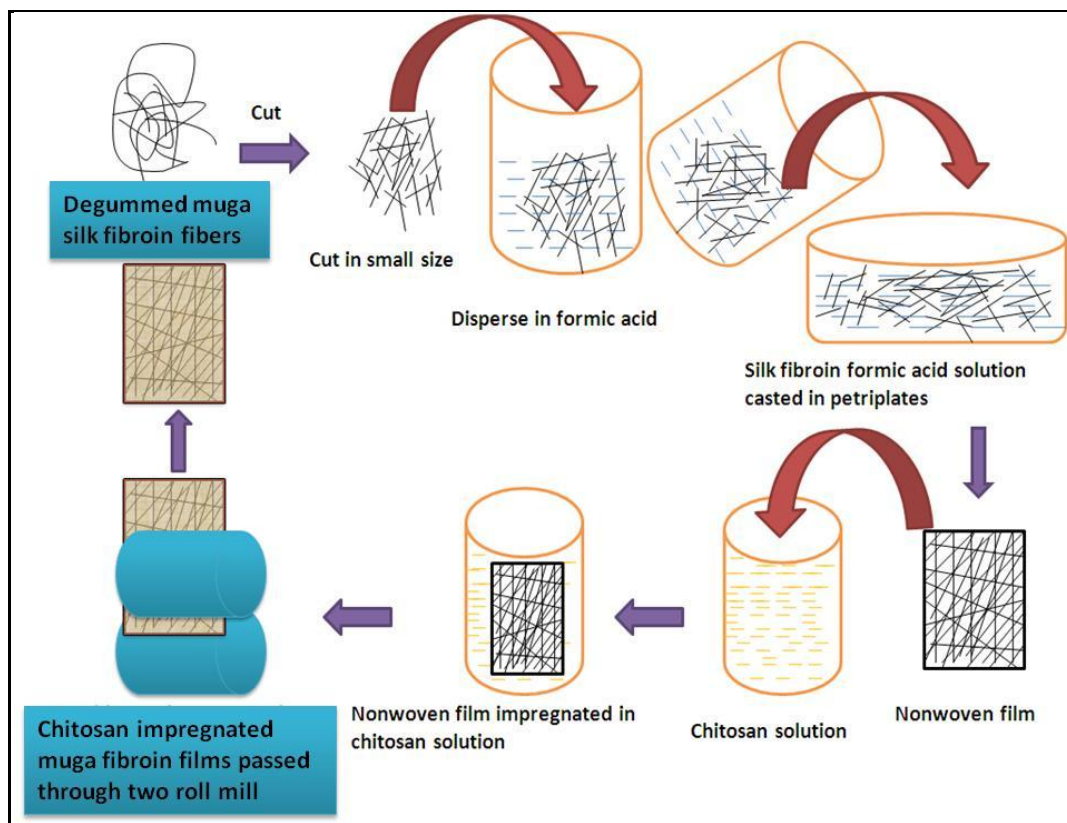
Scheme II: Schematic representation for preparation of chitosan finished muga nonwoven films

4.3 Results and Discussion

4.3.1 Structural Properties

FTIR analysis was carried out to investigate structural changes of tasar and muga silk fibroin before and after chitosan treatment.

FTIR spectra of TFF and 0.75 to 2% CMTFF are shown in the Figure 4.1. TFF scaffolds showed two broad absorption peaks with a center around 1616 cm^{-1} (amide I) and 1509 cm^{-1} (amide II), corresponding to silk II conformation (β-sheet). Tasar fibroin nonwoven films treated with different concentrations of chitosan (0.75 to 2%) showed peaks of amide I and II regions. These are 1626 and 1519 cm^{-1} for 0.75% CMTFF, 1613 and 1529 cm^{-1} for 1% CMTFF, 1619 and 1520 cm^{-1} for 1.5% CMTFF and finally 1636 and 1517 cm^{-1} for 2% CMTFF, which are characteristic of less ordered β-sheet conformation.
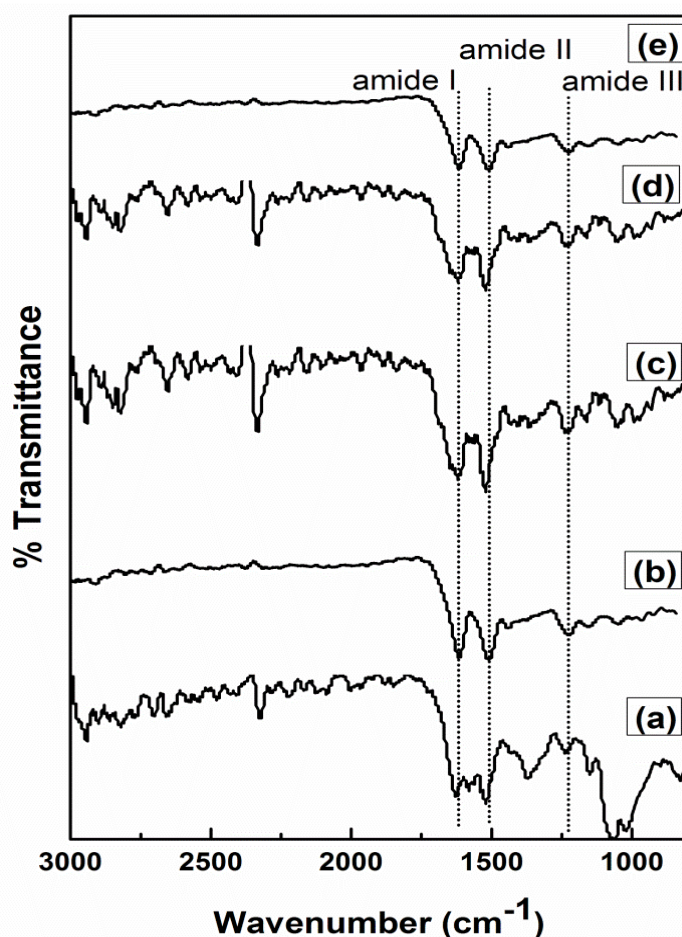
Figure 4.1: FTIR spectra of (a) TFF, (b) 0.75% CMTFF, (c) 1% CMTFF, (d) 1.5% CMTFF and (e) 2% CMTFF
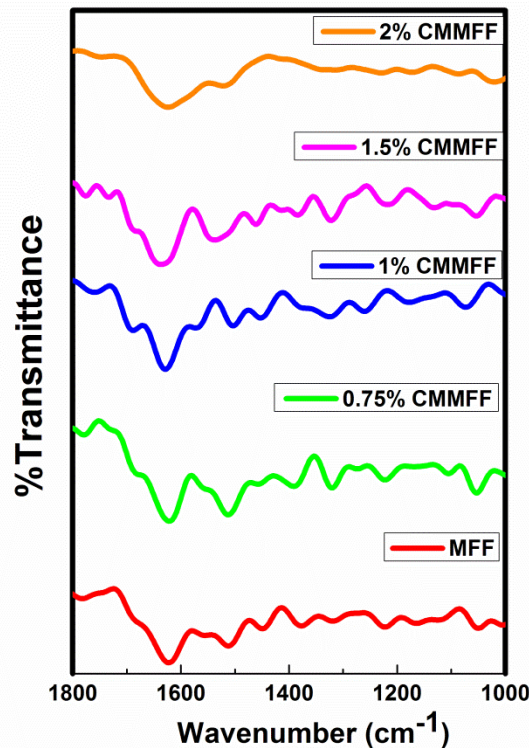
Figure 4.2: FTIR spectra of MFF, 0.75% CMMFF, 1% CMMFF, 1.5% CMMFF and 2% CMMFF

Similarly, muga nonwoven scaffolds (MFF) showed (Figure 4.2) two absorption bands at 1621 and 1510 cm^{-1}, for amide I and II region respectively, corresponding to silk II conformation (β-sheet). Chitosan finishing does not affect the secondary structural conformation of muga protein. These peaks appeared at 1621 and 1512 cm^{-1} for 0.75% CMMFF, 1627 and 1510 cm^{-1} for 1% CMMFF, 1624 and 1536 cm^{-1} for 1.5% CMMFF & finally 1621 and 1515 cm^{-1} for 2% CMMFF. These peaks are characteristics of β-sheet conformation.

She *et* al. [129] found that chitosan can induce conformational transitions in mulberry silk fibroin/chitosan blends. It is also reported by Mandal *et* al. [74] that these transition also take place in regenerated tasar fibroin gland proteins after alcohol treatment. The absorbance band at 1154 and 900 cm^{-1}, are characteristic of

asymmetric vibration of –C-O in the saccharide structure of chitosan. Teimori *et* al. [161] reported that for silk fibroin the amide peak appeared at 1653 cm^{-1} (random coil) which is shifted to 1633 cm^{-1} (β-sheet) after blending with chitosan. However in case of chitosan finished tasar and muga silk fibroin, chitosan does not have any remarkable effect on β-sheet conformation of tasar silk fibroin [162–165].

4.3.2   Morphology of nonwoven composite films

Figure 4.3 shows the SEM images of TFF and different CMTFF. From Figure 4.3, it is clear that TFF shows loosely packed structure, but as the concentration of chitosan increases the structure become more compact. The average diameter of fibers was 20 ± 10 μm (mean ± SD, n=5) and fibers are randomly oriented. TFF film is highly porous in nature with pore size distribution in the range of 50 ± 5 to 150 ± 50 μm. Due to chitosan treatment the nonwoven films become more consolidate and porosity is slightly reduced (50 ± 5 to 100 ± 50 μm).

SEM images of MFF and chitosan modified muga nonwoven films (CMMFF) are shown in the Figure 4.4. Similarly, MFF also show loosely packed structure but as we impregnate these non-woven structures with chitosan solution its compactness is enhanced and it further enhances with increase in concentration. MFF also showed highly porous architecture with pore size range from 50 ± 5 to 160 ± 50 μm. SEM images clearly indicate that due to chitosan finishing the nonwoven loosely packed structure became more compact and porosity slightly reduced (50 ± 5 to 110 ± 50 μm). Chitosan spread uniformly throughout the nonwoven films and no aggregates were observed. Chitosan finished macro architecture could be ideal design for wound dressing which mimics natural extracellular matrix and promotes regeneration of damage tissues and provides good mechanical support [3,166].
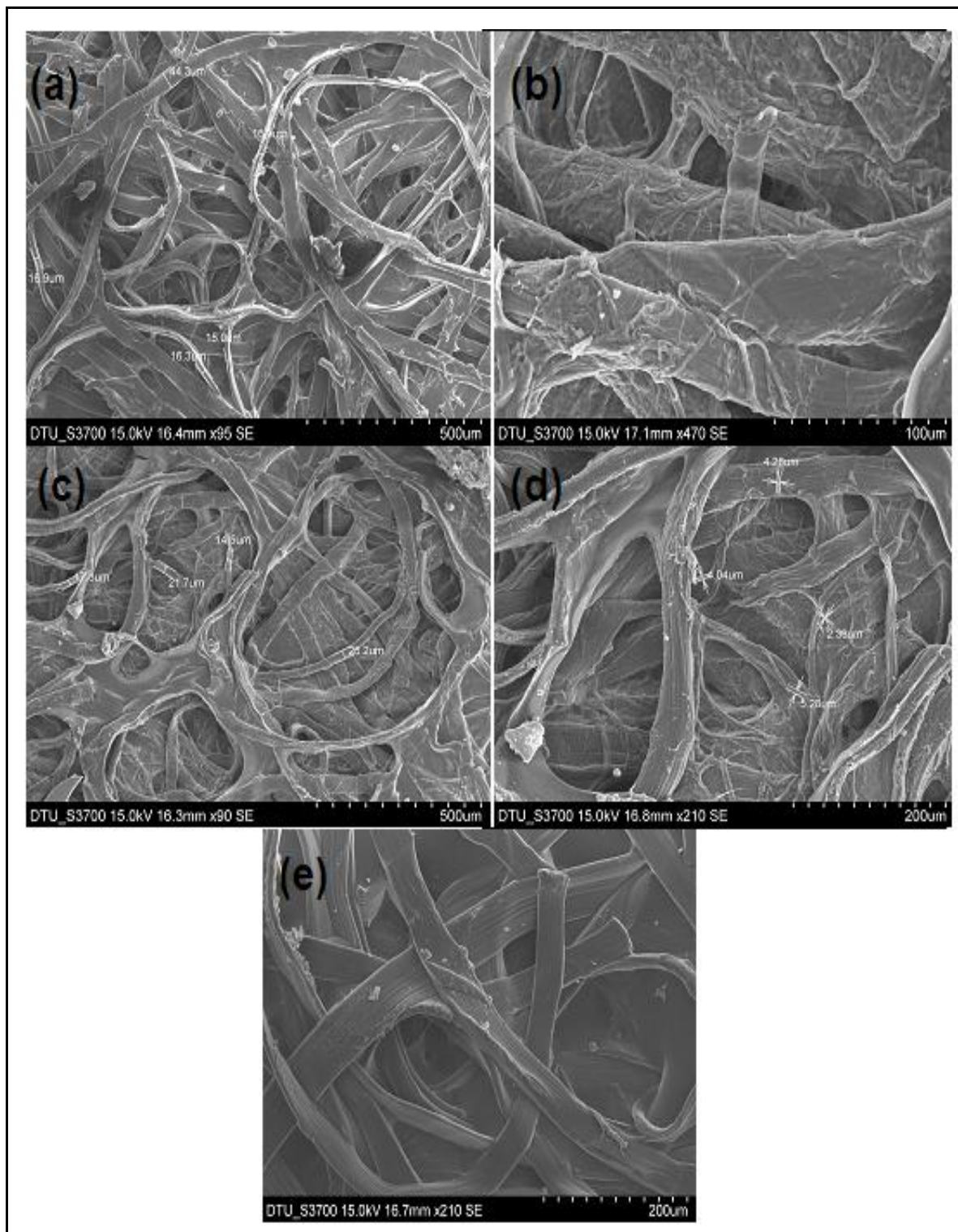
Figure 4.3: SEM images of (a) TFF, (b) 0.75% CMTFF, (c) 1% CMTFF, (d) 1.5% CMTFF and (e) 2% CMTFF
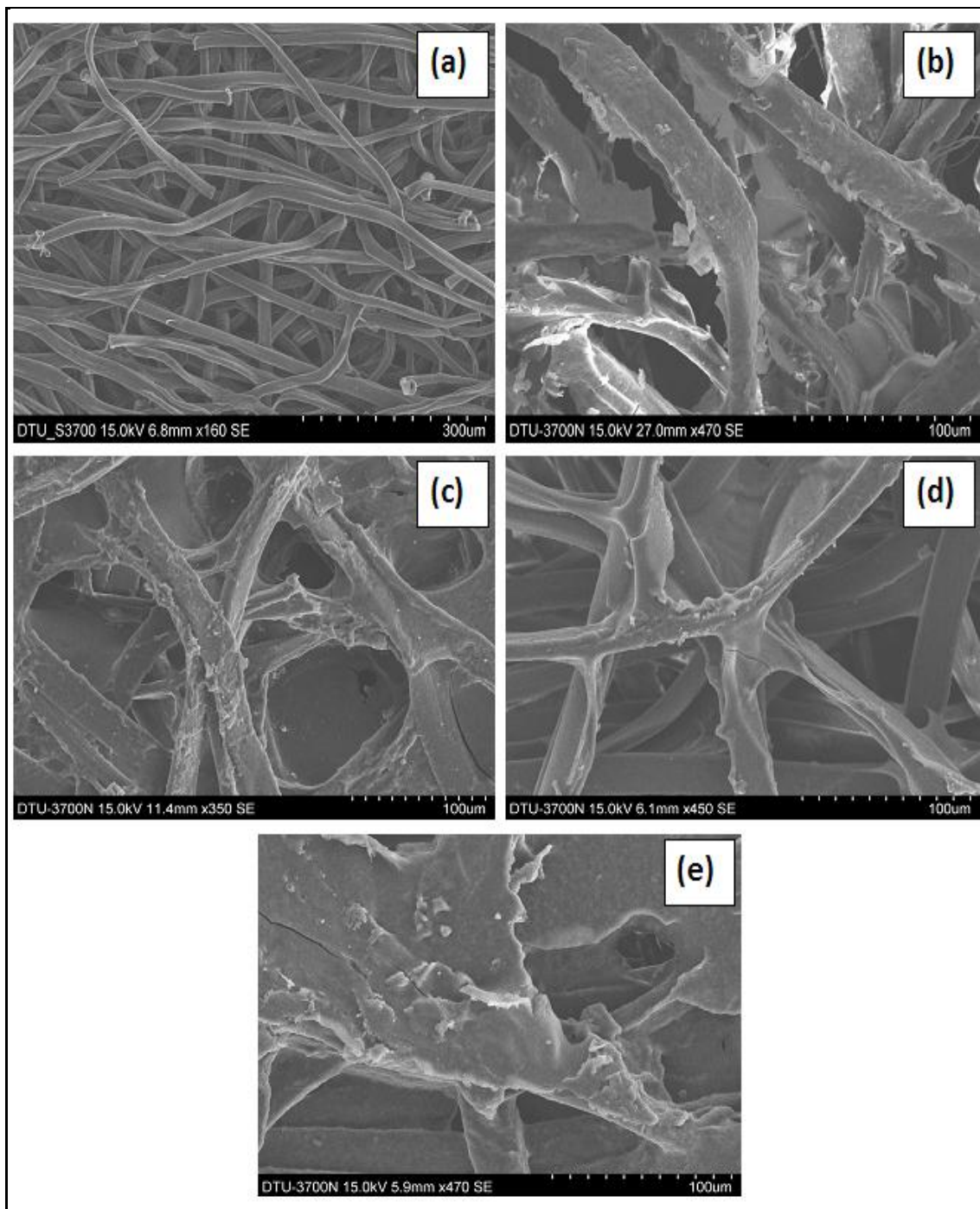
Figure 4.4: SEM images of (a) MFF, (b) 0.75% CMMFF, (c) 1% CMMFF, (d) 1.5% CMMFF and (e) 2% CMMFF

4.3.3   Mechanical characterization

Chitosan finished composite films showed higher tensile strength and modulus compared to unmodified tasar and muga nonwoven film. Tensile strength and

modulus of TFF are 6.5 and 218 MPa, respectively. Variation of tensile properties with change in weight and thickness of films after chitosan finishing are shown in the Figure 4.7 and Figure 4.5. Tensile strength and modulus of tasar fibroin nonwoven films increases with increase in chitosan concentration, started at 9 and 274 MPa for 0.75% CMTFF, 12 and 353 MPa for 1% CMTFF, 14 and 450 MPa for 1.5% CMTFF and reached 21 and 550 MPa for 2% CMTFF, showing significant difference (P<0.05) among each other. For TFF, elongation at break values was 16 mm which decreased to 13, 8, 4 and 3 mm for 0.75, 1, 1.5 and 2% CMTFF, respectively.
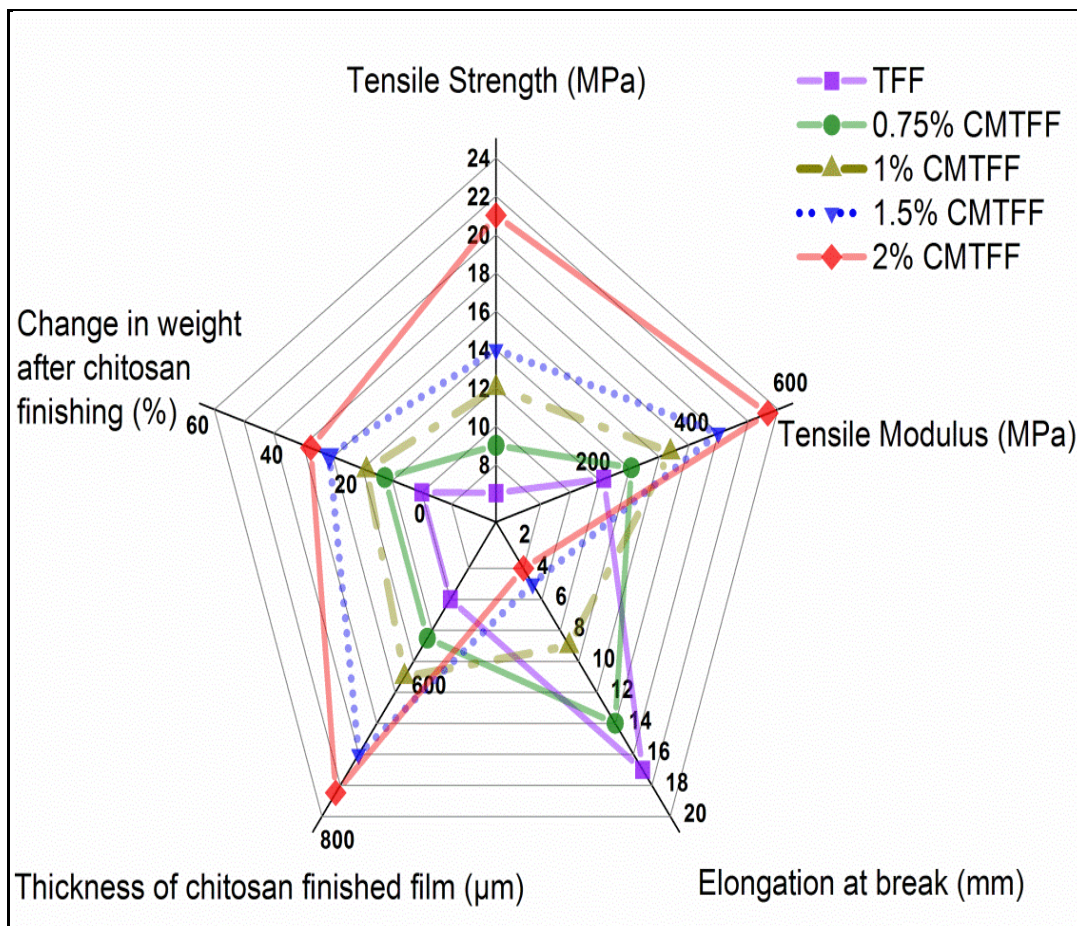
Figure 4.5: **Variation of tensile properties of tasar nonwoven films after finishing with chitosan**
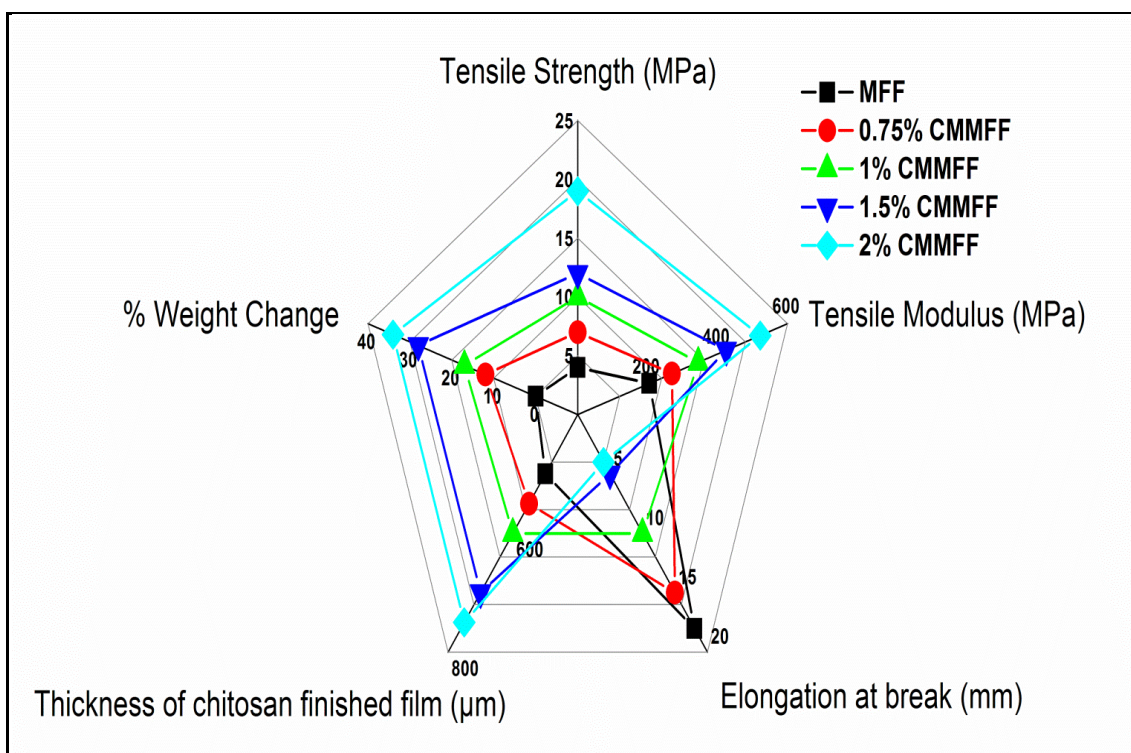
Figure 4.6: Variation of tensile properties of muga nonwoven films after finishing with chitosan

Muga fibroin nonwoven mat shows lower mechanical strength and higher elongation compared to tasar nonwoven mat (Figure 4.6). Tensile strength and modulus of MFF is 4 and 205 MPa, respectively. Chitosan finishing enhanced the tensile strength and modulus of MFF, which is 7 and 270 for 0.75% CMMFF, 10 and 345 MPa for 1% CMMFF, 12 and 425 MPa for CMMFF & further enhanced to 19 and 522 MPa for 2% CMMFF, that is significantly higher than MFF (P<0.05). Elongation at break for MFF is 18 mm which is reduced to 15, 10, 5 and 4 mm for 0.75 % CMMFF, 1% CMMFF, 1.5% CMMFF and 2% CMMFF, respectively.

Higher tensile strength of chitosan modified tasar and muga nonwoven mats compared to unmodified tasar (MFF) and muga (MFF) nonwoven mats are due to the mechanical properties of fibrous mats which depends upon adhesion between the fibers. In nonwoven mats, fibers are randomly oriented; hence, due to anisotropy as

well as less interaction between fibers stress concentrates that results in slippage of fibers. Thickness of TFF and MFF film was 500 μm which increased up to 750 μm after finishing with 2% (w/v) chitosan solution. Similarly, chitosan acts as a matrix, binds the fiber together, receives stress and transfers to the fiber. Due to more efficient contact and strong secondary bonding interaction between fibers, the mechanical properties of chitosan finished fibrous nonwoven films increases. Tensile strength and modulus was increased by 69 & 60 for tasar nonwoven and 78 & 58% for muga nonwoven mats by treating with chitosan solution from 0.75 to 2% (w/v), suggesting a possible way to improve the tensile properties of nonwoven fibrous films by finishing with chitosan [3].

4.3.4   Dynamic mechanical thermal analysis

Dynamic mechanical thermal analysis is a tool to find out the effect of temperature on viscoelastic properties of the silk biomaterials. Figure 4.7 shows the temperature dependence of the dynamic storage modulus of TFF and CMTFF. From Figure 4.7, it is clear that CMTFF shows higher storage modulus value compared to TFF. At 20 °C, storage modulus of TFF was 200 MPa, while for 0.75% CMTFF, 1% CMTFF, 1.5% CMTFF and 2% CMTFF it was 320, 400, 590 and 700 MPa, respectively. The increase in modulus after chitosan treatment is due to an increase in stiffness. Above 30 °C, for all the samples storage modulus value increased, which continues up to 100 °C, until completely drops at 250 °C due to thermal relaxation of fibroin chains. Initial increase in storage modulus in between 30 to 100 °C indicates an increase in the intrinsic stiffness of individual fibroin chains due to stronger interaction between fibroin chains with an increase in temperature.
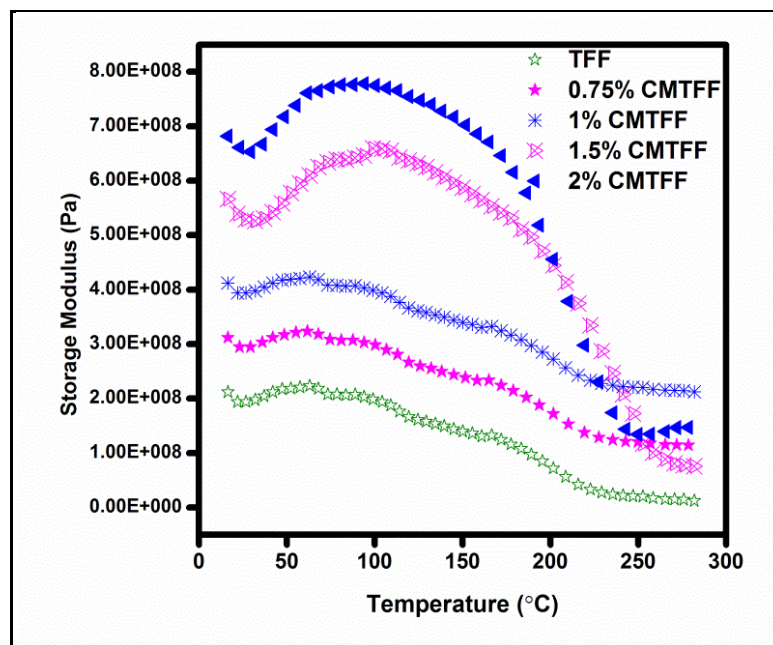
Figure 4.7: Storage modulus curves for: (a) TFF, (b) 0.75% CMTFF, (c) 1% CMTFF, (d) 1.5% CMTFF and (e) 2% CMTFF
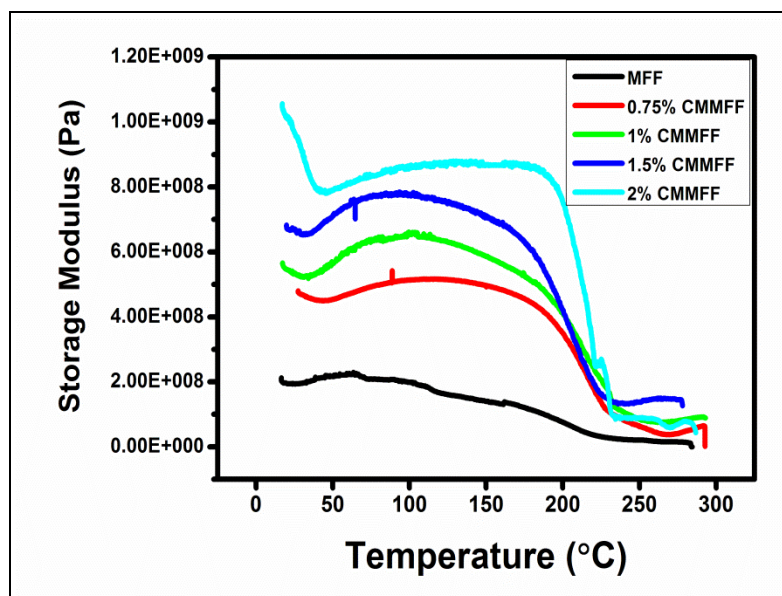
Figure 4.8: Storage modulus curves for: (a) MFF, (b) 0.75% CMMFF, (c) 1% CMMFF, (d) 1.5% CMMFF and (e) 2% CMMFF

Storage modulus of CMMFF was significantly higher compared to MFF. Figure 4.8, shows that storage modulus of MFF was 195 MPa, while for 0.75% CMMFF, 1% CMMFF, 1.5% CMMFF and 2% CMMFF it was 315, 390, 582 and 695 MPa,

respectively. Similarly, above 30 °C, storage modulus value enhanced, which continues up to temperature of 100 and finally drops down at 250 °C. Tsukada *et al.* [167] also observed that storage modulus of tussah silk fiber increases initially in the temperature range of 30 to 60 °C due to rearrangement of molecules in amorphous region during heating process that increases the interchain interaction. Similar trend has also been reported for mulberry silk fibroin [168].
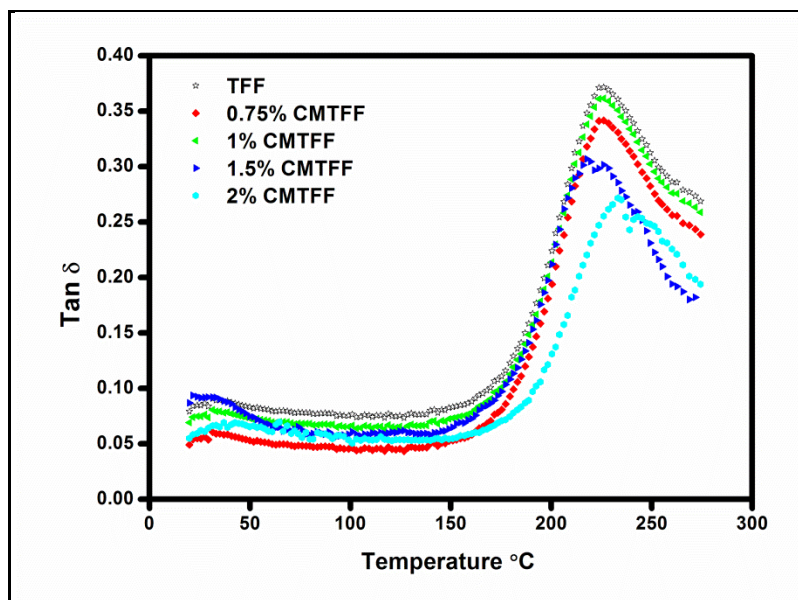
Figure 4.9: Tan δ curves for: TFF, 0.75% CMTFF, 1% CMTFF, 1.5% CMTFF and 2% CMTFF

Figure 4.9 & 4.10, show the temperature dependence of tan δ values of TFF, MFF, CMMFF and CMTFF. Tan δ curves for all the samples show a little change up to 175 °C, where the tan δ peak appeared and reached a maximum. The tan δ peak for TFF sample appeared at 226 °C, which is related to the molecular motion in the amorphous region, is designated as α-relaxation of fibroin chains. The α-relaxation peak does not affect due to chitosan treatment up to 1.5%. As it is clear from the Figure 4.9, for 2% CMTFF samples, tan δ peak shifted to higher temperature and

appeared at 245 °C, which can be attributed to strong inter- and intra-molecular hydrogen bonding interaction between the fibroin and chitosan that restricted the molecular motion of tasar fibroin molecules [169]. A small shoulder at 217 and 234 °C also appeared for 1.5% CMTFF and 2% CMTFF, which might be due to local molecular motion in pseudostable state [125].
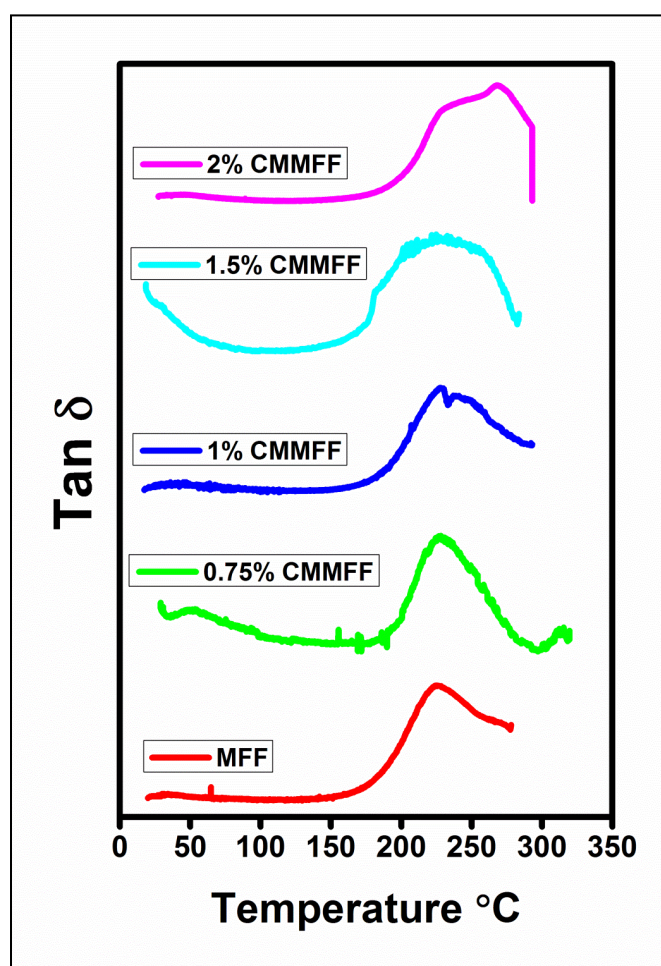
Figure 4.10: Tan δ curves for: MFF, 0.75% CMMFF, 1% CMMFF, 1.5% CMMFF and 2% CMMFF

Figure 4.10, shows the tan δ curve of different samples as a function of temperature. The tan δ peaks (α-relaxation) appear to begin at a temperature of 175 °C and reached maximum at 225 °C for MFF while it was 226, 228, 232 and 269 °C for 0.75

CMMFF, 1% CMMFF, 1.5% CMMFF and 2% CMMFF, respectively. The shifting of glass transition temperature to higher range is due to restricted molecular motion of fibroin chains caused by strong inter and intra molecular secondary interaction between chitosan and fibroin.

4.3.5   Water Uptake

Water absorbing capacity is an important function of biomaterials used as wound dressing. Figure 4.11 shows the water uptake capacity of TFF and CMTFF. For each type of sample water uptake capacity increases with time and saturate within 360 h. After 36 h maximum water uptake capacity of TFF film is 80%, while it is 96, 110 and 115% for 0.75, 1 and 1.5% CMTFF, respectively. The water uptake capacity of 2% CMTFF film is significantly higher (122%) than TFF film ($p < 0.05$).
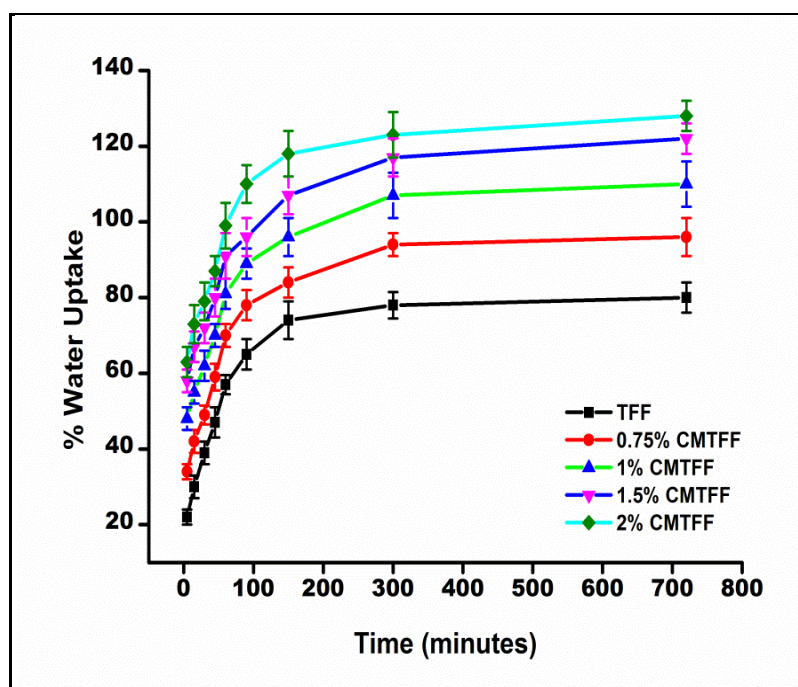
Figure 4.11: Water uptake capacity of TFF, 0.75% CMTFF, 1% CMTFF, 1.5% CMTFF and 2% CMTFF , Error bar represent mean±SD for n= 3
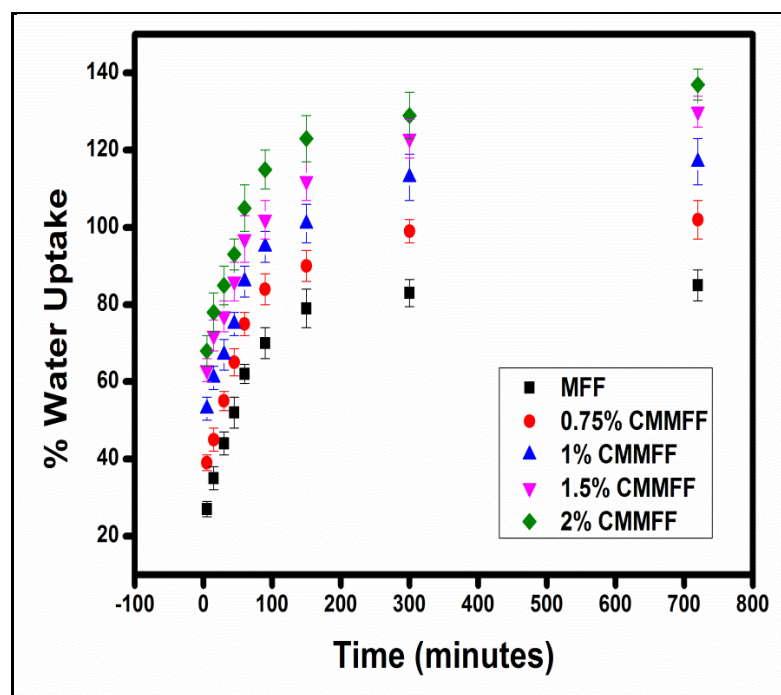
Figure 4.12: Water uptake capacity of MFF, 0.75% CMMFF, 1% CMMFF, 1.5% CMMFF and 2% CMMFF , Error bar represent mean±SD for n= 3

Water uptake capacity of MFF and CMMFF is shown in Figure 4.12. All types of sample were found to saturate after 360 h immersion in water. Water uptake ability of MFF was 85% which is slightly higher as compared to TFF may be due to high hydrophilic to hydrophobic amino acid ratio. After chitosan treatment water uptake tendency of muga nonwoven mats was increased. Maximum water uptake for 0.75% CMMFF, 1% CMMFF, 1.5% CMMFF and 2% CMMFF was 102, 117, 130 and 137%, respectively.

Water uptake capacity of TFF and MFF film is 80 and 85% which is comparable to muga nonwoven film (83%) prepared by Kasoju *et* al. [3] Silva et al. [127] have reported that for mulberry silk fibroin/chitosan water uptake capacity was 155%. On the basis of water absorption study, we can conclude that chitosan finished tasar fibrous films will absorb more exudates compared to unfinished films, so it could be a better biomaterial to be used as a wound dressing.

4.3.6 Porosity

Nonwoven structure always show porosity due to the interconnecting fiber architecture [79]. Highly porous tasar fibrous films are most advantageous for wound dressing applications, because porous architect of interconnected pores provides gas, water vapor and nutrient exchange, which are very crucial for cellular growth and wound healing [170,171].

Table 4.1: Change in weight, thickness and extent of porosity of tasar nonwoven films after finishing with chitosan

Samples	Conc. of chitosan solution used for finishing (% w/v)	% increase in weight after chitosan finishing	Thickness of the films (µm)	WVTR (g/m^2/day)	Porosity (%)	
TFF	-	-	500	2800±30	80±3	
0.75% CMTFF	0.75	10	550	2600±41	79±2	
1% CMTFF	1	15	600	2350±37	75±4	
1.5% CMTFF	1.5	25	700	2180±35	68±3	
2% CMTFF	2	30	750	1870±32	65±2.5	
Normal Skin	-	-	-	204	-	[172]
First Degree Wound	-	-	-	278	-	[172]
Second Degree Wound	-	-	-	4274	-	[172]
Third Degree Wound	-	-	-	3436	-	[172]
Granulating Wound	-	-	-	5138	-	[172]
Donor site	-	-	-	3590	-	[172]
Bilayer Chitosan	-	-	250-800	1187-1230	-	[86]
Bombyx mori Silk fibroin film	-	-	30-80	1900-2100	-	[173]

Table 4.1 shows the porosity of TFF and CMTFF. The porosity of TFF is 80%, while for 0.75, 1, 1.5 and 2% CMTFF the value of porosity is 79, 75 and 71%, respectively.

Table 4.2 shows the porosity of muga nonwoven (MFF) and different chitosan finished muga nonwoven mat (CMMFF). The apparent porosity of MFF was 75%, while it was 72, 68, 63 and 60% for 0.75%, 1%, 1.5% and 2% CMMFF, respectively.

After chitosan modification porosity was significantly reduced ($p < 0.05$). The values of porosity obtained for different films is favorable for effective transfer of water vapor, gas, nutrient and metabolic byproducts, which is one of the most essential requirement for effective wound dressing products [168]. Vasconcelos *et* al. [36] found that mulberry fibroin/elastin wound dressing with 70% porosity is favorable for dermal wound healing.

Table 4.2: Change in weight, thickness and extent of porosity of muga nonwoven films after finishing with chitosan

Sample Code	Concentration of chitosan solution used for finishing (% w/v)	% increase in weight after chitosan finishing	Thickness of the films (µm)	WVTR (g/m^2/day)	Porosity (%)
MFF	-	-	500	2850±30	82±3
0.75% CMMFF	0.75	12	550	2640±41	80±2
1% CMMFF	1	18	600	2390±37	76±4
1.5% CMMFF	1.5	27	700	2225±35	69±3
2% CMMFF	2	32	750	1885±32	67±2.5

4.3.7 Water vapor transmission rate

Water vapor permeability of wound dressing plays an important role to prevent dehydration and inhibiting infection at wound site. A good wound dressing should control evaporative water loss from wound at optimal rate. The WVTR results of the chitosan finished and unfinished dressing under static condition are shown in Table 4.1 and Table 4.2. The WVTR for TFF films is 2800 g/m^2/day, which is significantly reduced to 2600 g/m^2/day for 0.75% CMTFF, 2300 g/m^2/day for 1% CMTFF, 2180 g/m^2/day for 1.5%

CMTFF and 1870 g/m^2/day for 2% CMTFF. The WVTR for MFF film is 2700 g/m^2/day, which was reduced to the value of 2500, 2300, 2100 and 1800 g/m^2/day for 0.75%, 1%, 1.5% and 2% CMMFF, respectively. The WVTR value of tasar and muga nonwoven films shifted to lower side as chitosan content increased due to the fact that chitosan fills up the pores and causes wetting and gluing of fibroin fibers which results in reduced porosity. The WVTR values of different wound dressing are also shown in Table 4.1 and Table 4.2. Lamke *et* al. [172] have found that WVTR for normal skin is 204 g/m^2/day, while that for injured skin can range from 278 g/m^2/day for first degree wound, 4274 for second degree wound and 3436 g/m^2/day for third degree wound. Granulating wound has the highest evaporative water loss (20 times that of normal skin). The water vapor permeability of wound dressing should prevent both excessive dehydration as well as build-up of exudates. In our case the WVTR ranges from 2800 to 1870 g/m^2/day for tasar wound dressing while it ranges from 2700 to 1800 g/m^2/day for muga wound dressings. The WVTR data obtained for chitosan modified nonwoven tasar fibrous films are comparable to bilayer chitosan and *Bombyx mori* silk fibroin based wound dressing materials reported earlier [86,173].

Based on structural, mechanical, morphological, water uptake and water vapor transmission property, it was observed 2% chitosan modified tasar and muga films have better properties than their corresponding unmodified films. Therefore the biological properties were tested only on unmodified and 2% modified films.

4.3.8 Biological Properties

4.3.8.1 Platelets Attachment

Surface initiation of materials play a key role for different reactions between biological moieties [174]. Attachment of platelets once in contact with different TFF and CMTFF was investigated and are presented in Figure 4.13.
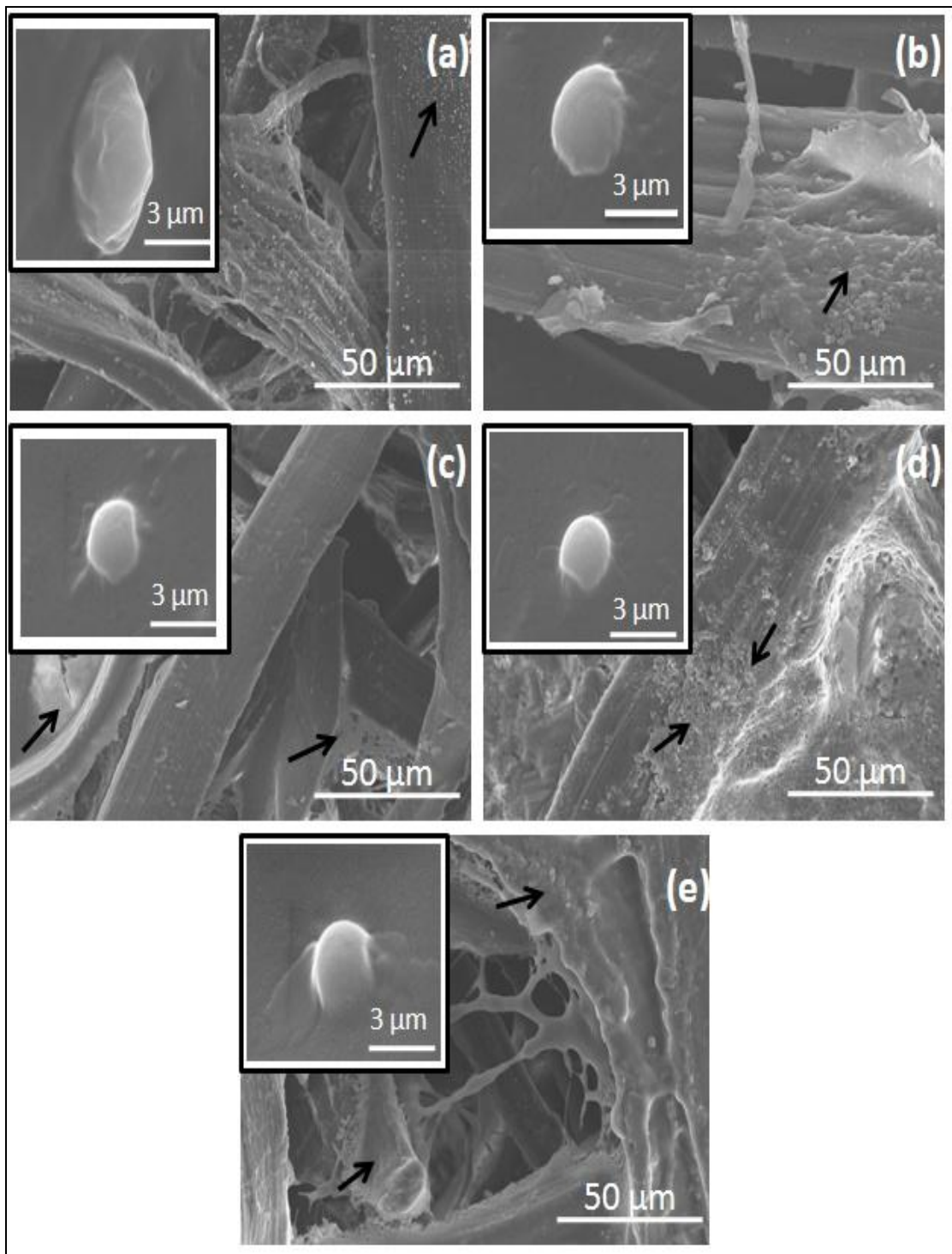
Figure 4.13: SEM images of platelet attachment to (a) TFF, (b) 0.75% CMTFF, (c) 1% CMTFF, (d) 1.5% CMTFF and (e) 2% CMTFF, arrow indicating platelets attached to films
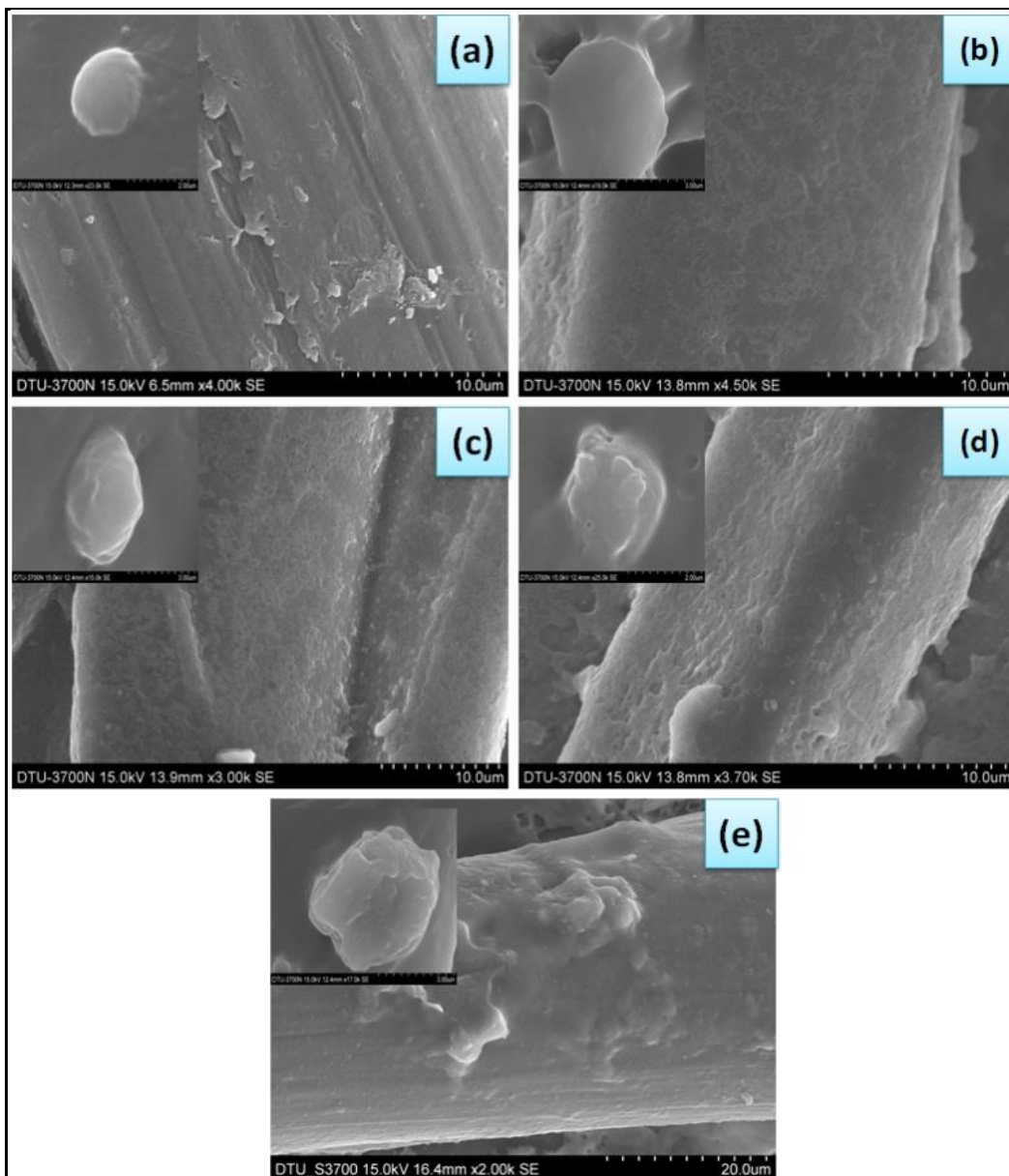
Figure 4.14: SEM images of platelet attachment to (a) MFF, (b) 0.75% CMMFF, (c) 1% CMMFF, (d) 1.5% CMMFF and (e) 2% CMMFF, arrow indicating platelets attached to films

The platelets adhesion increases with an increase in concentration of chitosan and gets deposited as a monolayer on 2% CMTFF. Attachment of platelets to the surface of MFF and CMMFF is shown in Figure 4.14. Only few platelets are attached at the surface of MFF while after chitosan finishing platelets adherence increases. Both chitosan finished muga and tasar nonwoven films show higher platelet adherence compared to unmodified

films, but there was no significant difference between muga and tasar modified and unmodified films. Blood proteins first absorbed on the surface of wound dressing, which results in platelets activation that triggers platelets aggregation [175]. The polycationic nature of chitosan is responsible for its nonspecific binding to cell membrane, especially with erythrocytes and platelets, which induces thrombosis. Tasar wound dressing films show little platelets attachment, chitosan modified tasar wound dressing binds more platelets and therefore acts as haemostatic, which may be a promising material for wound dressing applications.

4.3.8.2 Hemolysis Assay

Hemolysis is considered to be a very simple and reliable measure of estimating blood compatibility of materials. TFF and CMTFF were incubated with RBCs and effects on erythrocyte hemolysis were observed. The percentages of hemolysis are 0.15 ± 0.04, 0.23 ± 0.02, 0.34 ± 0.01, 0.45 ± 0.02 and 0.92 ± 0.04 for TFF, 0.75%, CMTFF, 1% CMTFF, 1.5% CMTFF and 2% CMTFF, respectively. Hemolytic activity of MFF and CMMFF was also analyzed. The percentages of hemolysis are 0.13 ± 0.09, 0.20 ± 0.02, and 0.31 ± 0.02, 0.40 ± 0.03 and 0.88 ± 0.03 for MFF, 0.75% CMMFF, 1% CMMFF, 1.5% CMMFF and 2% CMMFF, respectively. Muga and chitosan finished muga nonwoven mats are found to be less hemolytic as compared to tasar and chitosan finished tasar nonwoven mats. However, chitosan finished films have higher hemolytic value as compared to unfinished films. This may be due to the fact that chitosan is slight hemolytic in nature because of the presence of amino groups on the surface. When the chitosan comes in contact with blood, the electrostatic attraction between chitosan surface and erythrocyte membrane containing anionic glycoproteins induces curvature off erythrocyte membrane, ultimately leading to rupture and release of hemoglobin [176].

4.3.8.3 Cell adherence, spreading and viability of tasar nonwoven film and chitosan modified tasar nonwoven film

The viability of L929 fibroblast cells are measured by MTT assay as a function of culture time and types of films. The formazan absorbance value was calculated as number of viable cells as shown in Figure 4.15(a). It was observed that the absorbance values increased with increase in chitosan concentration over 5 days of *in vitro* culture ($p < 0.05$). Based on MTT assay, it was observed that viability of cells on 2% CMTFF was more and close to tissue culture plate (TCP); therefore other cytocompatibility tests were carried out only on TFF and 2% CMTFF.
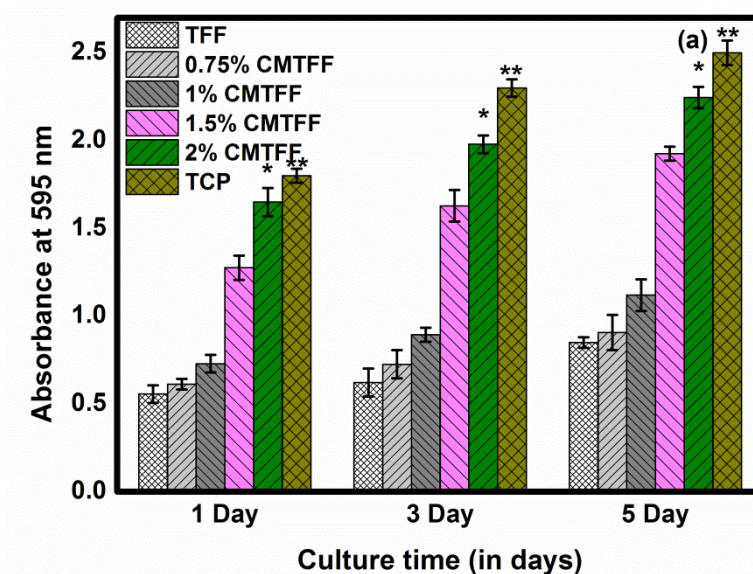
Figure 4.15(a): MTT assay of L929 fibroblast cell seeded on different TFF and CMTFF scaffolds, Data represent Mean±SD, n=3, *p<0.05; significant against the TFF, **p>0.05; insignificant against TCP

The adherence and spreading of L929 cells cultured on different TFF and 2% CMTFF scaffolds were monitored at 1, 3 and 5 days after seeding. Figure 4.15(b) shows the morphology and distribution of L929 cells on TFF and 2% CMTFF scaffolds after being cultivated for 1, 3 and 5 days. Cell spreading is highly dependent on surface properties of the silk fibroin films. SEM revealed that adherence and spreading of

L929 cells on 2% CMTFF is higher as compared to TFF scaffolds ($p < 0.05$) after 1 day of incubation. In contrast, cells seeded on TFF exhibited granular morphology of cells over 1 day culture period. After 3 days of culture, L929 cells spreads well on TFF scaffolds, but were unable to cover entire surface of TFF scaffolds over 5 days of culture. After 5 days of incubation, cell monolayer was formed that completely covered the surface of 2% CMTFF scaffold, indicating very good biocompatibility.
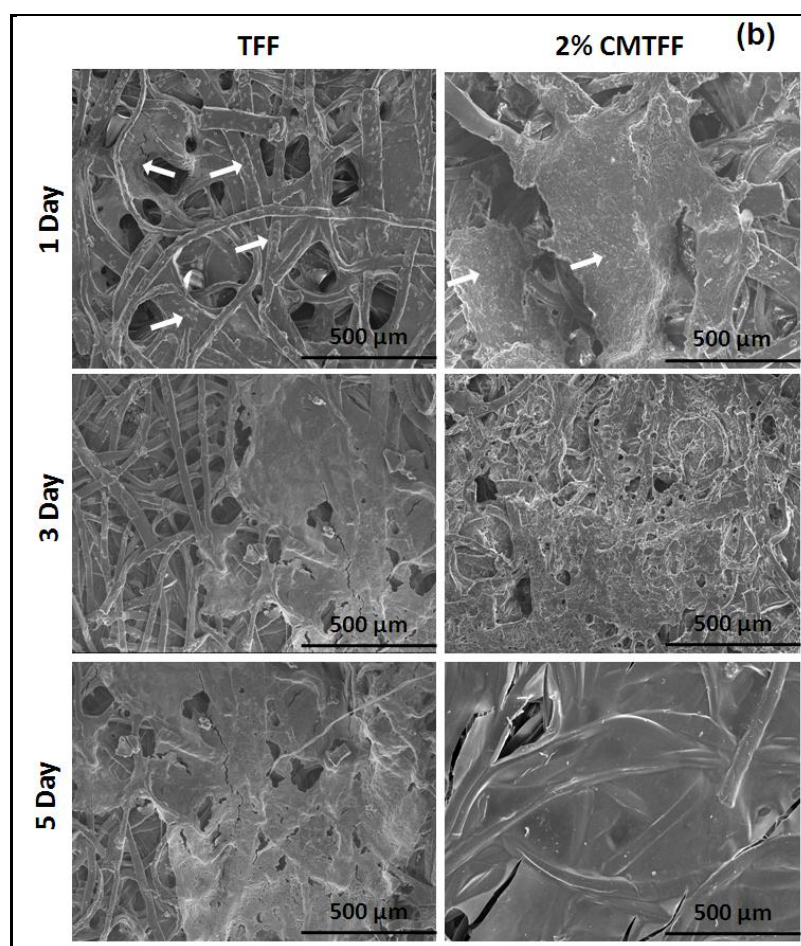
Figure 4.15(b): **SEM images of L929 cell seeded on TFF and 2% CMTFF films over 1, 3 and 5 days of incubation**

Fluorescence microscopy of DAPI stained L929 cells nuclei gave a good measure of cell spreading as a function of time [75]. Figure 4.15(c) shows DAPI stained L929 cells proliferation seeded on TFF and 2% CMTFF films over the time. It is observed

that nuclei density increases with time for both TFF and 2% CMTFF films, but 2% CMTFF showed significantly higher rate of proliferation as compared to TFF films ($p < 0.05$). The L929 fibroblast cells adhered and proliferated well on these chitosan finished nonwoven tasar films.
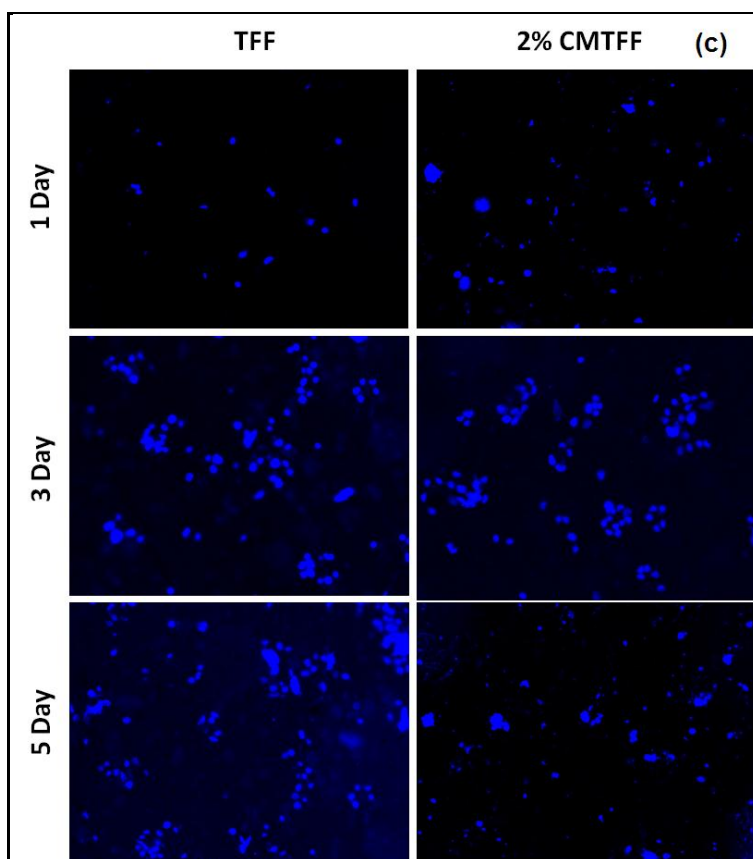
Figure 4.15(c): Fluorescence microscopy of DAPI stained nuclei of L929 cells seeded on TFF and CMTFF films over 1, 3 and 5 days of incubation

The viability of L929 fibroblast cells seeded on MFF and CMMFF was also measured by MTT assay (Figure 4.16b). It is observed that number of cells increased with time for all types of sample but it was higher in case of chitosan finished samples. We also found that number of cells increased with an increase in the concentration of chitosan and cell number was highest after 5 days of incubation ($p < 0.05$) (Figure 4.16a). Based on MTT assay, we found that viability of L929 cells on 2% CMMFF is higher than

MFF but not significantly higher than that of 2% CMTFF and were found to be close to tissue culture plate (TCP); therefore other cytocompatibility tests were carried out only on MFF and 2% CMMFF.
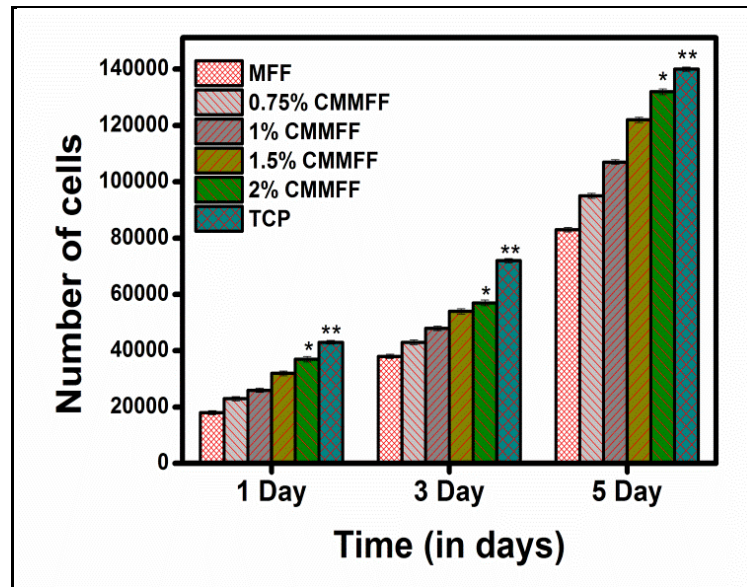
Figure 4.16(a): Number of cells over time for estimation of L929 fibroblast cell viability seeded on MFF and CMMFF films, Data represent Mean±SD, n=3, *p<0.05; significant against the MFF, **p>0.05; insignificant against TCP
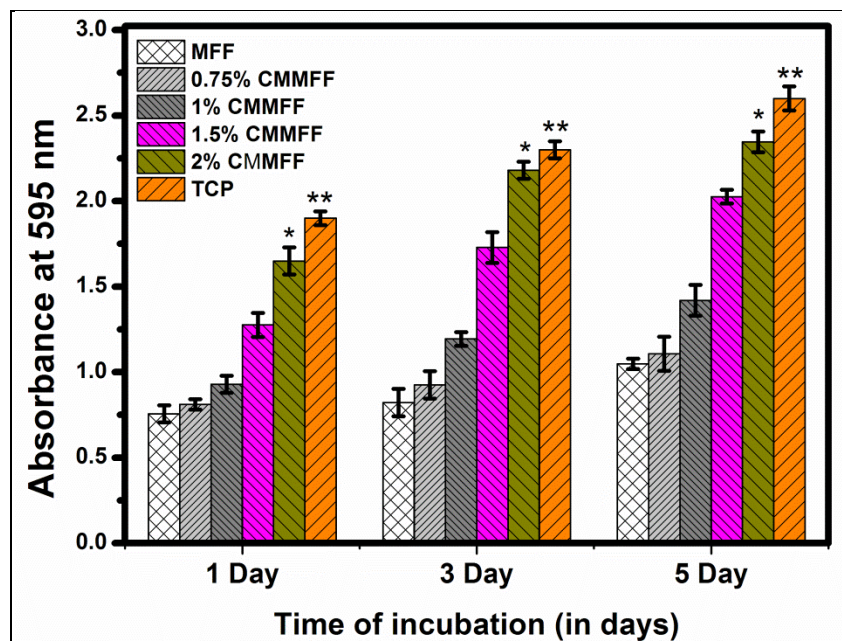
Figure 4.16(b): MTT assay of L929 fibroblast cell seeded on MFF and CMMFF films, Data represent Mean±SD, n=3, *p<0.05; significant against the MFF, **p>0.05; insignificant against TCP

4.3.8.4 Cell adherence, spreading and viability of muga nonwoven and chitosan modified muga nonwoven films

Adherence, proliferation and spreading of L929 fibroblast cells seeded on different MFF and 2% CMMFF scaffolds were determined after 1, 3 and 5 days of incubation. Figure 4.16(c) clearly depicted the morphology and spreading of L929 fibroblast cells seeded on MFF and 2% CMMFF after 1, 3 and 5 days of incubation. It is evident from SEM images that L929 cells adhered well on both MFF and 2% CMMFF after 1 day of incubation. The adherence and proliferation of L929 cells on 2% CMMFF was significantly higher ($p < 0.05$) than that for MFF over 5 days of incubation. After 5 days incubation, L929 cells formed monolayer and completely covered the surface of the 2% CMMFF but in the case of MFF scaffolds surface was not completely covered after 5 days of incubation. This higher adherence and proliferation of L929 cells on the chitosan finished tasar and muga nonwoven mats indicates good biocompatibility of these materials that would results in successful development of ideal tissue construct for skin tissue engineering and regeneration of damaged skin.

Chitosan promoting cell growth and proliferation and tasar nonwoven interconnected network providing enough space for fibroblast migration and growth for the favorable stable environment for cell adhesion and migration which will promote formation of dermal substitute for skin regeneration and wound healing. The higher adherence, spreading and proliferation of cells on tasar silk fibroin films may be due to the presence of tripeptide Arg(R)-Gly(G)-Asp(D) in tasar silk fibroin, which is recognition site for integrin-mediated cell adhesion. One possible reason is that with chitosan treatment, hydrophilicity of scaffolds increases which promotes cell

attachment on scaffolds [75]. In addition of RGD peptide of tasar fibroin and increase hydrophilicity of chitosan, cationic nature of chitosan, onto which a negatively charged cell membrane can adhere by electrostatic forces; consequently, spread more on the surface. Although the cell attachment on the surfaces of 2% CMTFF film is very important for cell growth and proliferation, which makes it a better substrate for wound dressing and skin regeneration applications.
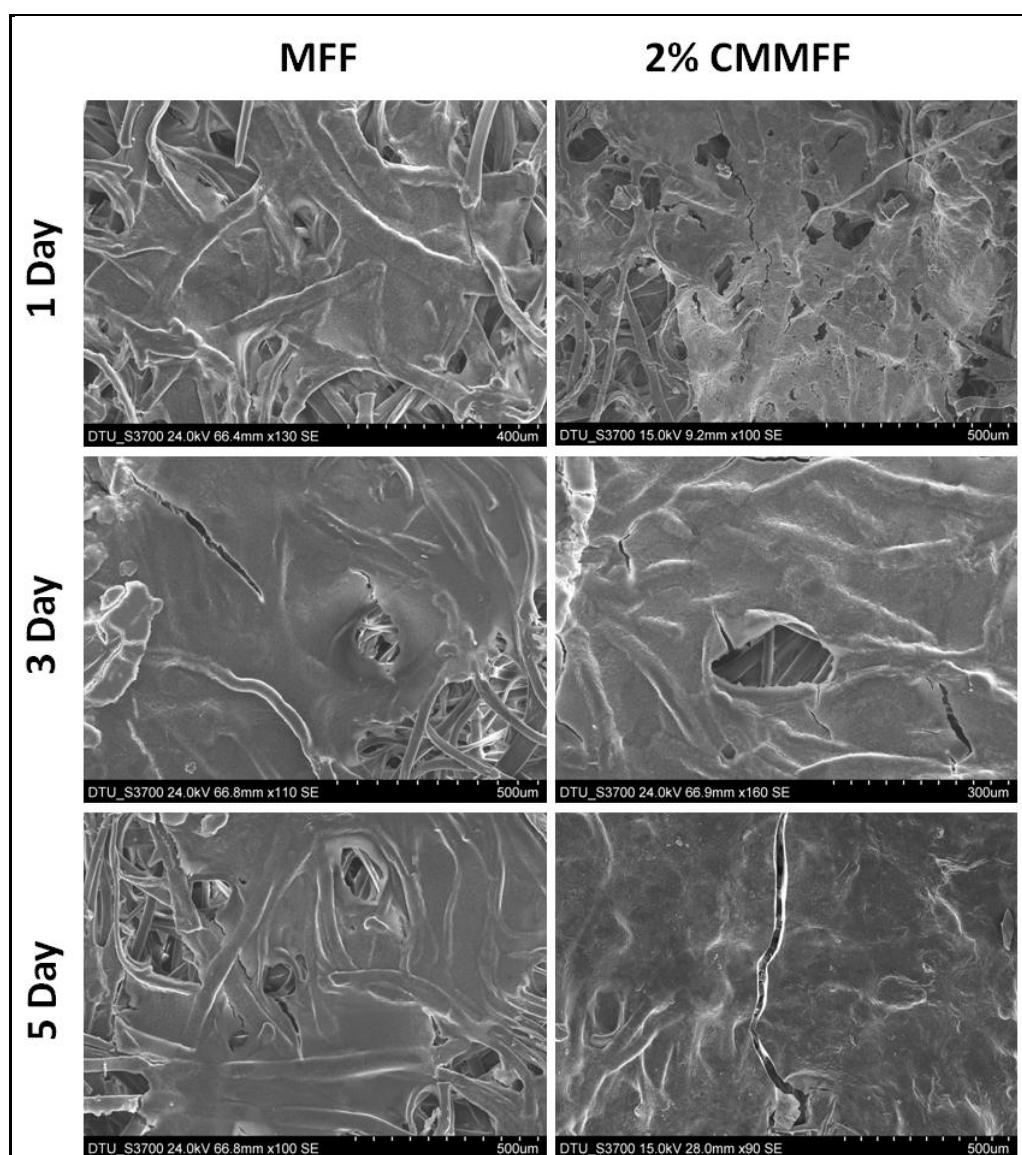
Figure 4.16(c):   SEM images of L929 cell seeded on MFF and 2% CMMFF films over 1, 3 and 5 days of incubation

4.3.9 *In vitro* biodegradation test

In vitro biodegradation of different films was investigated by monitoring the weight remained after respective time period during incubation in PBS and in presence of protease XIV. Protease XIV based enzymatic degradation assay was used on the basis of prior studies reported in literature [177]. The TFF and CMTFF samples kept in phosphate buffered saline without protease enzyme showed little degradation after 15 weeks and mass loss was 2% for TFF film and 8% for 2% CMTFF film. MFF and 2% CMMFF incubated in phosphate saline buffer shows same amount of biodegradation i.e. 2 for MFF and 9% for 2% CMMFF after 15 weeks of incubation. Figure 4.17 shows that on incubation with proteases, TFF and 0.75-2% CMTFF films showed predictable degradation patterns over a period of 15 weeks. Proteolytic degradation of TFF was significant (Figure 4.17) with a residual mass of about 52% after 15 week. Biodegradation of 0.75, 1 and 1.5% CMTFF films was comparable to TFF films with mass remaining % of 49, 46 and 47, respectively after 15 weeks of incubation. Similarly after 15 weeks 2% CMTFF films show residual weight of 44% (Figure 4.17), which is significantly higher compared to TFF film ($p > 0.05$). Figure 4.18 shows protease mediated *in vitro* biodegradation of MFF and 0.75%-2% CMMFF. Protease mediated biodegradation of MFF was significantly higher with residual mass of 48% as compared to control PBS without enzyme (2%) after 15 weeks of degradation. The residual mass of 0.75%, 1% and 1.5% CMMFF was 45, 44 and 43% after 15 weeks of enzymatic biodegradation. The enzymatic biodegradation of 2% CMMFF was significantly higher ($p > 0.05$) having residual mass of 41% which is

close to the value obtained for 2% CMTFF (44%). The higher degradation for 2% CMTFF and 2% CMMFF may be due to higher absorption of water which facilitated penetration of enzyme in tasar and muga fibroin fibers. Statistical analysis showed that biodegradation rate for all type of samples was significantly higher ($p > 0.05$) after 15 weeks of incubation. In PBS solution alone, which was tested for determination of non-enzymatic weight loss, TFF and MFF as well as CMMFF and CMTFF films did not indicate a significant weight loss ($p > 0.05$).

Figure 4.19 shows SEM images of TFF and CMTFF before and after 15 weeks of enzymatic degradation. It is evident from SEM images that the surface of TFF, 0.75 and 1% CMTFF was smooth before degradation. SEM images shows that surface of 1.5 and 2% CMTFF was slightly rough due to deposition of higher amount of chitosan. SEM images showed etched structure for all the degraded films. Effective mass removal was noticed after 15 weeks enzymatic treatment in all types of films. Figure 4.20 shows SEM images of MFF and CMMFF before and after 15 weeks of *in vitro* biodegradation. It is clearly depicted from the micrographs that surface of MFF before enzymatic degradation was smooth but MFF, 0.75% 1 and 1.5% showed significantly higher biodegradation and have highly eroded surface after 15 weeks of enzymatic degradation. The highest enzymatic erosion was found in the case of 2% CMMFF. Jin *et al.* [178] have studied protease based degradation of low molecular weight chitosan. These results indicated the possibility of using the CMTFF and CMMFF films as ideal wound dressing material to ensure that the films would not be completely degraded during the healing of wound.
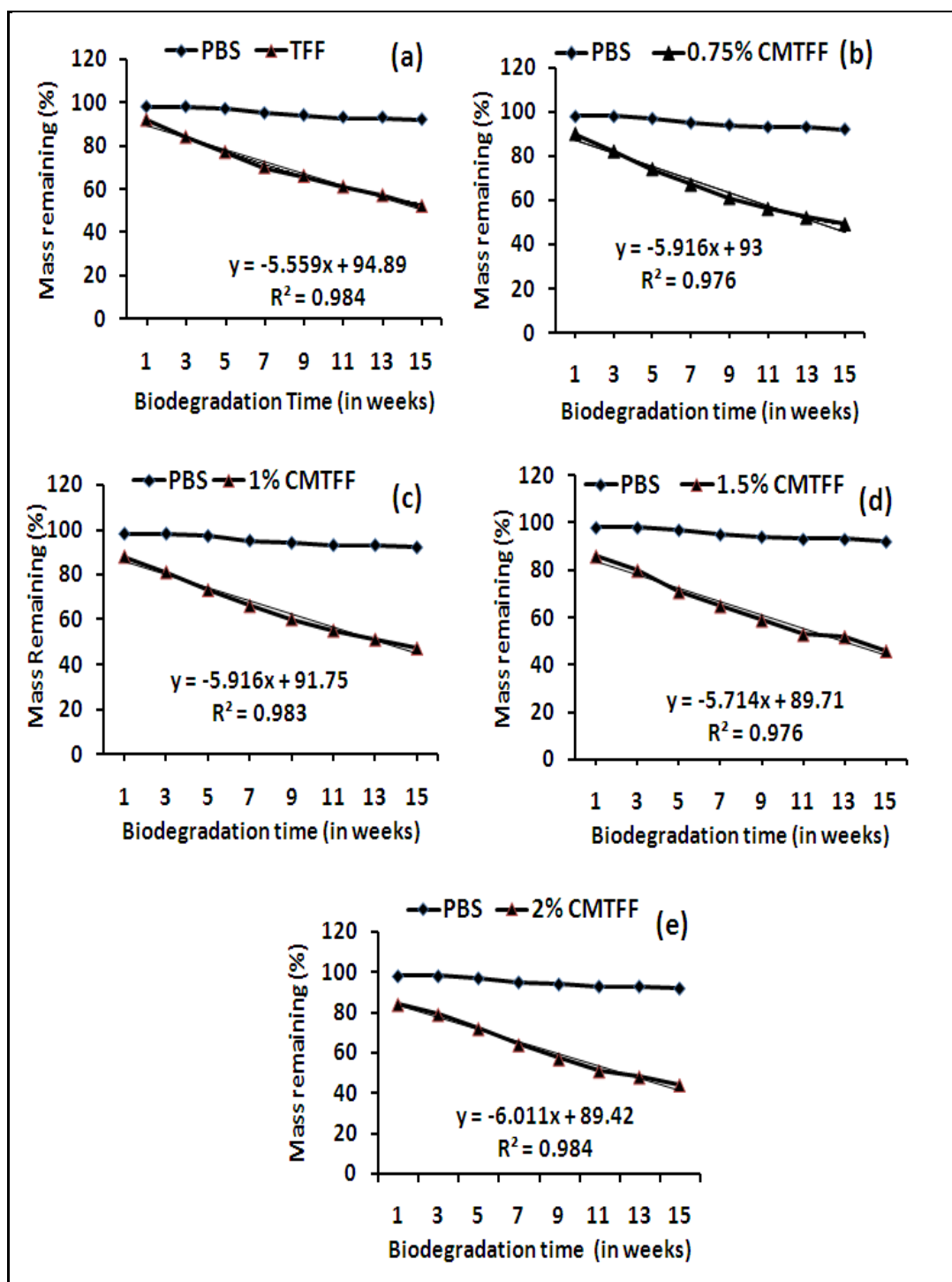
Figure 4.17: *In vitro* **protease XIV mediated biodegradation of: (a) TFF, (b) 0.75% CMTFF, (c) 1% CMTFF, (d) 1.5% CMTFF and (e) 2% CMTFF films**
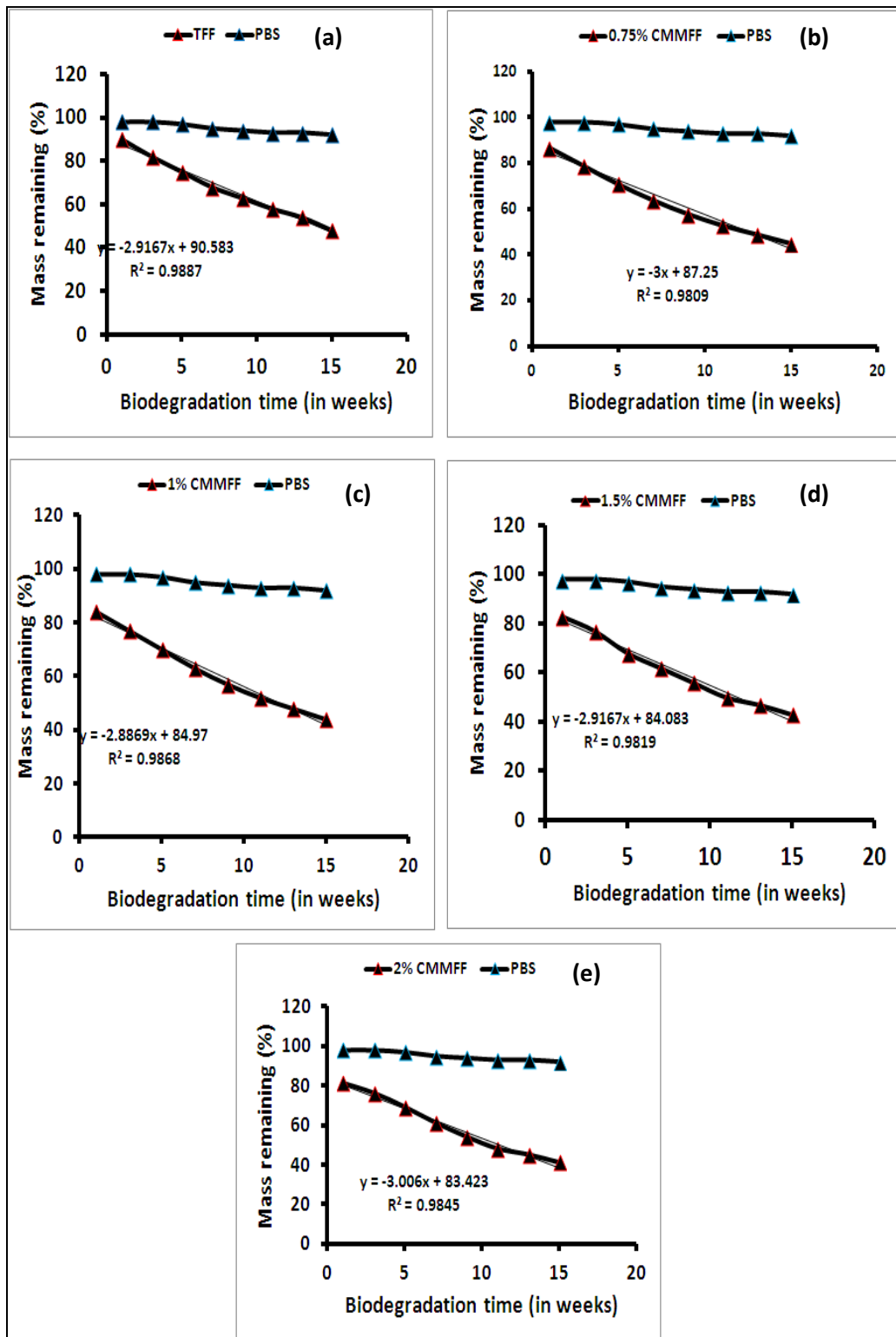
Figure 4.18: *In vitro* **protease XIV mediated biodegradation of: (a) MFF, (b) 0.75% CMMFF, (c) 1% CMMFF, (d) 1.5% CMMFF and (e) 2% CMMFF films**
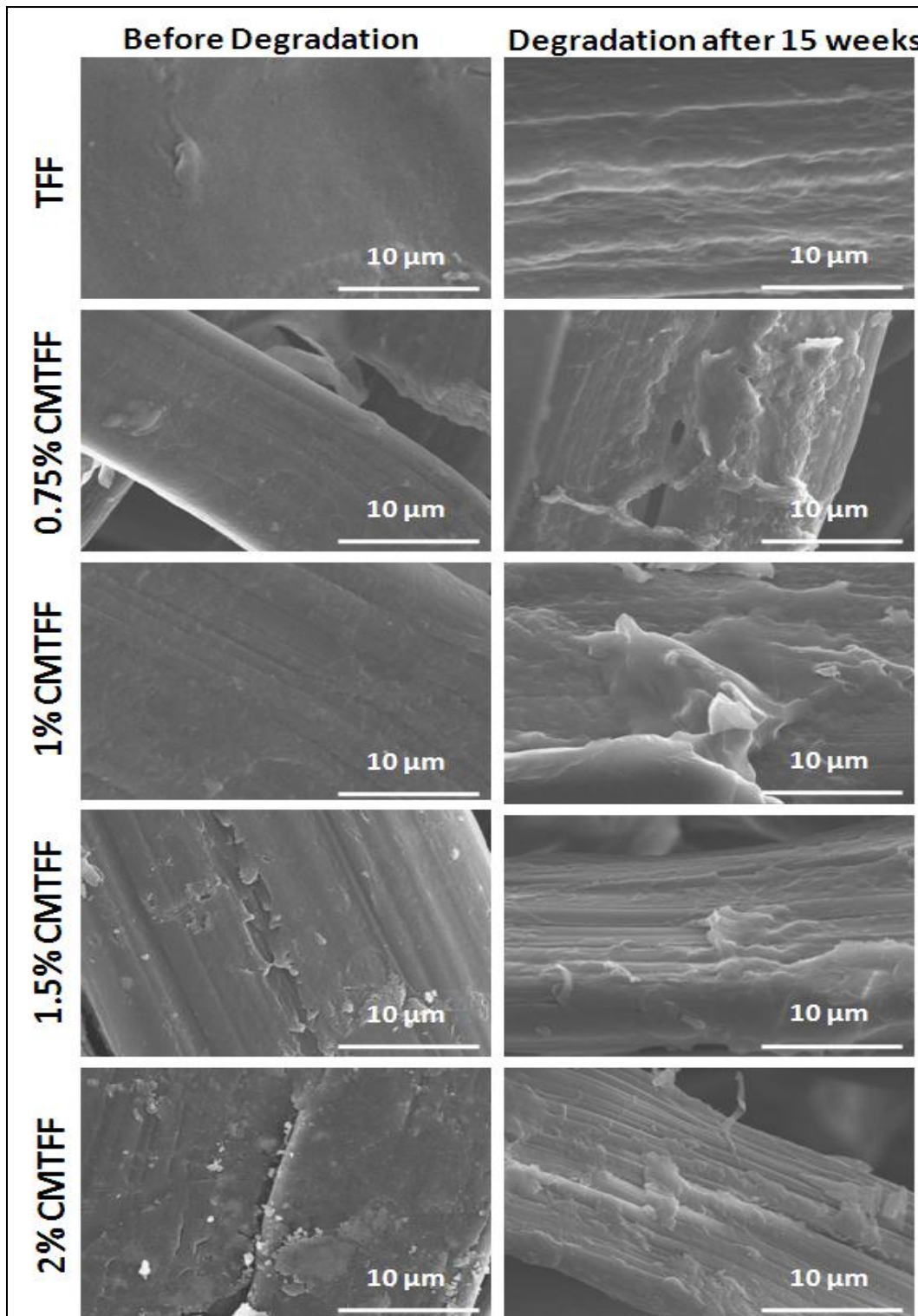
Figure 4.19: **SEM images of TFF, 0.75% CMTFF, 1% CMTFF, 1.5% CMTFF and 2% CMTFF films before and after *in vitro* biodegradation**
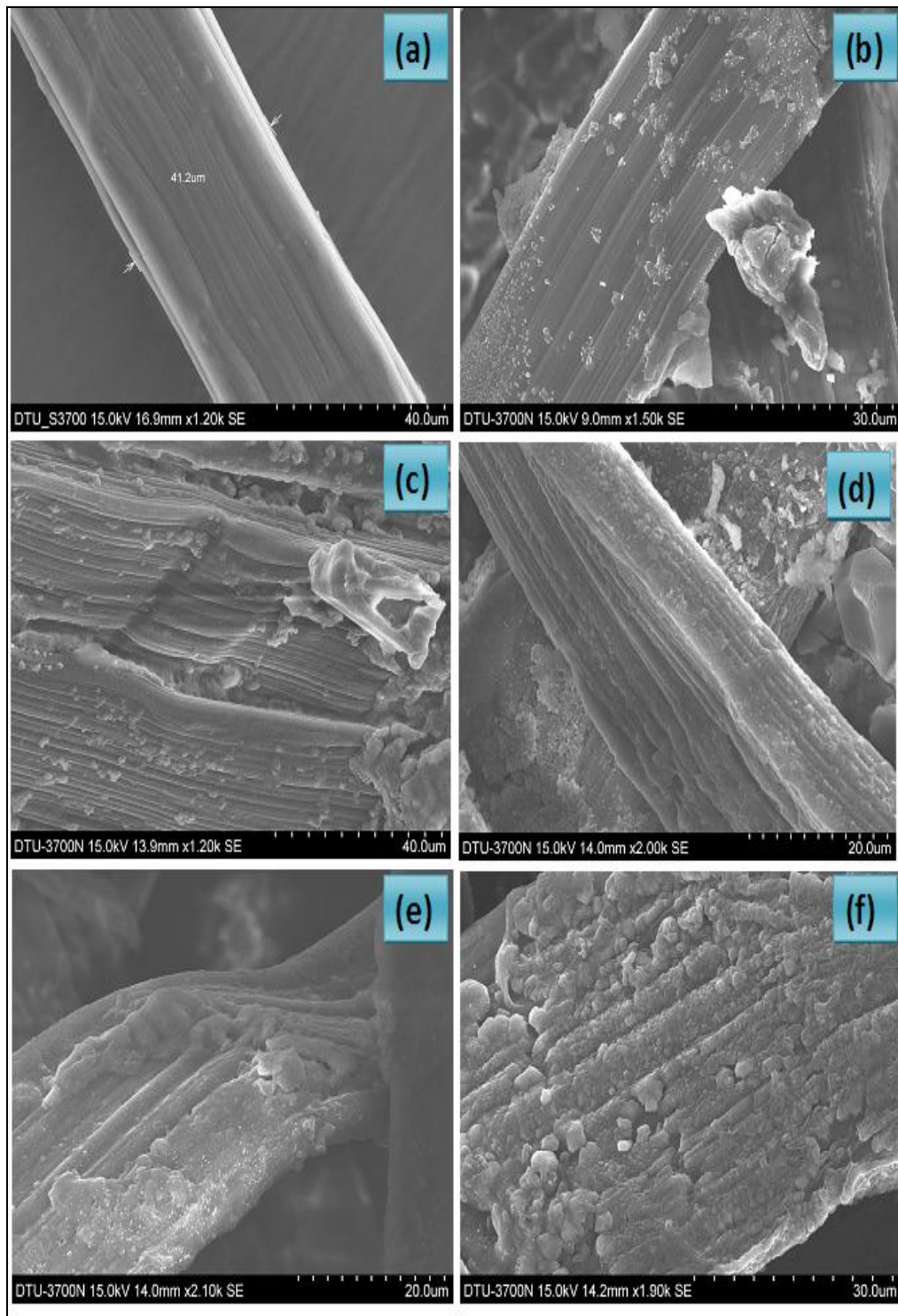
Figure 4.20: **SEM images of (a) MFF (incubated in PBS only), (b) MFF, (c) 0.75% CMMFF, (d) 1% CMMFF, (e) 1.5% CMMFF and (f) 2% CMMFF films after *in vitro* biodegradation**

4.3.10 Antimicrobial Activity

Antimicrobial activity is one of the most essential requirements of ideal wound dressing. The antimicrobial activity of chitosan is well known. The most acceptable model related to antimicrobial action of chitosan is the interaction between positively charged chitosan molecules and negatively charged microbial cell membranes. In this model the interaction is mediated by the electrostatic forces between the protonated NH_3^+ groups and the negative residues [179], presumably by competing with Ca^{2+} for electronegative sites on the membrane surface [180]. It is pertinent to note that due to insolubility of chitosan in water, absence of inhibition zone has been observed in agar disc diffusion assay [181]. In order to get best antimicrobial activity of chitosan, our wound dressing requires activation causing protonation of amine groups by acetic acid (AA). Therefore in present study, for the enhancement of the antimicrobial activity of CMTFF and CMMFF were dipped in the 1% (v/v) acetic acid aqueous solution for 5 min before placing on the agar plate. The disc diffusion assay showed that TFF film has no activity against gram −ve and gram +ve bacteria, but AA impregnated TFF showed antimicrobial action against both gram positive (9 mm) and gram negative (8 mm) bacteria (Figure 4.21a). Similarly MFF shows no zone of inhibition but acetic acid impregnated MFF exhibited prominent zone of inhibition against both gram +ve bacteria (*S. aureus*) (10 mm) and gram −ve bacteria (*E. coli*) (9 mm) (Figure 4.21b). Acetic acid has been used as sterilizing agents in food industry [182]. Antimicrobial activity of chitosan finished tasar film against gram +ve bacteria (*S. aureus*) and gram −ve bacteria (*E. coli*) were determined by disc diffusion assay. It is clear that AA activated chitosan modified nonwoven films are effective against both gram −ve and gram +ve bacteria and antimicrobial activity becomes more prominent as the concentration of chitosan increases. In this study 2% CMTFF and 2%

CMMFF films show strong antimicrobial activity having values of 21 mm and 22 mm against gram +ve and 25 and 27 mm against gram −ve bacteria, respectively. It is evident from the data that antimicrobial activity of chitosan finished films are significantly higher (p<0.05) for gram −ve bacteria as compared to gram +ve bacteria. Chung *et* al. [183] have found that strong −ve charge on the surface of gram −ve bacteria as compared to gram +ve bacteria, which causes higher amount of chitosan to absorb & a high inhibition effect against the gram −ve bacteria with minimum inhibition concentration value of 288 ppm for both strains. The higher antimicrobial activity of chitosan finished tasar nonwoven fibroin is due to the combined effect of acetic acid and chitosan. Moreover, in presence of very small amount of acetic acid low molecular weight chitosan fraction may swell and diffuse in agar which results in higher antimicrobial activity.
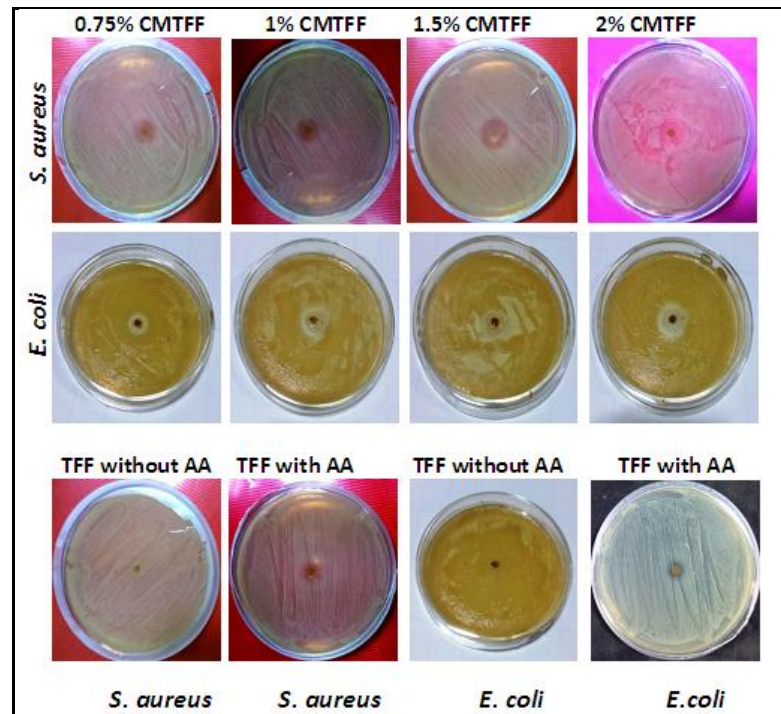
Figure 4.21(a): Disc diffusion assay of 1% (v/v) acetic acid solution treated TFF and CMTFF films against gram -ve and gram +ve bacteria
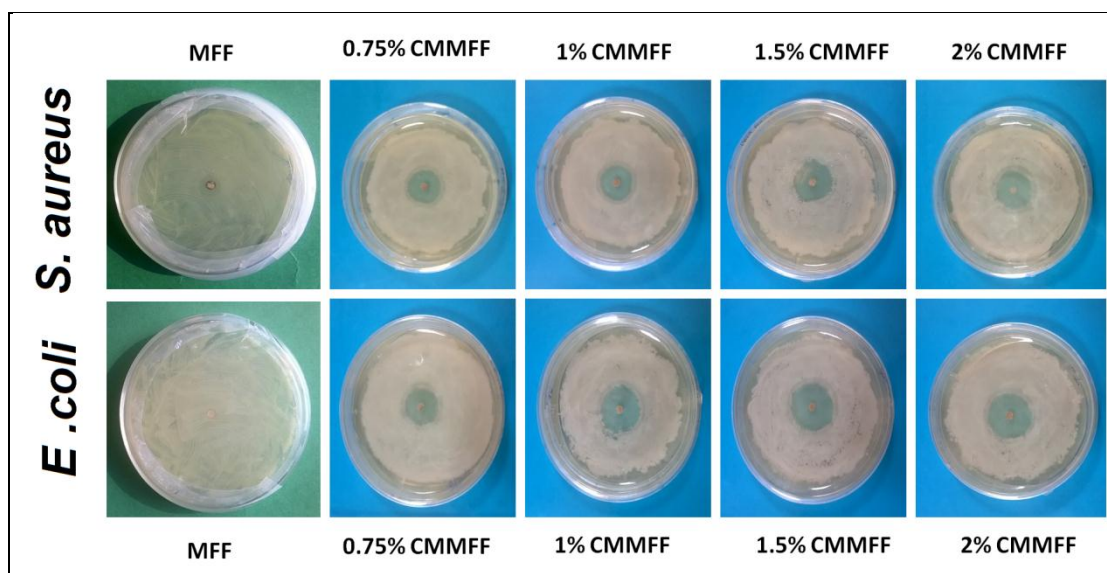
Figure 4.21(b): Disc diffusion assay of 1% (v/v) acetic acid solution treated MFF and CMMFF films against gram -ve and gram +ve bacteria

4.4 Conclusions

In this chapter chitosan finished nonwoven tasar and muga films are characterized and compared with their corresponding non-modified films. The observed results of chitosan finished nonwoven tasar and muga fibroin composite films show sufficient porosity, water vapor permeability, with adequate mechanical properties and thermal properties. Tensile strength and modulus of TFF and MFF were significantly increased after chitosan treatment. The structural properties of TFF & MFF as well as different CMTFF & CMMFF films were investigated by FTIR and XRD, which demonstrate that crystalline structure of tasar and muga silk fibroin is not affected by chitosan modification. The physicochemical study of chitosan modified tasar and muga films shows that these have good porosity, WVTR and water absorption ability as compared to TFF and MFF. Low hemolysis and higher attachment of platelets to chitosan modified tasar and muga nonwoven films may be advantageous to be utilized

as ideal wound dressing. MTT assay showed that chitosan finishing further increased the cytocompatibility of tasar and muga nonwoven films. The results from scanning electron microscopy showed an improved cellular growth and favorable morphological feature of tasar and muga nonwoven films after modification with chitosan.

CHAPTER 5

FABRICATION OF NONMULBERRY SILK FIBROIN NANOFIBROUS MATS FOR WOUND DRESSING APPLICATIONS

Nanofibrous mats prepared through electrospinning process have been utilized as alternative to skin grafts such as allografts [83], autografts [32] and xenografts [84] due to their structural similarity to extracellular matrix (ECM). The electrospun scaffolds made of nanofibers with individual fiber diameter in submicron to nano range provides higher surface area, allowing the seeded cells to proliferate and produce their own ECM [85]. The antimicrobial agents can be incorporated to these electrospun mats. These functionalized mats would have potential to reduce the bacterial infection and power to accelerate skin tissue regeneration [184]. Electrospun mats possess a very high surface area and porosity, which promotes moisture retention, exudates absorption, tissue regeneration and hemostasis [86].

This chapter is divided in two sections. The first section of this chapter is focused on the preparation of regenerated muga cocoon fibroin nanofibrous mats by electrospinning. The second chapter is focused on the fabrication of tasar fibroin nanofibrous mats. In this study, we have utilized the ionic liquid for regeneration of muga and tasar nanofibrous mats. The different properties of these nanofibrous mats were evaluated to check efficacy of these materials for wound dressing and skin tissue engineering applications.

SECTION 5.1: FABRICATION OF MUGA FIBROIN NANOFIBROUS MATS

5.1.1   Introduction

Based on literature search it is found that very limited work has been carried out on muga silk fibroin extracted from cocoons. There is no work reported on regeneration of muga silk fibroin in the form of nanofibrous mat using ionic liquid. Further, cytocompatibility of regenerated muga silk fibroin materials is not evaluated, which is a promising material for skin tissue engineering.

This section of the chapter is focused on the preparation of regenerated muga fibroin nanofibrous mat (MNF) using electrospinning technique. Muga fibroin was dissolved in ionic liquid, 1-butyl-3-methylimidazolium acetate (BMIMAc). The solution of muga fibroin was characterized for its structural and rheological properties. The process parameters of electrospinning machines were optimized to prepare muga nanofibrous mat. The nanofibrous mats were characterized for physicochemical, structural, thermal, mechanical, morphological and biological properties. The nanofibrous mat was loaded with antibiotic drug and drug release profile was evaluated. These properties of muga nanofibrous mat were also compared with muga cast film.

5.1.2   Experimental

5.1.2.1 Preparation of dope solution

Dissolution of silk fibroin in the ionic liquid was performed according to the protocol reported earlier [123]. Briefly, degummed muga silk fibroin fibers were dissolved in ionic liquid (1-butyl-3-methylimidazolium acetate) at 95 ℃ in the concentrations ranging from 5, 7, and 10% (w/v) under nitrogen atmosphere. Muga silk fibroin fibers

dissolved completely in BMIMAc within 2h under nitrogen atmosphere on constant stirring. After dissolution, the solution is filtered through mesh.

5.1.2.2 Preparation of silk fibroin cast film

Muga fibroin-BMIMAc solution (10% w/v) was poured into polystyrene petriplates under laminar air flow to prepare a film of thickness (0.50 ±0.1 mm). After 2 h, methanol was added to each plate and was allowed to crystallize for 5 h. The ionic liquid was removed from film samples as reported by Silva *et* al. [116]. Briefly, aliquots were replaced with fresh methanol at an interval of 12 h to extract ionic liquid form muga fibroin cast films. Conductivity of aliquots was measured by Conductivity meter (Decibell Scientific Industrie-14671). Conductivity of BMIMAc is 1500 μS/cm, while it was only 4 μS/cm for methanol. Initially large amount of ionic liquid was extracted from film so conductivity of aliquot was found to be very high near to conductivity of BMIMAc, but with time as the aliquot was replaced with fresh methanol, amount of ionic liquid extracted became low and finally after 108 h it became equal to conductivity of pure methanol indicating there is no any trace of ionic liquid released in aliquot as shown in Figure 1. Ionic liquid recovered back after evaporation of methanol at 50 °C and 150 mb pressure by using rotary evaporator.

5.1.2.3 Preparation of muga silk fibroin nanofibous mats by electrospinning

Muga silk fibroin nano-fibrous mats were prepared by electrospinning machine (Royal Enterprises, India) using 10 mL syringe with a needle diameter of 0.55 mm. The spinning of muga silk fibroin was performed by varying the concentration of dope solution and spinning voltage, with a constant distance of 8 cm between tip to rotating drum (1000 rpm) and a flow rate of 0.5 mL/h. The fibrous mats were collected on aluminum foil

mounted on rotating drum collector, which is slightly submerged on methanol coagulating bath. Finally, a film deposited on aluminum foil having a thickness of 0.5 ±0.1 mm. The ionic liquid was extracted from nanofibrous mats by the same procedure followed above in cast film. The removal of ionic liquid from nanofibrous mats was checked by conductivity experiment as shown in Scheme III.
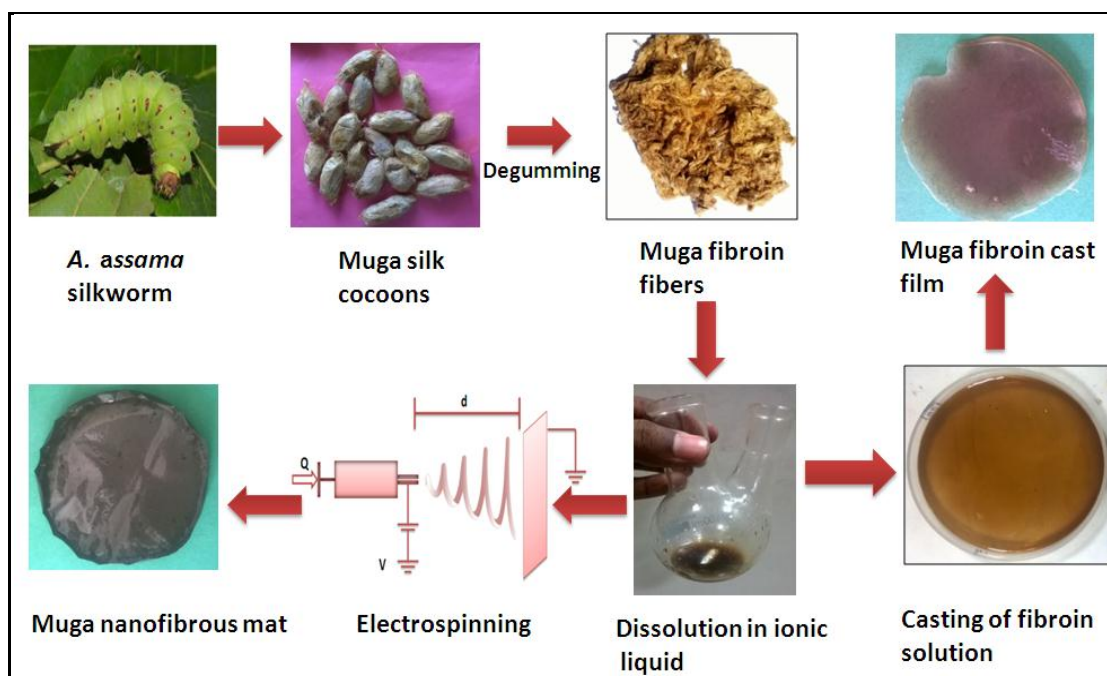
Scheme III: Schematic representation for preparation of muga nanofibrous mats using electrospinning

5.1.3 Results and discussion

5.1.3.1 Characterization of dope solution

5.1.3.1.1 Molecular weight

The molecular weight of muga fibroin after dissolution in ionic liquid was determined using SDS-PAGE. SDS-PAGE resolved muga fibroin shown in the Figure 5.1.1. It is reported that muga fibroin is a homodimer made of two peptide chains of 230 KDa linked with disulphide bonds. During dissolution of native muga fibroin at high

temperature these disulphide bonds between homodimers break that resulted in a single band resolved at 230 kDa [152].
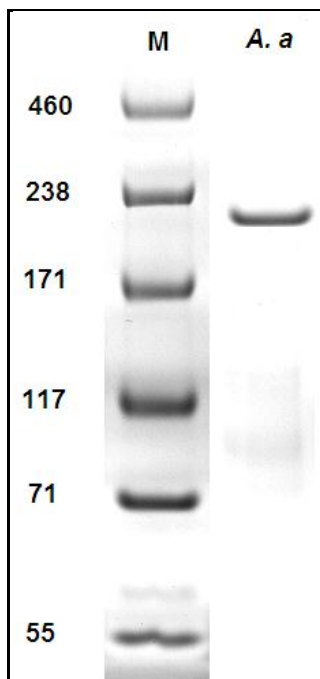
Figure 5.1.1: Photograph of SDS-PAGE after distaining

In our case molecular weight of regenerated muga fibroin is found to be about 230 kDa, which corresponds to weight of single peptide chain of homodimer, due to cleavage of disulphide bonds between homodimer during regeneration in ionic liquid. Gupta *et* al. [152] have found that an extra band may also be observed at 460 kDa due to the partial reduction of disulphide linkages by β-mercaptoethanol at the time of sample preparation corresponding to the uncleaved disulphide linkages of homodimer in the muga cocoon silk fibroin.

5.1.3.1.2 Rheological Studies

The rheological properties of polymer solution can often be investigated by analyzing the interactions between solvent and polymer species. Flow behavior of the polymer

solution can also be determined with rheological studies which is very useful to set process parameter of electrospinning machine. Solution viscosity is one of the most important parameter for preparation of electrospun fibers.
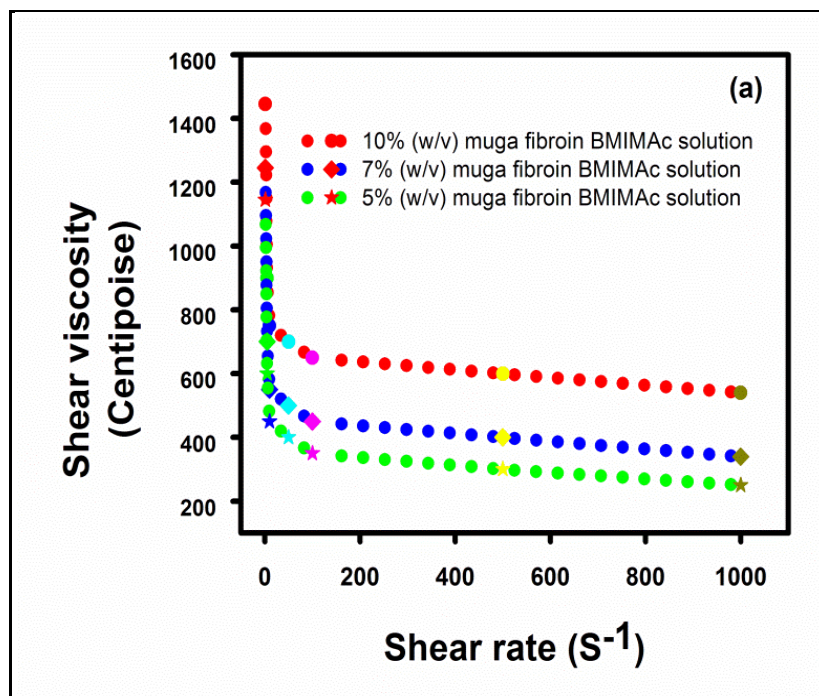
Figure 5.1.2(a): Variation of shear viscosity of muga-BMIMAc dope solutions with time

It is pertinent to note that at very low viscosity, continuous and smooth nanofibers cannot be obtained, while hard ejection of jet occurs at very high viscosity so there is a requirement of optimum viscosity for electrospinning of polymeric solutions [185]. Shear viscosity of muga fibroin-BMIMAc dope solution is plotted against shear rate and the relationship is depicted in Figure 5.1.2(a).The shear viscosity of 5, 7 and 10% w/v dope solution is 1145, 1243 and 1446 centipoises, respectively at 1 S^{-1}. As the concentration of muga fibroin increased the viscosity of dope solution increases due to more entanglements. The regenerated muga fibroin dope solution showed evidently non-Newtonian and shear thinning behavior [186]. The decrease of shear viscosity

against shear rate is due to the fact that some entanglement of polymer chain in

solution gets destroyed by applying the shear force.
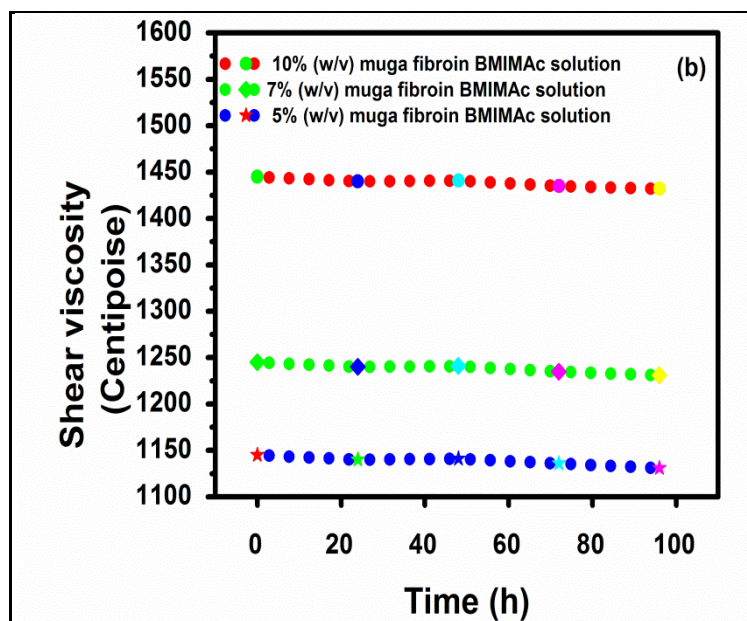
Figure 5.1.2(b): Variation of shear viscosity of muga fibroin-BMIMAc dope solution with shear rate (1 S^{-1})

BMIMAc, a green solvent was used to prepare muga fibroin solution. For

commercialization, it is important to know the storage stability of the dope solution.

The shear viscosity of different muga-BMIMAc solutions (5, 7 and 10% w/v) is

nearly unchanged for 4 days (Figure 5.1.2b), indicating that silk fibroin molecular

chains are stable in BMIMAc without any severe degradation within our experimental

period.

5.1.3.1.3 Structural properties of muga fibroin after dissolution in BMIMAc

To investigate secondary structure of muga fibroin protein dissolved in ionic liquid,

CD spectroscopy was carried out [153]. The results are shown in Fig 5.1.3(a). A

strong negative peak at 230 nm and positive peak at 202 nm are characteristic of

random coil conformation. Circular dichroism spectral behavior of muga fibroin is similar to *Antheraea pernyi* fibroin [3-4].
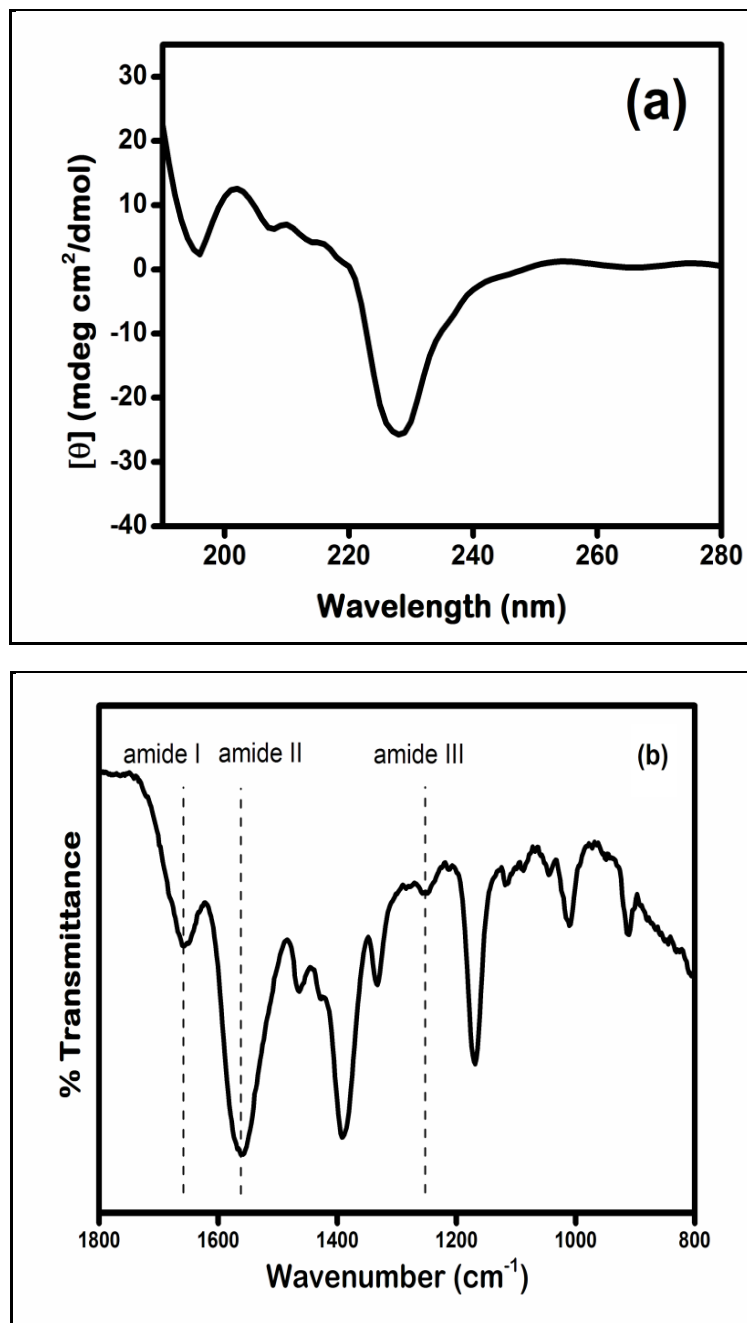
Figure 5.1.3: (a) Circular dichroism spectra (b) FTIR spectra of muga fibroin dissolve in BMIMAc solution

Random coil conformation of muga fibroin after dissolution in ionic liquid was further confirmed by FTIR spectrum (Figure 5.1.3b). FTIR spectrum of muga ionic

liquid solution shows characteristic protein bands at 1656 cm^{-1} (amide I), 1560 cm^{-1} (amide II) and 1253 cm^{-1}, attributed to random coil conformation of fibroin protein, which further corroborates the result of CD spectra.

5.1.3.2 Electrospinning

To prepare electrospun nanofibrous mat of muga fibroin, the process parameters such as concentration of polymer and voltage are varied. After each electrospinning the samples are collected and the morphology of the nanofibrous mats is observed under SEM. The distribution of fiber diameter was determined using Image J software. Thirty images of fiber diameter distribution were taken from different place at same magnification to plot the histogram for each sample.

(i)   Effect of concentration

Concentration is a very important parameter and has remarkable effect on the electro-spinnability of polymer solution. Fig 5.1.4(a) reveals that at low concentration of muga fibroin (5% w/v), nanofibers not formed. This is due to the fact that at very low concentration of muga (5% w/v) there is no ejection of jet from the Taylor cone, which leads to the phenomena of electro-spraying [185]. It is seen from Figure 5.1.4(b) that bead formation occurs for 7% (w/v) muga fibroin-BMIMAc solution, while for 10% (w/v) muga fibroin-BMIMAc there was no bead formation. The average fiber diameter was found to be 220 nm for 10% (w/v) silk ionic liquid solution (Figure 5.1.4c).   In the case of low concentrated polymer solution, the molecular entanglements was not enough to cause break up of jet before reaching the collector which results in formation of beads. When the concentration of solution was high (10% w/v), the viscosity of muga fibroin-BMIMAc dope solution was

sufficiently high (1446 cP) with sufficient chain entanglements which prevent breaking of electrically driven jet & allow electrostatic forces to further stretch the jet & draw it into fibers during electrospinning that results in bead less fiber morphology.
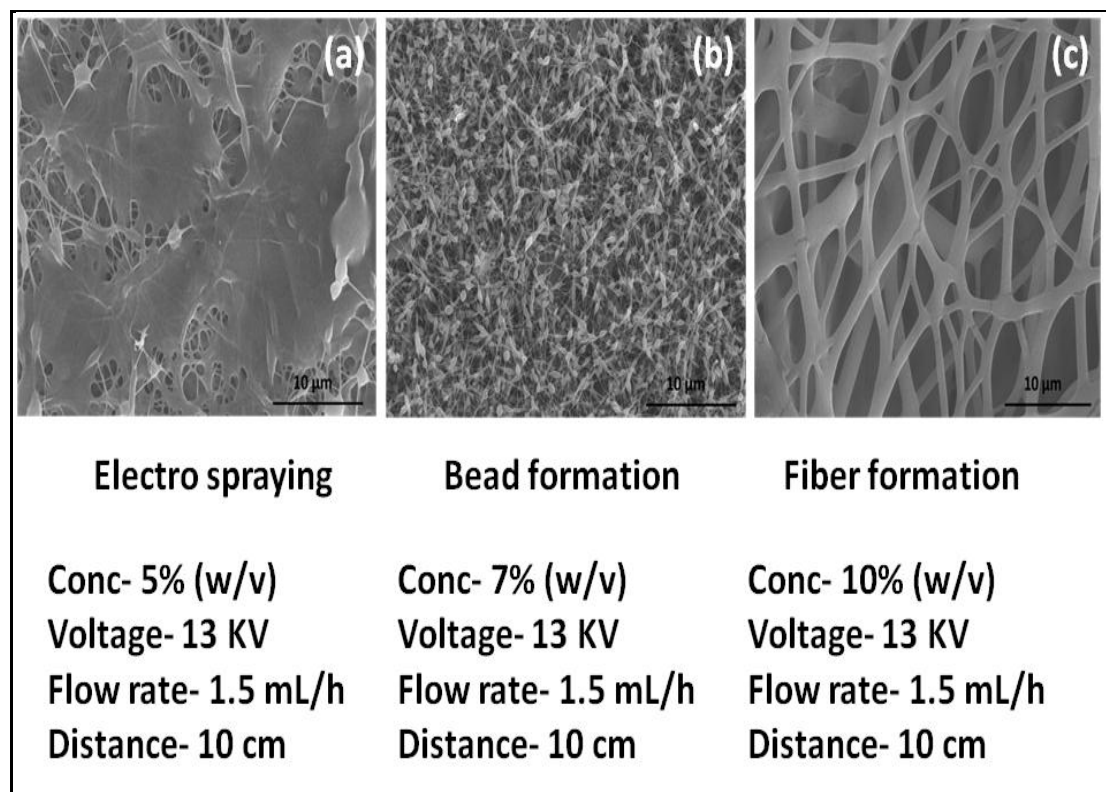
Figure 5.1.4: SEM images of muga fibroin nanofibrous mat prepared from: (a) 5% (w/v), (b) 7% (w/v) and (c) 10% (w/v) muga fibroin-BMIMAc solutions

(ii)   Effect of voltage

It can be seen from Figure 5.1.5(a) that for 10% (w/v) muga fibroin dope solution, the fiber diameter ranges from 80 to 250 nm with an average of 220 nm when 13 kV voltage was applied. When electric potential was increased from 13 to 18 kV, the average diameter of muga nanofibers decreased upto 200 nm (Figure 5.1.5b). This is due to the fact that sufficient electrostatic force can overcome solution surface tension and causes stretching of jet. Further, as we continue to increase the electric potential

up to 20 kV, the diameter of fiber reduced to an average value of 160 nm (Figure 5.1.5c). This is because of the fact that with high voltage, the higher electrostatic power made the concentrated solution flow easily and caused more stretching of jet, so the resultant fiber have narrower morphology [185]. It is clear from SEM images [Figure 5.1.5(a-c)] that nanofibres had a solid surface and are randomly oriented with interconnected pores among the fibers, presenting a porous morphology.
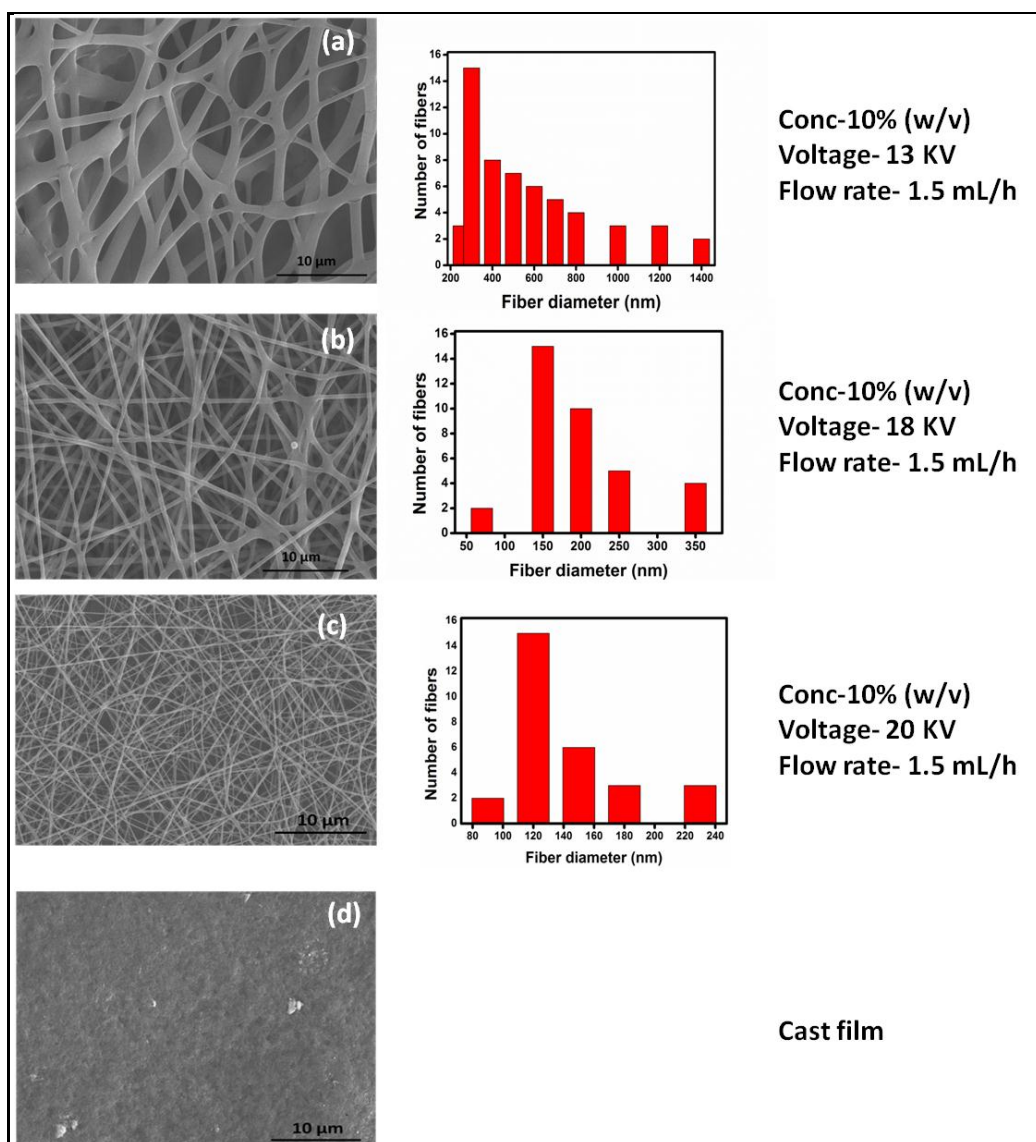
Figure 5.1.5: SEM images of muga fibroin nanofibrous mat prepared from 10% (w/v) muga fibroin-BMIMAc solution with: (a) 13 kV, (b) 18 kV, (c) 20 kV applied electric potential and (d) muga cast film

It can be seen from Figure 5.1.5(d) that muga cast film has rough surface morphology. Based on above studies, we have chosen 10% w/v concentration of muga fibroin and 20 kV voltage as optimized parameter for the formation of nanofibrous mat. This mat has been designated as MNF-20. Further, all subsequent properties are tested on MNF-20 nanofibrous sample and compared with muga cast film (MCF).

5.1.3.3 Mechanical properties of muga nanofibrous mat and cast film

Mechanical properties of electrospun MNF-20 and MCF film are critical for their successful application in skin tissue engineering. The appropriate mechanical strength of scaffolds is a prerequisite for functioning of soft tissue substitute in close proximity of neotissues [188]. Besides the biocompatibility, high tensile strength and flexibility are prerequisite condition for scaffolds used for load bearing area such as knee and elbow joints. Stress-strain curve shows that MNF-20 has higher extensibility as compared to MCF (Figure 5.1.6).
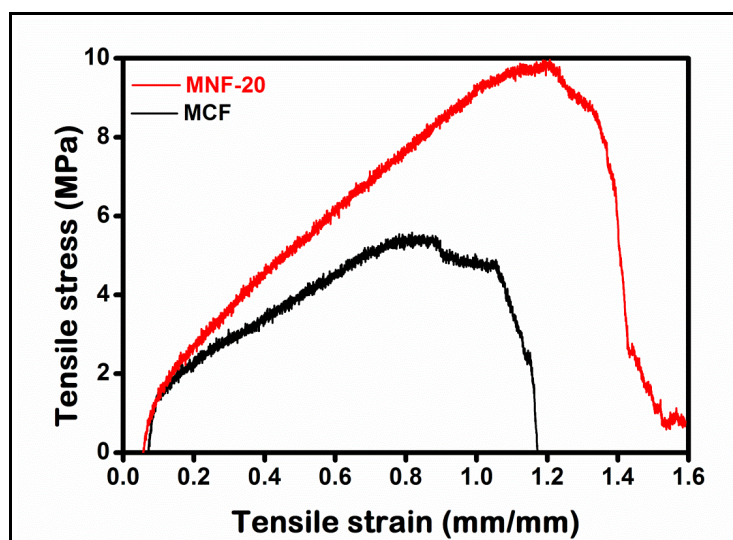
Figure 5.1.6: Stress-strain curve of muga fibroin nanofibrous mat and cast film

Table 5.1.1 showed that nanofibrous mats have higher tensile strength and elongation at break as compared to cast film (p<0.05). This is due to the fact that under tensile

stress, cohesive forces between nanofibers will break, resulting in absorption of more energy as compared to muga cast film. The tensile strength and modulus of MNF-20 and MCF lies well within the range of human skin (5 to 30 MPa) [188] and cell derived skin graft (713 kPa) [189].

Table 5.1.1: **Mechanical properties of muga nanofibrous mat and cast film. Data are represented as mean±SD for n=3. *P<0.05; significant against MCF**

Samples	Tensile strength (MPa)		Tensile Modulus (MPa)	Elongation at Break (mm)	
MNF-20	10		20	31	
MCF	5.6	*	12	25	*

5.1.3.4 Structural characterization of nanofibrous mat and film

Most of the fibroin protein properties depend upon its conformation. The conformation of fibroin changes during regeneration process. During dissolution in ionic solvents its conformation changes from β-sheet to random coil structure which again reverts back during crystallization. So it is very important to study the conformational changes in fibroin during regeneration.Three types of conformation have been proposed for silk fibroin, namely silk I that refers random coil conformation of water soluble silk fibroin in gland of silkworm. Silk II conformation represents extended β-sheet structure present in silk fibroin fibers after spinning by insect, and third is unstable silk III conformation reported at the air-water interface [190]. The conformations of regenerated MNF-20 and MCF were determined by FTIR and XRD techniques.
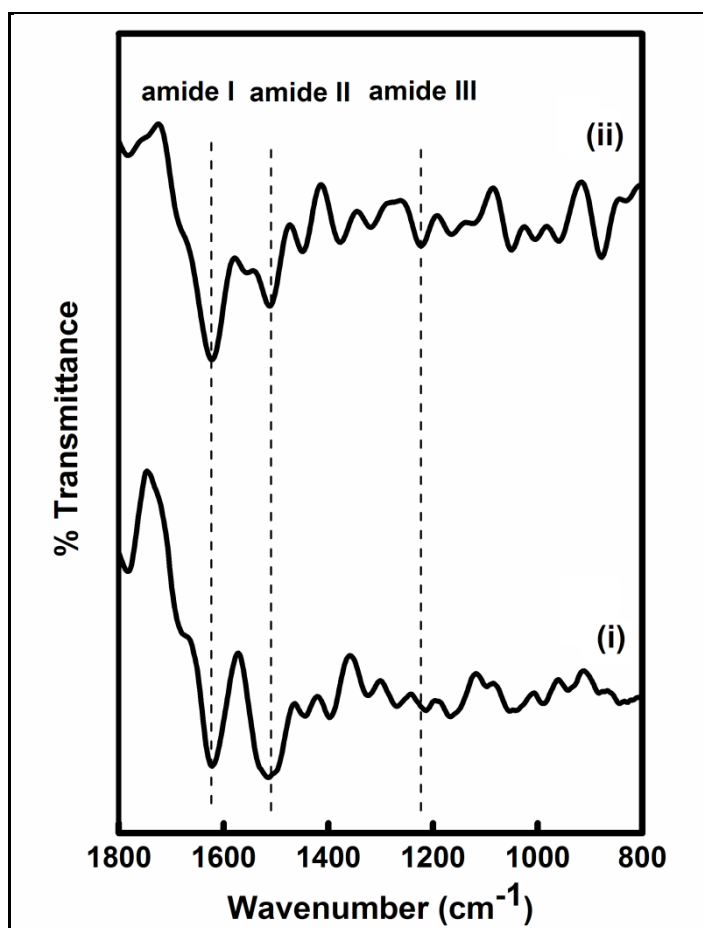
Figure 5.1.7: FTIR spectra of: (i) Muga cast film and (ii): Muga fibroin nanofibrous mat

FTIR spectra of MNF-20 and MCF are shown in Figure 5.1.7. MNF-20 and MCF exhibited peaks centered at 1619, 1511 and 1220 cm^{-1}, corresponding to amide I, amide II and amide III respectively. These peaks are attributed to β-sheet conformation of fibroin. In order to extract the ionic liquid, regenerated nanofibrous mats and cast film were dipped in methanol for 24 h which induces β-sheet conformation in regenerated muga fibroin. A small shoulder for amide II region at 1554 cm^{-1} occurred which is characteristic of α-helical structure of protein. Devi *et* al. [130] have found that both α-helical and β-sheet structures are present in degummed muga fiber.

X-ray diffractogram of MNF-20 is shown in Figure5.1.8. X-ray diffractogram of MNF-20 showed peaks at 12.7°, 20.6° and 24.5° with corresponding d-spacing of 6.96, 4.3 and 3.62 nm, respectively. These peaks represent β-sheet conformation of MNF-20. The d-spacing and crystal size corresponding to different peaks of muga fibroin are determined using Bragg's and Debye Scherrer's equation.

Table 5.1.2: XRD data of muga nanofibrous mat and cast film

S. No.	Muga nanofibrous mat (MNF-20)				Muga cast film (MCF)			
	2θ (FWHM)	d spacing (nm)	Crystal size (Å)	% Crystallinity	2θ (FWHM)	d spacing (nm)	Crystal size (A°)	% Crystallinity
1	12.7	6.96	13.3		12.2	7.2	15.6	
2	20.6	4.3	28.7	32	19.68	4.5	32.7	29
3	24.5	3.62	86.1		-	-	-	

As shown in the Table 5.1.2, the size of crystallite for MNF-20 is 13.3, 28.7 and 86.1 Å, corresponding to 2θ values of 12.7°, 20.6° and 24.5°, which concurred with the results reported by Bubrata *et* al. [72] for regenerated muga fibroin and Sen *et* al. [10] for degummed muga fibroin fiber. A small peak at 11.6 indicates existence of small amount of silk I structure which further supports the FTIR data. Muga cast film has similar diffraction pattern, showed 2θ peaks at 12.2° and 19.68° which correspond to d spacing of 7.2 and 4.5 nm, respectively. The percent crystallinity of MNF-20 and MCF was found to be 32 and 29, respectively.
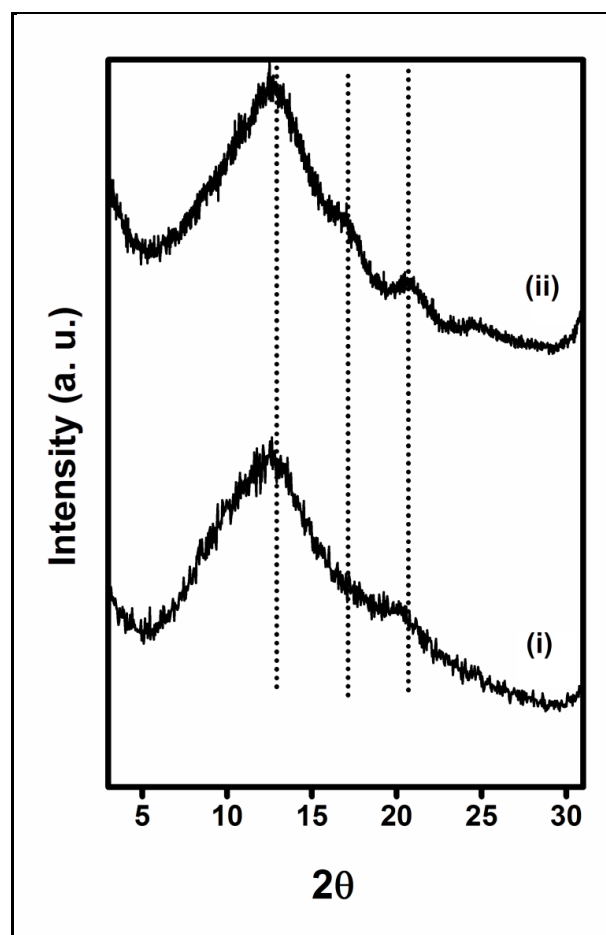
Figure 5.1.8: X-ray diffractogram of: (i) Muga cast film and (ii) Muga nanofibrous mat

5.1.3.5 Thermal properties

To study the thermal degradation profile of regenerated MNF-20 and MCF, thermogravimetric analysis was performed. Figure 5.1.9(a) shows the weight loss of MNF-20 and MCF during heating from room temperature to 700 ℃. First weight loss for MCF and MNF-20 within the range of 30 ℃ to 115 ℃ was related to bound water. MCF shows stable masses in the temperature ranges from 100 ℃ to about 185 ℃. Above 220 ℃ major degradation of muga fibroin started which continued up to 369 ℃ with weight loss of around 65%, while in case of MNF-20 degradation started from 225 ℃ which continued up to 365 ℃. Third step of weight loss started from 369 ℃ which continued to 680 ℃ for MCF, while for MNF-20 it is 370 ℃ which further continued to 640 ℃ for

nearly complete mass loss. Degradation pattern of regenerated MNF-20 is not much different than that MCF. This may be due to the fact that crystalline structure of regenerated muga film is not much different than that of muga fiber.
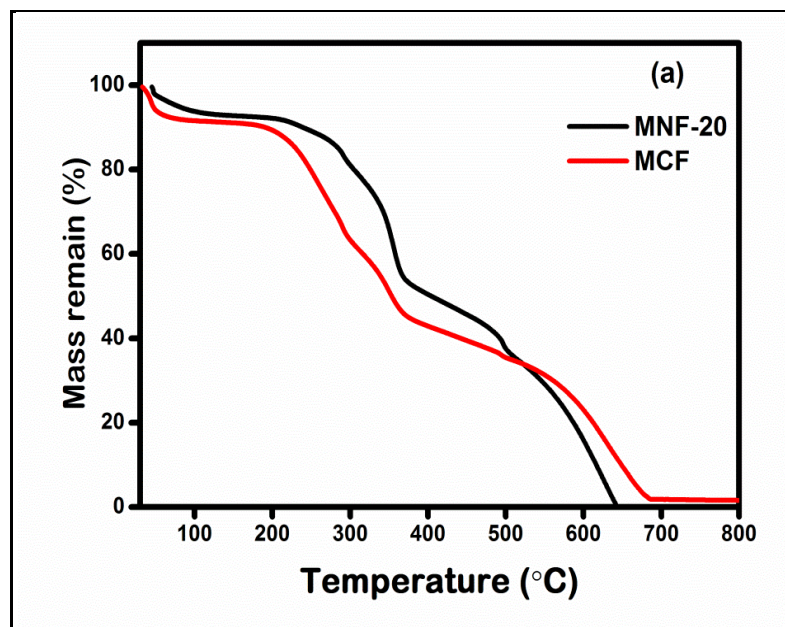
Figure 5.1.9(a): Thermogravimetric analysis of muga nanofibrous mat and cast film
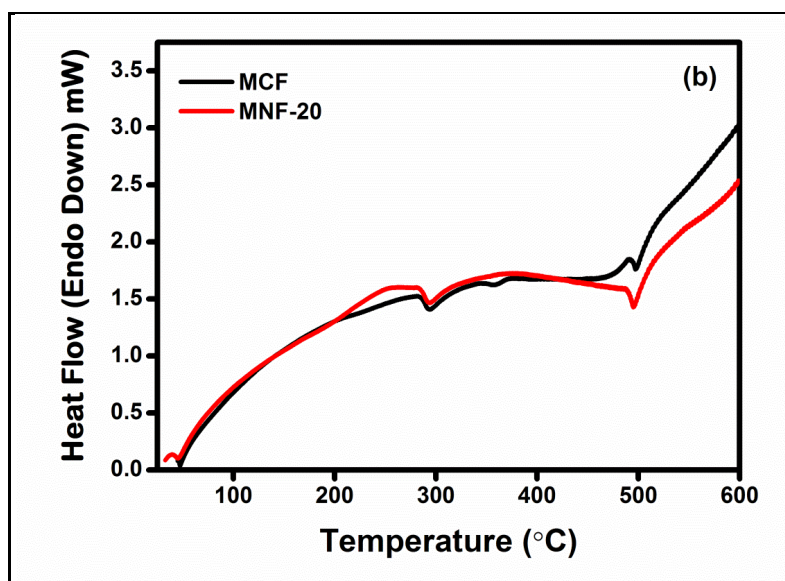
Figure 5.1.9(b): Differential thermal analysis of muga nanofibrous mat and cast film

Figure 5.1.9(b) shows the DTA scans of MNF-20 and MCF. During heating scan, MNF-20 and MCF showed a bound water evaporation peak around 70-115 ºC. MNF-20 and MCF exhibited an endothermic peak at 294 ºC, which attributed to thermal degradation of less ordered fraction of fibroin. Second endothermic peak for MCF and MNF-20 exhibited at 495 and 498 ºC, corresponds to the degradation of highly ordered structure within molecules. Thermal properties of regenerated nanofibrous mat and cast films show similar trends that were reported for muga fibroin films obtained from silkworm gland [72,117].

5.1.3.6 Porosity, pore size and surface roughness

Porosity measurement is very important in biomedical and tissue engineering applications as a highly porous matrix provide larger surface area that promotes better cell growth due to easy passage of nutrients and other essential materials required for growing cells [36].

Porosity measurements of MNF-20 and MCF were carried out by liquid displacement method, using hexane as a displacement liquid. Hexane being non-polar solvent easily permeates through interconnected pores without any remarkable swelling and shrinkage. Muga nanofibrous mat showed average porosity of 75%, while it was only 10% for muga cast film.

To further demonstrate the porosity, pore size and surface roughness of optimized muga nanofibers mats (MNF-20 as well as cast film MCF), AFM analysis was performed and results are depicted in Figure 5.1.10 (a&b) and Table 5.1.3. AFM measurements of MNF-20 and MCF were performed in noncontact mode. The average roughness value for the cast film was found to be very low (2.2 nm) as

compared to MNF-20 for which roughness value was 25 nm. AFM study revealed that MNF-20 mat is highly porous and having pores of 200-500 nm. In case of MCF, porosity was not observed. The apparent porosity value of muga cast film obtained by liquid displacement method may only be due to adsorption and entrapment of hexane to rough surface of cast film.The higher roughness and porosity of MNF-20 will be advantageous for cell adherence, proliferation and organization as well as transport of gases and essential nutrients.

Table 5.1.3: Surface roughness of muga nanofibrous mat and cast film. *P<0.05; significant against MCF

S. No.	Sample	Surface roughness	
		RMS (nm)	**Ra (nm)**
1	Muga cast film (MCF)	3	2.2
2	Muga nanofibrous mat (MNF 20)	25 *	20 *
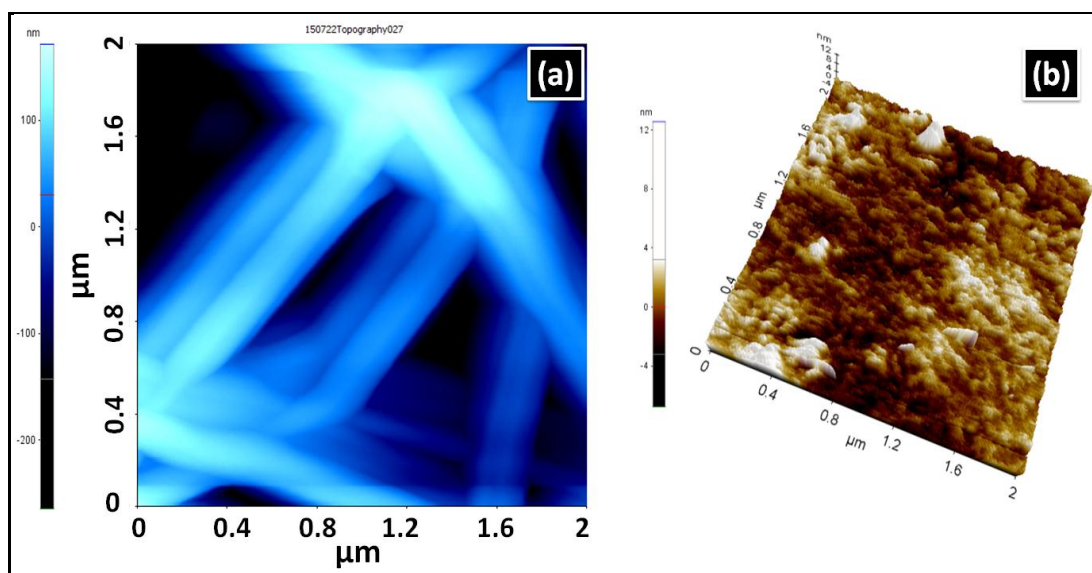
Figure 5.1.10: AFM image of (a) muga nanofibrous mat and (b) cast film

5.1.3.7 Water vapor transmission rate

Water vapor permeability of wound dressing plays a very important role in controlling excessive loss of body fluid. For rapid healing, wound must have moist environment by preventing dehydration of wound as well as building up of exudates. So there is a need of wound dressing that causes permeation of water vapor at optimum rate. WVTR for normal skin is 204 $g/m^2/day$, while that for an injured skin can range from 278 $g/m^2/day$ for first degree wound, 4274 $g/m^2/day$ for second degree wound and 3436 $g/m^2/day$ for third degree wound [172]. The WVTR of MCF and MNF-20 was found to be 990 $g/m^2/day$ and 2250 $g/m^2/day$, respectively. The higher WVTR of nano-fibrous mat is due to its porous structure. Since the WVTR of nano-fibrous mat is lower than second/third degree wound, so these nano-fibrous mats may be used for such types of wound, which can facilitate the cell migration and re-epithializaton that enhanced regeneration of damaged tissue [191].

5.1.3.8 Water uptake

Figure 5.1.11 shows the water uptake capacity of muga nano-fibrous mat (MNF-20) and cast film (MCF) over the time. From Figure 5.1.11 it is clear that water uptake capacity of MNF-20 and MCF increases with time and attains equilibrium after 48 h. The MNF-20 showed higher water uptake capacity (56%) as compared to muga cast film (45%). The water uptake value obtained for MNF-20 is slightly comparable to eri-tasar electrospun mat reported by Panda *et* al. and commercially available wound dressing Tegasorb (59%) [192]. This is only due to difference in porosity and surface area. Water holding capacity is very important to provide moist environment and would also be favorable for regeneration of neo-tissues to heal the wound.
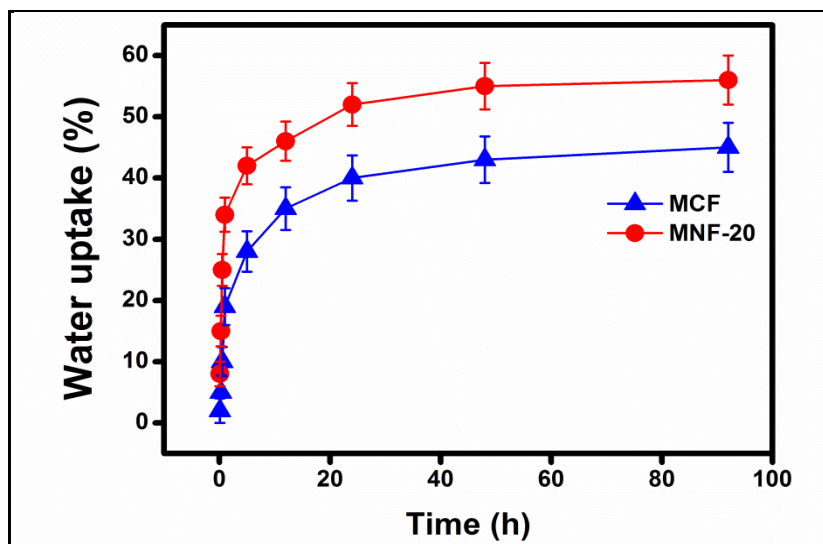
Figure 5.1.11: Water uptake behavior of muga nanofibrous mat and cast film

5.1.3.9 Cell adherence, morphology and proliferation

SEM revealed better attachment of cells after one day of seeding on MNF-20 as compared to MCF (Figure 5.1.12a).
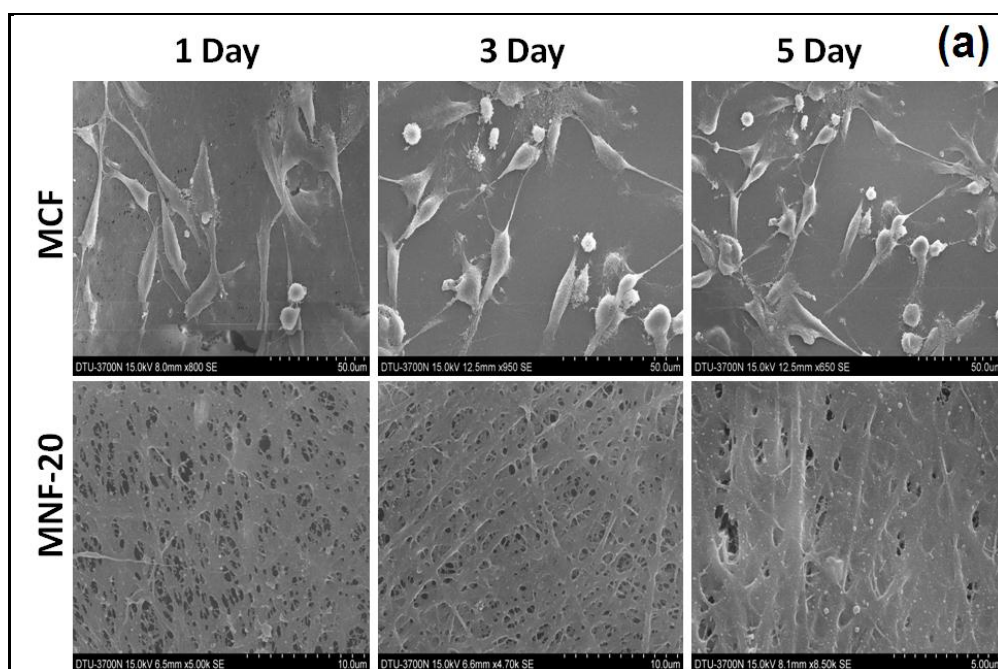
Figure 5.1.12(a):   SEM images of L929 cells seeded on muga nanofibrous mat (MNF-20) and muga cast film (MCF) after 1, 3 and 5 days of incubation. All experiments performed in triplicate

After 1 day of incubation L929 cell adhered well onto MNF-20 and MCF. L929 cells showing good integration with MNF-20 mat and highly colonized nanofibrous network was formed after 5 days of incubation as compared to MCF. After 5 days of cell seeding L929 cells proliferate & spread well in the form of monolayer and completely cover the surface of MNF-20 mat, but it does not happen with MCF.

To study cell proliferation and spreading on MNF-20 and MCF, fluorescence and phase contrast microcopy were carried out. Fluorescence microscopic images revealed that cells with distinct round nuclei were attached throughout the films (Figure 5.1.12b).
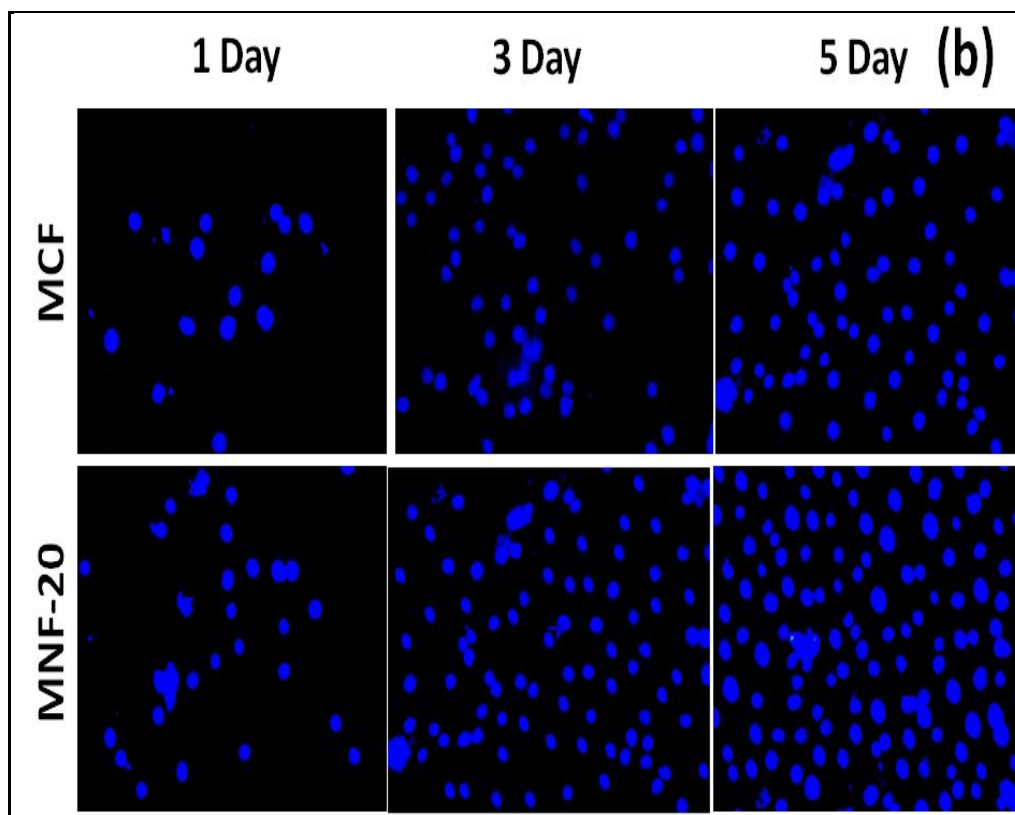
Figure 5.1.12(b): Fluorescence images of L929 cells seeded on muga nanofibrous mat (MNF-20) and muga cast film (MCF) after 1, 3 and 5 days of incubation. All experiments performed in triplicate

Cell number increases with time suggesting the normal growth of cells on film over the period of 5 days. The number of nuclei attached to MNF-20 was significantly higher ($p < 0.05$) as compared to MCF. The proliferation and growth of L929 cells seeded on MNF-20 and MCF was also examined by using phase contrast microscopy (Figure 5.1.12c). The phase contrast microscopy also revealed that L929 cells adhered to MNF-20 and MCF after 1 day of incubation.
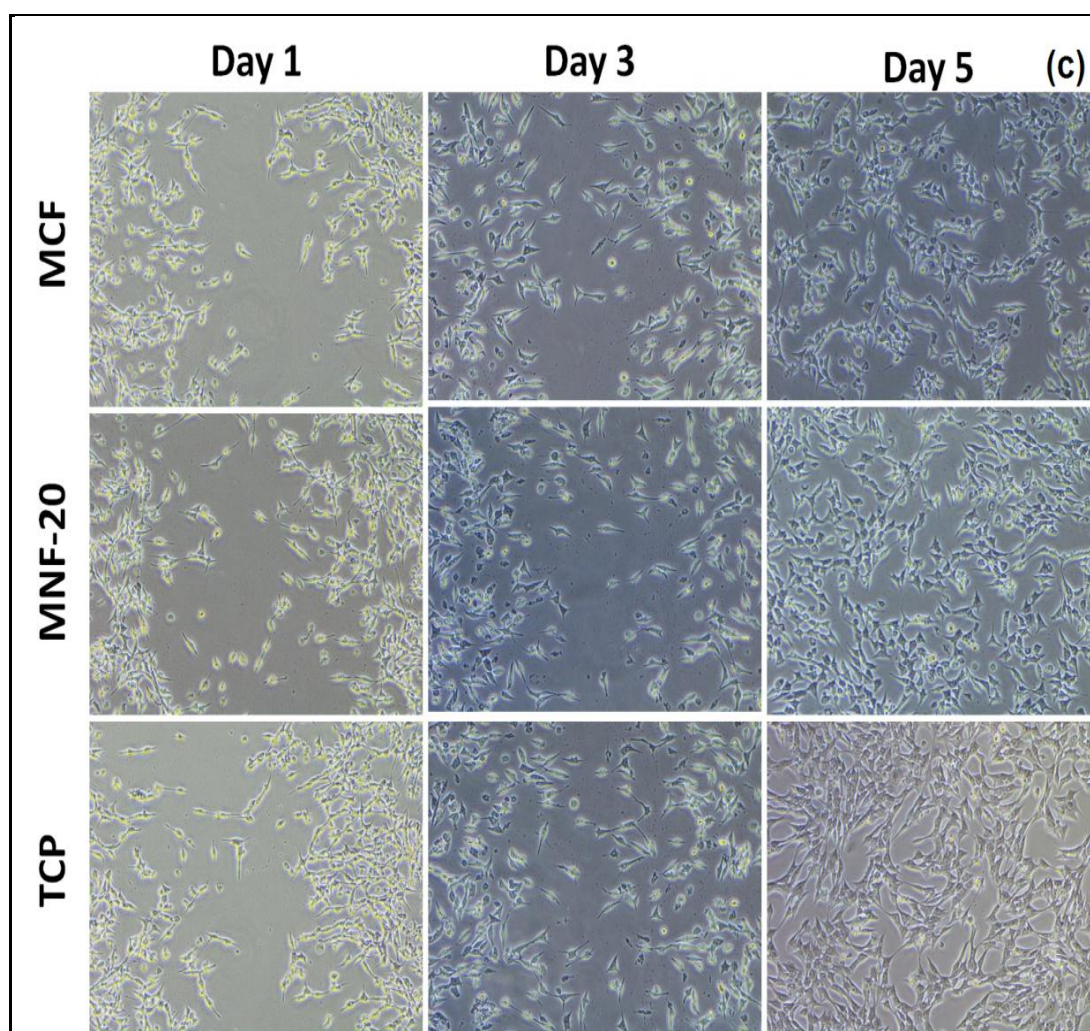
Figure 5.1.12(c): **Phase contrast microscopic images of L929 cells seeded on muga nanofibrous mat (MNF-20) and muga cast film (MCF) after 1, 3 and 5 days of incubation. All experiments performed in triplicate**

Cells attached to MNF-20 and MCF attain their normal morphology within 3 days of incubation and cell density increases with time for both MNF-20 and MCF. The number of cells attached to MNF-20 was significantly higher (p<0.05) than MCF after 5 days of incubation and it was found significantly closer to tissue culture plate. The cells seeded on MNF-20 reaches to confluence after 5 days of incubation, but it was not found for MCF.

5.1.3.10 Cell growth and viability

Adherence and spreading of cells to muga nanofibrous mat (MNF-20) and cast film (MCF) were monitored over 1, 3 and 5 days after cells seeding. Figure 5.1.12(d) shows that number of cells attached to MNF-20 increases with time.
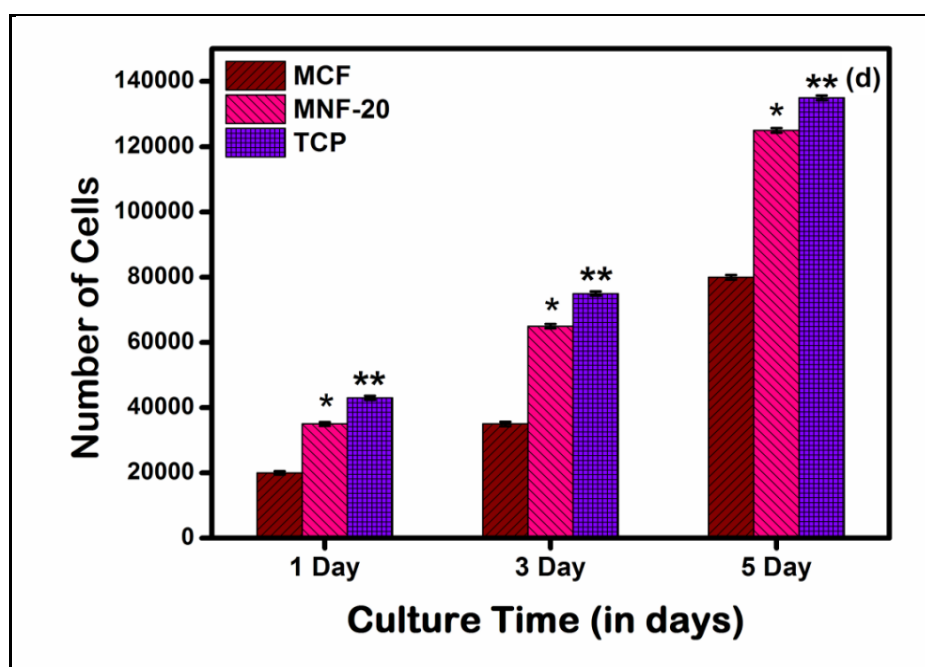
Figure 5.1.12(d): **Number of cells of L929 cells seeded on muga nanofibrous mat (MNF-20) and muga cast film (MCF) after 1, 3 and 5 days of incubation. All experiments performed in triplicate and bar represented as mean±SD. *P<0.05 significant against MCF and ** p>0.05 no significant against TCP**
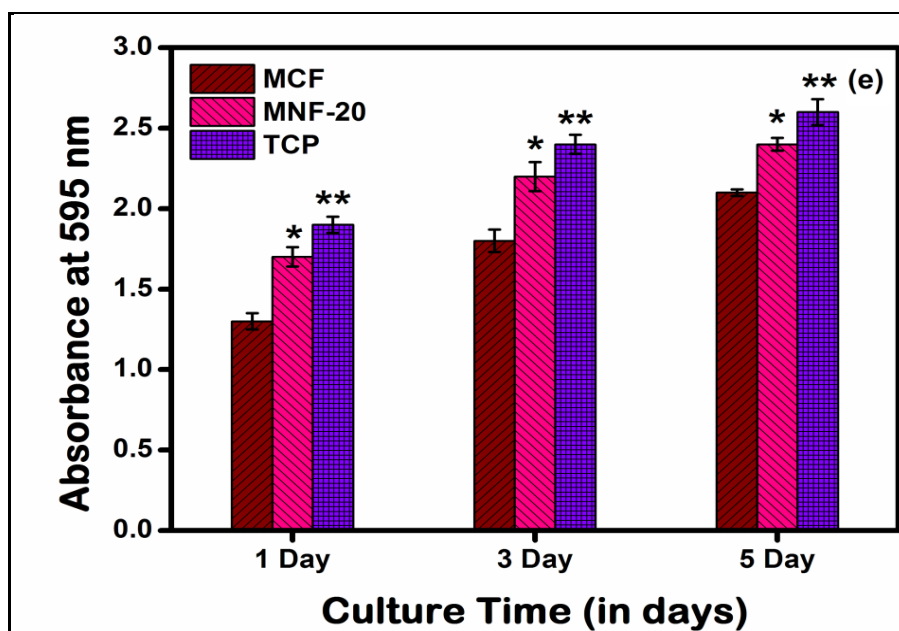
Figure 5.1.12(e): **MTT Assay of L929 cells seeded on muga nanofibrous mat (MNF-20) and muga cast film (MCF) after 1, 3 and 5 days of incubation. All experiments performed in triplicate and bar represented as mean±SD. *P<0.05 significant against MCF and ** p>0.05 no significant against TCP**

However, this increased cell adherence is significantly higher in MNF-20 as compared to MCF (p<0.05). It is also found that after 3 days of incubation, cell growth on nanofibrous mat is comparable to tissue culture plate (p>0.05).

MTT assay was performed to determine the viability of L929 fibroblast cells seeded on MNF-20 and MCF (Figure 5.1.12e). MTT assay is a tool to determine cellular metabolic activity that indirectly indicates the viability of cells seeded on regenerated muga samples over the time. Figure 5.1.12(e) showed that after 5 days of incubation there was no significant difference (p>0.05) between the MNF-20 and control, which is due to higher biocompatibility, surface area and porosity of MNF-20.

This indicates that MNF-20 is highly biocompatible and nontoxic. Previously, it has been reported that nonmulberry silk fibroin showed higher biocompatibility over the

mulberry fibroin. Nonmulberry fibroin belonging to genera *Antheraea* were reported to contain Arg(R)-Gly(G)-Asp(D) motif, AAC32606 (*A. pernyi*); AAK83145 (*A. yamamai*); and AY136 274 (*A. mylitta*), which are responsible for adherence of cells due to activation of cells surface integrin receptor [75]. Recently, Gupta *et* al. [152] reported about the molecular structure of muga fibroin (KJ862544). The unique feature of muga fibroin is the presence of hexa-serine residue that juxtaposes N-amorphous motif and the crystalline core. The crystalline core of muga fibroin generally made of 54% Arginine rich R-motif and 53.4% of Gly rich motif. The primary sequence of heavy muga fibroin chain has 17 Arginine rich R-motif, which is the highest number among all reported saturniidae heavy fibroin. These positively charged arginine rich R-motif may be responsible for attachment of cells, considering that surface of mammalian cells possess negative charge [75]. Beside this, the higher rate of spreading and proliferation of L929 cells over MNF-20 was related to their surface morphology and architecture. The porous architecture and higher surface area of MNF-20 provides favorable environment causing ease transport of gases and essential nutrients, which permits the cells to adhere and proliferate faster onto MNF-20 as compared to MCF. AFM observations revealed that MNF-20 has very high roughness value as compared to MCF, which is an advantageous feature, as cells adhered more strongly to rough surface as compared to smooth one. Hence the results of cell adherence, growth, viability & proliferation collectively suggest a very good cellular compatibility of MNF-20 scaffolds which is found to have good agreement with work reported previously for nonmulberry biomaterials [72,75,79]. These studies also hold good promise & encouragement for the development of nanofibrous construct towards the regeneration of damage tissue.
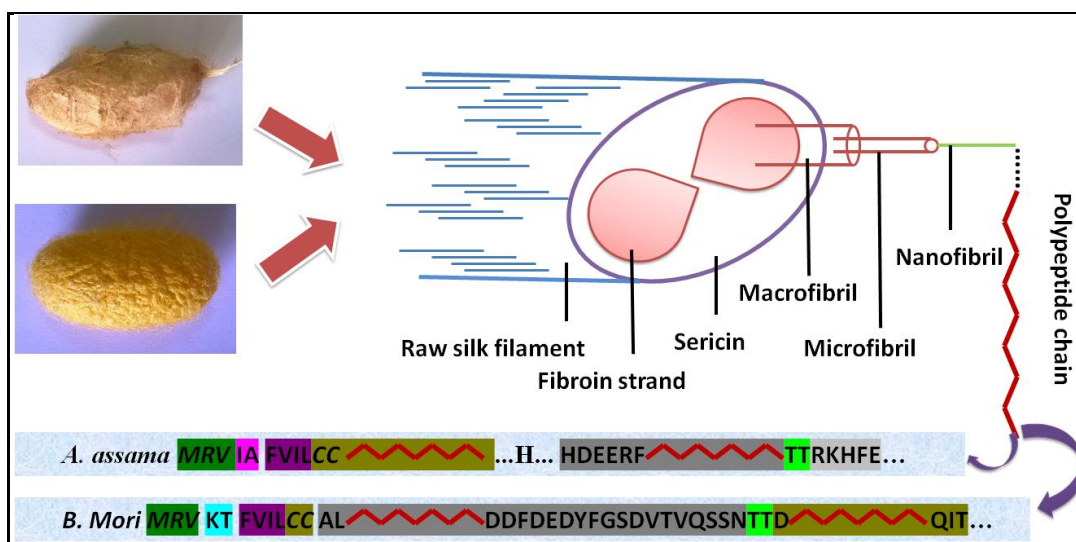
Figure 5.1.13: Schematic presentation of amino acid sequences of heavy chains of fibroins

A schematic presentation for N-terminal amino acid sequence of heavy chain fibroin for *Bombyx mori* and *Antheraea assama* are shown in Figure 5.1.13 as reported by Gupta *et* al. [152].

In order to develop biomaterials for skin tissue engineering and other biomedical applications, it needs higher surface area, porosity and adequate interaction between cells and biomaterial. The higher surface area porosity and nanofibrous architecture of MNF-20 mimic extracellular matrix component that results in ease of exchange of gases, nutrients and necessary components required for optimum growth of cells seeded on it.

5.1.3.11 Antimicrobial activity

Antimicrobial activity of gentamicin loaded MNF-20 and MCF was determined by agar disc diffusion test and results are depicted in Figure 5.1.14. Control samples did not show any zone of inhibition. Both drug loaded MNF-20 and MCF films exhibited antimicrobial activity against both *E. coli* (gram negative) and *S. aureus* (gram

positive) strains. The mean diameter of zone of inhibition (ZOI) for MNF-20 was 13 and 15 mm against *E. coli* and *S. aureus*, while it was 10 and 13 mm for MCF. Antimicrobial activity of MNF-20 was higher as compared to MCF. This behavior is related to surface architecture of both films. The MNF-20 being nanofibrous mat having large surface area and porosity, causes fast release of gentamicin as compared to cast film. The *E. coli* and *S. aureus* colonies were collected from inhibition zone of gentamicin loaded MNF-20 and MCF. These gentamicin treated *E. coli* and *S. aureus* bacterial cells were fixed with 2.5% gluteraldehyde followed by their morphological studies through SEM. SEM images of gentamicin treated *E. coli* and *S. aureus* are shown in Figure 5.1.15(a-d).
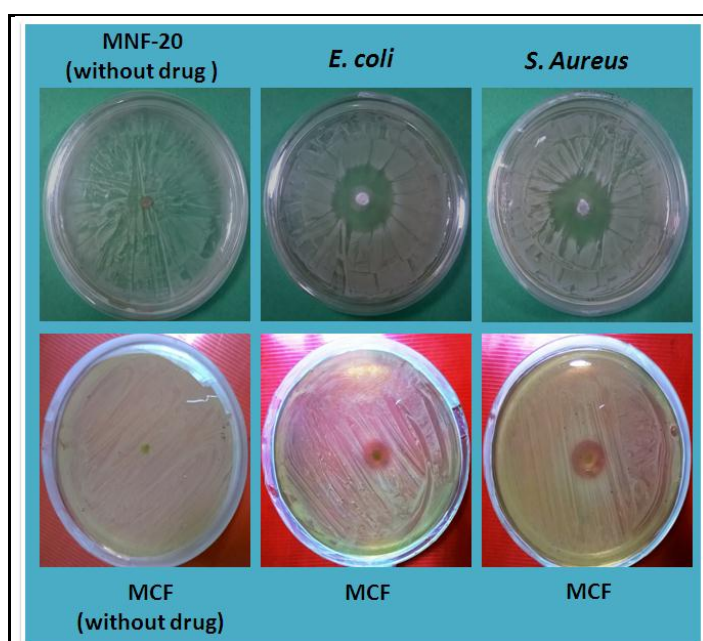
Figure 5.1.14: Disc diffusion test of gentamicin loaded muga nanofibrous mat and cast film

The gentamicin released from MNF-20 as well as MCF destroyed the cell walls of both bacterial strains. From Figure 5.1.15(a-d) it is observed that cell walls of *S. aureus* cultured with MNF-20 and MCF is highly damaged, which is shown by

arrows. The circle shows residues of dead bacteria. Similarly, cell walls of *E. coli* cultured with MNF-20 and MCF is also damaged, that results in the leakage out of cytoplasmic contents from the cell, which inhibits the multiplication for further bacterial growth [158].
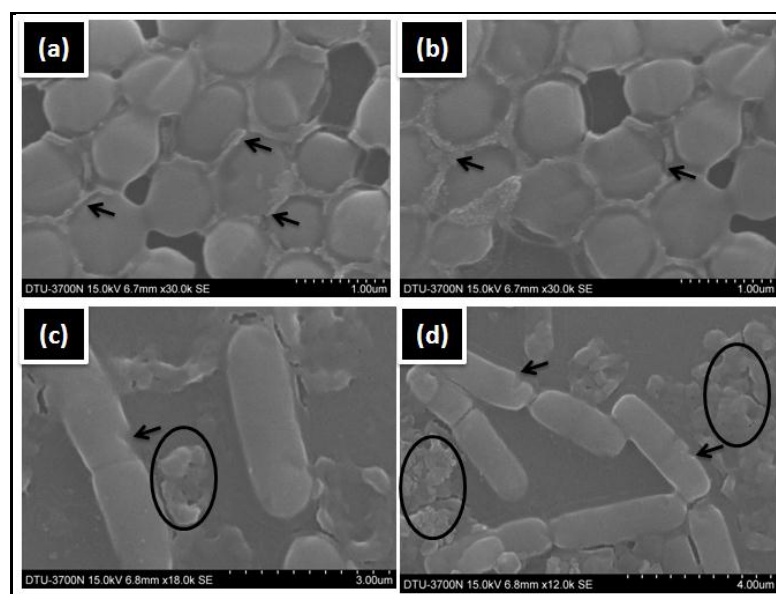
Figure 5.1.15: SEM images of gentamicin treated *E. coli* and *S. aureus*

5.1.3.12 Release study

Gentamicin is very effective against many gram +ve and −ve bacteria, so used as an effective drug in the treatment of superficial infection of skin. Figure 5.1.16 shows the release behavior of gentamicin loaded regenerated MNF-20 and MCF samples. The release of gentamicin from MCF and MNF-20 was carried out in PBS at physiological pH 7.4. From the Figure 5.1.16 it is clear that there is initial burst release of gentamicin within 24 h due to drug absorbed at the surface of nanofibrous mat, followed by continuous release of drug for rest period of time. The release of a drug from wound dressing materials always depends upon size of drug, nature of drug and pore size of wound dressing. From the SEM and AFM analysis as discussed

previously, it is clear that nanofibrous mat has higher porosity (pore size of 200-300 nm) as compared to the cast film. So an initial higher rate of release has been noted in the case of nanofibrous mat as compared to cast film. This is due to the fact that release of gentamicin through cast film is difficult so that it attains slow release profile as compared to porous nanofibrous mat. To determine the release mechanism of gentamicin as shown for muga nanofibrous mat and cast film, the data were fitted to Ritger-Peppas equation, a semi-empirical power law model as reported by Vasconcelos *et* al. [36]. This equation is further modified to determine exponent n, that depends upon the release mechanism and matrix architecture.

The value of n characterizes the release mechanism of drug from matrix. For the cylindrical matrices, $0.45 \leq n$ corresponds to a Fickian diffusion mechanism, $0.45 < n < 0.89$ to non-Fickian, where as $n = 0.89$ corresponds to Case II (relaxation) transport, and $n > 0.89$ to super case II transport. To find out the exponent of 'n', the portion of release curve where $M_t/M_\infty < 0.6$ should only be used. From Table 5.1.4 it is clear that for both sample 'n' value is higher than 0.45, which showed that release of gentamicin from muga nanofibrous mat and cast film follow anomalous diffusion behavior. The value of k is higher for muga nanofibrous mat than cast film, indicating higher rate of gentamicin release from muga nanofibrous mat due to the higher porosity as well as swelling capacity. Additionally, the lower value of diffusion exponent n for muga nanofibrous mat as compared to muga cast film further support the higher diffusion of muga nanofibrous mat over cast film.

Table 5.1.4: Kinetic data obtained by fitting the drug release data

	K	n	R^2
Muga nanofibrous film	0.32	0.53	0.98
Muga cast film	0.19	0.69	0.95
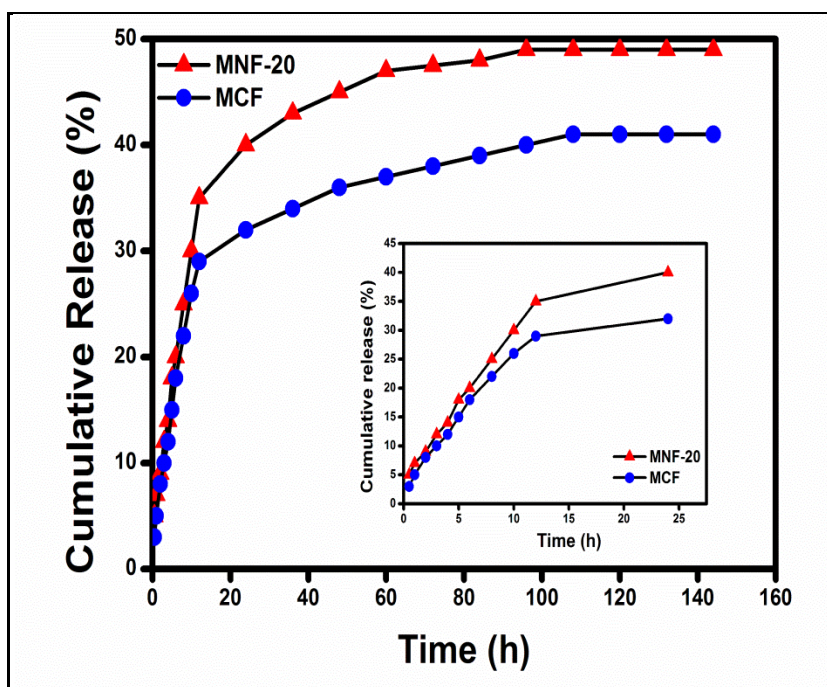
Figure 5.1.16: Release behavior of gentamicin sulphate loaded in muga nanofibrous mat and muga cast film

5.1.3.13 *In vitro* biodegradation

The biodegradation of materials is a key factor for the success of any biomaterials to be utilized in the field of biomedical and tissue engineering applications. The degradation of biomaterials should match with regeneration of neo-tissue in order to minimize localized stress or infection. *In vitro* biodegradation of MNF-20 and MCF was investigated by analyzing the mass remained during the incubation in PBS and in the presence of trypsin (Figure 5.1.17). The trypsin was used in biodegradation assay on the basis of previous study reported in the literature [11]. The biodegradation of

both the samples in PBS showed a controlled rate up to the value of 7% over 30 days of incubation. The enzyme mediated degradation of both the sample was significantly higher up to 30 days of incubation. After 30 days of incubation, biodegradation was higher in the case MNF-20, with a weight loss of 50% as compared to MCF for which mass loss was found to be 42% (Figure 5.1.17a-b). It may probably be due to higher surface area and porosity of MNF-20 mat as compared to MCF which results in higher interaction of materials surface with enzyme. Enzymatic materials erosion was also confirmed by SEM images of biodegraded MCF and MNF-20 (Figure 5.1.17 c-d).
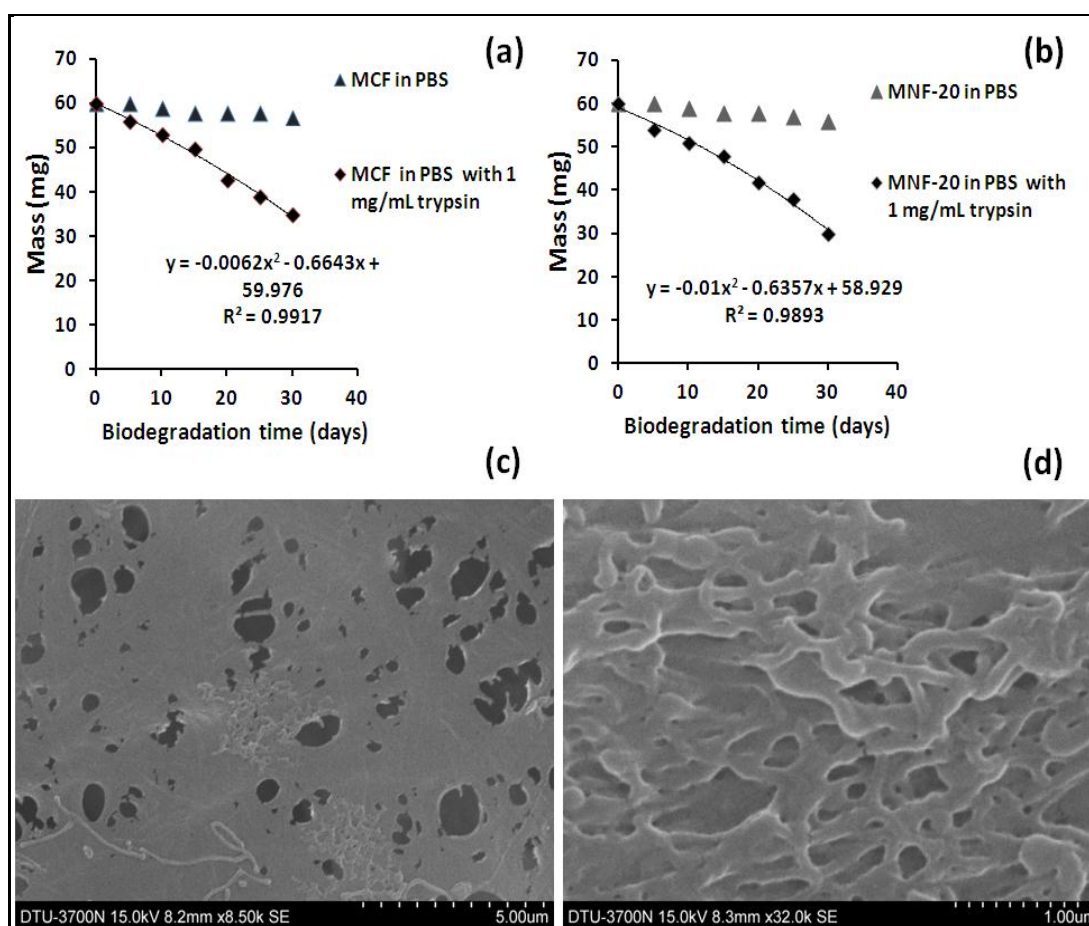
Figure 5.1.17: *In vitro* **biodegradation of (a) MCF, (b) MNF-20, (c) SEM image of MCF and (d) SEM image of MNF-20 after 30 days of incubation**

5.1.4   Conclusions

Cocoon extracted muga fibroin fibers have been successfully regenerated as nanofibrous mat by using ionic liquid. Muga fibroin nanofibrous mat exhibited unique properties, including adequate mechanical strength, porosity, water absorption and enhanced biocompatibility drug release over the muga cast film that makes it an excellent candidate in the field of skin tissue engineering.

SECTION 5.2: GREEN FABRICATION OF SILVER NANOPARTICLES COATED TASAR NANOFIBROUS MATS FOR WOUND DRESSING

5.2.1 Introduction

This section of the chapter is focused on the preparation of tasar fibroin nanofibrous mat using electrospinning technique. Electrospun mats from tasar fibroin blends have been prepared by various researchers. Andiappan *et* al. [71] developed eri and tasar silk fibroin based nanofibrous mat for biomedical applications. These nanofibrous mats show good cytocompatibility with skin fibroblast as well as low hemolysis. Bhattacharjee *et* al.[42] have prepared PVA/tasar silk fibroin electrospun mats for bone tissue regeneration.

In the present study, we have successfully prepared tasar fibroin nanofibrous mats using green solvent 1-butyl-3-methylimidazolium acetate for skin tissue engineering. The prepared tasar nanofibrous mat was further coated by silver nanoparticles (AgNPs) *insitu* via green synthesis using dandelion (*Tridax procumbens*) leaf extract. The kinetic of silver nanoparticles formation was studied by UV Vis spectrophotometer. The prepared silver nanoparticles were further confirmed by XRD and TEM. The coating of tasar nanofibrous mat with silver nanoparticles was confirmed by EDX and EDX mapping techniques. The physical, mechanical, antimicrobial and biological properties of these silver nanoparticles coated tasar nanofibrous mat were determined in order to check its suitability for skin tissue engineering and wound dressing applications.

5.2.2 Experimental

5.2.2.1 Preparation of dope solution

Dissolution of silk fibroin in the ionic liquid was performed according to the protocol reported earlier [123]. Briefly, degummed tasar silk fibroin fibers were dissolved in ionic liquid (1-butyl-3-methylimidazolium acetate) at 95 ºC in concentrations ranging from 5, 7, and 10% (w/v) under nitrogen atmosphere. Tasar silk fibroin fibers were dissolved completely in BMIMAc ionic liquid within 2h under nitrogen atmosphere with constant stirring. After dissolution the solution is filtered through mesh.

5.2.2.2 Preparation of tasar silk fibroin nanofibrous mats by electrospinning

Tasar silk fibroin nanofibrous mats were prepared as per protocol used above for muga fibroin nanofibrous mats with slight modifications (Scheme IV). Tasar silk fibroin nanofibrous mats were prepared by spinning of different concentration of tasar fibroin ionic liquid solutions (5, 7 and 10% w/v) at the fixed tip to collector drum (1000 rpm) distance of 8 cm. The applied voltage was varied from 15, 20 and 25 kV to prepare nanofibers which were further collected at drum that was submerged in methanol tank. The flow rate was 0.5 mL/h.

5.2.2.3 Preparation and deposition of silver nanoparticles on the surface of tasar nanofibrous mat

Tasar nanofibrous mat was coated with silver nanoparticles synthesized by green route using leaf extract of *Tridax procumbens*. Schematic diagram shows the coating of tasar nanofibrous mat with green synthesized silver nanoparticles (Scheme V). Briefly, the

aqueous extract of *Tridax procumbens* leaves was prepared by boiling 5 gm of leaves in 50 mL of milli Q water for 30 min. A rectangular piece of tasar nanofibrous mat was placed at the bottom of clean beaker. Slowly add 1 L of 10^{-3} M AgNO$_3$ solution over the nanofibrous mat. After that 5 mL freshly prepared leaf extract solution was added and left it for two days at ambient temperature. It is reported that polyhydroxy molecules of plant are responsible for reduction of silver nitrate to silver nanoparticles, as well as stabilization of prepared silver nanoparticles by capping. *Tridax procumbens* leaf extract contains many polyhydroxy molecules such as luteolin which may be responsible for reduction and capping of silver nanoparticles. Scheme VI & VII shows the synthesis and capping nanoparticles using leaf extract. These synthesized silver nanoparticles settle down and deposit on the surface of tasar nanofibrous mat. After 2 days, nanoparticles coated tasar nanofibrous mat are removed from solution and remaining nanoparticles that are suspended in solution are collected by centrifugation and are characterized.
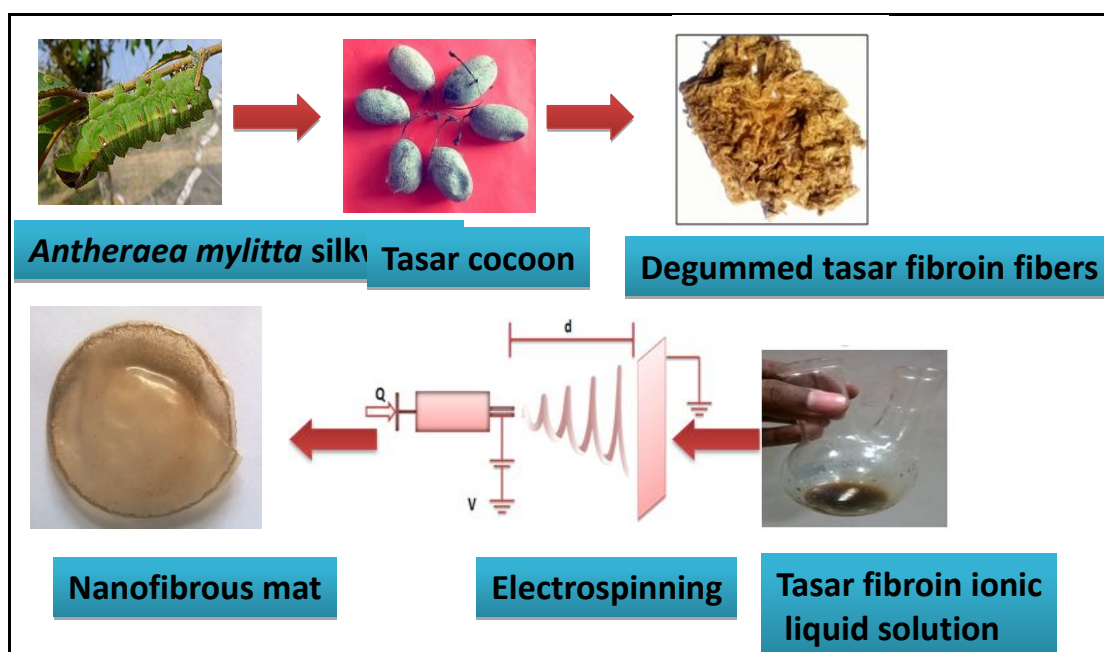
Scheme IV: Schematic representation for preparation of tasar nanofibrous mats using electrospun
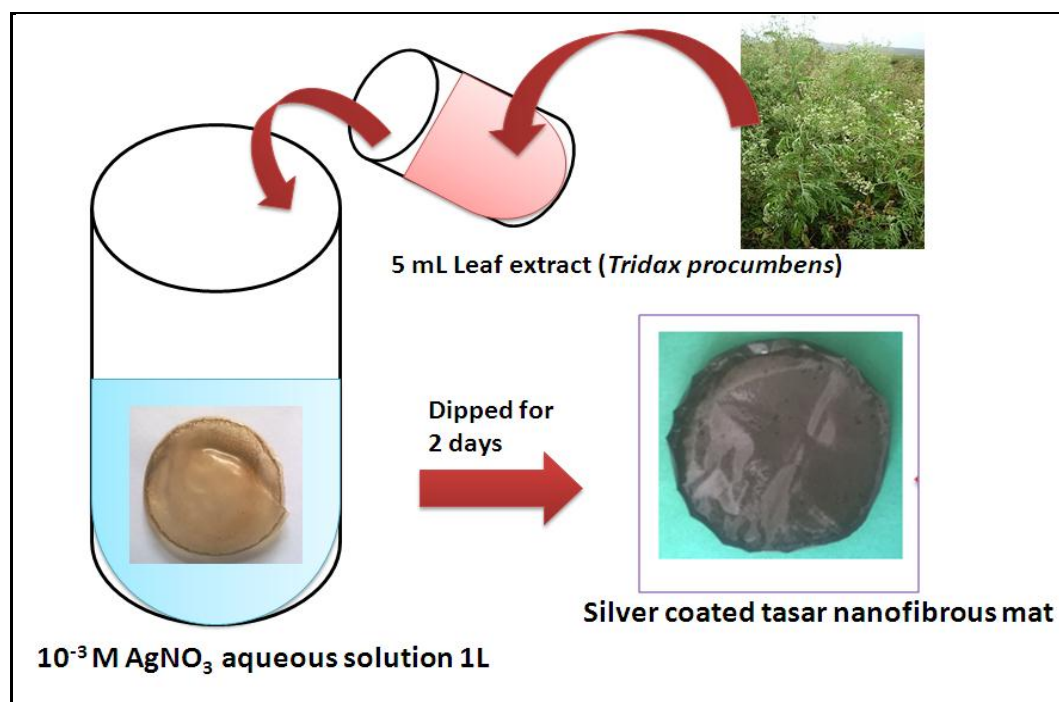
Scheme V: **Coating of tasar nanofibrous mat by in situ preparation and deposition of silver nanoparticles**

5.2.3 Results and discussion

5.2.3.1 Characterization of dope solution

5.2.3.1.1 Molecular weight

The sodium dodecyl sulphate polyacrylamide gel electrophoresis (SDS-PAGE) was performed to check molecular weight of tasar fibroin protein after dissolution in ionic liquid. SDS-PAGE resolved tasar fibroin protein is shown is Figure 5.2.1. Tasar fibroin showed a band corresponding to 195 kDa. Tasar fibroin protein is a homodimer made of two peptide segments of 195 kDa linked with disulphide bridge bond. At the time of dissolution of tasar fibroin protein these disulphide bonds of homodimers break due to which one band gets resolved at 195 kDa. Mandal *et* al. [47] have analyzed molecular weight of tasar fibroin proteins in different regeneration conditions and found that tasar fibroin protein has molecular weight 390 kDa in non-

reducing condition and 197 kDa in reducing condition. In our case molecular weight of tasar fibroin protein was 195 kDa due to the reduction of disulphide bonds by β-mercaptoethanol during sample preparation corresponding to the uncleaved disulphide bond of homodimer in the tasar cocoon silk fibroin.
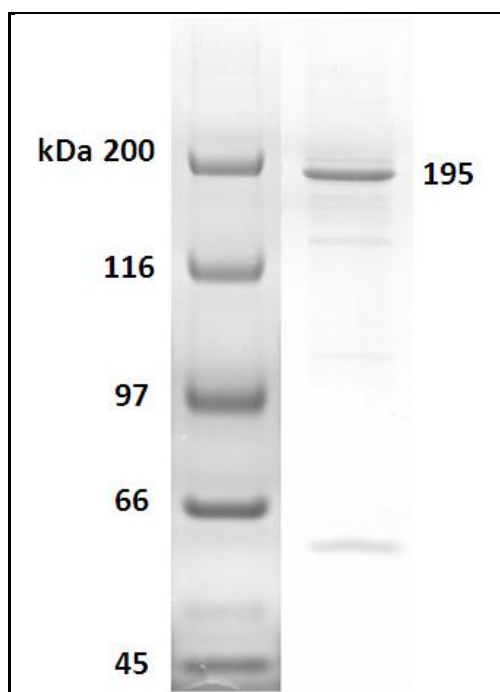
Figure 5.2.1: SDS PAGE analysis of tasar silk fibroin after dissolution in ionic liquid

5.2.3.1.2 Rheological Studies

The rheological properties of tasar fibroin ionic liquid solutions were determined to study flow behavior of solution which is very important to optimize process parameters of electrospinning machine. Concentration and viscosity are the most important parameters for processing of electrospun mats because at very low viscosity or concentration continuous and smooth nanofibers cannot be formed due to insufficient entanglement between molecules while at a very high concentration there is difficulty in ejection of jet so it is very important to set optimum concentration of solution used for electrospinning [33].

Shear viscosity of tasar fibroin ionic liquid solutions is determined by varying the concentration and results are depicted in Figure 5.2.2. As the concentration of tasar fibroin protein increases, shear viscosity increase due to more entanglements between tasar fibroin chains. Shear viscosity of 5, 7 and 10% w/v dope solution is 535, 1132 & 1542 centipoise, respectively at the shear rate of $1S^{-1}$.Shear viscocity of pure BMIMAc is 140 centipoise at the shear rate of $1S^{-1}$. Shear viscosity of pure BMIMAc is 140 centipoise at $1S^{-1}$.

Tasar silk fibroin ionic liquid solutions show non-Newtonian as well as shear thinning behavior. As we increase shear rate the viscosity of all types of tasar fibroin solution decreases due to the fact that under shear force some entanglement and secondary forces such as Vander Waal forces between fibroin chains destroy [34].
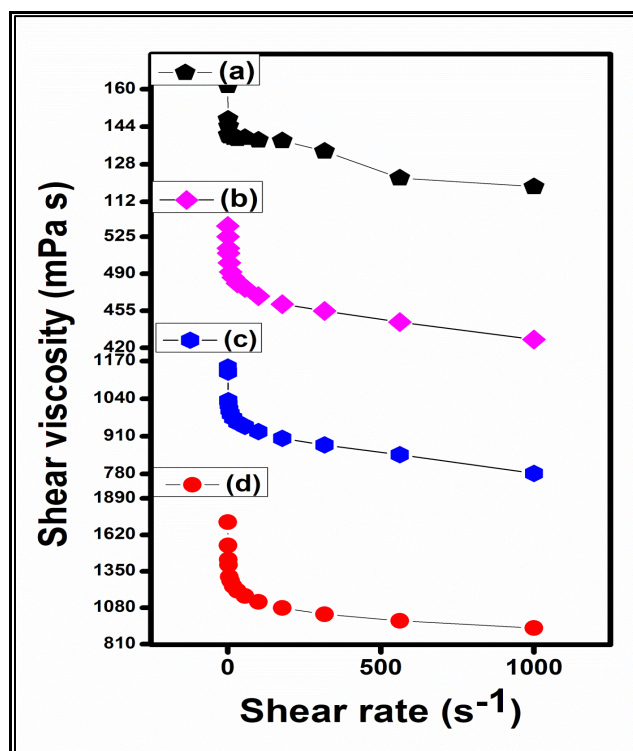
Figure 5.2.2: **Variation of shear viscosity with shear rate (S^{-1}) (a) Pure BMIMAc, (b) 5% (w/v), (c) 7% (w/v) and (d) 10% (w/v) tasar fibroin-BMIMAc dope solution**

5.2.3.1.3 Structural properties of tasar fibroin proteins after dissolution in ionic liquid

Water soluble silk fibroin protein inside gland of silkworm has silk I (random coil) conformation but during spinning by silkworm through spinnerette a shear force is applied that changes its conformation from random coil to β-sheet. Degummed silk fibroin cocoon fibers having β-sheet conformation change to random coil after dissolution in solvent. To study the conformation of tasar fibroin protein after dissolution in ionic liquid, FTIR analysis was performed. The bands positioned at 1645, 1535 and 1260 cm^{-1} are characteristic of random coil conformation.
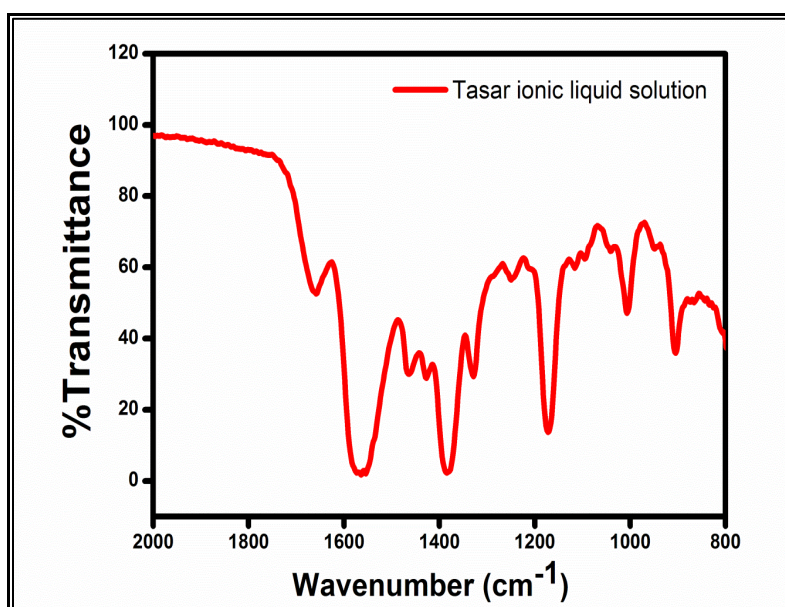
Figure 5.2.3: FTIR analysis of tasar fibroin protein after dissolution

5.2.3.2 Electrospinning

In the present study we have varied two process parameters such as concentration and voltage in order to prepare the nanofibrous mat. After electrospinning each sample is collected and morphology of these samples was analyzed by SEM. The diameter of these nanofibers was analyzed by using image J software. About 30 images of fiber

diameter distribution were taken from different places at same magnification to plot the histogram for each sample.

(i)   Effect of concentration

Concentration is one of the most important parameter that has profound effect on electrospinning of solution. SEM images of fiber spun at various concentrations are shown in Figure 5.2.4. At low concentration of tasar ionic liquid solution (5% w/v) beaded morphology of nanofibers was obtained (Figure 5.2.4a). This is due to the fact at very low concentration molecular entanglement is not sufficient that results in breaking of jet before reaching the collector. As we increase the concentration of tasar fibroin protein up to 7% w/v, nanofibers were formed but there was lack of uniformity. The diameter of fibers ranges from 200 to 1400 nm with average diameter of 800 nm (Figure 5.2.4.b). On further increase in concentration of tasar fibroin protein up to 10% w/v, uniform flat morphology of tasar fibroin nanofibers was obtained. This is due to the fact that the viscosity of tasar fibroin-ionic liquid dope solution was sufficiently high (1532 cP) with sufficient molecular entanglements which prevent breaking of electrically driven jet & allow electrostatic forces to further stretch the jet & draw it into fibers during electrospinning that results in bead less fiber morphology. The average fiber diameter of 10% (w/v) tasar fibroin ionic liquid solution was found to be 900 nm (Figure 5.2.4.c) at voltage of 15 kV. As the ionic liquid does not evaporate during flight reaching to collector so a wet jet falls on the collector submerged in methanol (80% v/v) solution resulting in flat morphology of nanofibers instead of round one.
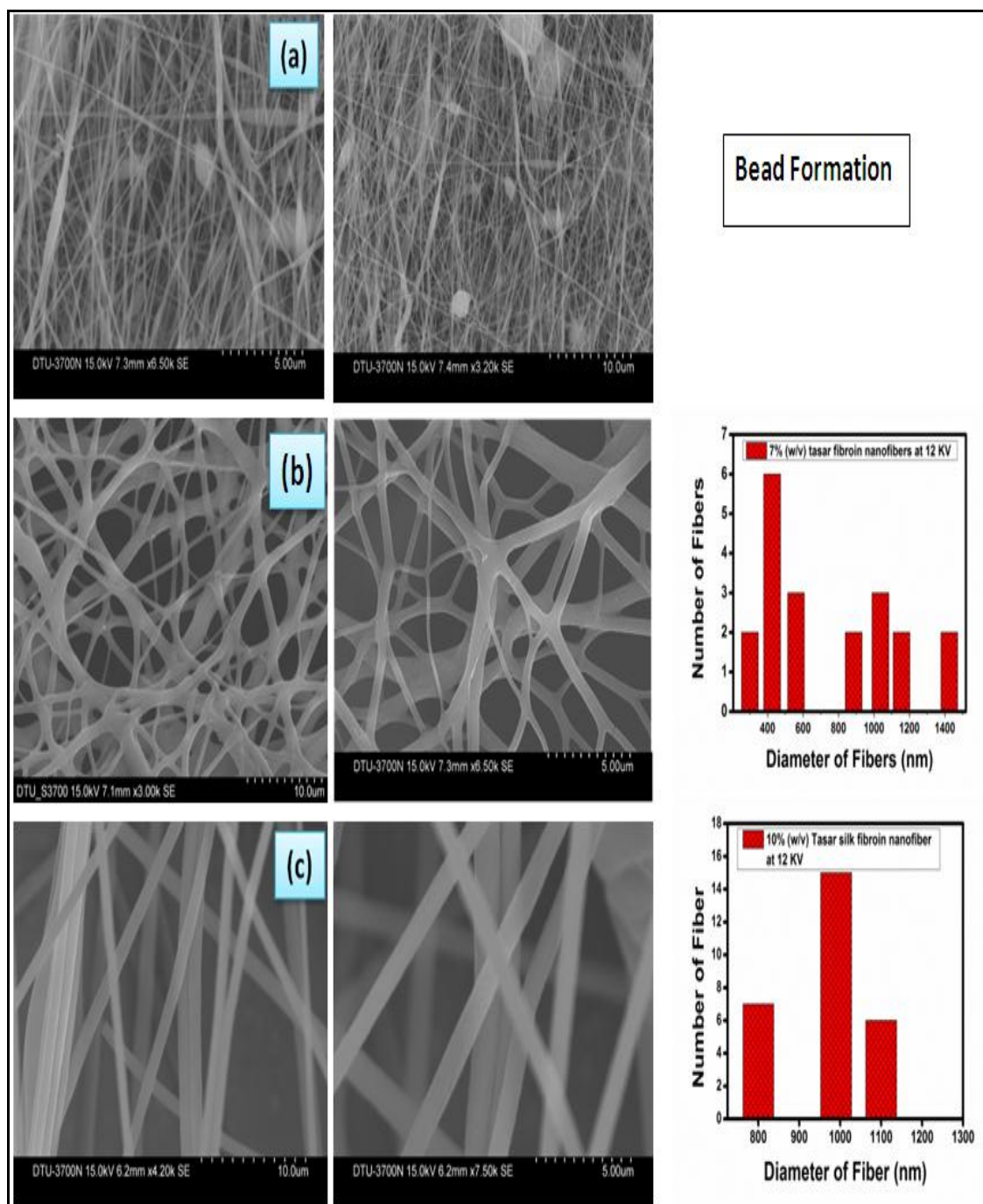
Figure 5.2.4: SEM images of tasar fibroin nanofibrous mat prepared from: (a) 5% (w/v), (b) 7% (w/v) and (c) 10% (w/v) tasar fibroin-BMIMAc solutions

(ii) Effect of voltage

Figure 5.2.5 shows that for 10% w/v tasar silk fibroin dope solution the fiber diameter ranges from 200 to 1300 nm with an average of 900 nm when 15 kV voltage was applied. As we increase the voltage from 15 to 20 kV, the average diameter of tasar fibroin nanofibers decreased up to 700 nm.
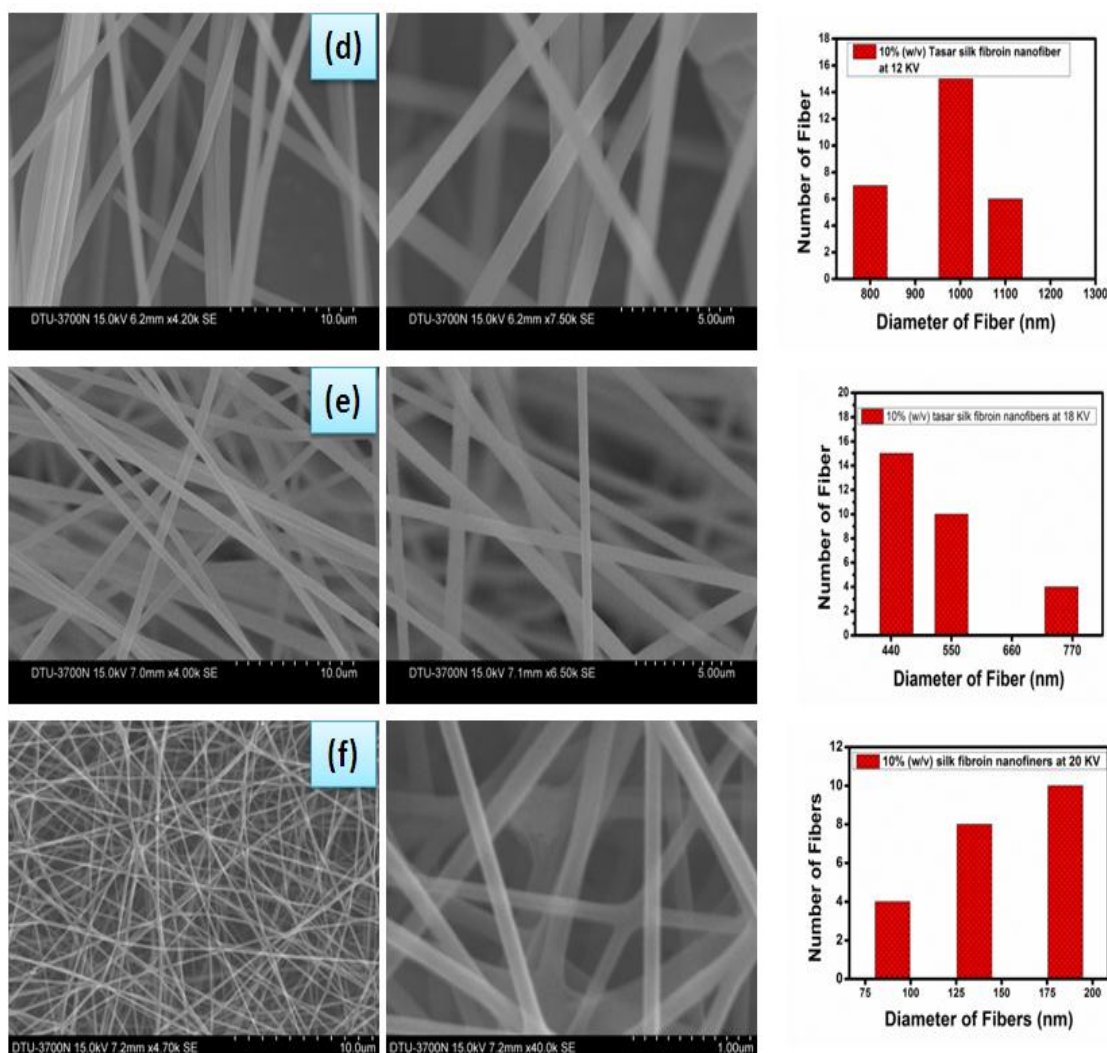
Figure 5.2.5: SEM images of tasar fibroin nanofibrous mat prepared from 10% (w/v) tasar fibroin-BMIMAc solution with: (d) 15 kV, (e) 20 kV and (f) 25 kV applied electric potential

This is due to the fact that at critical voltage surface tension is overcome by applied electrical potential and causes stretching of jet before reaching the collector. Further

increase in voltage to 25 kV, results in reduction of average diameter of nanofibers to 185 nm due to more stretching of electrically driven jet that result in narrow morphology of the nanofibers [33]. It is clearly evident that nanofibers are randomly oriented & has interconnected and porous morphology.

5.2.3.3 Characterization of silver nanoparticles

Bioreduction of silver ions to silver nanoparticles as function of time was carried out by UV-VIS spectrophotometer at room temperature. Figure 5.2.6(a) shows the UV-VIS spectra of silver nanoparticles aqueous solution at different time interval.
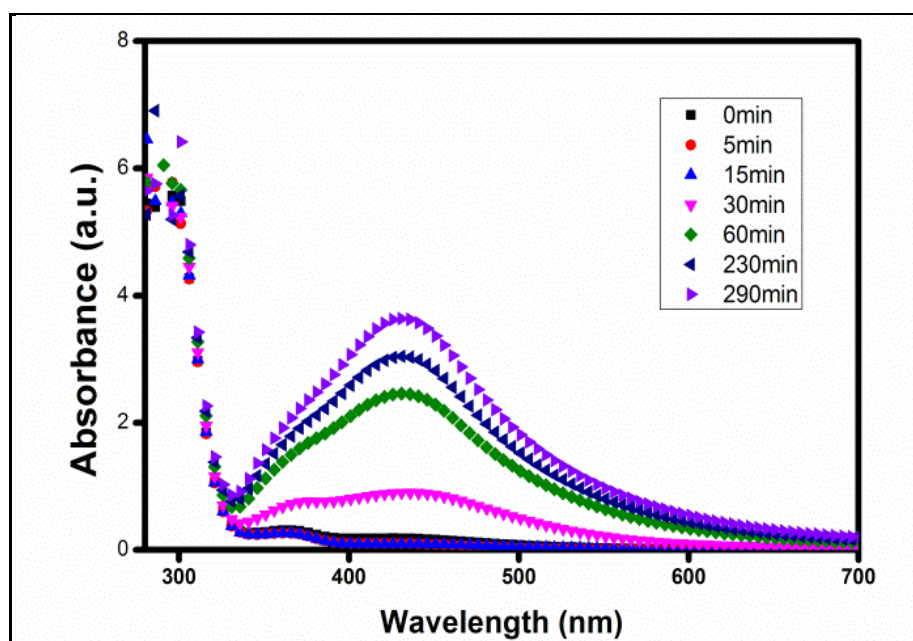
Figure 5.2.6(a): Kinetics of silver nanoparticle formation by UV-VIS spectroscopy

The characteristic absorption band at 420 nm is observed after 5 min of reaction between *Tridax procumbens* leaf extract and silver nitrate solution. The intensity of absorption band at 420 nm increases with time. With increase in reaction time up to 290 min, absorption intensity increases steadily, this indicates continuous reduction of silver ions to silver nanoparticles.

Figure 5.2.6(b) shows that color of reduced silver solution gradually turned from light yellow to dark brown with reaction periods of 5 to 290 min, further indicating the generation of silver nanostructure. This characteristic color variation is due to the excitation of the surface plasmon resonance in the metal nanoparticles.

Figure 5.2.6(b): Change in colour with time due to the formation of silver nanoparticles

The morphology of synthesized silver nanoparticles was characterized by high resolution transmission electron microscopy (HR-TEM). Figure 5.2.7 represents high resolution TEM images of synthesized silver nanoparticles. The prepared silver nanoparticles are nearly spherical in shape. Particle size of synthesized silver nanoparticles is in range from 5-45 nm. The crystalline structure of silver nanoparticles was further analyzed by X-ray diffraction.
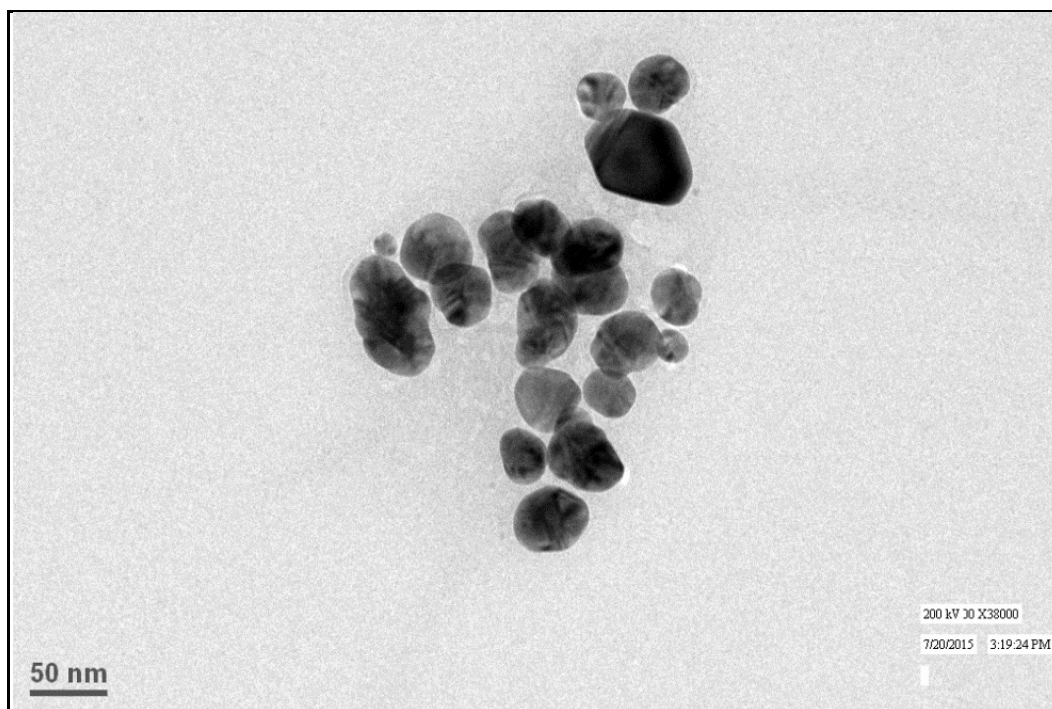
Figure 5.2.7: HR-TEM image of silver nanoparticles

Figure 5.2.8 shows the XRD pattern of the synthesized silver nanoparticles. The pattern shows the peaks at (2θ) 38.18°, 44.42°, 64.18° and 70.38° corresponds to (1 1 1), (2 0 0), (2 2 0) and (3 1 1) planes, respectively with the majority of particles showing (1 1 1) plane having face centered cubic (fcc) structure. The average crystal size of synthesized silver nanoparticles calculated by the Debye-Scherrer equation was found to be 20 nm ± 2nm.

It was observed that the silver nanoparticles solution was extremely stable for several days with only a little aggregation of particles in solution. Stability of nanoparticles in solution is due to its capping with biomolecules of plant extract as suggested in scheme VI and VII. The biomolecules can provide a good protecting environment for metal hydrosol during their growth processes [193].

Reference Code. 00-003-0921
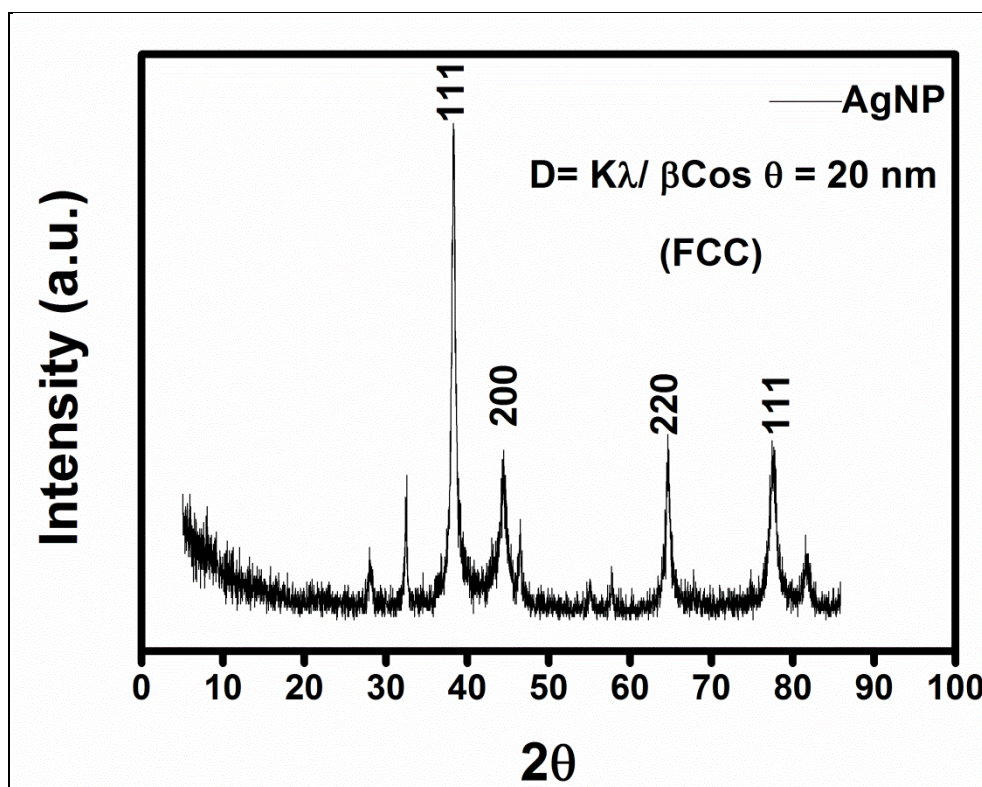
Figure 5.2.8: X-ray diffractogram of silver nanoparticles

FTIR spectroscopy of leaf extract solution was performed to know the functional groups present in active ingredients of leaf extract that actively take part in capping of AgNPs [194,195]. FTIR spectra of fresh leaf extract and after the treatment of $AgNO_3$ are shown in Figure 5.2.9. The FTIR spectrum of leaf extract shows significant absorption bands at 3258, 1640, 1389, 1172 cm^{-1}. The broad absorption band at 3358 cm^{-1} is because of O–H stretching of a phenol group in biomolecules present in plant leaves such as luteolin molecules. Similarly the band at 1640 cm^{-1} indicates conjugated carbonyl group. In the fingerprint region, the band at 1389 cm^{-1} corresponds to in-plane O–H bending of polyphenols, the band at 1070 cm^{-1} is because of C–O stretching of polyphenols (which usually appeared at 1075 and 1025 cm^{-1} for phenol). The presence of the above band indicates that the leaf extract having

multiple substituted aromatic rings (polyphenol) may be responsible for capping of silver nanoparticles. The functional group and finger print region shows the band pattern that is similar to polyphenols as specified by Chuan-xiang and Shao-lin [196].
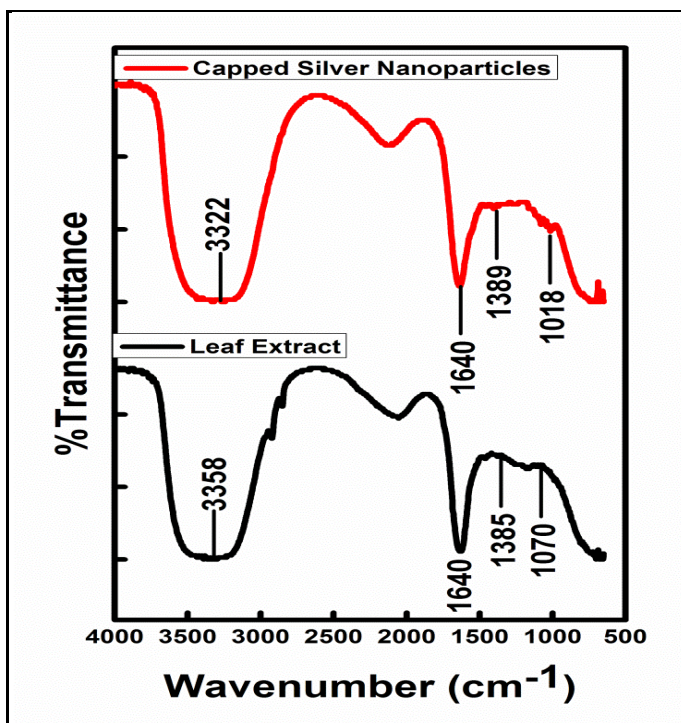
Figure 5.2.9: FTIR spectra of leaf extract and capped silver nanoparticles

FTIR spectrum of capped silver nanoparticles is shown in the Figure 5.2.9. FTIR spectrum of capped silver nanoparticles shows major bands at 3322, 1622, 1385 and 1018 (cm^{-1}). The biomolecules (polyphenols) present over the surface of silver nanoparticles act as capping agent. This suggests that the biological molecules could possibly perform dual functions of formation and stabilization of silver nanoparticles in the aqueous medium.

It is reported that biomolecules of plant extract are responsible for reduction and capping of silver nanoparticles. The possible mechanism of the reduction of Ag$^+$ to Ag° and capping of synthesized silver nanoparticles is shown in scheme VI and VII.

$$2Ag^+ + 2e^- \rightarrow Ag^0$$

$$2H^+ + 2e^- \rightarrow H_2$$

$$2Ag^+ + H_2 \rightarrow 2Ag^0 + 2H^+$$
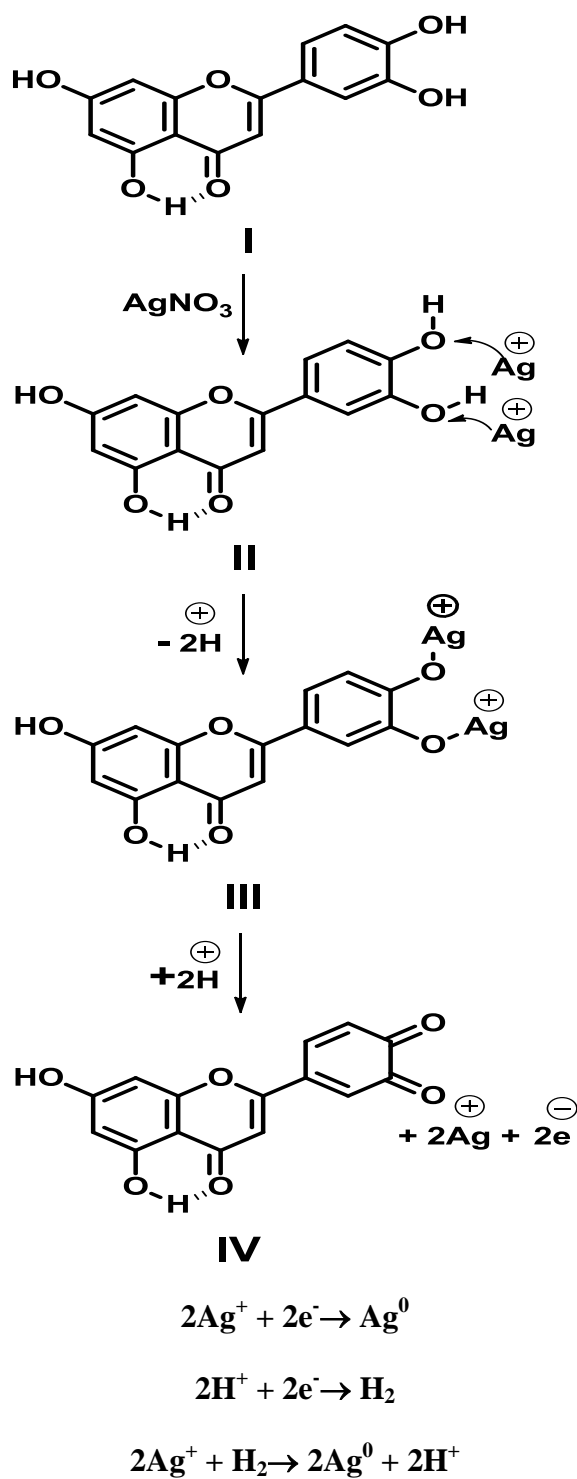
Scheme VI: Mechanism of silver nanoparticles formation by luteolin
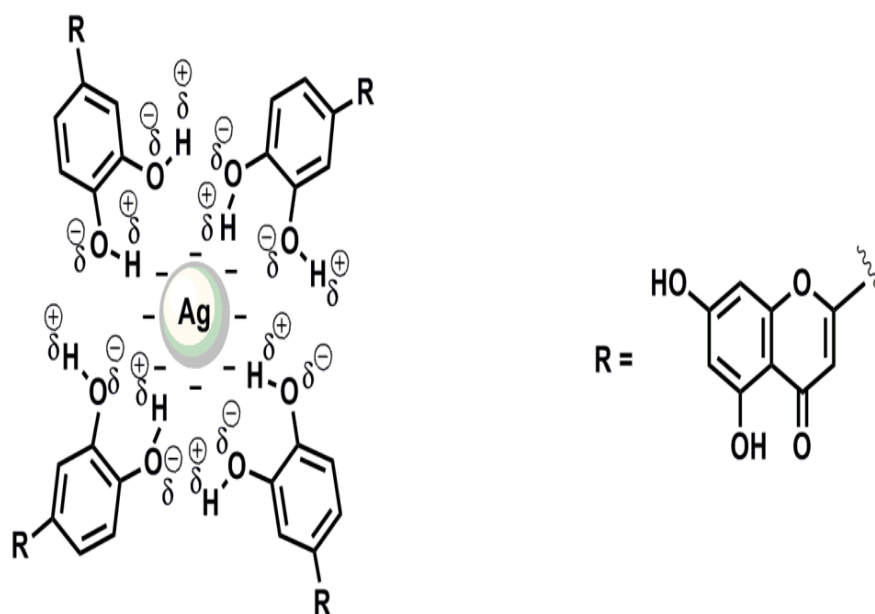
Scheme VII: Probable capping effect of luteolin (polyphenols) compound

5.2.3.4 Morphology of tasar nanofibrous mat after coating with silver nanoparticles

Deposition of silver nanoparticles on the surface of tasar nanofibrous mat was evaluated by FE-SEM (Figure 5.2.10). Micrographs show that silver nanoparticles are uniformly deposited over the surface of tasar nanofibrous mat. The size of the nanoparticles deposited on the surface of the nanofibers is in the range of 5-45 nm. However, in some portion of the fiber surface, aggregation of nanoparticles also appeared. Silver nanoparticles coated tasar nanofibrous mats are also porous in nature, i.e. apparent porosity does not get affected by deposition of silver nanoparticles.
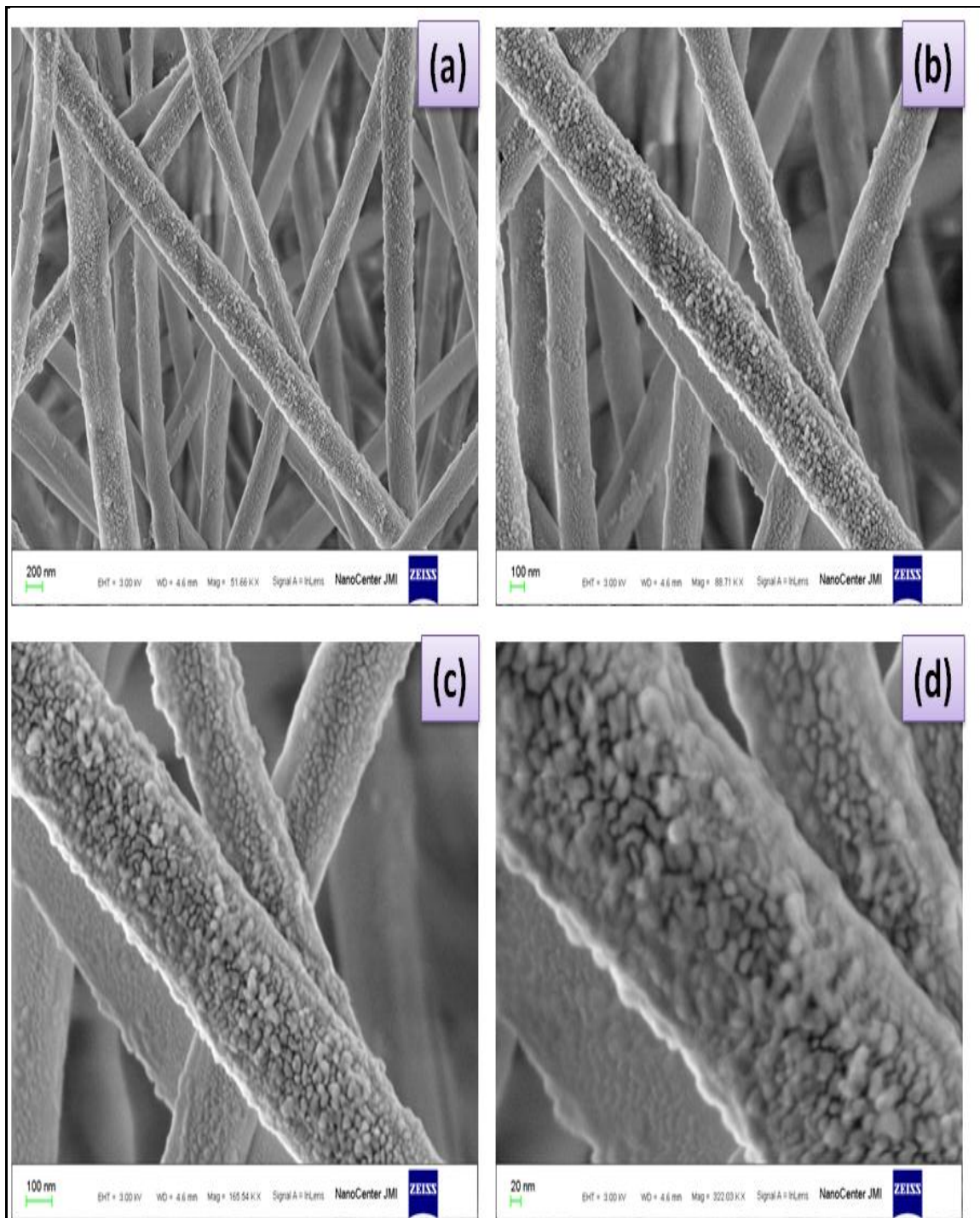
Figure 5.2.10: FESEM images of tasar fibroin nanofibrous mat coated with AgNPs at different magnification (a-d)

5.2.3.5 EDX and EDX mapping analysis of silver nanoparticles coated tasar nanofibrous mat
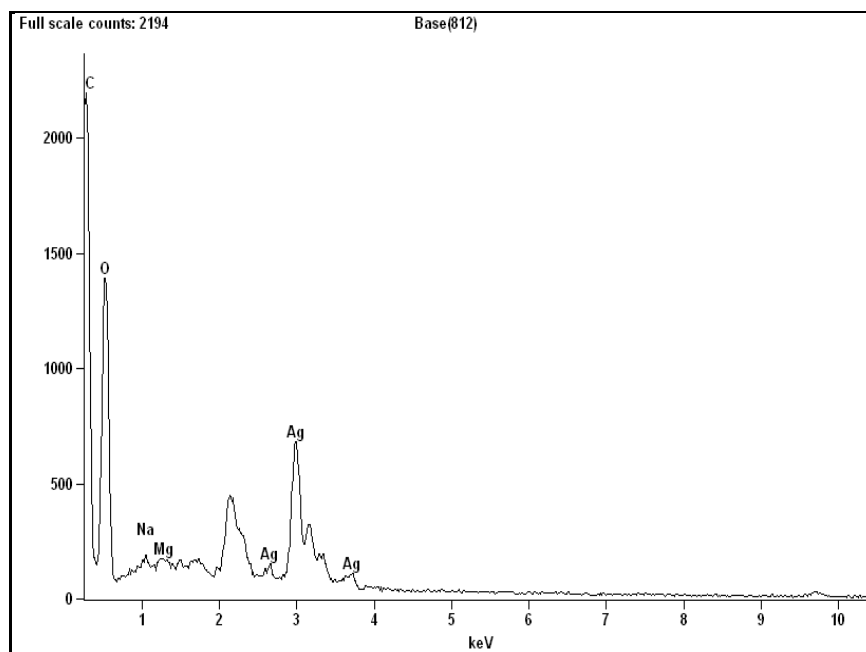
Figure 5.2.11: EDX of silver nanoparticles coated tasar nanofibrous mat

Deposition of the silver nanoparticles on the surface of tasar nanofibrous mat was further confirmed through EDX and EDX mapping. Figure 5.2.11 showed a peak at 3 keV which confirms the deposition of silver nanoparticles on the surface of tasar nanofibrous mat. Deposition of silver nanoparticles on the surface of tasar nanofibrous mats were further confirmed by EDX mapping analysis. EDX mapping analysis of silver nanoparticles coated tasar nanofibrous mat showed that silver nanoparticles are uniformly deposited on the surface of nanofibrous mat which is indicated by purple color dots in Figure 5.2.12. The deposition of silver nanoparticles on the surface of nanofibrous mat will provide fast delivery of AgNPs to wounding surface having initial high loading of microorganism.
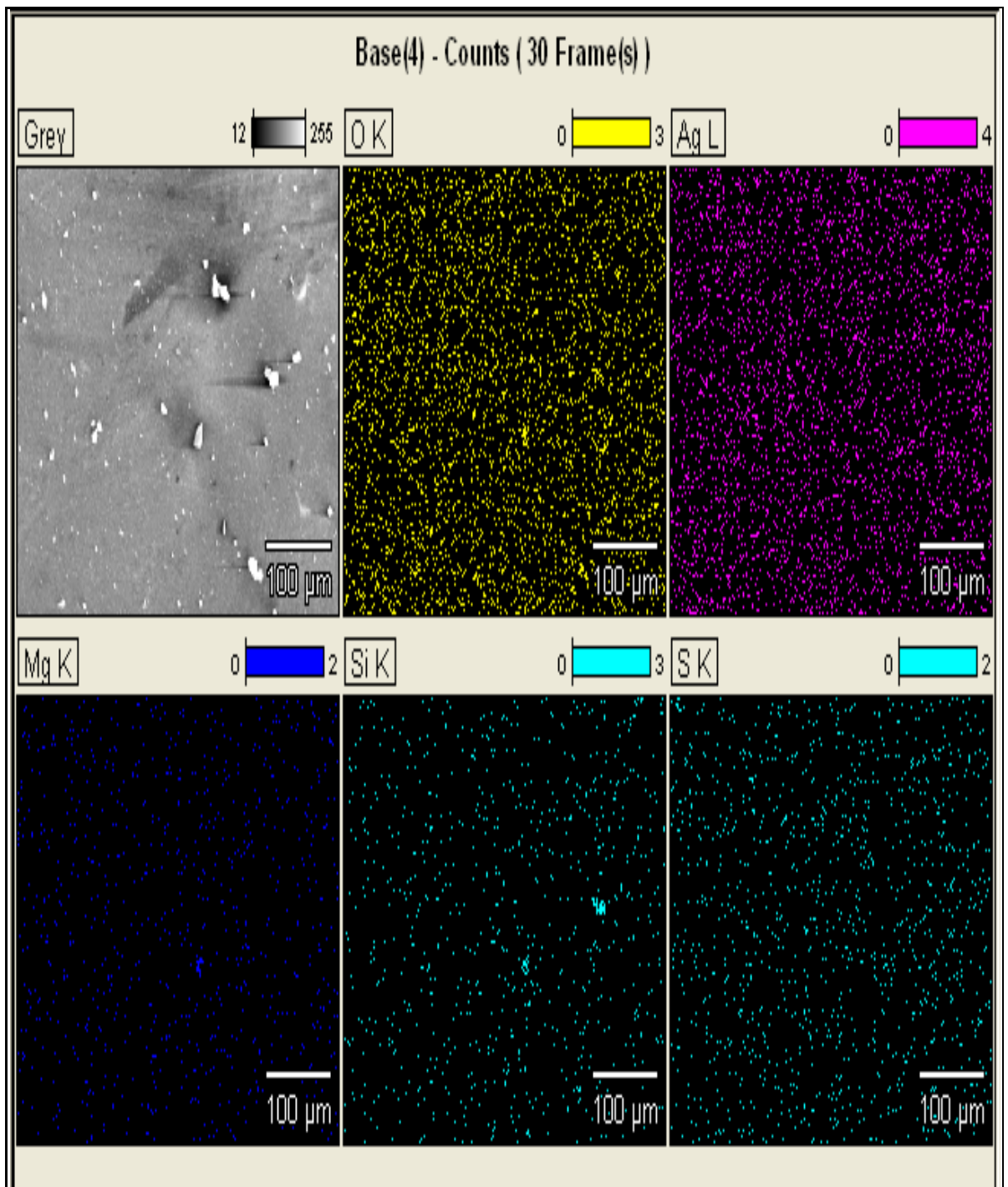
Figure 5.2.12: EDX mapping of silver nanoparticles coated tasar nanofibrous mat

5.2.3.6 Mechanical Properties of tasar nanofibrous mat

Appropriate mechanical strength of tasar nanofibrous mats are critical for their successful application as wound dressings and skin tissue engineering applications [188]. Tasar nanofibrous mat exhibit higher extensibility with tensile strength and modulus values of 12 MPa and 35 MPa respectively. The elongation at break value of nanofibrous mat was found to be 28 mm. The tensile strength and modulus values of tasar nanofibrous mat is slightly higher as compared to muga nanofibrous mat that we have discussed in our previous chapter. This silver nanoparticles coated tasar nanofibrous mats have enough extensibility and flexibility compared to commercial cellular grafts so it can be utilized as wound dressing material in load bearing areas such as knee and joints [189].

5.2.3.7 Structural characterization of silver nanoparticles coated nanofibrous mat

The mechanical and biological properties of silk fibroin proteins depend on its conformation. Native silk fibroin fibers have β-sheet conformation which is responsible for its good mechanical properties. The regenerated silk fibroin films having random coil conformation are mechanically unstable and easily dissolved in aqueous environment. Therefore these films coagulate in methanol to induce crystallinity. The conformation of tasar fibroin protein after regeneration and coagulation was evaluated by FTIR [190].

FTIR spectra of AgNPs coated tasar nanofibers are shown in the Figure 5.2.13. The bands centered at 1616, 1521 and 1225 cm^{-1} are due to stretching of peptide bonds in amide I, II and III region. These bands are characteristics of β-sheet conformation. This indicates that during coagulation of nanofibrous mat in methanol its

conformation changes from random coil to β-sheet and deposition of silver nanoparticles does not affect its conformation.
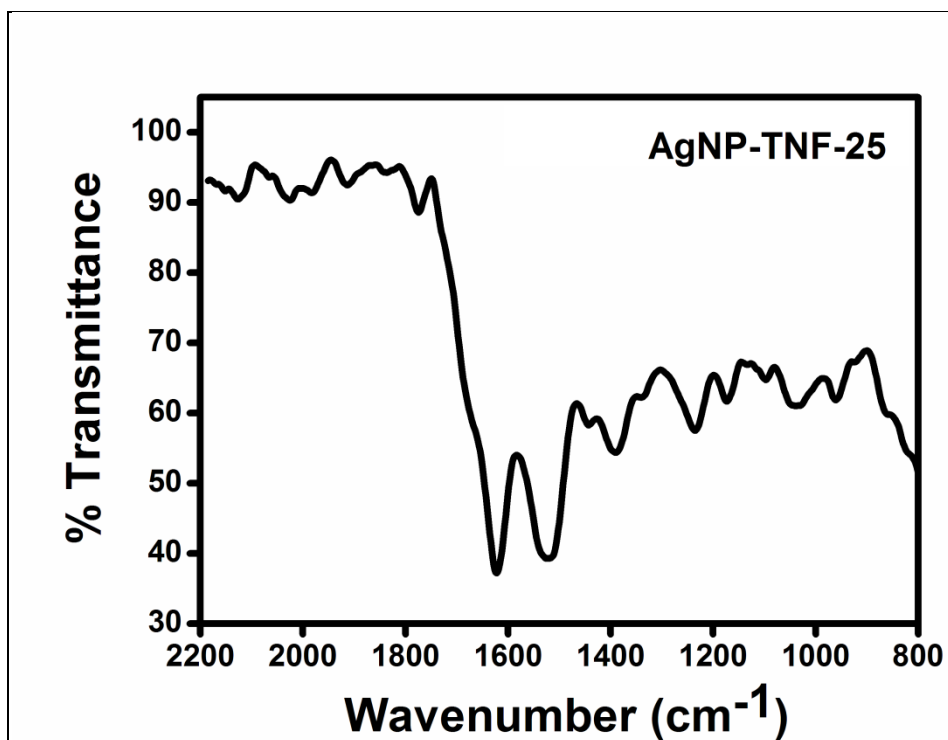
Figure 5.2.13: **FTIR analysis of AgNPs coated tasar fibroin nanofibrous mat prepared from 10% (w/v) tasar fibroin-BMIMAc solution at 25 kV applied electric potential**

5.2.3.8 Porosity, pore size and surface roughness

Porosity is very important factor for a material to be used as a wound dressing or tissue engineered scaffold. A porous material provides larger surface area that favors adherence and growth of seeded cells due to ease passage of nutrients and metabolites which is very important for growth of neo-tissues [36]. Porosity measurement of the silver nanoparticles coated tasar silk fibroin nanofibers mat was performed by liquid displacement technique. Hexane was used as displacement liquid due to its non-polar characteristic it easily penetrates through interconnected pores without any significant

swelling or shrinkage. Silver nanoparticle coated tasar nanofibrous mats showed average porosity of 80%.

Porosity, pore size and average roughness of silver nanoparticles coated tasar silk fibroin nanofibrous mat was further analyzed by AFM and the results are presented in Figure 5.2.14 (a & b) and Table 5.2.1. AFM analysis shows that the tasar nanofibrous mat & silver nanoparticles coated tasar nanofibrous mat is highly porous in nature with well interconnected network having pore size of 250-550 nm.
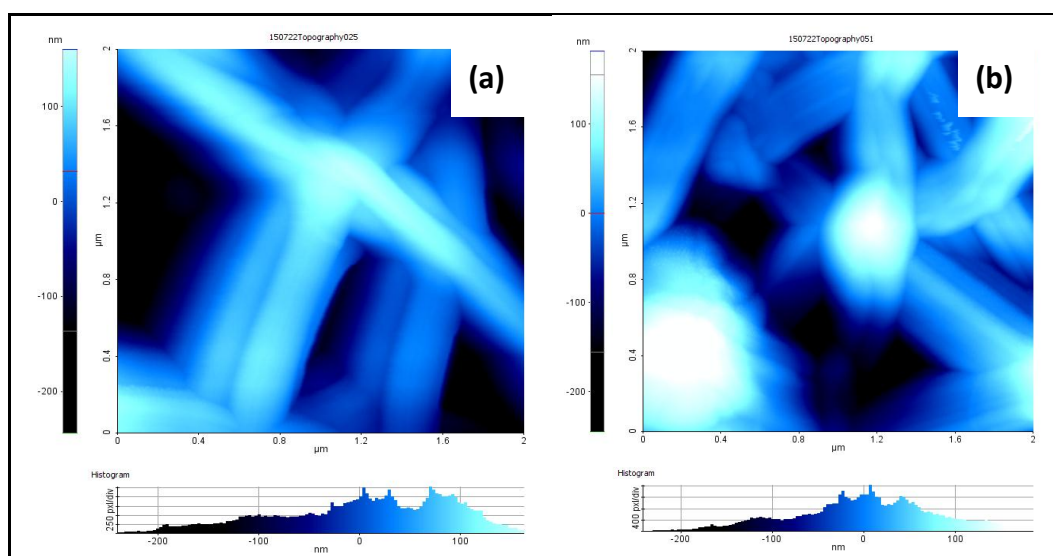
Figure 5.2.14: AFM images of (a) tasar nanofibrous mat and (b) silver nanoparticles coated nanofibrous mat

The nanophase roughness of silver nanoparticles coated tasar nanofibrous mat is slightly higher (38 nm) as compared to tasar nanofibrous mat (30 nm). The nanophase roughness and porosity play a very important role in adherence, growth and proliferation of cells to develop neo-tissue due to ease transport of nutrient, metabolites, permeation of water vapor as well as migration of cells for successful development of skin substitute.

Table 5.2.1: Surface roughness of tasar nanofibrous mat and silver nanoparticles coated nanofibrous mat

S. No.	Samples	Surface roughness	
		RMS (nm)	Ra (nm)
1	Tasar nanofibrous mat	26	22
2	AgNPs coated Tasar nanofibrous mat	30	26

5.2.3.9 Water vapor permeability

Water vapor permeability of materials used as wound dressing should be optimum because a high water vapor transmission rate causes dehydration of wound while low water vapor permeation would result in development of exudates on the surface of wound. The WVTR of silver nanoparticles coated tasar nanofibrous mat is 2300 $g/m^2/day$. It is reported that WVTR of normal skin is 204 $g/m^2/day$ while an injured skin show different degree of WVTR which depends on type & condition of wound. It is found that WVTR of first degree, second degree and third degree wound is 278, 4274 and 3436 $g/m^2/day$, respectively [172]. Kaplan et al. [191] have found that WVTR of mulberry silk fibroin cast films is 1000 $g/m^2/day$. In our case the higher WVTR of silver nanoparticles coated tasar nanofibrous mat than that of cast films due to highly porous matrix architecture. WVTR of silver nanoparticles coated tasar nanofibrous mat is well suited for second degree wound.

5.2.3.10 Water uptake

A material used as wound dressing should absorb good amount of water so that it provides moist environment to promote healing. Water uptake is one of the most important characteristic of material used as wound dressing. Water uptake of AgNPs coated tasar nanofibrous mat is 70%, which is higher than that of nonmulberry mats prepared by Panda *et al.* [192] and commercially available wound dressing which may be due to higher porosity and surface area.
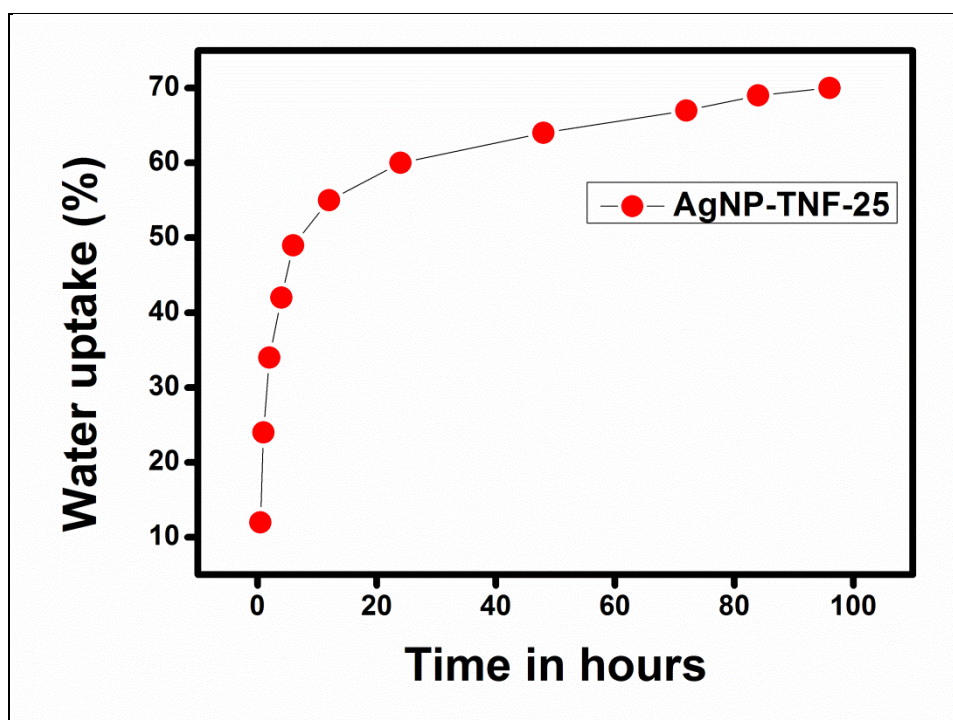
Figure 5.2.15: Water uptake of AgNPs coated tasar nanofibrous mat

5.2.3.11 Biocompatibility Test

Dermal fibroblast cells play a vital role in regeneration of wound. So it is very important to evaluate the cytocompatibility of the wound dressing materials using skin fibroblast. Adherence and growth of cells highly depend on the surface properties as well as architecture of the biomaterials used as scaffold and wound dressing.

5.2.3.11.1 Growth and viability

MTT is a colorimetric technique used to evaluate cellular metabolic activity that indicates the growth and viability of cells. MTT assay of L929 fibroblast cells seeded AgNP coated tasar nanofibrous mat (AgNP-TNF-25) was performed as a function of time and results are shown in Figure 5.2.16.

From Figure 5.2.16, it is evident that cell population increases with time for both the silver nanoparticles coated tasar nanofibrous mat and tissue culture plate. After 5 days of incubation absorbance value for silver nanoparticles coated tasar nanofibrous mat was nearly close to tissue culture plate. This higher cells proliferation was due to the higher surface area and porosity of nanofibrous mat.
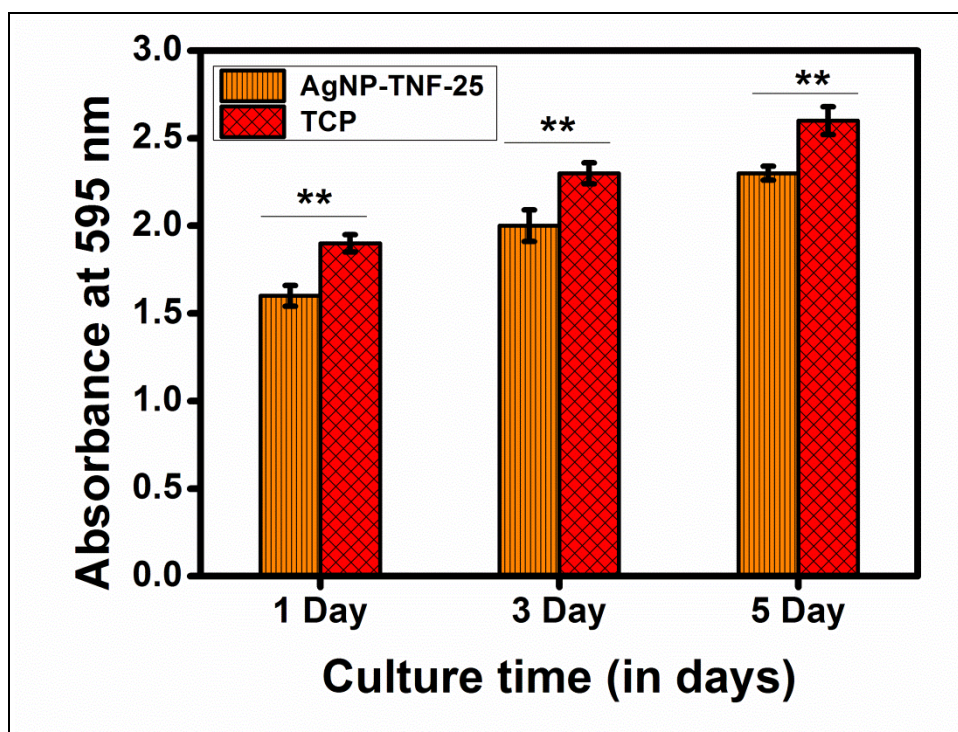
Figure 5.2.16: MTT assay of L929 fibroblast cells seeded on silver nanoparticles coated tasar nanofibrous mat (AgNP-TNF-25) after 1, 3 and 5 days of incubation. All experiments performed in triplicate and bar represented as mean±SD, ** p>0.05, significant against tissue culture plate (TCP)

5.2.3.11.2 Spreading and proliferation of L929 fibroblast cells seeded on nanofibrous mat (TNF-25) after 1, 3 and 5 days of incubation using phase contrast and fluorescence microscopy

Spreading and proliferation of L929 cells seeded on silver nanoparticles coated tasar nanofibous mat were studied by Phase contrast and Fluorescence microscopy (Figure 5.2.17).
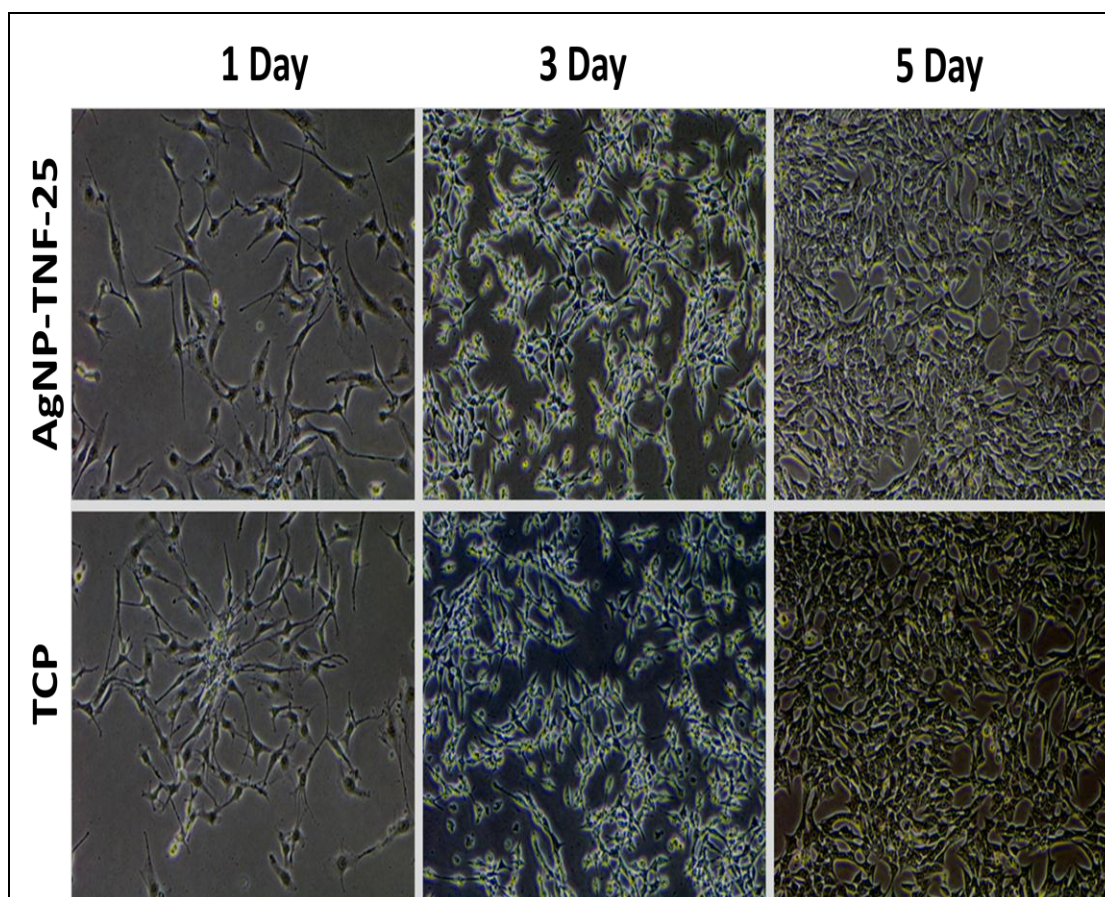
Figure 5.2.17: Phase contrast microscopic images of L929 cells seeded on silver nanoparticle coated tasar nanofibrous mat (AgNP-TNF-25) after 1, 3 and 5 days of incubation. All the experiments are performed in triplicate

Phase contrast microscopic images show that L929 cells adhered well and attain their normal morphology after one day of incubation. Cell density increases with time and attains confluence stage after 5 days of incubation. After 5 days of incubation there

was not a significant difference between silver nanoparticles coated tasar nanofibrous mat and tissue culture plate (p>0.05). Adherence and proliferation of L929 cells seeded on silver nanoparticles coated tasar nanofibrous mat was further evaluated by using Fluorescence microscopy (Figure 5.2.18).
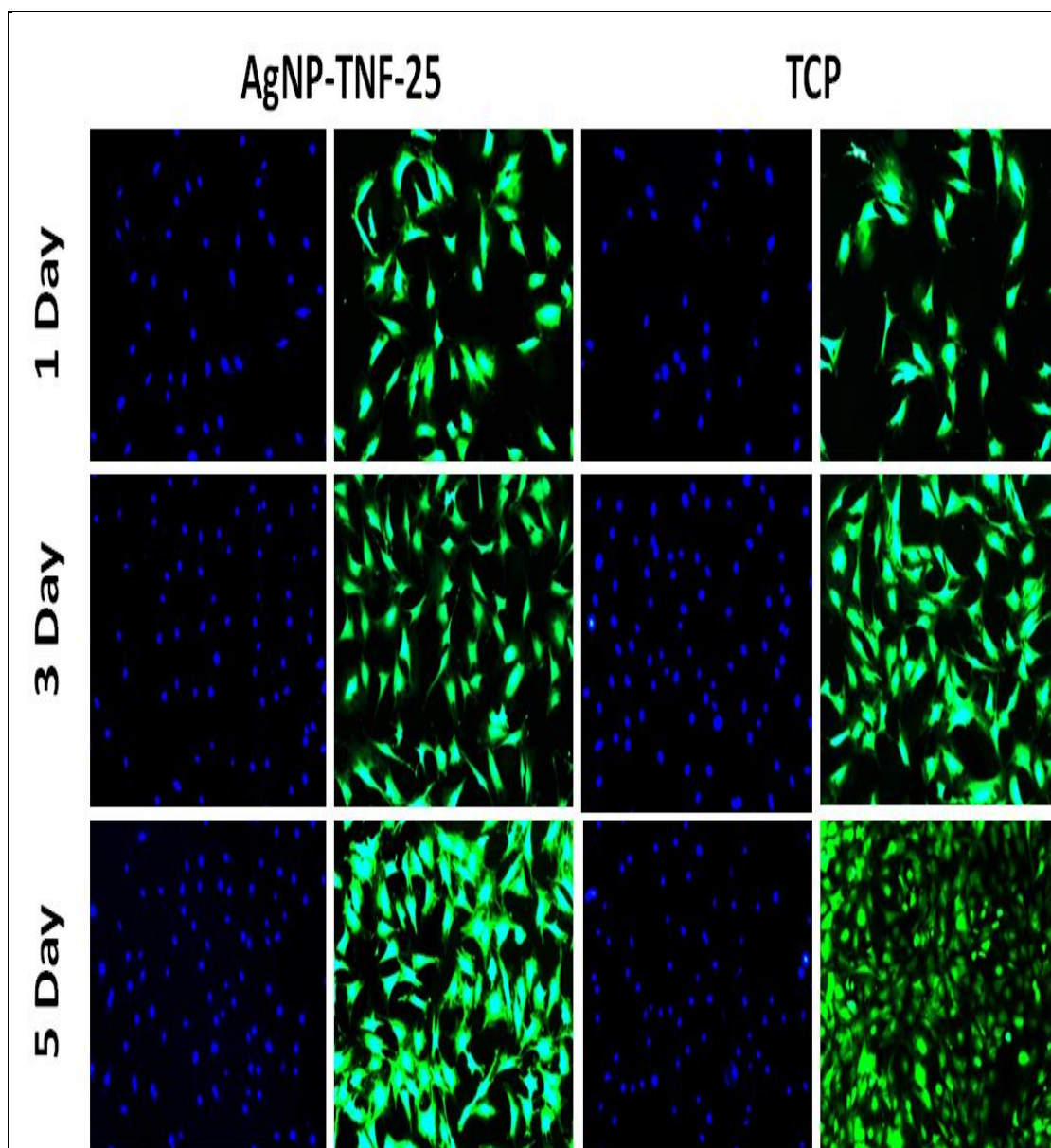
Figure 5.2.18: Fluorescence microscopic images of L929 cells seeded on silver nanoparticle coated tasar nanofibrous mat (AgNP-TNF-25) after 1, 3 and 5 days of incubation. All the experiments are performed in triplicate

Fluorescence microscopic images showed that fibroblarst cells with distinct, round nucleus were adhered though out the mat with well-defined cytoskeleton. Cells attain normal morphology after 1 day of incubation and cells population increases with time and no significant difference was found compared with tissue culture plate. Good cell growth on silver nanoparticles coated tasar nanofibrous mat is due to higher surface roughness and porosity. The porous morphology of this matrix is responsible for permeation of water vapor and gases as well as transport of essential biomolecules and nutrients that are responsible for growth of cells and promotes regeneration of wound.

5.2.3.12 Antimicrobial activity

As the wounds are highly prone to microbial attack so it is very important to add some active molecules that prevent the growth of infectious microbe and promotes healing. Here we have coat tasar nanofibrous mat with silver nanoparticles to provide antimicrobial resistance and results are shown in the Figure 5.2.19.

Antimicrobial potential of silver nanoparticles coated tasar nanofibrous mat was determined by disc diffusion assay against gram +ve and gram −ve bacteria. Silver nanoparticles coated tasar nanofibrous mat shows a prominent zone of inhibition against gram +ve (*S. aureus*) and gram −ve (*E. coli*) bacteria. Mean diameter of zone of inhibition for silver nanoparticles coated tasar nanofibrous mat was 10 and 14 mm against *S. aureus* and *E. coli*, respectively. Silver nanoparticles have good antimicrobial activity that made them a promising candidate as new generation antimicrobial agent. The mechanism of antibacterial activity of silver nanoparticles is not clearly understood. It is reported that silver nanoparticles accumulate in the

bacterial cell wall due to the formation of pet that result in increase in the permeability of cell, causing death of cell [197].
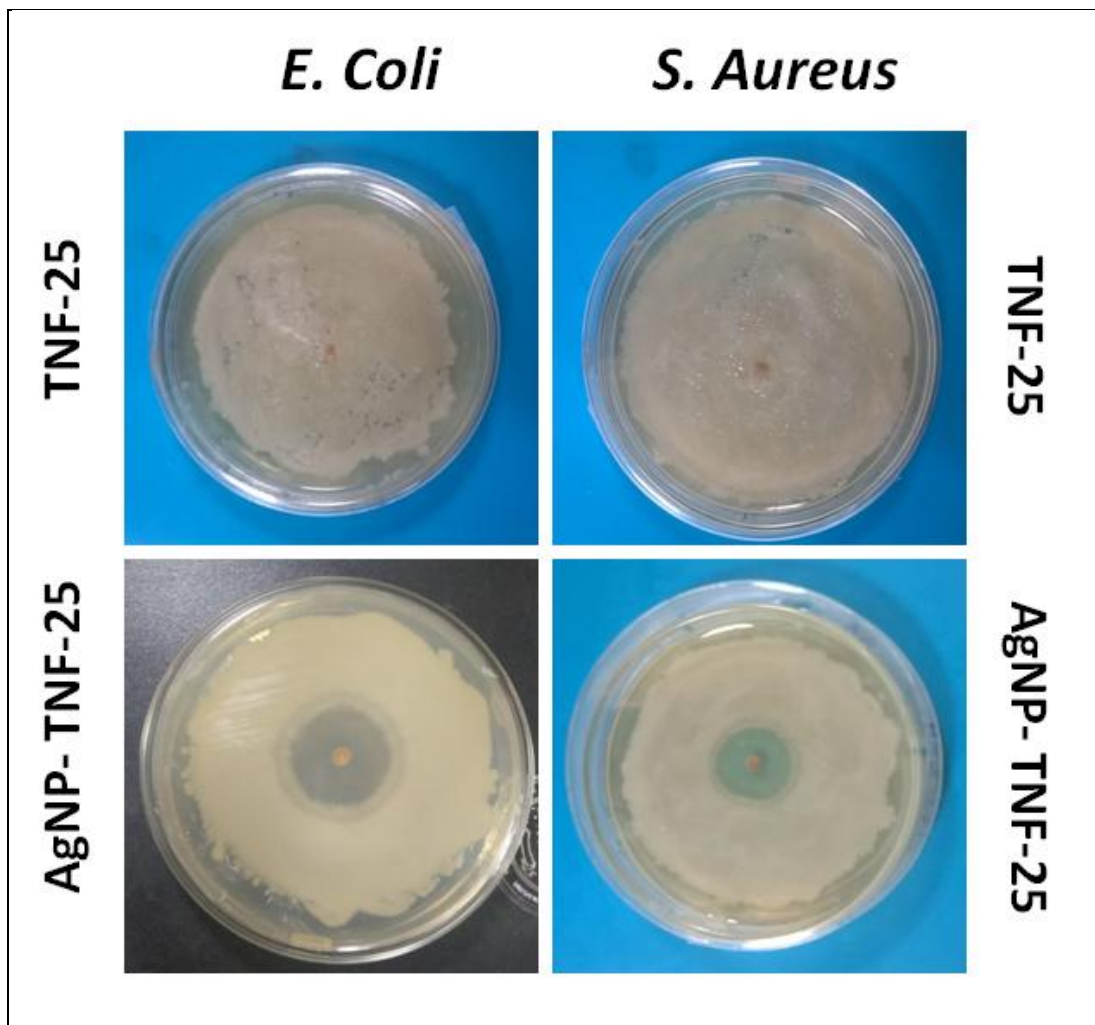
Figure 5.2.19: Disc diffusion assay of silver nanoparticles coated and uncoated TNF-25 against *E. coli* and *S. aureus*

Another proposed mechanism suggests that antimicrobial action of silver nanoparticles is closely related to their interaction with the thiol groups (-SH) of the cysteine as well as other compounds on cell wall to form (R-S-S-R) bonds in the presence of oxygen, thereby blocking respiration and causing cell death. Silver nanoparticles are able to bind irreversibly to functional group of different enzymes of cytoplasmic membrane of bacterial wall [198,199].

5.2.3.13 *In vitro* biodegradation

Biodegradation of a material used as wound dressing or scaffolds should be optimum. The rate of biodegradation of scaffolds should match with regeneration of neo-tissue because high rate of biodegradation causes build up of exudates and slow rate of biodegradation will cause stress on developing neo-tissues. *In vitro* biodegradation of silver nanoparticles coated tasar nanofibrous mat was studied by incubation in PBS with and without trypsin enzyme. The silver nanoparticles coated tasar nanofibrous mat showed controlled rate of degradation in PBS (only 6%) after 30 days of incubation. Nanofibrous mat incubated in trypsin showed significantly higher mass loss of 48% Figure 5.2.20(a). Enzymatic erosion of nanofibrous mat was further confirmed by SEM. SEM images clearly show that nanofibrous network completely destroyed and only few fibers remained after 30 days of incubation Figure 5.2.20(b).
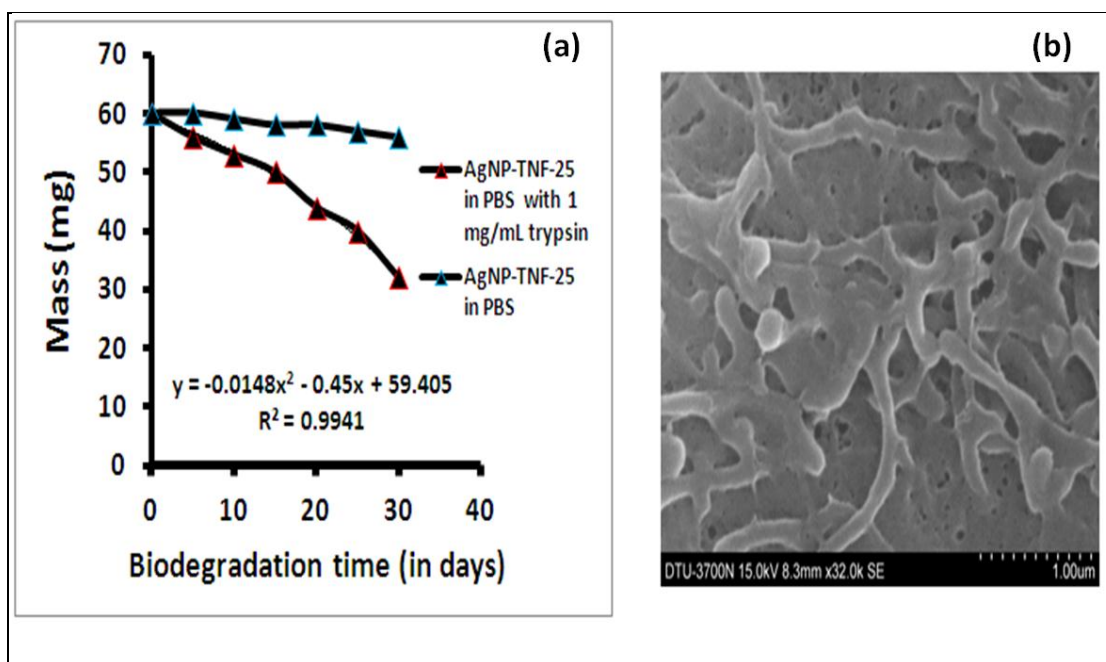
Figure 5.2.20: *In vitro* biodegradation of (a) AgNP-TNF-25 and (b) SEM micrograph of TNF-25 after 30 days of incubation in trypsin

5.2.3.14 Conclusions

In this study an effort has been made for the preparation of tasar nanofibrous mat by green route. Therapeutic efficacy of this nanofibrous mat was further enhanced by coating with silver nanoparticles. Silver nanoparticles coated tasar nanofibrous mat show good mechanical strength, water absorption with adequate porosity. The higher surface roughness, porosity and water absorption properties are responsible for higher adherence, growth and proliferation of cells that make it an excellent candidate in the field of wound dressing and regenerative medicine. Silver nanoparticles coated highly active tasar nanofibrous mat has potential to open new facile way to be utilized as therapeutic device, drug delivery vehicle, and tissue engineered constructs. From commercial point of view there is a requirement for some animal tests and clinical trial to evaluate its utility and responses *in vivo*.

CHAPTER 6

DEXTROSE PLASTICIZED TASAR AND MUGA FIBROIN FILMS FOR WOUND DRESSING

6.1 Introduction

In order to regenerate muga and tasar cocoon fibroin proteins films, the degummed cocoon fibroin fibers were dissolved in ionic liquid and regenerated by coagulating in alcohol [55]. These regenerated fibroin films are highly brittle in nature so it becomes unsuitable for wound dressing & regenerative medicine [105]. It is also observed that mechanical properties of different non-mulberry silk fibroin proteins regenerated from the cocoon have not been reported, which is very important for a material to be used as wound dressing. In the previous chapter muga cast films were prepared and found to be brittle. Regenerated silk fibroin films require flexibility to be used as wound dressing especially when they are used in load bearing areas such as knee joints & elbow joints. Beside this, to promote healing these films should provide good biocompatibility, moist environment & protection against pathogens [36,85,106].

Flexibility of biomaterial films can be improved by incorporating glucose [105], sorbitol and mannitol [200]. Lu *et* al. [201] have developed flexible mulberry silk fibroin films using glycerol. Glucose is a simple polyhydroxy carbohydrate which increases water absorbance ability of fibroin proteins from humid environment.

This chapter is focused on the regeneration of muga and tasar fibroin flexible films by incorporating dextrose. These plasticized muga and tasar fibroin films were characterized for their physical, mechanical and structural properties. The cytocompatibility and *in vitro* biodegradation of different plasticized and un-plasticized films were also determined. In order to protect the wound against

pathogens, gentamicin was further incorporated in these films. The release kinetics of gentamicin from different films was also carried out.

6.2   Experimental

6.2.1 Preparation of dextrose incorporated muga and tasar silk fibroin films

Degummed muga and tasar fibroin fibers were dissolved in the 1-butyl-3-methylimidazolium acetate (BMIMAc) ionic liquid (10% w/v) at 90 ^{o}C for 2h under nitrogen atmosphere with constant stirring. The molecular weight of tasar and muga fibroin proteins after dissolution in ionic liquid was measured with Sodium dodecyl sulphate polyacrylamide gel electrophoresis (SDS-PAGE). The molecular weight of tasar and muga proteins was found to be 195 and 230 kDa. Different concentrations of dextrose (5 to15% w/w of fibroin) were mixed with muga and tasar ionic liquid solution separately and then poured into petriplates under laminar air flow to prepare films of thickness 0.5±0.1 mm. After 2 h, methanol was added to each petriplate in order to crystallize them for 5 h. The residual ionic liquid trapped in the cast films was extracted by the protocol described earlier [116]. Briefly, aliquots were replaced continuously with fresh methanol at 12 h in each petriplate in order to extract the residual ionic liquid from muga and tasar cast films. Residual ionic liquid was checked by measuring the conductivity of the aliquots at different time intervals. Conductivity of the pure methanol and ionic liquid was 4 μS/cm and 1500 μS/cm, respectively. Initially, large amount of ionic liquid was released from cast films so conductivity of the aliquots was found to be higher, which was nearly close to the conductivity of pure ionic liquid. With time as the aliquots were replaced with fresh methanol the amount of ionic liquid released from the films reduced, finally after 96 h the conductivity of the aliquots became equal to pure methanol which indicated that there was no trace of ionic liquid released from the films.

Ionic liquid was recovered back from aliquots by evaporation of methanol at 60 $^{\circ}$C and 150 mb pressure by using rotatory evaporator. Regenerated muga and tasar films are designated as MF and TF. Dextrose modified muga and tasar films are designated as DMMF and DMTF, respectively. Amount of dextrose (in w/w) is written before the abbreviation. For example 5% dextrose incorporated muga regenerated film is designated as 5% DMMF.

6.3   Results and discussion

6.3.1. Mechanical properties

Strength and elasticity of different plasticized and un-plasticized silk fibroin films were determined in terms of tensile strength, elongation at break and Young's modulus, which are depicted in Table 6.1. Stress-strain curves (Figure 6.1) revealed that with an increase in the dextrose content from 5 to 15%, the elongation at break of muga and tasar silk fibroin increased. Further it is evident from Table 6.1 that with increase in dextrose content, tensile strength & modulus values decreased significantly, whereas elongation at break values of plasticized silk films increased sharply as compared to un-plasticized films. Highly brittle and hard films showed higher tensile strength, modulus and low elongation at break while flexible films show lower tensile strength, modulus and higher elongation. Many studies revealed that flexibility of protein and polysaccharide films can be increased by the incorporation of hydrophilic molecules [200,201]. These hydrophilic molecules break the inter-chain interactions and establish new interaction with the polymer chains. Being hydrophilic in nature, dextrose attracts the water molecules from surrounding environment that increase the inter-chain space between polymer molecules. Similarly, we found that elasticity of dextrose plasticized mulberry silk fibroin films

increased by increasing dextrose content. Lu *et* al. [201] have prepared glycerol blended mulberry silk fibroin films and found that glycerol is very effective to act as plasticizer that increase the flexibility of mulberry fibroin films. Kawahara *et* al. [202] studied the effect of water plasticization on the flexibility of mulberry silk fibroin films.
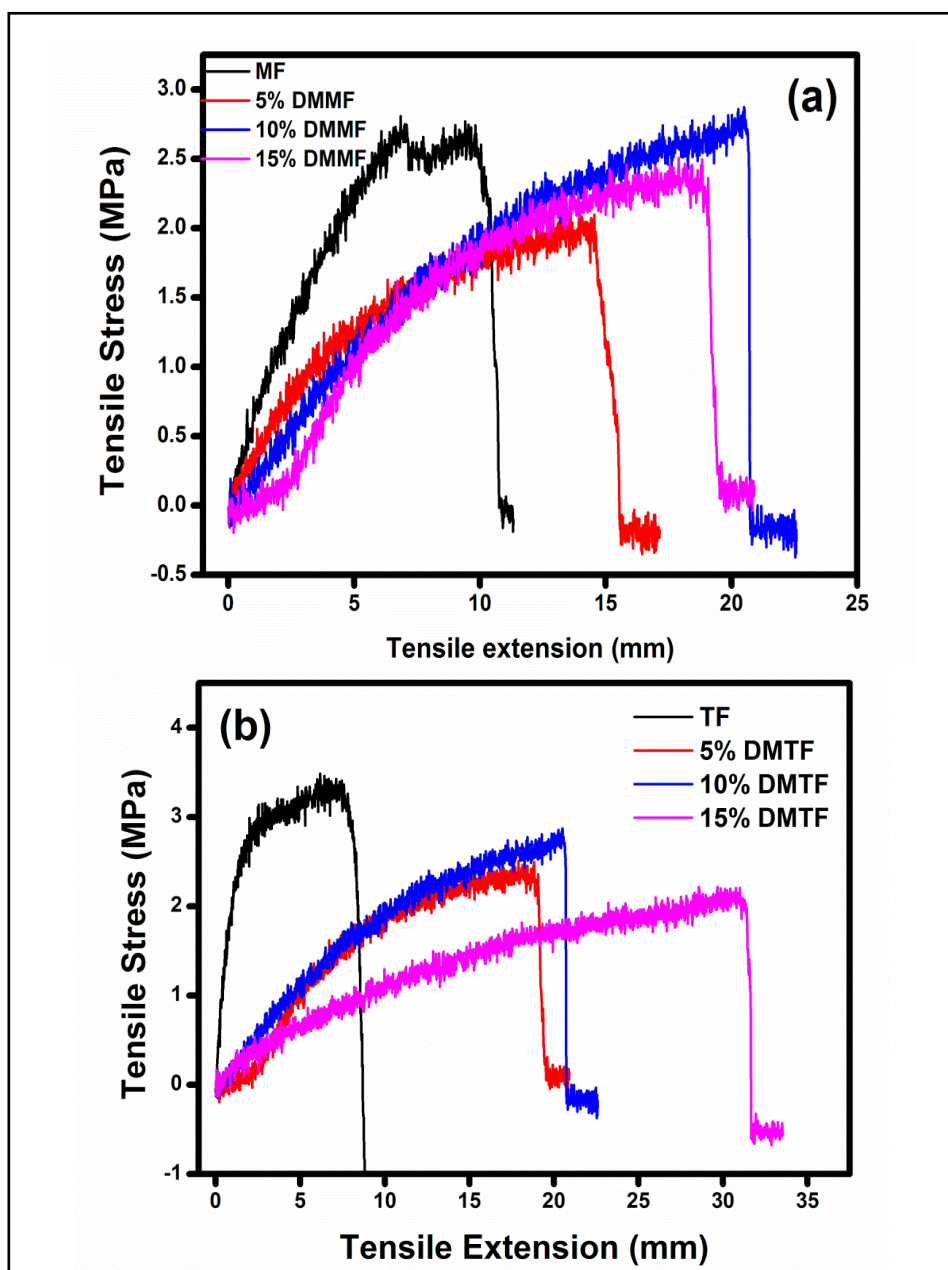
Figure 6.1: Stress-strain curves of different (a) muga and (b) tasar fibroin films

Table 6.1: Mechanical properties of dextrose modified muga and tasar fibroin films, Data were represented as mean±SD for n=3

Sample Name	Tensile Strength (MPa)	Tensile Modulus (MPa)	Extension at Break (%)
MF	2.8±0.3	24±2	12±1.7
5% DMMF	2±0.4	15±2.5	18±1.6
10% DMMF	2.5±0.25	13±1.5	21±1.5
15% DMMF	2.3±0.3	11±1.2	23±2.1
TF	3.2±0.32	30±1.6	7±2.4
5% DMTF	2.3±0.26	18±1.8	19±1.5
10% DMTF	2.7±0.28	14±2	25±2
15% DMTF	2±0.27	12±1	32±2.5

Plasticization effect of dextrose on the muga and tasar fibroin films were further confirmed by measuring the tan δ peak at different temperatures using dynamic mechanical thermal analyzer. The results are shown in Figure 6.2. The tan δ peaks for TF and MF were found at the temperature of 228 and 224 ^{o}C respectively.

As we incorporated dextrose, the peak shifted towards lower temperature region and was observed at 218 and 210 ^{o}C, for 15% DMTF and 15% DMMF, respectively. This behavior was observed due to increase in segmental mobility of muga and tasar fibroin molecules as the amount of bound water increased by dextrose plasticization. As shown in the schematic representation (Figure 6.3), dextrose molecules absorb water from the environment that increases interchain space which results in increased segmental mobility of fibroin molecules. The higher glass transition temperature of the un-plasticized muga and tasar fibroin was associated with limited polymer chain mobility due to the presence of strong secondary forces such as hydrogen bonds in amorphous motifs. These findings are concurred with results reported by Yuon *et* al.

[203]. They found that tan δ peak of mulberry silk fibroin films shifted from 195 to 162 °C as the initial water content increased from 6 to 13 wt%.
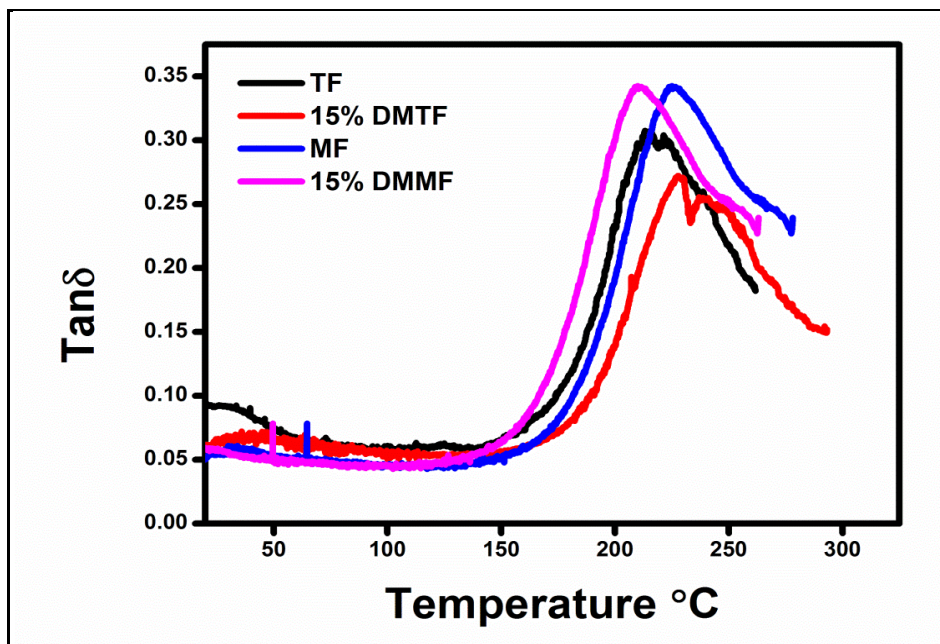
Figure 6.2: Tan δ curves of different muga and tasar fibroin films
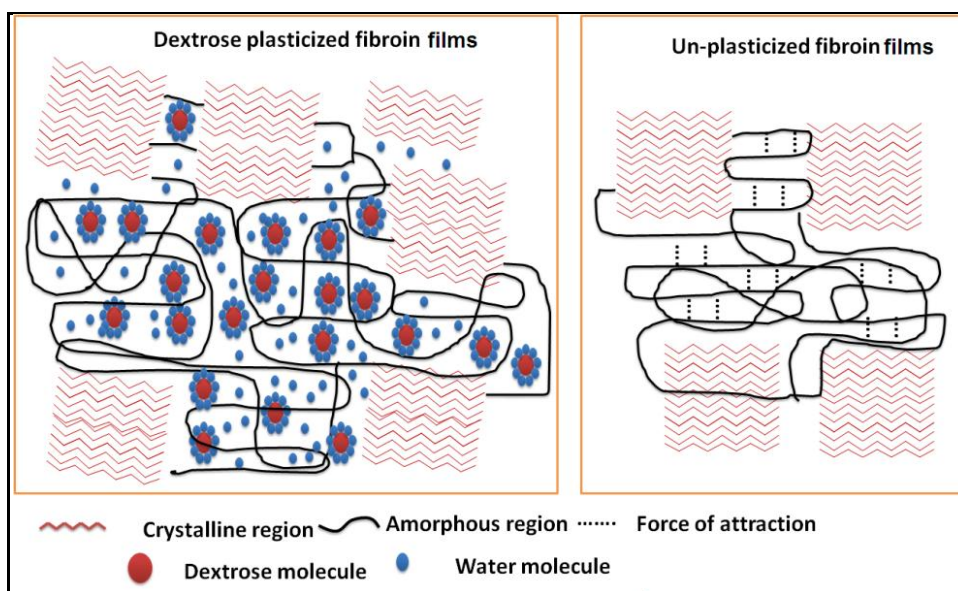
Figure 6.3: Schematic representation for dextrose plasticized and un-plasticized silk fibroin films

6.3.2 Morphological characterization

Surface morphology of different plasticized and un-plasticized muga and tasar silk fibroin films was analyzed by scanning electron microscope. The SEM images of different films are shown in Figure 6.4. Regenerated muga (MF) and tasar (TF) films showed comparatively smooth surface morphology (Figure 6.4 a&e) as compared to dextrose incorporated films.
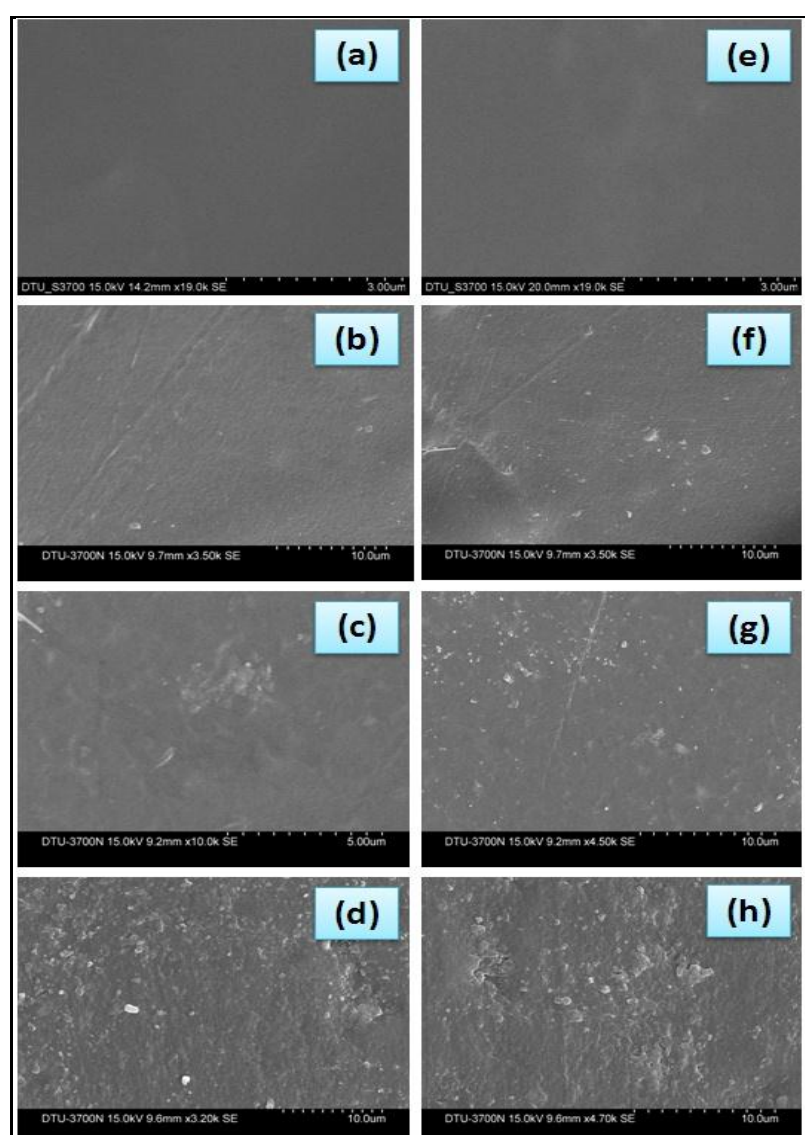
Figure 6.4: SEM images of different muga and tasar fibroin films (a) MF, (b) 5% DMMF, (c) 10% DMMF & (d) 15% DMMF and (e) TF, (f) 5% DMTF, (g) 10% DMTF & (h) 15% DMTF

The surface roughness of muga and tasar fibroin films increased with increase in dextrose content from 5 to 15% (w/w).
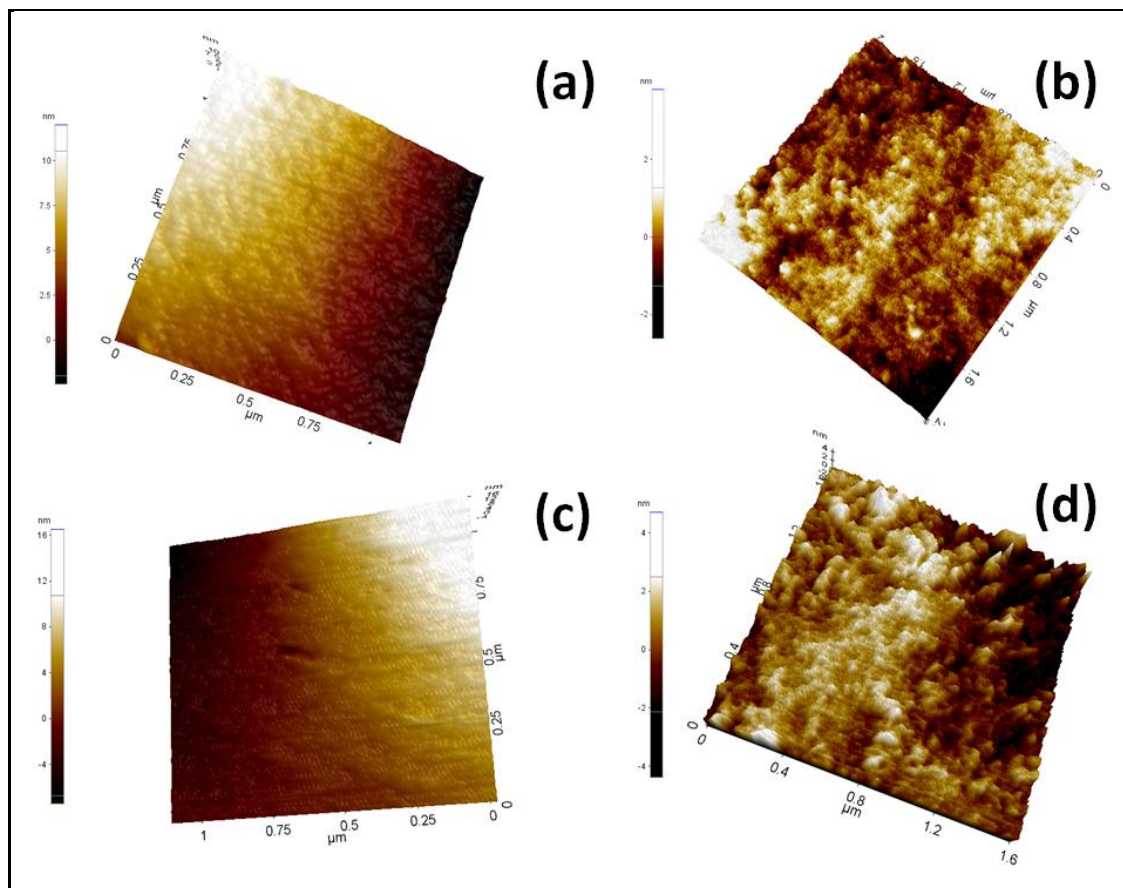
Figure 6.5: AFM micrographs of different muga and tasar fibroin films (a) MF, (b) 15% DMMF, (c) TF & (d) 15% DMTF

For the quantitative analysis, surface roughness and nano-featured topographies of different plasticized and un-plasticized silk fibroin films were further determined by atomic force microscope (Park-100). Results are depicted in the Figure 6.5. The average roughness values of different films are shown in Table 6.2. The root mean square (Rq) and average roughness (Ra) of dextrose (15% w/w) incorporated muga (15% DMMF) and tasar silk fibroin films (15% DMTF) were significantly higher as compared to that of un-plasticized tasar (TF) and muga (MF) film. It was observed that tasar fibroin film had higher surface roughness (Rq & Ra) as compared to muga

fibroin film. The surface roughness of 15% DMTF was significantly higher ($p < 0.05$) as compared to 15% DMMF.

The higher surface roughness of dextrose incorporated films may be due to some phase separation and leaching off dextrose from surface during the crystallization of films as well as extraction of ionic liquid from plasticized films. It may also be possible that in the presence of dextrose the interactions between fibroin molecules disrupt which lead to higher aggregation at molecular level and caused higher roughness.

Table 6.2: Surface Roughness (Root Mean Square and Arithmetic Average) of dextrose plasticized and un-plasticized muga and tasar fibroin films

Samples	Rq (nm)	Ra(nm)
MF	1.08	0.83
15% DMMF	2.5	2.2
TF	1.19	1.2
15% DMTF	3.0	2.5

6.3.3 Water uptake

Water uptake ability is an indicator of the hydrophilicity of the material, which is an essential requirement of any material to be used as wound dressing. The material to be used as wound dressing should be efficient to absorb fluid for preventing the accumulation of exudates that can cause infection by the bacteria. Water uptake ability of different plasticized and un-plasticized muga and tasar fibroin films were determined and are shown in Figure 6.6. Water uptake for 5% DMTF was found to be 37% , which was significantly higher ($p < 0.05$) than that of pure tasar fibroin (17%), while for 5% DMMF the value of water uptake was 39% as compared to pure muga

fibroin (19%). The water uptake ability of tasar and muga fibroin films increased with an increase in dextrose content from 5 to 15% (w/w) and was found to saturate after 48 h. This difference in water absorbance was due to the difference in amount of dextrose present in the films. The amount of water absorbed by un-plasticized muga and tasar fibroin films were nearly same, which may be due to the fact that hydrophilic to hydrophobic amino acid ratio for both fibroin proteins is nearly same. The maximum water uptake for TF and 15% (w/w) DMTF was 17 and 64%, respectively, which is not significantly ($p > 0.05$) different from the water uptake value of MF (19%) and 15% (w/w) DMMF (65%). This is due to the fact that no significant difference in hydrophilic to hydrophobic amino acid ratio for the tasar and muga fibroin [11].
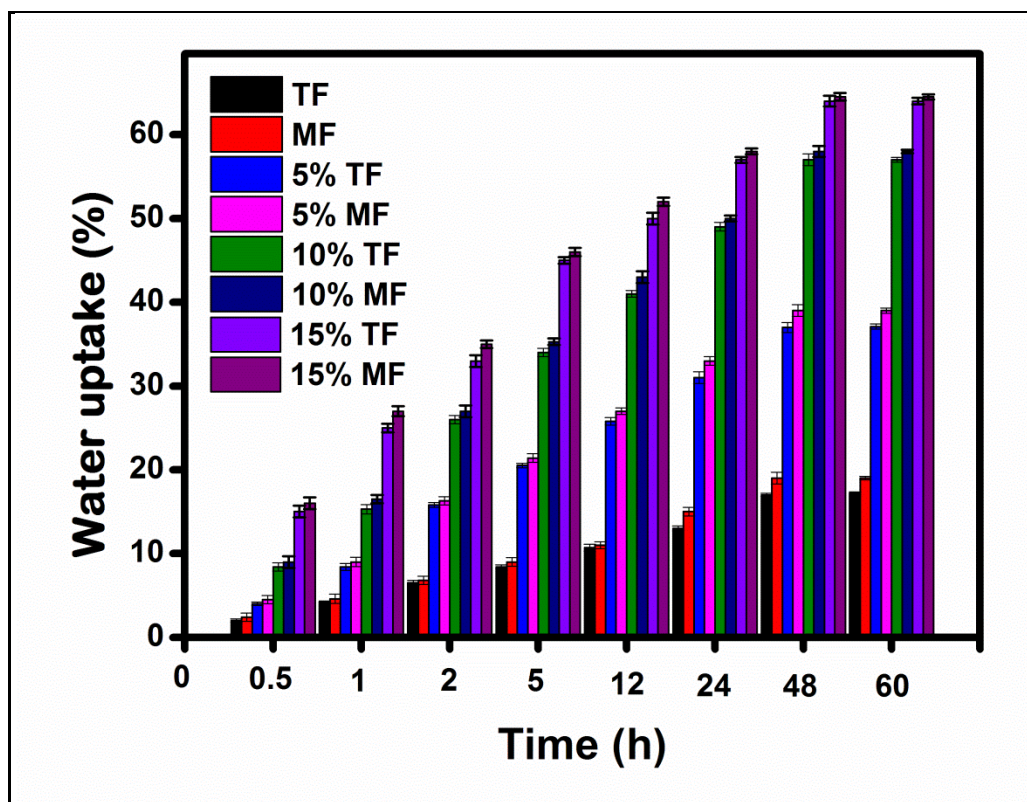
Figure 6.6: Water uptake behavior of different muga and tasar silk fibroin films

Based on the improvement in flexibility, surface roughness and water uptake by incorporating 15% dextrose in both muga and tasar films, further studies were focused only on 15% dextrose plasticized tasar and muga films.

6.3.4 Structural properties

ATR-FTIR measurements were carried out to access the conformational changes of plasticized and un-plasticized muga and tasar fibroin films. The infrared region between 1700-1600, 1600-1500 to 1300-1200 cm^{-1}, corresponds to amide I, amide II and amide III, used for the study of secondary structure of fibroin proteins.
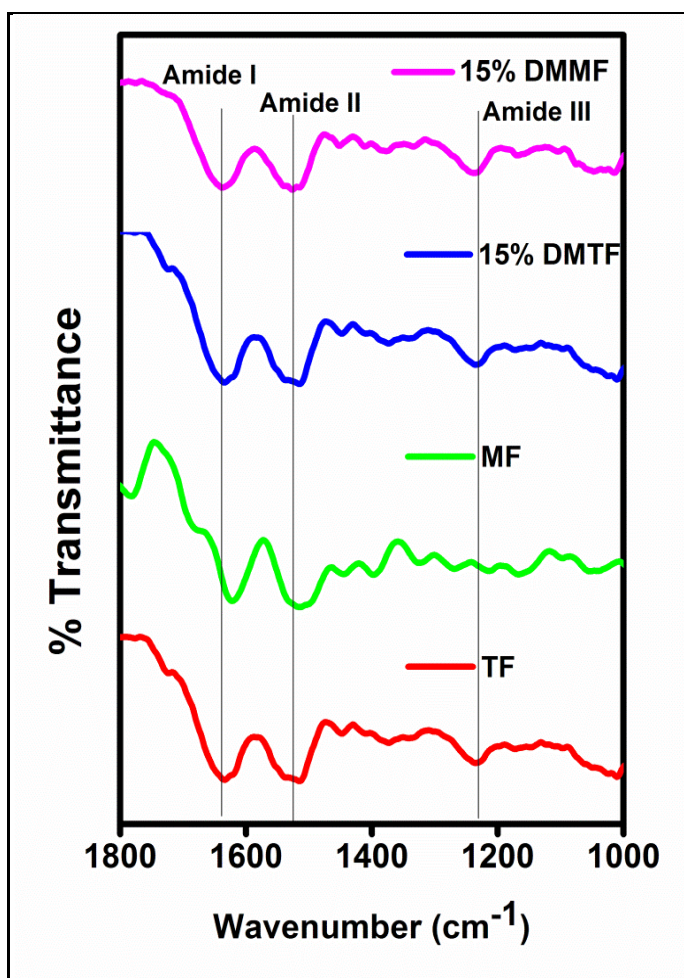
Figure 6.7: FTIR spectra of different muga and tasar fibroin films

The peaks positioned at 1630-1610, 1520-1510 and 1230-1220 cm^{-1} were characteristic of silk II (β-sheet) conformation. From Figure 6.7 it is evident that bands which appeared at 1635 & 1521 cm^{-1}, 1633 & 1527 cm^{-1}, 1625 & 1515 cm^{-1} and 1635 & 1525 cm^{-1} for 15% DMMF, 15% DMTF, MF and TF, respectively, were characteristic of β-sheet conformation. These results showed that dextrose incorporation did not affect the β-sheet conformation of fibroin proteins after coagulation with methanol. Kaplan *et* al. [201] also observed that incorporation of glycerol does not affect silk II structure of regenerated mulberry silk fibroin.

6.3.5 Thermal properties

Differential scanning calorimetric (DSC) thermograms of different plasticized and un-plasticized muga and tasar silk fibroin films are shown in Figure 6.8. The endothermic transitions found in the temperature range below 120 °C associate to evaporative water loss during heating. The bound water evaporation peaks of 15% DMTF and 15% DMMF were larger compared to TF and MF due to higher water absorption tendency of dextrose incorporated silk films. The other endothermic peaks above the temperature boundary of 390 °C were associated to thermal degradation of high ordered fraction of TF and 15% DMTF, while major endothermic peak for the degradation of MF and 15% DMMF was found at 295 °C. This further signifies that addition of dextrose does not affect crystalline structure of muga and tasar fibroin proteins. It has been reported that T_g in lower temperature region (bound water evaporation peak) indicates the interaction between fibroin protein and bound water. High heat capacity of endothermic peaks below 150 °C indicate strong interaction between bound water and silk fibroin macromolecules [204,205].
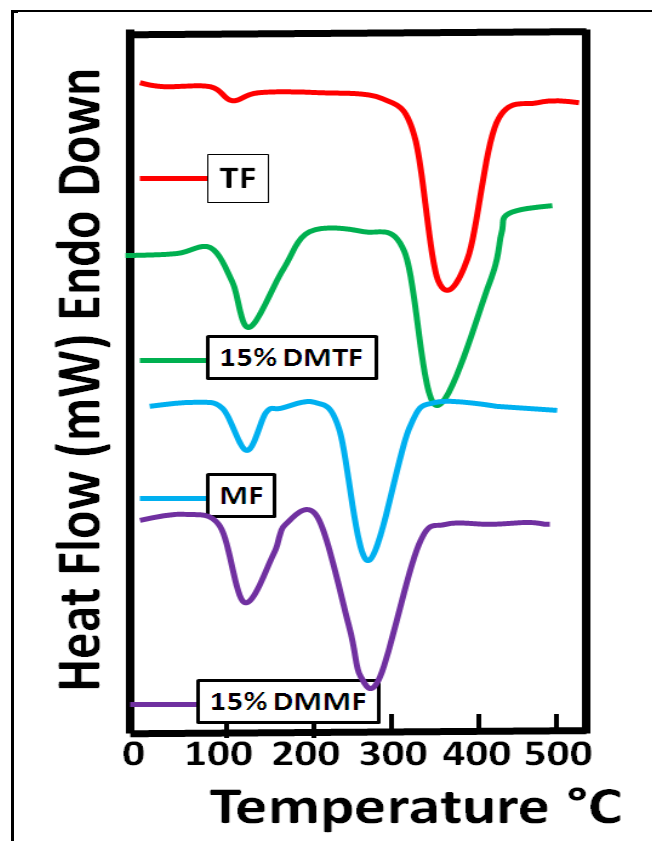
Figure 6.8: DSC thermogram of different muga and tasar fibroin films

6.3.6   Biocompatibility

6.3.6.1 Cell growth and viability of L929 cells seeded on different silk films by Trypan blue assay

The viability of L929 cells seeded on different plasticized and un-plasticized muga and tasar fibroin films can be determined by counting total number of viable cells by Trypan blue staining using hemocytometer. The number of viable cells seeded on different films is shown in the Figure 6.9(a). After one day of incubation number of viable cells seeded on 15% DMMF and 15% DMTF was significantly higher than the un-plasticized TF and MF, but there was not any significant difference found between the cells seeded on TF and MF as well as 15% DMMF and 15% DMTF, respectively. Similarly, after 3 and 5

days of incubation, number of cells increased for both plasticized and un-plasticized films, but cell proliferation was more significant for plasticized (15% DMMF and 15% DMTF) films as compared to un-plasticized TF and MF.

6.3.6.2 Growth and viability of L929 cells seeded on different silk films by MTT assay

The cellular metabolic activity of L929 cells seeded on different plasticized and un-plasticized films after 1, 3 and 5 days of incubation were determined by MTT assay. MTT assay determines the cellular metabolic activity, which is based on the fact that MTT is reduced to violet color formazan by the mitochondrial dehydrogenase. The optical density (OD) value of MTT formazan solution is directly related to cell population, so by measuring the OD value we can be able to evaluate the relative cells proliferation. For all the samples, cell proliferation was increased with incubation time.
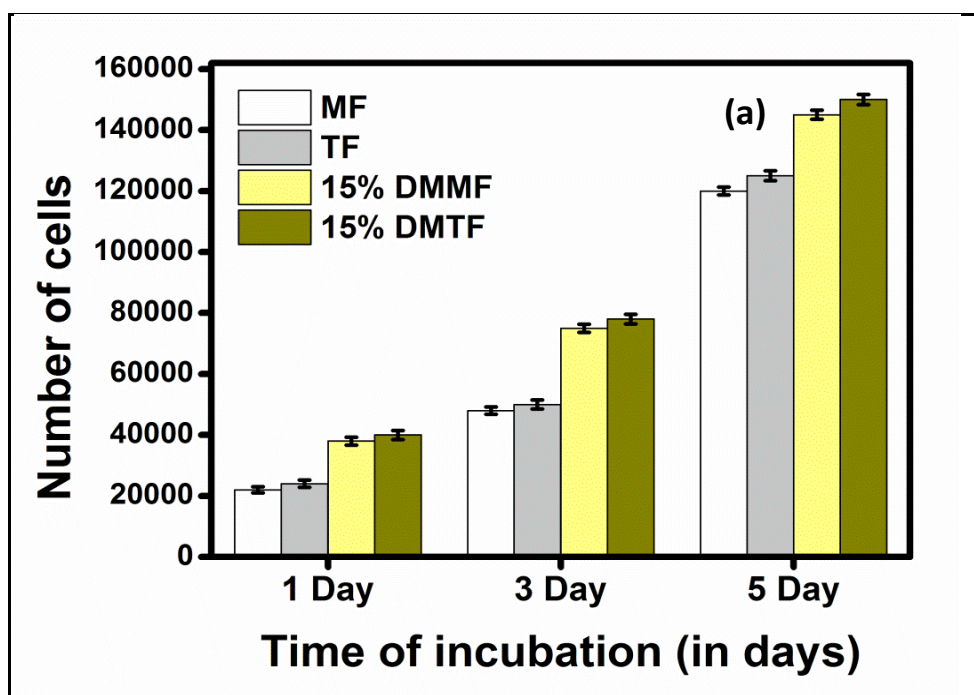
Figure 6.9(a): Trypan blue assay of L929 cells seeded on different muga and tasar fibroin films All experiments performed in triplicate and bar represented as mean±SD
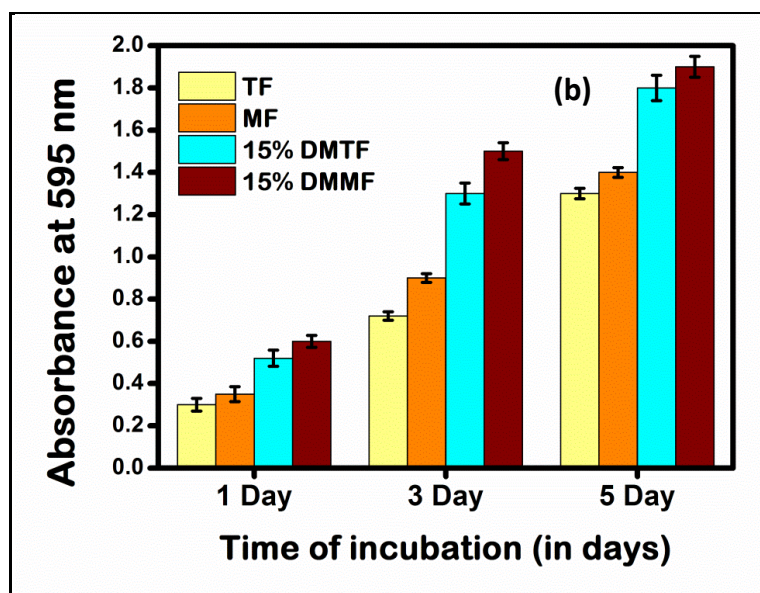
Figure 6.9(b): MTT assay of L929 cells seeded on different muga and tasar fibroin films. All experiments performed in triplicate and bar represented as mean±SD

From the Figure 6.9(b), it is evident that absorbance value for 15% DMMF and 15% DMTF was significantly higher as compared to MF and TF, but there was no significant difference found between MF & TF as well as 15% DMMF and 15% DMTF after 5 days of incubation.

6.3.6.3 Spreading and proliferation of L929 cells seeded on different silk films by phase contrast microscopy

The spreading and morphology of L929 cells seeded on plasticized and un-plasticized muga and tasar fibroin films after 1, 3 and 5 days of incubation were determined by phase contrast microscopy.

From Figure 6.9(c), it is clear that the cells attain their normal morphology after 1 day of incubation with all types of film. The spreading of cells increased with time and reached to confluence stage after 5 days of incubation for 15% DMMF and 15% DMTF, but cells did not reach to confluence state for un-plasticized muga and tasar

films. So it is clear that cell spreading and proliferation was significantly higher in case of plasticized muga and tasar fibroin as compared to un-plasticized muga and tasar fibroin films. However, no significant difference was observed for adherence and proliferation of L929 fibroblast cells seeded on 15% DMMF and 15% DMTF.
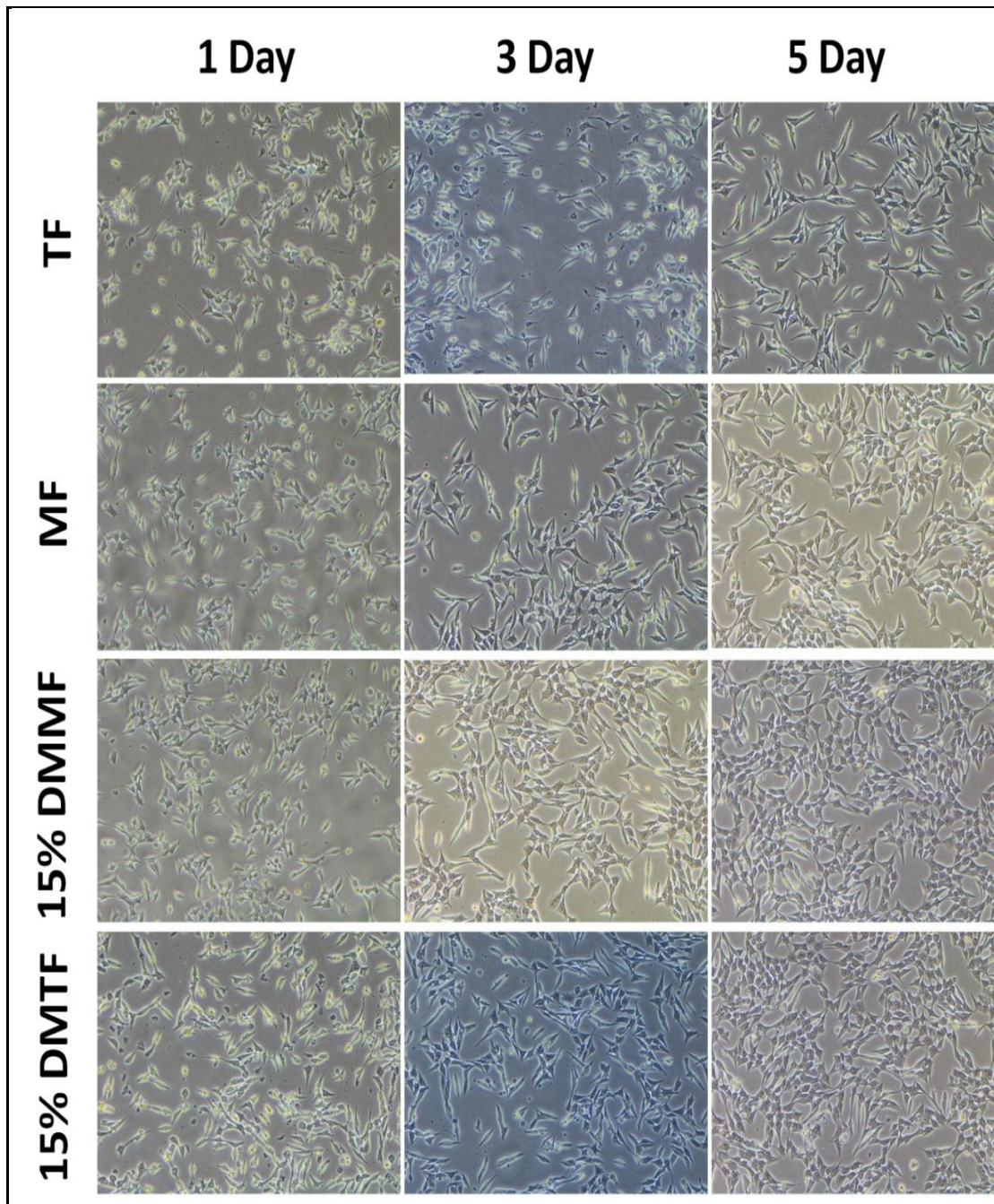
Figure 6.9(c): **Phase contrast microscopy of L929 cells seeded on different muga and tasar fibroin films**

Tripeptide Arg(R)-Gly(G)-Asp(D) motif of nonmulberry silk fibroin proteins is responsible for higher attachment of cells [206]. A research group of Kundu *et* al. [41,45,75,116,207] extensively studied biocompatibility of mulberry and nonmulberry silk fibroin proteins. They have reported that tasar and muga fibroin gland protein showed higher adherence and proliferation compared to mulberry silk fibroin protein.

Cells adherence and proliferation was further increased by incorporating dextrose content. The higher adherence and proliferation of the cells seeded on dextrose plasticized muga and tasar fibroin films over the un-plasticized muga and tasar film was mainly due to increased hydrophilicity and nanophase surface roughness. The dextrose being a hydrophilic molecule has tendency to increase the water absorbance capacity of fibroin films. Karahaliloğlu *et* al. [39] have found that mulberry silk fibroin films having nanophase surface roughness shows higher adherence and proliferation of dermal fibroblast cells compared to films having smooth morphology.

6.3.7 *In vitro* biodegradation

The stability of these muga and tasar fibroin films in physiological environment was studied by *in vitro* biodegradation assay. *In vitro* biodegradation was performed by incubating different plasticized and un-plasticized silk fibroin films in PBS with and without protease XIV enzyme. The mass change in plasticized and un-plasticized muga and tasar fibroin films after incubation in pure PBS and PBS-protease XIV solution is shown in Figure 6.10. It was observed that notable mass loss occurred for each type of films after 50 days of incubation in protease XIV enzyme. The 15% DMTF and 15% DMMF showed significantly higher mass loss as compared to TF and MF after 50 days of incubation. The higher biodegradation of dextrose

incorporated fibroin films over pure fibroin films was mainly related to the swelling characteristics of proteins. The crystalline portion of fibroin is highly resisted to degradation because enzyme cannot easily permeate β-sheet region. But with dextrose the swelling ability of fibroin increased which facilitated the permeation of enzyme to the inner extremes of β-sheet crystal that lead to significant mass loss. There was not any significant difference ($p > 0.05$) was found between mass loss of TF and MF over 50 days of incubation. This may be due to nearly same hydrophilic to hydrophobic amino acid ratio of tasar and muga fibroin proteins.
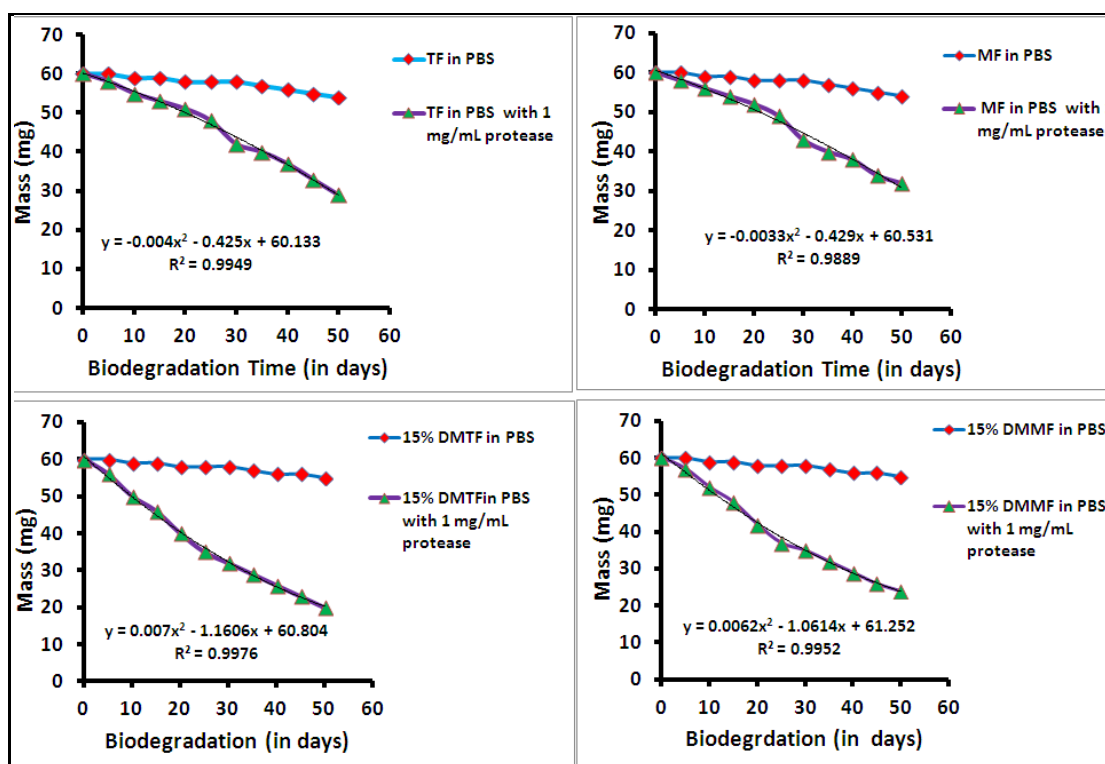
Figure 6.10: Protease XIV mediated *in vitro* biodegradation of different muga and tasar silk fibroin

The mass loss of TF, MF, 15% DMTF and 15% DMMF was found to be 52, 47, 67 and 60%, respectively which consistently followed second order trend line. No significant differences in mass loss were observed in PBS incubated samples for the same time.

6.3.8 Antimicrobial activity and drug release

6.3.8.1 Antimicrobial activity

Antimicrobial activity of gentamicin loaded plasticized and un-plasticized muga and tasar fibroin films were analyzed by agar disc diffusion assay. Amount of drug loaded in the dextrose plasticized films was significantly higher compared to the un-plasticized films, which was found to be 15 and 12 mg for muga and tasar fibroin films and was 25 and 20 mg for 15% DMMF and 15% DMTF, respectively.
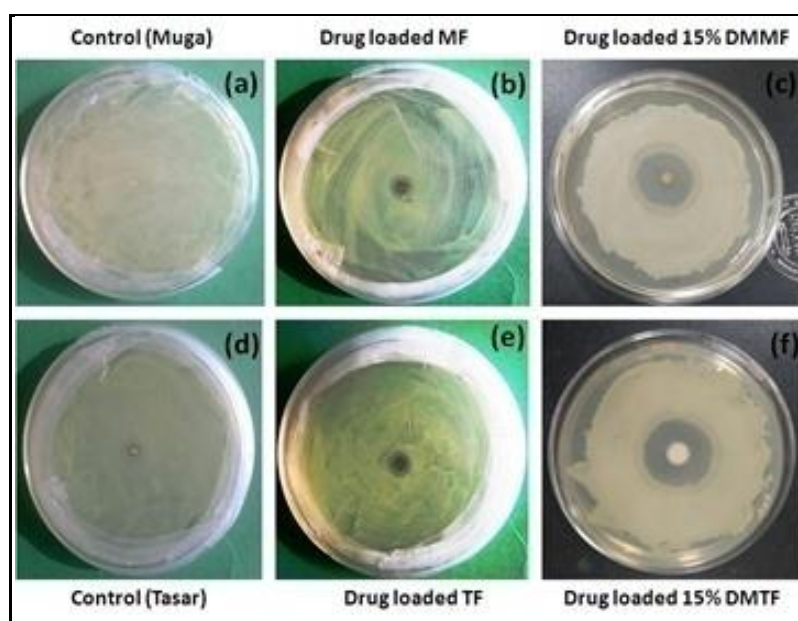
Figure 6.11: Disc diffusion assay of gentamicin loaded plasticized and un-plasticized muga and tasar silk fibroin films

Figure 6.11 shows the antimicrobial activity of different samples in the form of zone of inhibition. Antimicrobial results show that there was no zone of inhibition formed for plasticized and un-plasticized muga and tasar fibroin films without drug. The zone of inhibition for TF, MF, 15% DMMF and 15% DMTF against *E. coli* was found to be 10, 11, 16 and 18 mm, respectively. The zone of inhibition for TF, MF, 15% DMMF and 15% DMTF against *S. aureus* was found to be 11, 13, 19 and 21 mm, respectively. Antimicrobial activity of dextrose plasticized muga and tasar fibroin

films were higher compared to un-plasticized films. This behavior was related to amount of drug loaded and swelling behavior of films. The high swelling ability of dextrose plasticized films caused fast and high drug release as compared to un-plasticized films.

6.3.8.2 Drug release

Gentamicin is very effective antibiotic that has potential to kill gram +ve and gram -ve bacterial stain which reduces the infection at wound site and aids in normal wound healing profile. The cumulative release of gentamicin at physiological pH from loaded samples is shown in Figure 6.12. Initial burst release of gentamicin was found for all the samples within 24 h due to more drug absorbed at the surface, which was followed by normal release for the rest of the period of study time. Release of drug from any wound dressing depends upon the degree of porosity, pore size, nature of drug. It was found that initial burst release was 20 and 22% for MF and TF, respectively, while it was found to be 28 and 30% for 15% DMMF and 15% DMTF, respectively. The maximum drug released from TF and MF was 45 and 40%, while it was 55 and 50% for 15% DMTF and 15% DMMF, respectively and reached to saturation within 10 days of analysis. The amount of drug released from dextrose plasticized samples was significantly higher than that of un-plasticized films. This behavior may be related to surface roughness and water absorbance ability of films. Due to higher surface roughness as revealed by AFM as well as water absorbance capacity of dextrose plasticized films, amount of drug loaded in the dextrose plasticized films was significantly higher compared to the un-plasticized films. The higher burst release could be the result of high amount of drug adsorbed at the rough surface of dextrose

plasticized films compared to un-plasticized films, similarly gradual release of drug up to 6 days was due to the presence of higher amount of drug in the reservoirs of the films.
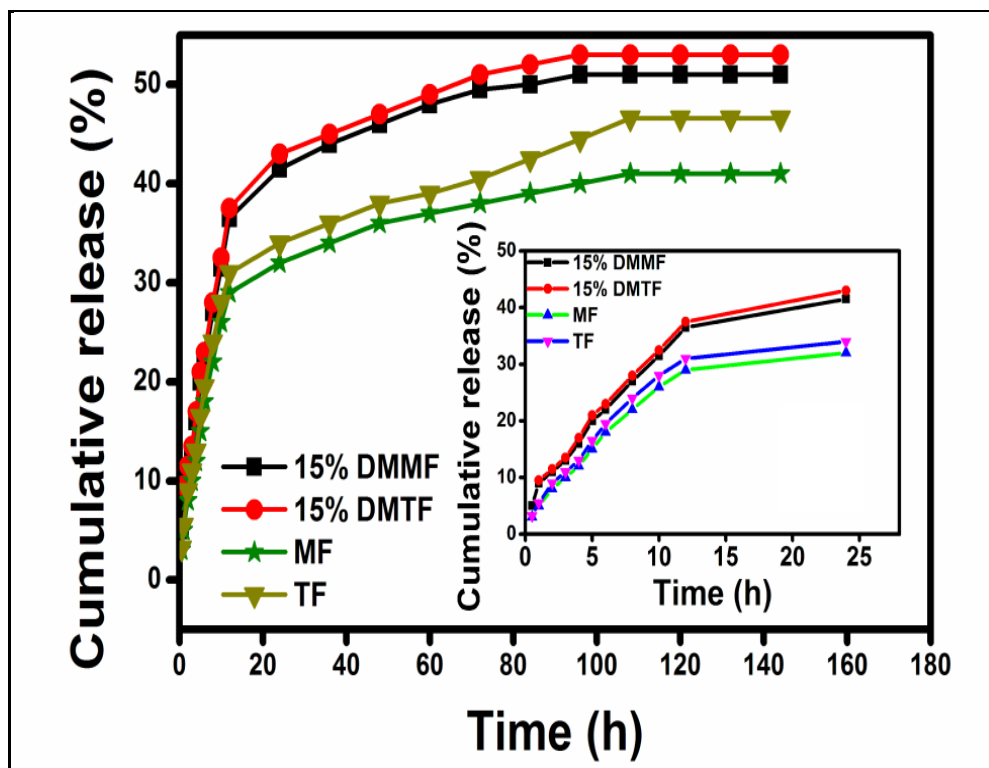
Figure 6.12: Cumulative release of gentamicin from different plasticized and un-plasticized muga and tasar fibroin films

The release mechanism of gentamicin from different muga and tasar fibroin films were determined by putting the data to semi empirical model known as Ritger-Peppas model to determine value of 'n' exponent [36]. The release data are shown in the Table 6.3. Vasconales *et* al. [36] have also found that value of exponent 'n' depend upon release mechanism and architecture of matrix. To determine the value of exponent 'n' we should consider the portion of curve for which value of M_t/M_o should be less than 0.6. The value of exponent 'n' for Fickian diffusion must be $0.45 \leq n$, for

non Fickian diffusion it is $0.45 < n < 0.89$, while $n > 0.89$ corresponds to super case II transport and $n = 0.89$ corresponds to Case II (relaxation) transport [208].

The value of 'n' for muga, tasar, 15% DMMF and 15% DMTF was found to be 0.68, 0.65, 0.51, and 0.52, which depicted anomalous release behavior of drug for all type of films. Additionally, lower 'n' value of dextrose plasticized muga and tasar films compared to the un-plasticized films further supported higher diffusion of dextrose plasticized films compared to un-plasticized films. Similarly the higher 'k' value of dextrose plasticized muga and tasar films over the un-plasticized films was responsible for higher release of gentamicin. This phenomena was related to higher surface roughness and swelling capacity of dextrose plasticized films over un-plasticized.

Table 6.3: Kinetic data obtained by fitting the drug release data

	K	n	R^2
MF	0.19	0.68	0.98
TF	0.18	0.65	0.95
15% DMMF	30	0.51	0.97
15% DMTF	29	0.52	0.98

6.4 Conclusions

Dextrose plasticized flexible and biocompatible muga and tasar fibroin films were prepared by using ionic liquid. Increase in elongation at break value and lowering of tan δ value of dextrose plasticized tasar and muga fibroin films indicates that flexibility of films increased by the addition of dextrose. Dextrose content does not affect the secondary structure of silk fibroin protein. Higher water absorption and increased nanophase surface roughness was responsible for significantly improved cellular compatibility.

CHAPTER 7

HYDROGEL PARTICLES DOPED *ANTHERAEA MYLITTA* AND *ANTHERAEA ASSAMA* SILK FIBROIN FLEXIBLE FILMS FOR WOUND DRESSING

7.1 Introduction

Nonmulberry silk fibroin proteins have been successfully utilized for tissue engineering and regenerative medicine but only limited work has been carried out in the field of wound dressing and skin regeneration.

Hydrogels are three dimensional, crosslinked and water insoluble networks which have most of the desirable properties of ideal wound dressing [26]. Hydrogels provide moist environment, cool the surface of wound and absorb excess exudates. Hydrogels based wound dressing are non-adherent so reduce the dressing change pain. Highly porous structure and aqueous swelling of hydrogels can easily be tuned up by controlling the crosslink density of matrix which is responsible for loading of drugs into the gel matrix. The drug release rate depends on the diffusion coefficient of drug molecules through porous gel structure [209].

The chapter is focused on the preparation and properties of muga and tasar flexible films fabricated by incorporating hydrogel particles. These hydrogels were broken into small particles of size ranging from 0.1 to 1 µm with the help of Ball milling machine. Muga and tasar fibroin flexible silk films were prepared by incorporating hydrogel particles. These hydrogels particles are highly hydrophilic in nature which absorbs the moisture from humid environment that makes the silk films flexible. **An Indian patent has been filed for the process of preparation of hydrogel particles and its incorporation in muga and tasar films (Patent Application Numbered 201711011922 dated 01-04-2017)** so only few data has been shown in this chapter.

7.2 Experimental

7.2.1 Preparation of hydrogel particles

Natural polysaccharide has been used for the preparation of hydrogel using radical polymerization. Hydrogel particles was prepared using ball milling machine. Briefly, 1 gm dried hydrogel sample was ball milled with 5 balls for a period of 1 week. The prepared hydrogel particles were filtered out using 100 μm mechanical meshes in order to remove large particles.

7.2.2 Preparation of hydrogel particle doped silk fibroin films

Different concentration of hydrogel particles (1, 3 and 5% w/w of silk fibroin) were mixed with muga and tasar silk fibroin ionic liquid solution separately and then poured into petriplates under laminar air flow to prepare films of thickness 0.5±0.1 mm. After 2 h, methanol was added to each petriplate in order to crystallize them for 5 h. The residual ionic liquid trapped in the cast films was extracted by the protocol described in earlier chapters.

7.3 Results and Discussion

7.3.1 Mechanical Properties

Plasticity and strength of different hydrogel doped muga and tasar silk fibroin is shown in the Table 7.1. Due to incorporation of hydrogel particles, strength and plasticity of muga and tasar silk fibroin films increased. Tensile strength and modulus of muga and tasar silk fibroin films increased with increase in hydrogel particles from 1 to 5% w/w. This behavior is due to fact that hydrogel particles entrapped between networks of fibroin chains and stabilizes strong secondary interactions such as hydrogen bonding and Vander Waal forces with them. These hydrogel particles

absorbed water from humid environment that increased the segmental mobility of the fibroin chain. Due to the water plasticization effect, elongation at break value of muga and tasar silk fibroin films also increased due to incorporation of hydrogel particles. These hydrogel particles are highly hydrophilic molecules which absorb water from environment and increase the interchain space of molecules that makes plasticization of fibroin films. Elasticity of muga and tasar fibroin films increased with increase in hydrogel particles.

Table 7.1: Mechanical properties of hydrogel doped muga and tasar silk fibroin films

Samples	Tensile Strength (MPa)	Tensile Modulus (MPa)	Elongation at break (%)
MF	2.8	24	12
1% HDMFF	4	26	22
3% HDMFF	5.5	30	30
5% HDMFF	6	35	38
TF	3.2	30	10
1% HDTFF	4.5	33	21
3% HDTFF	7	36	28
5% HDTFF	8	38	35

7.3.2 Biocompatibility of hydrogel particle doped tasar and muga fibroin films

Growth and viability of L929 cells seeded on tasar, muga, 5% hydrogel doped muga and tasar fibroin films were determined by MTT assay. MTT is rapid calorimetric technique which is based on the fact that yellow MTT is reduced to violet formazan due to the action of mitochondrial dehydrogenase enzyme inside the cells. Optical density of DMSO formazan solution is directly related to the cells population so it gives the direct indication about cell population as well as proliferation over the time of incubation. Optical density of formazan after 1, 3 and 5 days of incubation is

shown in Figure 7.1. From Figure 7.1, it is evident that OD value increases with the time for all types of samples but cell proliferation is significantly higher in the case hydrogel doped muga and tasar silk fibroin films but there is no significant difference between undoped muga and tasar silk fibroin as well as 5% hydrogel doped muga and tasar silk fibroin films.
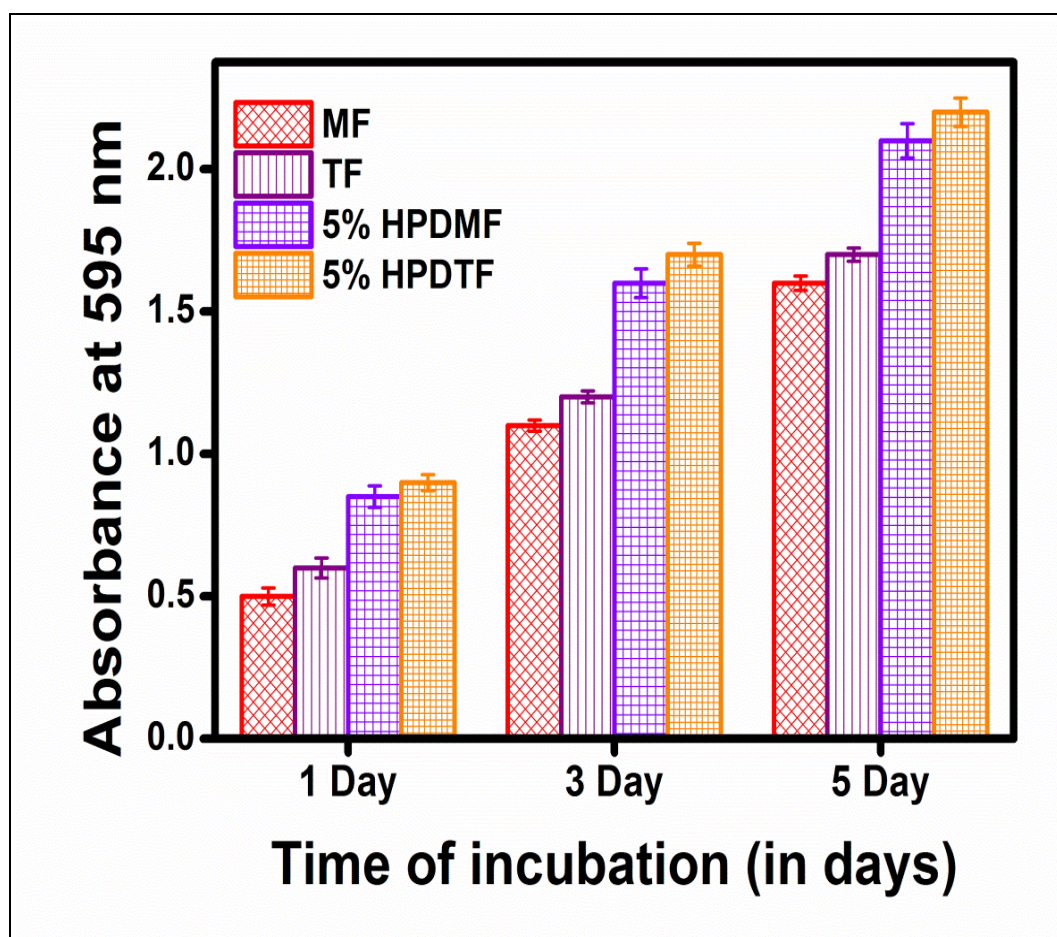
Figure 7.1: MTT assay of L929 skin fibroblast cells seeded on hydrogel particle doped flexible muga and tasar fibroin films

The morphology and spreading of L929 fibroblast cells seeded on different film samples were studied by Fluorescence microscope. From Figure 7.2, it is clear that L929 cells attached to surface of all type of samples and were able to attain their

normal morphology within one day of incubation. Spreading and proliferation of L929 cells seeded on 5% hydrogel doped muga and tasar silk fibroin films are higher as compared to control undoped muga and tasar silk fibroin films. Adherence and proliferation of L929 cells seeded on 5% hydrogel doped muga and tasar silk fibroin is significantly higher as compared to undoped muga and tasar silk fibroin films and reached near confluence stage after 5 days of incubation.

Few research groups that are working on the nonmulberry silk fibroin studied the biocompatibility of tasar silk fibroin proteins and they reported that these nonmulberry varieties of silk fibroin showed higher growth and proliferation of cells compared to mulberry silk fibroin proteins. It is reported that nonmulberry silk fibroin proteins have positively charged tripeptide sequences R(Arg)-G(Gly)-D(Asp) which are responsible for adherence of animal cells due to the fact that animal cell surface are negatively charged. Beside this polycationic nature of chitosan present in hydrogel could also be responsible for adherence of cells.

Adherence and proliferation of cells was significantly enhanced by doping hydrogel particles. Doping of hydrogel particles significantly increased the nanophase surface roughness as well as hydrophilicity of the muga and tasar silk fibroin films. Hydrogels being hydrophilic in nature increased the water absorbance capacity of the films. The higher swelling ability and nanophase roughness of hydrogel doped films are responsible for higher growth and proliferation of the cells.
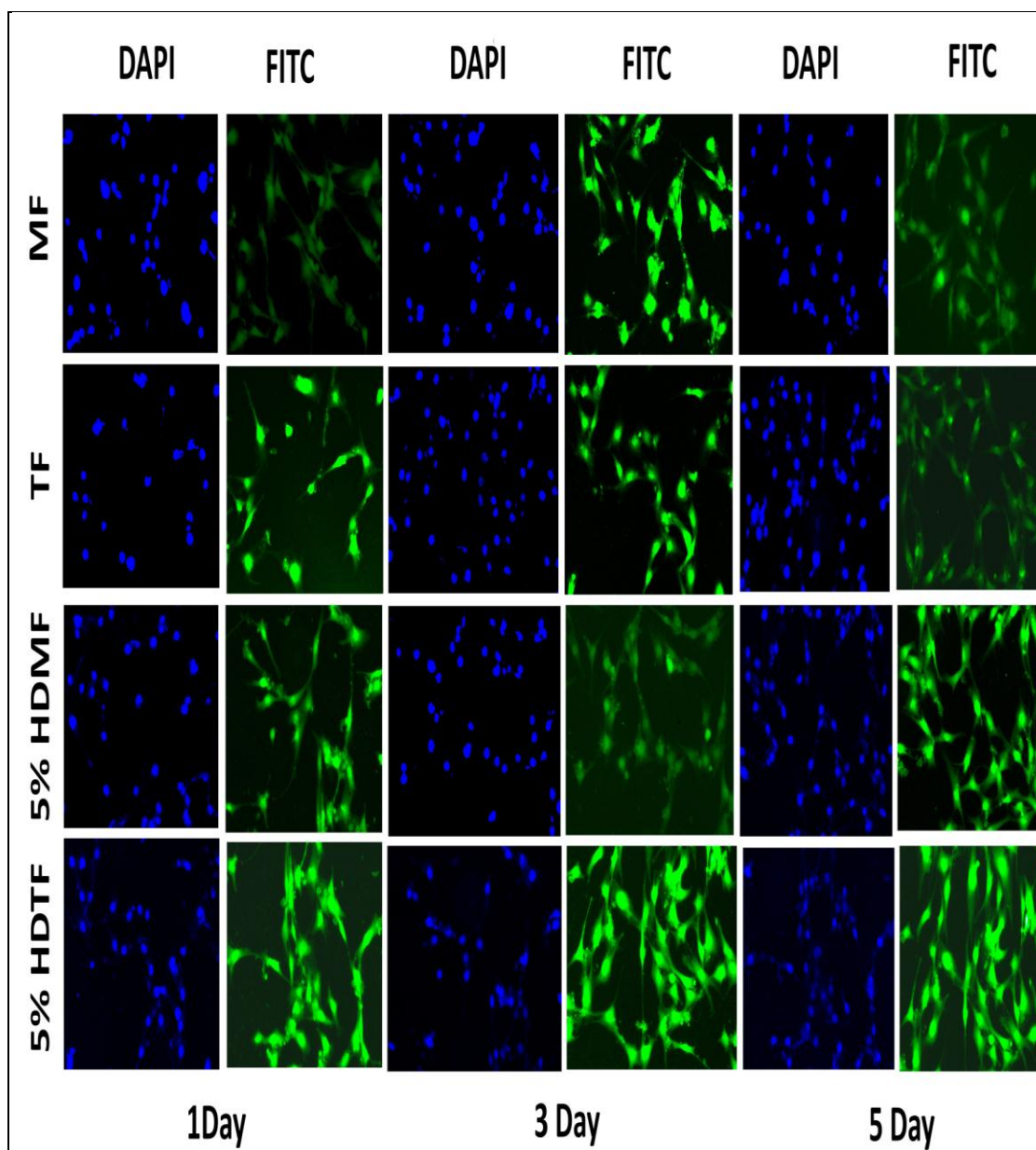
Figure 7.2: Fluorescence microscopy of L929 fibroblast cells seeded on hydrogel particle doped tasar and muga fibroin films

7.3.3 Release study

Gentamicin is a broad spectrum antibiotic and highly effective against gram positive and gram negative bacteria and having ability to reduce bacterial contamination and stimulates normal healing of wound. Figure 7.3 shows cumulative release of gentamicin sulphate from different loaded samples at a physiological pH of 7.4 for 144 h. From

Figure 7.3, it is clear that initial burst release was found for all types of sample within 24 h due to high amount of drug absorbed at the surface of the samples after that normal release of drug was reported for the rest period of study. Release of drug from the wound dressing depends upon the nature of drug, porosity, pore size, swelling ability of matrix. It is found that initial burst release was reported (58%) for hydrogel (having 5% w/w MBA) while it is found to be 53 and 55% for 5% hydrogel doped tasar and muga fibroin films. The maximum drug release from 5% hydrogel doped muga (5% HDMF) and 5% hydrogel doped tasar (5% HDTF) films was 69 and 71%, while it was 80% for hydrogel and reached to saturation after 144 h of study. Mechanism of drug from different film samples were determined by putting the release data to semi-empirical model known as Ritger-Peppas model to obtain the value of release exponent [160,208]. Value of release exponent depends upon the architecture of matrix as well as type of release mechanism. To determine the value of release exponent n we should use the release data for which value of the M_t/M_o should be less than 0.6. For the Fickian diffusion value of release exponent must be $0.45 \leq n$, for non-Fickian diffusion it is $0.45 < n < 0.89$, if $n > 0.89$ correspond to super case II transport and $n = 0.89$ for case II (relaxation) transport [36].

The value of 'n' for 5% hydrogel doped muga and tasar silk fibroin films was 0.58 and 0.55, which shows anomalous release behavior of drug (Non-Fickian), while it was 0.48 for hydrogel which followed Fickian diffusion. The higher value of release constant 'k' was 14 for hydrogel, responsible for higher release of gentamicin sulphate as compared to the value of 'k' for 5% hydrogel doped muga and tasar silk fibroin films for which it was found to be 12 and 10. In our previous study we have found that value of n and k for pure muga and tasar silk fibroin films was 0.68 & 0.65 and 0.19 & 0.18, respectively.
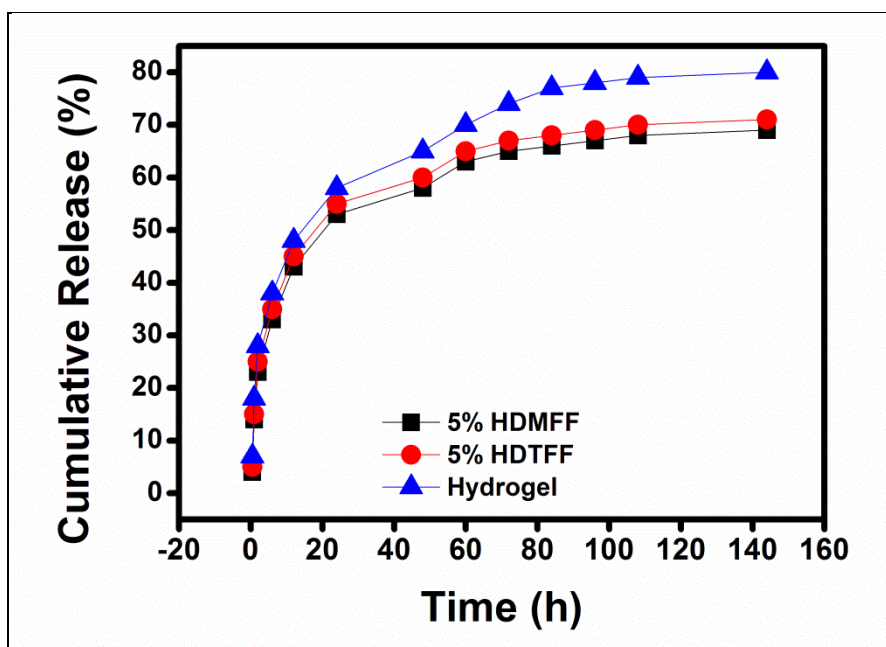
Figure 7.3: Release behavior of gentamicin sulphate loaded in hydrogel particle doped tasar and muga fibroin films

High rate of drug release was found for hydrogel particles over 5% hydrogel particles doped muga and tasar silk fibroin films which in turn were higher than pure muga and tasar silk fibroin films. This behavior was related to higher swelling ability of hydrogel particles over 5% hydrogel particles doped muga and tasar films. The higher drug release rate of 5% hydrogel doped muga and tasar silk fibroin films over pure muga and tasar silk fibroin films is due to higher surface roughness as revealed by AFM and higher swelling ability of the films is due to entrapment of hydrogel particles inside the muga and tasar silk fibroin molecules, which are responsible for higher absorption of drug solution and release of drug molecules. The nanophase roughness value for MF, 1% DMMF, 3% DMMF and 5% DMMF was 3.4, 20, 25 and 32, respectively whereas the values for TF, 1% DMTF, 3% DMTF and 5% DMTF was 4, 24, 28 and 35, respectively. Hydrogels are highly hydrophilic materials having very high swelling ability (7.5 g/g). Addition of hydrogel particles (5% w/w) significantly increases the swelling ratio of muga and tasar

silk fibroin films which is further responsible for high loading of drug. Swelling ratio of muga fibroin films was found to be 1.9 as compared to tasar fibroin films for which it was 1.5. This difference in swelling value of muga and tasar silk fibroin films is not significant due to the fact that there is no significant difference between hydrophilic to hydrophobic amino acid ratio for tasar and muga fibroin. Swelling value for 5% w/w hydrogel doped muga fibroin films (5% HDMFF) was 2.9 as compared to 5% w/w hydrogel doped tasar fibroin films (5% HDTFF) that has the swelling value of 2.7. The loading of drug was found to be 6 mg/gm of hydrogel while it was 3 mg/gm for tasar and muga silk fibroin films [18, 37].

7.4 Conclusions

Hydrogel was successfully prepared with N,N'-methylenebis (acrylamide) (5% w/w of polymer) has optimum swelling capacity. Hydrogel particles are prepared by ball milling of dry hydrogels. Toughness and plasticity of muga and tasar silk fibroin films was successfully enhanced with the incorporation of hydrogel particles which influence its silk II conformation. Hydrogel doped muga and tasar silk fibroin films exhibited significantly higher water absorption and roughness as compared to control muga and tasar silk fibroin films which are responsible for higher adherence and proliferation of L929 fibroblast cells. These tough and flexible silk fibroin films will further explore efficacy of silk based biomaterials to be utilized as wound dressing and regenerative medicine, advance drug vehicle and therapeutic devices as well as scaffolds for tissue engineering, but still there is a need to further explore the *invivo* response of these materials so that we would be able to fully exploit them for wound dressing and regenerative medicine.

CHAPTER 8

CONCLUSIONS AND FUTURE PROSPECTS

8.1 Conclusions

The whole research work was focused on the fabrication of chitosan finished nonmulberry micro-fibrous nonwoven composites, nano-fibrous mats, dextrose plasticized flexible films as well as hydrogel particles doped films. All these constructs showed good mechanical integrity, water uptake capacity, water vapor transmission ability, biocompatibility and antimicrobial activity. Tasar and muga nanofibrous mats have very good porosity. Dextrose plasticized and hydrogel particles doped nonmulberry silk fibroin films have good extensibility, flexibility. The important findings of whole thesis are concluded below:

❖ Chitosan finished tasar and muga fibroin composite films showed good physical, mechanical and biological properties. Tensile strength and modulus of tasar fibroin nonwoven mat were 6.5 and 218 MPa, respectively. Tensile strength and modulus of tasar fibroin nonwoven films increased with increase in chitosan concentration started at 9 and 274 MPa for 0.75% chitosan finished tasar fibroin nonwoven films, 12 and 353 MPa for 1% chitosan finished tasar fibroin nonwoven films, 14 and 450 MPa for 1.5% chitosan finished tasar fibroin nonwoven films and reached 21 and 550 MPa for 2% chitosan finished tasar fibroin nonwoven films, respectively. For tasar fibroin nonwoven films, elongation at break values was 16 mm which was decreased to 13, 8, 4 and 3 mm for 0.75, 1, 1.5 and 2% chitosan finished tasar fibroin nonwoven mat, respectively. Tensile strength and modulus of muga fibroin nonwoven mat were

4 and 205 MPa, respectively. Chitosan finishing enhanced the tensile strength and modulus of muga fibroin nonwoven mats, which is 7 and 270 for 0.75% chitosan finished muga fibroin nonwoven mat, 10 and 345 MPa for 1% chitosan finished muga fibroin nonwoven mat, 12 and 425 MPa for 1.5% chitosan finished muga fibroin nonwoven mat & further enhanced to 19 and 522 MPa for 2% chitosan finished muga fibroin nonwoven mat. Elongation at break for muga fibroin nonwoven mat was 18 mm which was reduced to 15, 10, 5 and 4 mm for 0.75 % chitosan finished muga fibroin nonwoven, 1% chitosan finished muga fibroin nonwoven, 1.5% chitosan finished muga fibroin nonwoven and 2% chitosan finished muga fibroin nonwoven, respectively.

❖ Storage modulus of chitosan finished muga fibroin nonwoven was significantly higher compared to muga fibroin nonwoven. The storage modulus of muga fibroin nonwoven was 195 MPa, while for 0.75% chitosan finished muga fibroin nonwoven, 1% chitosan finished muga fibroin nonwoven, 1.5% chitosan finished muga fibroin nonwoven and for 2% chitosan finished muga fibroin nonwoven it was 315, 390, 582 and 695 MPa, respectively.

❖ Chitosan finished tasar fibroin nonwoven mats showed higher storage modulus value as compared to tasar fibroin nonwoven mat. At 20 °C, storage modulus of tasar fibroin nonwoven mat was 200 MPa, while for 0.75% chitosan finished tasar fibroin nonwoven mats, 1% chitosan finished tasar fibroin nonwoven mats, 1.5% chitosan finished tasar fibroin nonwoven mats and for 2% chitosan finished tasar fibroin nonwoven mats it was 320, 400, 590 and 700 MPa, respectively.

❖ Water uptake capacity of tasar and muga fibroin nonwoven matswas 80 and 85%, respectively. The maximum water uptake capacity of 0.75, 1 and 1.5% chitosan finished tasar fibroin nonwoven mats was 96, 110 and 115%, respectively. The water uptake capacity of 2% chitosan finished tasar fibroin nonwoven mat was significantly higher (122%) than TFF film. Maximum water uptake for 0.75% chitosan finished muga fibroin nonwoven mat, 1% chitosan finished muga fibroin nonwoven mat, 1.5% chitosan finished muga fibroin nonwoven mat and 2% chitosan finished muga fibroin nonwoven mat was 102, 117, 130 and 137%, respectively.

❖ The porosity of tasar fibroin nonwoven mat was 80%, while for 0.75, 1, 1.5 and 2% chitosan finished tasar fibroin nonwoven mats, the value of porosity was 79, 75,71 and 68%, respectively. The porosity of muga fibroin nonwoven mat was 75%, while it was 72, 68, 63 and 60% for 0.75%, 1%, 1.5% and 2% chitosan finished muga fibroin nonwoven mats, respectively. The WVTR for tasar fibroin nonwoven mat was 2800 $g/m^2/day$, which is significantly reduced to 2600 $g/m^2/day$ for 0.75% chitosan finished tasar fibroin nonwoven mat, 2300 $g/m^2/day$ for 1% chitosan finished tasar fibroin nonwoven mat, 2180 $g/m^2/day$ for 1.5% chitosan finished tasar fibroin nonwoven mat and 1870 $g/m^2/day$ for 2% chitosan finished tasar fibroin nonwoven mat. The WVTR for muga fibroin nonwoven mat was 2700 $g/m^2/day$, which was reduced to the value of 2500, 2300, 2100 and 1800 $g/m^2/day$ for 0.75%, 1%, 1.5% and 2% chitosan finished muga fibroin nonwoven mats, respectively.

❖ Proteolytic degradation of tasar fibroin nonwoven mat was significant with a residual mass of about 52% after 15 week. Biodegradation of 0.75, 1 and 1.5

and 2% chitosan finished tasar fibroin nonwoven mats was comparable to tasar fibroin nonwoven mat with mass remaining percentage of 49, 46, 47 and 44, respectively. Protease mediated biodegradation of muga fibroin nonwoven mat was significantly higher with residual mass of 48% as compared to control PBS without enzyme (2%) after 15 weeks of degradation. The residual mass of 0.75, 1, 1.5 and 2% chitosan finished muga fibroin nonwoven mats was 45, 44, 43 and 41% after 15 weeks of enzymatic biodegradation.

❖ Chitosan finished muga and tasar nonwoven mats showed higher growth and spreading of L929 fibroblast cells as compared to unmodified muga and tasar silk fibroin mats. Chitosan finished muga and tasar nonwoven mats showed good antimicrobial activity.

❖ Cocoon extracted muga and tasar fibroin fibers had been successfully regenerated as nanofibrous mat by using ionic liquid. Nonmulberry muga and tasar fibroin nanofibrous mat exhibited unique properties, including adequate mechanical strength, porosity, water absorption and enhanced biocompatibility drug release over the muga cast film, which makes it an excellent candidate in the field of skin tissue engineering.

❖ The shear viscosity of 5, 7 and 10% w/v muga fibroin ionic liquid dope solution was 1145, 1243 and 1446 centipoises, respectively at $1 S^{-1}$.

❖ FTIR spectra showed that coagulated muga fibroin nanofibrous mats have β-sheet conformation.

❖ Optimized nanofibrous mat prepared at 10% w/v concentration and 20 kV potential having diameter of 160 nm. Muga nanofibrous mat has higher tensile

strength and elongation at break value of 10 MPa and 31 mm, respectively, as compared to muga cast film having value of 5.6 MPa and 25 mm, respectively.

❖ Muga nanofibrous mat showed average porosity of 75%, while it was only 10% for muga cast film.

❖ The average roughness value for the cast film was found to be very low (2.2 nm) as compared to MNF-20 for which roughness value was 25 nm.

❖ The WVTR of muga cast film and muga nanofibrous mat was found to be 990 g/m^2/day and 2250 g/m^2/day, respectively.

❖ The muga nanofibrous mats howed higher water uptake capacity (56%) as compared to muga cast film (45%).

❖ Spreading and proliferation of L929 cells seeded on muga nanofibrous mat was higher as compared to muga cast film.

❖ The mean diameter of zone of inhibition (ZOI) for muga nanofibrous mat was 13 and 15 mm against *E. coli* and *S. aureus*, while it was 10 and 13 mm for muga cast film.

❖ Antimicrobial activity of muga nanofibrous mat was higher compared to muga cast film. For both the sample, value of 'n' was higher than 0.45, which showed that release of gentamicin from muga nanofibrous mat and cast film follow anomalous diffusion behavior. The value of k was higher for muga nanofibrous mat than cast film, indicating higher rate of gentamicin release from muga nanofibrous mat due to higher porosity as well as swelling capacity.

❖ After 30 days of incubation, biodegradation was higher in case of muga nanofibrous mat, with a weight loss of 50% as compared to muga cast film for which mass loss was found to be 42%.

❖ Shear viscosity of 5, 7 and 10% w/v tasar ionic liquid dope solution was 535, 1132 and 1542 centipoise, respectively at shear rate of $1S^{-1}$.

❖ Optimized tasar silk fibroin nanofibrous mat prepared with 10% w/v tasar silk fibroin dope solution at 25 kV had average diameter of 185 nm.

❖ Formation of silver nanoparticles confirmed by the characteristic absorption band at 420 nm after 5 min of reaction between *Tridax procumbens* leaf extract and silver nitrate solution. The average size of silver nanoparticles as revealed by HR-TEM was 20 nm. Tasar nanofibrous mat exhibited good mechanical strength with tensile strength and modulus values of 4 MPa and 220 MPa respectively.

❖ The nanophase roughness of AgNPs coated tasar nanofibrous mat was slightly higher (38 nm) as compared to tasar nanofibrous mat (30 nm). The WVTR of AgNPs coated tasar nanofibous mat is 2300 g/m^2/day. Water uptake of AgNPs coated tasar nanofibrous mat was 70%.

❖ AgNPs coated tasar nanofibrous mat showed good growth and spreading of L929 fibroblast cells after 5 day of incubation.

❖ AgNPs coated tasar nanofibrous mat exhibited prominent zone of inhibition against both Gram positive and Gram negative bacteria. Mean diameter of zone of inhibition for AgNPs coated tasar nanofibrous mat was 10 and 14 mm against *S. aureus* and *E. coli*, respectively.

❖ Nanofibrous mat incubated in trypsin showed significantly higher mass loss of 48%.

❖ Dextrose was found as an effective plasticizer for the silk fibroin films.

❖ Increase in the dextrose content from 5 to 15%, the elongation at break of muga and tasar silk fibroin increased from 12 to 23% and 7 to 32%, respectively. The tensile strength & modulus values decreased significantly from 2.8 & 24 to 2.3 & 11 for muga and 15% dextrose modified muga film whereas it was reduced from 3.2 & 30 to 2 & 12 for tasar fibroin and 15% dextrose modified tasar fibroin film, respectively.

❖ Plasticization effect of dextrose on the muga and tasar fibroin films was further confirmed by measuring the tan δ peak at different temperature using dynamic mechanical analyzer. The tan δ peaks of tasar fibroin and muga fibroin films was found at 228 and 224 ^{o}C, respectively, which is shifted toward lower temperature region and observed at 218 and 210 ^{o}C for 15% DMTF and 15% DMMF, respectively.

❖ The maximum water uptake for TF and 15% (w/w) DMTF was 17 and 64%, respectively, which is not significantly different from the corresponding water uptake value of MF (19%) and 15% (w/w) DMMF (65%).

❖ The amount of drug released from dextrose plasticized samples was significantly higher than that of un-plasticized films. The maximum drug released from tasar fibroin and muga fibroin films was 45 and 40%, while it was 55 and 50% for 15% dextrose modified tasar fibroin film and 15% dextrose modified muga fibroin film. Dextrose plasticized muga and tasar silk fibroin

films show significantly higher cell growth and proliferation as compared to un-plasticized silk fibroin films.

❖ The 15% dextrose modified tasar fibroin film and 15% dextrose modified muga fibroin film showed significantly higher mass loss as compared to tasar fibroin and muga fibroin films after 50 days of incubation. The mass loss of tasar fibroin, muga fibroin, 15% dextrose modified tasar fibroin and 15% dextrose modified muga fibroin films was found to be 52, 47, 67 and 60%, respectively. The maximum water uptake for tasar fibroin film and 15% dextrose modified tasar fibroin film was 17 and 64%, respectively, which is not significantly ($p > 0.05$) different from the water uptake value of muga fibroin film (19%) and 15% dextrose modified muga fibroin film (65%).

❖ Flexible tasar and muga fibroin films were prepared by incorporating hydrogel particles.

❖ The tensile strength and modulus value for muga fibroin film was 2.2 and 24 MPa, respectively that was increased upto 6 and 35 as we increase the amount of hydrogel particles upto 5% (w/w).

❖ Elongation at break (%) value for tasar and muga fibroin films was 10 and 12, respectively that was increased upto 35 and 38 as we increased hydrogel particles upto 5% w/w.

❖ The value of 'n' for 5% hydrogel doped muga and tasar silk fibroin films was 0.58 and 0.55, which shows anomalous release behavior of drug (Non-Fickian). The value of 'k' for 5% hydrogel doped muga and tasar silk fibroin films was found to be 12 and 10, respectively.

❖ The value of n and k for pure muga and tasar silk fibroin films was 0.68 & 0.65 and 0.19 & 0.18, respectively

❖ Adherence and proliferation of L929 cells seeded on tasar and muga fibroin films was significantly higher as compared to pure muga and tasar fibroin films.

8.2 Future Prospects

Further, some clinical studies and animal tests of these wound dressing materials will be carried out in future to compare its suitability over the commercial wound dressing. Nonmulberry silk fibroin based light weight, highly porous materials such as aerogels can be fabricated that would be highly advantageous for biomedical applications. 3D printed nonmulberry fibroin based construct are yet to be explored for wound dressing applications.

REFERENCES

[1]   C. Vepari, D.L. Kaplan, Silk as a biomaterials, Prog. Polym Sci. 32 (2007) 991–1007.

[2]   N. Panda, A. Bissoyi, K. Pramanik, A. Biswas, Development of novel electrospun nanofibrous scaffold from P. Ricini And A. Mylitta silk fibroin blend with improved surface and biological properties., Mater. Sci. Eng. C. Mater. Biol. Appl. 48 (2015) 521–32. doi:10.1016/j.msec.2014.12.010.

[3]   N. Kasoju, R.R. Bhonde, U. Bora, Fabrication of a novel micro–nano fibrous nonwoven scaffold with Antheraea assama silk fibroin for use in tissue engineering, Mater. Lett. 63 (2009) 2466–2469. doi:10.1016/j .matlet.2009.08.037.

[4]   S. Fan, Y. Zhang, H. Shao, X. Hu, Electrospun regenerated silk fibroin mats with enhanced mechanical properties., Int. J. Biol. Macromol. 56 (2013) 83–8. doi:10.1016/j.ijbiomac.2013.01.033.

[5]   Y. Wang, D.D. Rudym, A. Walsh, L. Abrahamsen, H.-J. Kim, H.S. Kim, et al., In vivo degradation of three-dimensional silk fibroin scaffolds., Biomaterials. 29 (2008) 3415–28. doi:10.1016/j.biomaterials.2008.05.002.

[6]   C. Bettinger, K. Cyr, Silk fibroin microfluidic devices, Adv. …. 19 (2007) 2847–2850. doi:10.1002/adma.200602487.Silk.

[7]   R.L. Horan, K. Antle, A.L. Collette, Y. Wang, J. Huang, J.E. Moreau, et al., In vitro degradation of silk fibroin., Biomaterials. 26 (2005) 3385–93. doi:10.1016/j.biomaterials.2004.09.020.

[8]   Z. Shao, F. Vollrath, Surprising strength of silkworm silk., Nature. 418 (2002) 741. doi:10.1038/418741a.

[9]   K. Ohgo, C. Zhao, M. Kobayashi, T. Asakura, Preparation of non-woven nanofibers of Bombyx mori silk, Samia cynthia ricini silk and recombinant hybrid silk with electrospinning method, Polymer (Guildf). 44 (2002) 841–846. doi:10.1016/S0032-3861(02)00819-4.

[10]   K. Sen, M. Babu K, Studies on Indian silk. II. Structure-property correlations, J. Appl. Polym. Sci. 92 (2004) 1098–1115. doi:10.1002/app.13610.

[11]   K. Sen, M. Babu K, Studies on Indian silk. I. Macrocharacterization and analysis of amino acid composition, J. Appl. Polym. Sci. 92 (2004) 1080–1097. doi:10.1002/app.13609.

[12]   S.P. Mishra, A text book of fibre science and technology, New Age International, 2000.

[13]   R.L. Moy, A. Lee, A. Zalka, Commonly used suture materials in skin surgery., Am. Fam. Physician. 44 (1991) 2123–8. http://www.ncbi.nlm.nih. gov/pubmed/1746393 (accessed September 23, 2016).

[14] B.-M. Min, G. Lee, S.H. Kim, Y.S. Nam, T.S. Lee, W.H. Park, Electrospinning of silk fibroin nanofibers and its effect on the adhesion and spreading of normal human keratinocytes and fibroblasts in vitro, Biomaterials. 25 (2004) 1289–1297. doi:10.1016/j.biomaterials.2003.08.045.

[15] B. Panilaitis, G.H. Altman, J. Chen, H.-J. Jin, V. Karageorgiou, D.L. Kaplan, Macrophage responses to silk, Biomaterials. 24 (2003) 3079–3085. doi:10.1016/S0142-9612(03)00158-3.

[16] Robert Lanza, Robert Langer and Joseph P. Vacanti, Principles of Tissue Engineering, 4th Edition, Academic Press (2014).

[17] D. Howard, L.D. Buttery, K.M. Shakesheff, S.J. Roberts, Tissue engineering: strategies, stem cells and scaffolds, J. Anat. 213 (2008) 66–72. doi: 10.1111/j.1469-7580.2008.00878.x

[18] A. Shai, H.I. Maibach, Wound Healing and Ulcers of the Skin : Diagnosis and Therapy : The Practical Approach, Springer-Verlag Berlin Heidelberg, 2005.

[19] Robert Lanza, Robert Langer, Joseph P. Vacanti, Principles of Tissue Engineering, I[st] Edition, Acedemic Press (1997).

[20] J.S. Boateng, K.H. Matthews, H.N.E. Stevens, G.M. Eccleston, Wound healing dressings and drug delivery systems: A review, J. Pharm. Sci. 97 (2008) 2892–2923.

[21] O.C. JB Debra, wound healing: technological innovaions and market overview - Google Scholar, Technol. Catal. Int. Corp. 2 (1998) 1–185. https://scholar.google.co.in/scholar?hl=en&q=wound+healing%3A+technologi cal+innovaions+and+market+overview&btnG= (accessed March 1, 2017).

[22] D. Morgan, Wounds-what should a dressings formulary include?, Pharm. J. (2009). http://www.pharmaceutical-journal.com/learning/learning-article/wou nds-what-should-a-dressings-formulary-include/10976442.article (accessed March 1, 2017).

[23] J.-H. Kim, H.-J. Moon, T.-H. Kim, J.-M. Jo, S.H. Yang, D. Naskar, et al., A novel in vivo platform for studying alveolar bone regeneration in rat., J. Tissue Eng. 4 (2013) 2041731413517705. doi:10.1177/2041731413517705.

[24] E.J. Chong, T.T. Phan, I.J. Lim, Y.Z. Zhang, B.H. Bay, S. Ramakrishna, C.T. Lim, Evaluation of electrospun PCL/gelatin nanofibrous scaffold for wound healing and layered dermal reconstitution, Acta Biomater. 3 (2007) 321–330

[25] B. Pomahac, T. Svensjo, F. Yao, H. Brown, E. Eriksson, Tissue Engineering of Skin, Crit. Rev. Oral Biol. Med. 9 (1998) 333–344. doi:10.1177/ 10454411980090030601.

[26] J.S. Boateng, K.H. Matthews, H.N.E. Stevens, G.M. Eccleston, Wound Healing Dressings and Drug Delivery Systems: A Review, J. Pharm. Sci. 97 (2008) 2892–2923. doi:10.1002/jps.21210.

[27]   B.L. Seala, T.C. Oterob, A. Panitch, Polymeric biomaterials for tissue and organ regeneration, Mater. Sci. Eng. 34 (2001) 147–230. doi:10.1016/S0927-796X(01)00035-3.

[28]   S. MacNeil, Progress and opportunities for tissue-engineered skin, Nature. 445 (2007) 874–880. doi:10.1038/nature05664.

[29]   T.M. Quynh, H. Mitomo, N. Nagasawa, Y. Wada, F. Yoshii, M. Tamada, Properties of crosslinked polylactides (PLLA & PDLA) by radiation and its biodegradability, Eur. Polym. J. 43 (2007) 1779–1785. doi:10.1016/j.eurpolymj.2007.03.007.

[30]   T.-M. Wu, C.-Y. Wu, Biodegradable poly(lactic acid)/chitosan-modified montmorillonite nanocomposites: Preparation and characterization, Polym. Degrad. Stab. 91 (2006) 2198–2204. doi:10.1016/j.polymde-gradstab.2006.01.004.

[31]   T.L. Khoo, A.S. Halim, A.Z.M. Saad, A.A. Dorai, The application of glycerol-preserved skin allograft in the treatment of burn injuries: an analysis based on indications., Burns. 36 (2010) 897–904. doi:10.1016/j.burns.2009.03.007.

[32]   F.M. Wood, M.L. Kolybaba, P. Allen, The use of cultured epithelial autograft in the treatment of major burn injuries: a critical review of the literature., Burns. 32 (2006) 395–401. doi:10.1016/j.burns.2006.01.008.

[33]   J.T. Shores, A. Gabriel, S. Gupta, Skin substitutes and alternatives: a review., Adv. Skin Wound Care. 20 (2007) 493-508–10. doi:10.1097/01. ASW.0000288217.83128.f3.

[34]   T. Liu, J. Miao, W. Sheng, Y. Xie, Q. Huang, Y. Shan, et al., Cytocompatibility of regenerated silk fibroin film: a medical biomaterial applicable to wound healing., J. Zhejiang Univ. Sci. B. 11 (2010) 10–6. doi:10.1631/jzus.B0900163.

[35]   P. Inpanya, A. Faikrua, A. Ounaroon, A. Sittichokechaiwut, J. Viyoch, W.K.R.W.T.M.B.D.G. and D.R.F. Menke N B, et al., Effects of the blended fibroin/aloe gel film on wound healing in streptozotocin-induced diabetic rats, Biomed. Mater. 7 (2012) 35008. doi:10.1088/1748-6041/7/3/035008.

[36]   A. Vasconcelos, A.C. Gomes, A. Cavaco-Paulo, Novel silk fibroin/elastin wound dressings, Acta Biomater. 8 (2012) 3049–3060. doi:10.1016/j.actbio .2012.04.035.

[37]   N. Bhardwaj, W.T. Sow, D. Devi, K.W. Ng, B.B. Mandal, N.-J. Cho, Silk fibroin-keratin based 3D scaffolds as a dermal substitute for skin tissue engineering., Integr. Biol. (Camb). 7 (2015) 53–63. doi:10.1039/c4ib00208c.

[38]   D.-H. Roh, S.-Y. Kang, J.-Y. Kim, Y.-B. Kwon, H. Young Kweon, K.-G. Lee, et al., Wound healing effect of silk fibroin/alginate-blended sponge in full thickness skin defect of rat., J. Mater. Sci. Mater. Med. 17 (2006) 547–52. doi:10.1007/s10856-006-8938-y.

[39] Z. Karahaliloğlu, B. Ercan, E.B. Denkbaş, T.J. Webster, Nanofeatured silk fibroin membranes for dermal wound healing applications., J. Biomed. Mater. Res. A. 103 (2015) 135–44. doi:10.1002/jbm.a.35161.

[40] E. Ruoslahti, M.D. Pierschbacher, New perspectives in cell adhesion: RGD and integrins., Science. 238 (1987) 491–7. http://www.ncbi.nlm.nih.gov/pubmed/2821619 (accessed August 10, 2016).

[41] C. Acharya, S.K. Ghosh, S.C. Kundu, Silk fibroin protein from mulberry and non-mulberry silkworms: cytotoxicity, biocompatibility and kinetics of L929 murine fibroblast adhesion, J. Mater. Sci. Mater. Med. 19 (2008) 2827–2836. doi:10.1007/s10856-008-3408-3.

[42] P. Bhattacharjee, B. Kundu, D. Naskar, T.K. Maiti, D. Bhattacharya, S.C. Kundu, Nanofibrous nonmulberry silk/PVA scaffold for osteoinduction and osseointegration, Biopolymers. 103 (2015) 271–284. doi:10.1002/bip.22594.

[43] N. Panda, A. Biswas, L.B. Sukla, K. Pramanik, Degradation Mechanism and Control of Blended Eri and Tasar Silk Nanofiber, Appl. Biochem. Biotechnol. 174 (2014) 2403–2412. doi:10.1007/s12010-014-1151-4.

[44] N. nath Panda, A. Biswas, K. Pramanik, S. Jonnalagadda, Enhanced osteogenic potential of human mesenchymal stem cells on electrospun nanofibrous scaffolds prepared from eri-tasar silk fibroin, J. Biomed. Mater. Res. Part B Appl. Biomater. 103 (2015) 971–982. doi:10.1002/jbm.b.33272.

[45] B. Kundu, S.C. Kundu, Bio-inspired fabrication of fibroin cryogels from the muga silkworm Antheraea assamensis for liver tissue engineering., Biomed. Mater. 8 (2013) 55003. doi:10.1088/1748-6041/8/5/055003.

[46] R.R. Mallepally, M.A. Marin, V. Surampudi, B. Subia, R.R. Rao, S.C. Kundu, et al., Silk fibroin aerogels: potential scaffolds for tissue engineering applications., Biomed. Mater. 10 (2015) 35002. doi:10.1088/1748-6041/10/3/035002.

[47] B.B. Mandal, S.C. Kundu, Non-Bioengineered Silk Fibroin Protein 3D Scaffolds for Potential Biotechnological and Tissue Engineering Applications, Macromol. Biosci. 8 (2008) 807–818. doi:10.1002/mabi.200800113.

[48] B.B. Mandal, S.C. Kundu, Cell proliferation and migration in silk fibroin 3D scaffolds, Biomaterials. 30 (2009) 2956–2965. doi:10.1016/j.biomaterials.2009.02.006.

[49] N. Bhardwaj, S.C. Kundu, Chondrogenic differentiation of rat MSCs on porous scaffolds of silk fibroin/chitosan blends, Biomaterials. 33 (2012) 2848–2857. doi:10.1016/j.biomaterials.2011.12.028.

[50] S. Hazra, S. Nandi, D. Naskar, R. Guha, S. Chowdhury, N. Pradhan, et al., Non-mulberry Silk Fibroin Biomaterial for Corneal Regeneration, Nat. Publ. Gr. (2016). doi:10.1038/srep21840.

[51]   C. Patra, S. Talukdar, T. Novoyatleva, S.R. Velagala, C. Mühlfeld, B. Kundu, et al., Silk protein fibroin from Antheraea mylitta for cardiac tissue engineering, Biomaterials. 33 (2012) 2673–2680. doi:10.1016/j. biomaterials.2011.12.036.

[52]   B.B. Mandal, S.C. Kundu, Calcium alginate beads embedded in silk fibroin as 3D dual drug releasing scaffolds, Biomaterials 30 (2009) 5170–5177.

[53]   J. Samal, S. Weinandy, A. Weinandy, M. Helmedag, L. Rongen, B. Hermanns-Sachweh, et al., Co-Culture of Human Endothelial Cells and Foreskin Fibroblasts on 3D Silk-Fibrin Scaffolds Supports Vascularization, Macromol. Biosci. 15 (2015) 1433–1446. doi:10.1002/mabi.201500054.

[54]   S. Talukdar, Q.T. Nguyen, A.C. Chen, R.L. Sah, S.C. Kundu, Effect of initial cell seeding density on 3D-engineered silk fibroin scaffolds for articular cartilage tissue engineering, Biomaterials. 32 (2011) 8927–8937. doi:10.1016/j.biomaterials.2011.08.027.

[55]   N. Goujon, R. Rajkhowa, X. Wang, N. Byrne, Effect of solvent on ionic liquid dissolved regenerated *antheraea assamensis* silk fibroin, J. Appl. Polym. Sci. 128 (2013) 4411–4416. doi:10.1002/app.38666.

[56]   D. Chouhan, B. Chakraborty, S.K. Nandi, B.B. Mandal, Role of non-mulberry silk fibroin in deposition and regulation of extracellular matrix towards accelerated wound healing, Acta Biomater. 48 (2017) 157-174.

[57]   C.M. Srivastava, R. Purwar, R. Kannaujia, D. Sharma, Flexible silk fibroin films for wound dressing, Fibers Polym. 16 (2015) 1020–1030. doi:10.1007/s12221-015-1020-y.

[58]   E.S. Gil, B. Panilaitis, E. Bellas, D.L. Kaplan, Functionalized Silk Biomaterials for Wound Healing, Adv. Healthc. Mater. 2 (2013) 206–217.

[59]   P. Uttayarat, S. Jetawattana, P. Suwanmala, J. Eamsiri, T. Tangthong, S. Pongpat, Antimicrobial electrospun silk fibroin mats with silver nanoparticles for wound dressing application, Fibers. Polym. 13 (2012) 999–1006.

[60]   G. Freddi, Y. Gotoh, T. Mori, I. Tsutsui, M. Tsukada, Chemical structure and physical properties of antheraea assama silk, J. Appl. Polym. Sci. 52 (1994) 775–781. doi:10.1002/app.1994.070520608.

[61]   G.S. Nadiger, N.V. Bhat, Investigation of amino acid composition in the crystallne region of silk fibroin., J. Appl. Polym. Sci. 30 (1985) 221–225.

[62]   M.L. Gulrajani, R. Purwar, R.K. Prasad, M. Joshi, Studies on Structural and Functional Properties of Sericin Recovered from Silk Degumming Liquor by Membrane Technology, (2009). doi:10.1002/app.

[63]   G. Freddi, G. Pessina, M. Tsukada, Swelling and dissolution of silk fibroin (Bombyx mori) in N-methyl morpholine N-oxide, Int. J. Biol. Macromol. 24 (1999) 251–263.

[64]   X. Chen, D.P. Knight, Z. Shao, F. Vollrath, Regenerated Bombyx silk solutions studied with rheometry and FTIR, (n.d.).

[65]   J. Yao, H. Masuda, C. Zhao, T. Asakura, Artificial Spinning and Characterization of Silk Fiber from Bombyx mori Silk Fibroin in Hexafluoroacetone Hydrate, (n.d.). doi:10.1021/ma011335j.

[66]   David M. Phillips, Lawrence F. Drummy, Deborah G. Conrady, Douglas M. Fox, Rajesh R. Naik, Morley O. Stone, et al., Dissolution and Regeneration of Bombyx mori Silk Fibroin Using Ionic Liquids, (2004). doi:10.1021/JA046079F.

[67]   N. Goujon, X. Wang, R. Rajkowa, N. Byrne, Regenerated silk fibroin using protic ionic liquids solvents: towards an all-ionic-liquid process for producing silk with tunable properties., Chem. Commun. (Camb). 48 (2012) 1278–80. doi:10.1039/c2cc17143k.

[68]   S. Shang, L. Zhu, J. Fan, Physical properties of silk fibroin/cellulose blend films regenerated from the hydrophilic ionic liquid, Carbohydr. Polym. 86 (2011) 462–468.

[69]   I.C. Um, C.S. Ki, H. Kweon, K.G. Lee, D.W. Ihm, Y.H. Park, Wet spinning of silk polymer, Int. J. Biol. Macromol. 34 (2004) 107–119. doi:10.1016/j.ijbiomac.2004.03.011.

[70]   I.C. Um, H. Kweon, K.G. Lee, D.W. Ihm, J.-H. Lee, Y.H. Park, Wet spinning of silk polymer I. Effect of coagulation conditions on the morphological feature of filament, Int. J. Biol. Macromol. 34 (2004) 89–105. doi:10.1016/j.ijbiomac.2004.03.007.

[71]   M. Andiappan, T. Kumari, S. Sundaramoorthy, G. Meiyazhagan, P. Manoharan, G. Venkataraman, Comparison of eri and tasar silk fibroin scaffolds for biomedical applications., Prog. Biomater. 5 (2016) 81–91. doi:10.1007/s40204-016-0047-5.

[72]   S. Kar, S. Talukdar, S. Pal, S. Nayak, P. Paranjape, S.C. Kundu, Silk gland fibroin from indian muga silkworm Antheraea assama as potential biomaterial, Tissue Eng. Regen. Med. 10 (2013) 200–210.

[73]   W. Tao, M. Li, C. Zhao, Structure and properties of regenerated Antheraea pernyi silk fibroin in aqueous solution, Int. J. Biol. Macromol. 40 (2007) 472–478.

[74]   B.B. Mandal, S.C. Kundu, Non-bioengineered silk gland fibroin protein: Characterization and evaluation of matrices for potential tissue engineering applications, Biotechnol. Bioeng. 100 (2008) 1237–1250. doi:10.1002/bit.21835.

[75]   C. Acharya, S.K. Ghosh, S.C. Kundu, Silk fibroin film from non-mulberry tropical tasar silkworms: A novel substrate for in vitro fibroblast culture., Acta Biomater. 5 (2009) 429–37.

[76] P. Pyo-Jam, J. Jae-Young, J. Won-Kyo, A.Chang-Bum, K. Se-Kwon, Anticoagulant activity of heterochitosans and their oligosaccharide sulfates, Eur Food Res Technol. 219 (2004) 529–533. doi:10.1007/s00217-004-0977-3.

[77] S.B. Rao, C.P. Sharma, Use of chitosan as a biomaterial: studies on its safety and hemostatic potential., J. Biomed. Mater. Res. 34 (1997) 21–8. http://www.ncbi.nlm.nih.gov/pubmed/8978649 (accessed January 17, 2017).

[78] W. Paul, C.P. Sharma, Chitosan and Alginate Wound Dressings: A Short Review, Trends Biomater. Artif. Organs. 18 (2004) 18–23. http://www.sbaoi.org (accessed January 17, 2017).

[79] N. Kasoju, R.R. Bhonde, U. Bora, Preparation and characterization of *Antheraea assama* silk fibroin based novel non-woven scaffold for tissue engineering applications, J. Tissue Eng. Regen. Med. 3 (2009) 539–552. doi:10.1002/term.196.

[80] U. Armato, I.D. Pra, C. Migliaresi, A. Motta, K. Kesenci, Method for the preparation of a non-woven silk fibroin fabrics, US 7285637 B2 (2001).

[81] S.H. Kim, Y.S. Nam, T.S. Lee, W.H. Park, Silk Fibroin Nanofiber. Electrospinning, Properties, and Structure, Polym. J. 35 (2003) 185–190. doi:10.1295/polymj.35.185.

[82] B.B. Mandal, S.C. Kundu, Biospinning by silkworms: Silk fiber matrices for tissue engineering applications, Acta Biomater. 6 (2010) 360–371. doi:10.1016/j.actbio.2009.08.035.

[83] T.L. Khoo, A.S. Halim, A.Z.M. Saad, A.A. Dorai, The application of glycerol-preserved skin allograft in the treatment of burn injuries: an analysis based on indications., Burns. 36 (2010) 897–904. doi:10.1016/j.burns.2009.03.007.

[84] J.T. Shores, A. Gabriel, S. Gupta, Skin substitutes and alternatives: a review., Adv. Skin Wound Care. 20 (2007) 493-508–10. doi:10.1097/01 ASW.0000288217.83128.f3.

[85] K.A. Rieger, N.P. Birch, J.D. Schiffman, Designing electrospun nanofiber mats to promote wound healing – a review, J. Mater. Chem. B. 1 (2013) 4531–4541.

[86] S.E. Wharram, X. Zhang, D.L. Kaplan, S.P. McCarthy, Electrospun silk material systems for wound healing, Macromol. Biosci. 10 (2010) 246–257.

[87] A. Formhals, Process and apparatus for preparing artificial threads, US 1975504 A (1934).

[88] H.-J. Jin, S. V Fridrikh, G.C. Rutledge, D.L. Kaplan, Electrospinning Bombyx mori Silk with Poly(ethylene oxide), Biomacromolecules, 3 (2002) (6) 1233–1239 doi:10.1021/bm025581u.

[89] J.M. Deitzel, J. Kleinmeyer, D. Harris, N.C.B. Tan, The effect of processing variables on the morphology of electrospun nanofibers and textiles, 42 (2001) 261–272.

[90] Y.M. Shin, M.M. Hohman, M.P. Brenner, G.C. Rutledge, Experimental characterization of electrospinning: the electrically forced jet and instabilities, Polymer 42 (2001) 09955–09967

[91] G.E. Wnek, M.E. Carr, D.G. Simpson, G.L. Bowlin, Electrospinning of Nanofiber Fibrinogen Structures, *Nano Letters*, *3* (2003) 213–216. doi:10.1021/nl025866c.

[92] X. Fang, D.H. Reneker, Journal of Macromolecular Science, Part B DNA Fibers by Electrospinning, J. Macromol. Sci. Part B J. MACROMOL. SCI. - PHYS. 36 (1997) 169–173. doi:10.1080/00222349708220422.

[93] K. Ohgo, C. Zhao, M. Kobayashi, T. Asakura, Preparation of non-woven nanofibers of Bombyx mori silk, Samia cynthia ricini silk and recombinant hybrid silk with electrospinning method, 44 (2003) 841–846.

[94] S. Sukigara, M. Gandhi, J. Ayutsede, M. Micklus, F. Ko, Regeneration of Bombyx mori silk by electrospinning—part 1: processing parameters and geometric properties, 44 (2003) 5721–5727. doi:10.1016/S0032-3861(03)00532-9.

[95] J. Ayutsede, M. Gandhi, S. Sukigara, M. Micklus, H.-E. Chen, F. Ko, Regeneration of Bombyx mori silk by electrospinning. Part 3: characterization of electrospun nonwoven mat, Polymer (Guildf). 46 (2005) 1625–1634. doi:10.1016/j.polymer.2004.11.029.

[96] S. Zarkoob, R.. Eby, D.H. Reneker, S.D. Hudson, D. Ertley, W.W. Adams, Structure and morphology of electrospun silk nanofibers, Polymer (Guildf). 45 (2004) 3973–3977. doi:10.1016/j.polymer.2003.10.102.

[97] K.H. Lee, C.S. Ki, D.H. Baek, G.D. Kang, I. Dae-Woo, Y.H. Park, Application of electrospun silk fibroin nanofibers as an immobilization support of enzyme, Fiber. Polym. 6 (2005) 181-185.

[98] K. Zhang, X. Mo, C. Huang, C. He, H. Wang, Electrospun scaffolds from silk fibroin and their cellular compatibility, J. Biomed. Mater. Res. Part A. 9999A (2009) NA-NA. doi:10.1002/jbm.a.32497.

[99] J. Zhu, H. Shao, X. Hu, Morphology and structure of electrospun mats from regenerated silk fibroin aqueous solutions with adjusting pH, Int. J. Biol. Macromol. 41 (2007) 469–474. doi:10.1016/j.ijbiomac.2007.06.006.

[100] K. Shanmugam, S. Sundaramoorthy, A.M. Reed, W. Czaja, A. Krystynowicz, S. Bielecki, et al., Development and characterization of an electrospun mat from Eri silk fibroin and PLA blends for wound dressing application, RSC Adv. 5 (2015) 31352–31364. doi:10.1039/C4RA15268A.

[101] L. Jeong, K.Y. Lee, W.H. Park, Effect of Solvent on the Characteristics of Electrospun Regenerated Silk Fibroin Nanofibers, Key Eng. Mater. 342–343 (2007) 813–816. doi:10.4028/www.scientific.net/KEM.342-343.813.

[102] J. Zhu, Y. Zhang, H. Shao, X. Hu, Electrospinning and rheology of regenerated Bombyx mori silk fibroin aqueous solutions: The effects of pH and

concentration, Polymer (Guildf). 49 (2008) 2880–2885. doi:10.1016/j.
polymer.2008.04.049.

[103] C. Meechaisue, P. Wutticharoenmongkol, R. Waraput, T. Huangjing, N. Ketbumrung, P. Pavasant, et al., Preparation of electrospun silk fibroin fiber mats as bone scaffolds: a preliminary study, Biomed. Mater. 2 (2007) 181–188. doi:10.1088/1748-6041/2/3/003.

[104] N. Amiraliyan, M. Nouri, M.H. Kish, Electrospinning of silk nanofibers. I. An investigation of nanofiber morphology and process optimization using response surface methodology, Fibers Polym. 10 (2009) 167–176. doi:10.1007/s12221-009-0167-9.

[105] Y. Baimark, P. Srihanam, Y. Srisuwan, Preparation of Flexible Silk Fibroin Films Plasticized with Glucose, Asian J. Mater. Sci. 1 (2009) 29–35. doi:10.3923/ajmskr.2009.29.35.

[106] G.S. Lazarus, D.M. Cooper, D.R. Knighton, D.J. Margolis, R.E. Percoraro, G. Rodeheaver, et al., Definitions and guidelines for assessment of wounds and evaluation of healing, Wound Repair Regen. 2 (1994) 165–170. doi:10.1046/j.1524-475X.1994.20305.x.

[107] H.-J. Jin, J. Park, V. Karageorgiou, U.-J. Kim, R. Valluzzi, P. Cebe, et al., Water-Stable Silk Films with Reduced β-Sheet Content, Adv. Funct. Mater. 15 (2005) 1241–1247. doi:10.1002/adfm.200400405.

[108] P. Monti, G. Freddi, A. Bertoluzza, N. Kasai, M. Tsukada, Raman spectroscopic studies of silk fibroin fromBombyx mori, J. Raman Spectrosc. 29 (1998) 297–304. doi:10.1002/(SICI)1097-4555(199804)29:4<297::AID-JRS240>3.0.CO;2-G.

[109] W.S. Muller, L.A. Samuelson, S.A. Fossey, D.L. Kaplan, Formation and Characterization of Langmuir Silk Films, Langmuir. 9 (1993) 1867–1861.

[110] X.-J. Lian, S. Wang, H.-S. Zhu, Surface properties and cytocompatibillity of silk fibroin films cast from aqueous solutions in different concentrations, Front. Mater. Sci. China. 4 (2010) 57–63. doi:10.1007/s11706-010-0013-4.

[111] J. Liu, B.D. Lawrence, A. Liu, I.R. Schwab, L.A. Oliveira, M.I. Rosenblatt, Silk Fibroin as a Biomaterial Substrate for Corneal Epithelial Cell Sheet Generation, Investig. Opthalmology Vis. Sci. 53 (2012) 4130. doi:10.1167/iovs.12-9876.

[112] F.P. Seib, M.F. Maitz, X. Hu, C. Werner, D.L. Kaplan, Impact of processing parameters on the haemocompatibility of Bombyx mori silk films., Biomaterials. 33 (2012) 1017–23. doi:10.1016/j.biomaterials.2011.10.063.

[113] A.B. Mathur, A. Tonelli, T. Rathke, S. Hudson, The dissolution and characterization of Bombyx mori silk fibroin in calcium nitrate-methanol solution and the regeneration of films, Biopolymers. 42 (1997) 61–74. doi:10.1002/(SICI)1097-0282(199707)42:1<61::AID-BIP6>3.0.CO;2-#.

[114] J. Kundu, Y.-I. Chung, Y.H. Kim, G. Tae, S.C. Kundu, Silk fibroin nanoparticles for cellular uptake and control release, Int. J. Pharm. 388 (2010) 242–250. doi:10.1016/j.ijpharm.2009.12.052.

[115] O. Hakimi, D.P. Knight, F. Vollrath, P. Vadgama, Spider and mulberry silkworm silks as compatible biomaterials, Compos. Part B Eng. 38 (2007) 324–337.

[116] S.S. Silva, E.G. Popa, M.E. Gomes, M.B. Oliveira, S. Nayak, B. Subia, et al., Silk hydrogels from non-mulberry and mulberry silkworm cocoons processed with ionic liquids, Acta Biomater. 9 (2013) 8972–8982.

[117] S. Dutta, B. Talukdar, R. Bharali, R. Rajkhowa, D. Devi, Fabrication and characterization of biomaterial film from gland silk of muga and eri silkworms., Biopolymers. 99 (2013) 326–33.

[118] H.J. Kim, I.C. Um, Effect of degumming ratio on wet spinning and post drawing performance of regenerated silk., Int. J. Biol. Macromol. 67 (2014) 387–93. doi:10.1016/j.ijbiomac.2014.03.055.

[119] M.A. de Moraes, C.R. Albrecht Mahl, M. Ferreira Silva, M.M. Beppu, Formation of silk fibroin hydrogel and evaluation of its drug release profile, J. Appl. Polym. Sci. 132 (2015) n/a-n/a. doi:10.1002/app.41802.

[120] N. Kasoju, U. Bora, Antheraea assama Silk Fibroin-Based Functional Scaffold with Enhanced Blood Compatibility for Tissue Engineering Applications, Adv. Eng. Mater. 12 (2010) B139–B147. doi:10.1002/adem.200980055.

[121] N. Sahu, P. Baligar, S. Midha, B. Kundu, M. Bhattacharjee, S. Mukherjee, et al., Nonmulberry Silk Fibroin Scaffold Shows Superior Osteoconductivity Than Mulberry Silk Fibroin in Calvarial Bone Regeneration, Adv. Healthcare Mater. 4 (2015) 1709-21. DOI:10.1002/adhm.201500283

[122] M. Andiappan, S. Sundaramoorthy, N. Panda, G. Meiyazhaban, S.B. Winfred, G. Venkataraman, et al., Electrospun eri silk fibroin scaffold coated with hydroxyapatite for bone tissue engineering applications, Prog. Biomater. 2 (2013) 6. doi:10.1186/2194-0517-2-6.

[123] N. Goujon, R. Rajkhowa, X. Wang, N. Byrne, Effect of solvent on ionic liquid dissolved regenerated antheraea assamensis silk fibroin, J. Appl. Polym. Sci. 128 (2013) 4411–4416.

[124] W. Luangbudnark, J. Viyoch, W. Laupattarakasem, P. Surakunprapha, P. Laupattarakasem, Properties and Biocompatibility of Chitosan and Silk Fibroin Blend Films for Application in Skin Tissue Engineering, Sci. World J. 2012 (2012) 1–10. doi:10.1100/2012/697201.

[125] S.J. Park, K.Y. Lee, W.S. Ha, S.Y. Park, Structural changes and their effect on mechanical properties of silk fibroin/chitosan blends, J. Appl. Polym. Sci. 74 (1999) 2571–2575. doi:10.1002/(SICI)1097-4628(19991209)74:11<2571:: AID-APP2>3.0.CO;2-A.

[126] R. Jayakumar, M. Prabaharan, P.T. Sudheesh Kumar, S.V. Nair, H. Tamura, Biomaterials based on chitin and chitosan in wound dressing applications, Biotechnol. Adv. 29 (2011) 322–337. doi:10.1016/j.biotechadv.2011.01.005.

[127] S.S. Silva, T.C. Santos, M.T. Cerqueira, A.P. Marques, L.L. Reys, T.H. Silva, et al., The use of ionic liquids in the processing of chitosan/silk hydrogels for biomedical applications, Green Chem. 14 (2012) 1463. doi:10. 1039/c2gc16535j.

[128] A. Sionkowska, A. Płanecka, Preparation and characterization of silk fibroin/chitosan composite sponges for tissue engineering, J. Mol. Liq. 178 (2013) 5–14. doi:10.1016/j.molliq.2012.10.042.

[129] Z. She, A. Chenrui, J. Ae, Z. Huang, B. Zhang, A. Qingling, et al., Silk fibroin/chitosan scaffold: preparation, characterization, and culture with HepG2 cell, J. Mater. Sci. Mater. Med. 19 (2008) 3545-53 doi:10.1007/s10856-008-3526-y.

[130] D. Devi, N. Sen Sarma, B. Talukdar, P. Chetri, K.C. Baruah, N.N. Dass, Study of the structure of degummed Antheraea assamensis (muga) silk fibre, J. Text. Inst. 102 (2011) 527–533.

[131] C. Patra, S. Talukdar, T. Novoyatleva, S.R. Velagala, C. Mühlfeld, B. Kundu, et al., Silk protein fibroin from Antheraea mylitta for cardiac tissue engineering, Biomaterials. 33 (2012) 2673–2680. doi:10.1016/j.biomaterials.2011.12.036.

[132] N. Bhardwaj, Q.T. Nguyen, A.C. Chen, D.L. Kaplan, R.L. Sah, S.C. Kundu, Potential of 3-D tissue constructs engineered from bovine chondrocytes/silk fibroin-chitosan for in vitro cartilage tissue engineering, Biomaterials. 32 (2011) 5773–5781. doi:10.1016/j.biomaterials.2011.04.061.

[133] J. Wang, S. Zhang, T. Xing, B. Kundu, M. Li, S.C. Kundu, et al., Ion-induced fabrication of silk fibroin nanoparticles from Chinese oak tasar Antheraea pernyi, Int. J. Biol. Macromol. 79 (2015) 316–325. doi:10.1016/j.ijbiomac.2015.04.052.

[134] S. Yodmuang, S.L. McNamara, A.B. Nover, B.B. Mandal, M. Agarwal, T.-A.N. Kelly, et al., Silk microfiber-reinforced silk hydrogel composites for functional cartilage tissue repair, Acta Biomater. 11 (2015) 27–36. doi:10.1016/j.actbio.2014.09.032.

[135] D. Naskar, S. Nayak, T. Dey, S.C. Kundu, Non-mulberry silk fibroin influence osteogenesis and osteoblast-macrophage cross talk on titanium based surface., Sci. Rep. 4 (2014) 4745. doi:10.1038/srep04745.

[136] N.J. Percival, Classification of Wounds and their Management, Surg. 20 (2002) 114–117. doi:10.1383/surg.20.5.114.14626.

[137] K.G. Harding, H.L. Morris, G.K. Patel, Science, medicine and the future: healing chronic wounds., BMJ. 324 (2002) 160–3. http://www.ncbi.nlm.nih.gov/pubmed/11799036 (accessed March 2, 2017).

[138] J.S. Boateng, K.H. Matthews, H.N.E. Stevens, G.M. Eccleston, Wound Healing Dressings and Drug Delivery Systems: A Review, J. Pharm. Sci. 97 (2008) 2892–2923. doi:10.1002/jps.21210.

[139] T. Liu, J. Miao, W. Sheng, Y. Xie, Q. Huang, Y. Shan, et al., Cytocompatibility of regenerated silk fibroin film: a medical biomaterial applicable to wound healing., J. Zhejiang Univ. Sci. B. 11 (2010) 10–6. doi:10.1631/jzus.B0900163.

[140] A. Vasconcelos, A.P. Pêgo, L. Henriques, M. Lamghari, A. Cavaco-Paulo, Protein Matrices for Improved Wound Healing: Elastase Inhibition by a Synthetic Peptide Model, Biomacromolecules. 11 (2010) 2213–2220. doi:10.1021/bm100537b.

[141] D.-H. Roh, S.-Y. Kang, J.-Y. Kim, Y.-B. Kwon, H. Young Kweon, K.-G. Lee, et al., Wound healing effect of silk fibroin/alginate-blended sponge in full thickness skin defect of rat, J. Mater. Sci. Mater. Med. 17 (2006) 547–552. doi:10.1007/s10856-006-8938-y.

[142] K. Karthikeyan, S. Sekar, M. Pandima Devi, S. Inbasekaran, C.H. Lakshminarasaiah, T.P. Sastry, Fabrication of novel biofibers by coating silk fibroin with chitosan impregnated with silver nanoparticles, J. Mater. Sci. Mater. Med. 22 (2011) 2721–2726. doi:10.1007/s10856-011-4462-9.

[143] Q. Lu, X. Zhang, X. Hu, D.L. Kaplan, Green Process to Prepare Silk Fibroin/Gelatin Biomaterial Scaffolds, Macromol. Biosci. 10 (2010) 289–298. doi:10.1002/mabi.200900258.

[144] Maneesh K. Gupta, Shama K. Khokhar, David M. Phillips, Laura A. Sowards, Lawrence F. Drummy, Madhavi P. Kadakia, et al., Patterned Silk Films Cast from Ionic Liquid Solubilized Fibroin as Scaffolds for Cell Growth, *Langmuir* 23 (2007) 1315–1319. doi:10.1021/LA062047P.

[145] C. Vepari, D. Matheson, L. Drummy, R. Naik, D.L. Kaplan, Surface modification of silk fibroin with poly(ethylene glycol) for antiadhesion and antithrombotic applications, J. Biomed. Mater. Res. Part A. 93 (2010) 595-606. doi:10.1002/jbm.a.32565.

[146] R.K. Mishra, K. Ramasamy, S.M. Lim, M.F. Ismail, A.B.A. Majeed, Antimicrobial and in vitro wound healing properties of novel clay based bionanocomposite films, J. Mater. Sci. Mater. Med. 25 (2014) 1925–1939. doi:10.1007/s10856-014-5228-y.

[147] B. Kundu, C.J. Schlimp, S. Nürnberger, H. Redl, S.C. Kundu, Thromboelastometric and platelet responses to silk biomaterials, Sci. Rep. 4 (2014) 4945. doi:10.1038/srep04945.

[148] S. Çalamak, C. Erdoğdu, M. Özalp, K. Ulubayram, Silk fibroin based antibacterial bionanotextiles as wound dressing materials, Mater. Sci. Eng. C. 43 (2014) 11–20. doi:10.1016/j.msec.2014.07.001.

[149] A. Schneider, X.Y. Wang, D.L. Kaplan, J.A. Garlick, C. Egles, Biofunctionalized electrospun silk mats as a topical bioactive dressing for accelerated wound healing., Acta Biomater. 5 (2009) 2570–8. doi:10.1016/j.actbio.2008.12.013.

[150] W.-Y. Lee, I.C. Um, M.-K. Kim, K.-J. Kwon, S.-G. Kim, Y.-W. Park, Effectiveness of Woven Silk Dressing Materials on Full-skin Thickness Burn Wounds in Rat Model., Maxillofac. Plast. Reconstr. Surg. 36 (2014) 280–4. doi:10.14402/jkamprs.2014.36.6.280.

[151] U.K. Laemmli, Cleavage of structural proteins during the assembly of the head of bacteriophage T4., Nature. 227 (1970) 680–5.

[152] A. Gupta K, K. Mita, K.P. Arunkumar, J. Nagaraju, Molecular architecture of silk fibroin of Indian golden silkmoth, Antheraea assama, Sci. Rep. 5 (2015) 12706.

[153] N.J. Greenfield, Using circular dichroism spectra to estimate protein secondary structure., Nat. Protoc. 1 (2006) 2876–90.

[154] B.B. Mandal, S.C. Kundu, Cell proliferation and migration in silk fibroin 3D scaffolds., Biomaterials. 30 (2009) 2956–65. doi:10.1016/j.bio materials.2009.02.006.

[155] E.S. Gadelmawla, M.M. Koura, T.M. a Maksoud, I.M. Elewa, H.H. Soliman, Roughness parameters, J. Mater. Process. Technol. 123 (2002) 133–145.

[156] Z. Pei, Q. Sun, X. Sun, Y. Wang, P. Zhao, Preparation and characterization of silver nanoparticles on silk fibroin/carboxymethylchitosan composite sponge as anti-bacterial wound dressing., Biomed. Mater. Eng. 26 Suppl 1 (2015) S111-8. doi:10.3233/BME-151296.

[157] M.A. de Moraes, R.F. Weska, M.M. Beppu, Effects of sterilization methods on the physical, chemical, and biological properties of silk fibroin membranes., J. Biomed. Mater. Res. B. Appl. Biomater. 102 (2014) 869–76.

[158] S.W. Ali, R. Purwar, M. Joshi, S. Rajendran, Antibacterial properties of Aloe vera gel-finished cotton fabric, Cellulose. 21 (2014) 2063–2072. doi:10.1007/s10570-014-0175-9.

[159] S.S. Sampath, D.H. Robinson, Comparison of new and existing spectrophotometric methods for the analysis of tobramycin and other aminoglycosides., J. Pharm. Sci. 79 (1990) 428–31.

[160] Nikolaos A. Peppas and Jennifer J. Sahlin, [PDF]A simple equation for description of solute release I. Fickian and non-fickian release from non-swellable devices in the form of slabs, spheres, cylinders or discs, 5 (1987) 23-36.

[161] A. Teimouri, R. Ebrahimi, A.N. Chermahini, R. Emadi, Fabrication and characterization of silk fibroin/chitosan/Nano γ-alumina composite scaffolds for tissue engineering applications, RSC Adv. 5 (2015) 27558–27570. doi:10.1039/C5RA01018G.

[162] D. Gogoi, A.J. Choudhury, J. Chutia, A.R. Pal, M. Khan, M. Choudhury, et al., Development of advanced antimicrobial and sterilized plasma polypropylene grafted muga (*antheraea assama*) silk as suture biomaterial, Biopolymers. 101 (2014) 355–365. doi:10.1002/bip.22369.

[163] S. Mobini, B. Hoyer, M. Solati-Hashjin, A. Lode, N. Nosoudi, A. Samadikuchaksaraei, et al., Fabrication and characterization of regenerated silk scaffolds reinforced with natural silk fibers for bone tissue engineering, J. Biomed. Mater. Res. Part A. 101A (2013) 2392–2404. doi:10.1002/jbm.a.34537.

[164] X. Chen, W. Li, T. Yu, Conformation transition of silk fibroin induced by blending chitosan, J. Polym. Sci. Part B Polym. Phys. 35 (1997) 2293–2296. doi:10.1002/(SICI)1099-0488(199710)35:14<2293::AID-POLB9>3.0.CO;2-X.

[165] Q. Yuan, J. Yao, L. Huang, X. Chen, Z. Shao, Correlation between structural and dynamic mechanical transitions of regenerated silk fibroin, Polymer (Guildf). 51 (2010) 6278–6283. doi:10.1016/j.polymer.2010.10.046.

[166] U. Armato, P.I. Dal, K. Kesenci, C. Migliaresi, A. Motta, Method for the preparation of a non-woven silk fibroin fabrics, WO 2002029141 A1 (2002).

[167] M. Tsukada, G. Freddi, M. Nagura, H. Ishikawa, N. Kasai, Structural changes of silk fibers induced by heat treatment, J. Appl. Polym. Sci. 46 (1992) 1945–1953. doi:10.1002/app.1992.070461107.

[168] Q. Yuan, J. Yao, L. Huang, X. Chen, Z. Shao, Correlation between structural and dynamic mechanical transitions of regenerated silk fibroin, Polymer (Guildf). 51 (2010) 6278–6283. doi:10.1016/j.polymer.2010.10.046.

[169] Q. Li, J. Zhou, L. Zhang, Structure and properties of the nanocomposite films of chitosan reinforced with cellulose whiskers, J. Polym. Sci. Part B Polym. Phys. 47 (2009) 1069–1077. doi:10.1002/polb.21711.

[170] S.J. Eichhorn, W.W. Sampson, Statistical geometry of pores and statistics of porous nanofibrous assemblies., J. R. Soc. Interface. 2 (2005) 309–318. doi:10.1098/rsif.2005.0039.

[171] K. Zhang, Y. Qian, H. Wang, L. Fan, C. Huang, A. Yin, et al., Genipin-crosslinked silk fibroin/hydroxybutyl chitosan nanofibrous scaffolds for tissue-engineering application., J. Biomed. Mater. Res. A. 95 (2010) 870–81. doi:10.1002/jbm.a.32895.

[172] L.-O. Lamke, G.E. Nilsson, H.L. Reithner, The evaporative water loss from burns and the water-vapour permeability of grafts and artificial membranes used in the treatment of burns, Burns. 3 (1977) 159–165.

[173] X. Li, B. Li, J. Ma, X. Wang, S. Zhang, Development of a silk fibroin/HTCC/PVA sponge for chronic wound dressing, J. Bioact. Compat. Polym. 29 (2014) 398–411. doi:10.1177/0883911514537731.

[174] T.-C. Chou, E. Fu, C.-J. Wu, J.-H. Yeh, Chitosan enhances platelet adhesion and aggregation, Biochem. Biophys. Res. Commun. 302 (2003) 480–483. doi:10.1016/S0006-291X(03)00173-6.

[175] L. Wang, M. Fazley Elahi, G. Guan, HEMOCOMPATIBILITY OF SURFACE MODIFIED SILK FIBROIN MATERIALS: A REVIEW, Rev. Adv. Mater. Sci. 38 (2014) 148–159.

[176] A. Nakajima, K. Shinoda, Complex formation between oppositely charged polysaccharides, J. Colloid Interface Sci. 55 (1976) 126–132. doi:10.1016/0021-9797(76)90017-5.

[177] S.H. Kim, Y.S. Nam, T.S. Lee, W.H. Park, Silk Fibroin Nanofiber. Electrospinning, Properties, and Structure, Polym. J. 35 (2003) 185–190. doi:10.1295/polymj.35.185.

[178] J. Li, Y.M. Du, H.B. Liang, P.J. Yao, Y.A. Wei, Effect of immobilized neutral protease on the preparation and physicochemical properties of low molecular weight chitosan and chito-oligomers, J. Appl. Polym. Sci. 102 (2006) 4185–4193. doi:10.1002/app.24555.

[179] G.J. Tsai, W.H. Su, Antibacterial activity of shrimp chitosan against Escherichia coli., J. Food Prot. 62 (1999) 239–43. http://www.ncbi.nlm.nih.gov/pubmed/10090242 (accessed January 19, 2017).

[180] D.H. Young, H. Kauss, Release of Calcium from Suspension-Cultured Glycine max Cells by Chitosan, Other Polycations, and Polyamines in Relation to Effects on Membrane Permeability., Plant Physiol. 73 (1983) 698–702. doi:10.1104/PP.73.3.698.

[181] Entsar I. Rabea, Mohamed E.-T. Badawy, Christian V. Stevens, Guy Smagghe, W. Steurbaut, Chitosan as Antimicrobial Agent: Applications and Mode of Action, Biomacromolecules 4 (2003) 1457–1465. doi:10.1021/BM034130M.

[182] S.Y. Lee, M.S. Rhee, R.H. Dougherty, D.H. Kang, Antagonistic effect of acetic acid and salt for inactivating *Escherichia coli* O157:H7 in cucumber puree, J. Appl. Microbiol. 108 (2010) 1361–1368. doi:10.1111/j.1365-2672.2009.04543.x.

[183] Y. Chung, Y. Su, C. Chen, G. Jia, H. Wang, J.C.G. Wu, et al., Relationship between antibacterial activity of chitosan and surface characteristics of cell wall., Acta Pharmacol. Sin. 25 (2004) 932–6. http://www.ncbi.nlm.nih.gov/pubmed/15210068 (accessed January 19, 2017).

[184] D.S. Katti, K.W. Robinson, F.K. Ko, C.T. Laurencin, Bioresorbable nanofiber-based systems for wound healing and drug delivery: Optimization of fabrication parameters, J. Biomed. Mater. Res. 70B (2004) 286–296.

[185] S. Sukigara, M. Gandhi, J. Ayutsede, M. Micklus, F. Ko, Regeneration of Bombyx mori silk by electrospinning—part 1: processing parameters and

geometric properties, Polymer (Guildf). 44 (2003) 5721–5727. doi:10.1016/S0032-3861(03)00532-9.

[186] A.E. Terry, D.P. Knight, D. Porter, F. Vollrath, pH induced changes in the rheology of silk fibroin solution from the middle division of Bombyx mori silkworm, Biomacromolecules. 5 (2004) 768–772.

[187] G. Li, P. Zhou, Z. Shao, X. Xie, X. Chen, H. Wang, et al., The natural silk spinning process, Eur. J. Biochem. 268 (2001) 6600–6606.

[188] J. Pan, N. Liu, H. Sun, F. Xu, Preparation and characterization of electrospun PLCL/Poloxamer nanofibers and dextran/gelatin hydrogels for skin tissue engineering., PLoS One. 9 (2014) e112885. doi:10.1371/journal.pone.0112885.

[189] J.-E.W. Ahlfors, K.L. Billiar, Biomechanical and biochemical characteristics of a human fibroblast-produced and remodeled matrix., Biomaterials. 28 (2007) 2183–91. doi:10.1016/j.biomaterials.2006.12.030.

[190] R. Valluzzi, S.P. Gido, W. Zhang, W.S. Muller, D.L. Kaplan, Trigonal Crystal Structure of Bombyx mori Silk Incorporating a Threefold Helical Chain Conformation Found at the Air−Water Interface, Macromolecules. 29 (1996) 8606–8614.

[191] W.-C. Jao, M.-C. Yang, C.-H. Lin, C.-C. Hsu, Fabrication and characterization of electrospun silk fibroin/TiO2 nanofibrous mats for wound dressings, Polym. Adv. Technol. 23 (2012) 1066–1076.

[192] N. Panda, A. Bissoyi, K. Pramanik, A. Biswas, Directing osteogenesis of stem cells with hydroxyapatite precipitated electrospun eri-tasar silk fibroin nanofibrous scaffold., J. Biomater. Sci. Polym. Ed. 25 (2014) 1440–57.

[193] R. Narayan Mitra, P. Kumar Das, In situ Preparation of Gold Nanoparticles of Varying Shape in Molecular Hydrogel of Peptide Amphiphiles, J. Phys. Chem. C 112 (2008) 8159–8166. doi:10.1021/jp712106d.

[194] Anand Gole, Chandravanu Dash, Vidya Ramakrishnan, S. R. Sainkar, A. B. Mandale, Mala Rao, et al., Pepsin−Gold Colloid Conjugates: Preparation, Characterization, and Enzymatic Activity, Langmuir, 17 (2001) 1674–1679. doi:10.1021/LA001164W.

[195] Frank Caruso, D. Neil Furlong, Katsuhiko Ariga, Izumi Ichinose, T. Kunitake, Characterization of Polyelectrolyte−Protein Multilayer Films by Atomic Force Microscopy, Scanning Electron Microscopy, and Fourier Transform Infrared Reflection−Absorption Spectroscopy, Langmuir 14 (1998) 4559–4565. doi:10.1021/LA971288H.

[196] Chuan-xiang C & Shao-lin M, The electrochemical preparation of polyphenol with Conductibility, Chinese J. Polym. Sci. 20 (2002) 309–316.

[197] I. Sondi, B. Salopek-Sondi, Silver nanoparticles as antimicrobial agent: a case study on E. coli as a model for Gram-negative bacteria, J. Colloid Interface Sci. 275 (2004) 177–182. doi:10.1016/j.jcis.2004.02.012.

[198] V.S. Kumar, B.M. Nagaraja, V. Shashikala, A.H. Padmasri, S.S. Madhavendra, B.D. Raju, et al., Highly efficient Ag/C catalyst prepared by electro-chemical deposition method in controlling microorganisms in water, J. Mol. Catal. A Chem. 223 (2004) 313–319. doi:10.1016/j.molcata.2003.09.047.

[199] I.A. Wani, S. Khatoon, A. Ganguly, J. Ahmed, T. Ahmad, Structural characterization and antimicrobial properties of silver nanoparticles prepared by inverse microemulsion method, Colloids Surfaces B Biointerfaces. 101 (2013) 243–250. doi:10.1016/j.colsurfb.2012.07.001.

[200] M.J. Franco, A.A. Martin, L.F.B. Jr, J. Caetano, G.A. Linde, D.C. Dragunski, EFFECT OF PLASTICIZER AND MODIFIED STARCH ON BIODEGRADABLE FILMS FOR STRAWBERRY PROTECTION, 0 (2016) 1–9. doi:10.1111/jfpp.13063.

[201] S. Lu, X. Wang, Q. Lu, X. Zhang, J.A. Kluge, N. Uppal, et al., Insoluble and Flexible Silk Films Containing Glycerol, Biomacromolecules 11 (2010) 143–150. doi:10.1021/bm900993n.

[202] Y. Kawahara, K. Furukawa, T. Yamamoto, Self-Expansion Behavior of Silk Fibroin Film, Macromol. Mater. Eng. 291 (2006) 458–462. doi:10.1002/mame.200500350.

[203] Q. Yuan, J. Yao, L. Huang, X. Chen, Z. Shao, Correlation between structural and dynamic mechanical transitions of regenerated silk fibroin, Polymer (Guildf). 51 (2010) 6278–6283. doi:10.1016/j.polymer.2010.10.046.

[204] Q. Lu, X. Hu, X. Wang, J.A. Kluge, S. Lu, P. Cebe, et al., Water-insoluble silk films with silk I structure, Acta Biomater. 6 (2009) 1380–1387. doi:10.1016/j.actbio.2009.10.041.

[205] A. Motta, L. Fambri, C. Migliaresi, Regenerated silk fibroin films: Thermal and dynamic mechanical analysis, Macromol. Chem. Phys. 203 (2002) 1658–1665. doi:10.1002/1521-3935(200207)203:10/11<1658::AID-MACP1658>3.0.CO;2-3.

[206] A. Gupta K, K. Mita, K.P. Arunkumar, J. Nagaraju, L. Pauling, R.B. Corey, et al., Molecular architecture of silk fibroin of Indian golden silkmoth, Antheraea assama, Sci. Rep. 5 (2015) 12706. doi:10.1038/srep12706.

[207] J. Kundu, R. Mohapatra, S.C. Kundu, Silk fibroin/sodium carboxymethylcellulose blended films for biotechnological applications., J. Biomater. Sci. Polym. Ed. 22 (2011) 519–39. doi:10.1163/092050610X487864.

[208] P.L. Ritger, N.A. Peppas, A simple equation for description of solute release II. Fickian and anomalous release from swellable devices, J. Control. Release. 5 (1987) 37–42. doi:10.1016/0168-3659(87)90035-6.

[209] T.R. Hoare, D.S. Kohane, Hydrogels in drug delivery: Progress and challenges, Polymer (Guildf). 49 (2008) 1993–2007. doi:10.1016/j.polymer.2008.01.027.

PUBLICATIONS (FROM THESIS WORK)

Publication in International Journals

1. **Chandra Mohan Srivastava** and Roli Purwar, Fabrication of robust *Antheraea assama* fibroin nanofibrous mat using ionic liquid for skin tissue engineering, *Materials Science and Engineering C*, 2016, 68, 276-290. Impact factor: 3.42

2. **Chandra Mohan Srivastava**, Roli Purwar, Anuradha Gupta, Deepak Sharma, Dextrose modified flexible tasar and muga fibroin films for wound healing applications, *Materials Science and Engineering C*, 2017, 75, 104-114. Impact factor 3.42

3. **Chandra Mohan Srivastava** and Roli Purwar, Chitosan finished *Antheraea mylitta* silk fibroin nonwoven composite films for wound dressing, *Journal of Applied Polymer Science*, 2017, 134, 1-16, Impact factor: 1.866

4. **Chandra Mohan Srivastava**, Roli Purwar, Rekha Kannaujia, and Deepak Sharma, Flexible Silk Fibroin Films for Wound Dressing, *Fibers and Polymers,* 2015, 16, 1020-1030. Impact factor: 1.022

5. **Chandra Mohan Srivastava** and Roli Purwar, Recent developments in regenerated silk fibroin fibers, *International Journal of Research in Advent Technology*, 2014, 2, 267-277.

6. **Chandra Mohan Srivastava** and Roli Purwar, Fabrication of silk fibroin based spider web like structure for biomedical applications, *Materials Letter*, Submitted

7. **Chandra Mohan Srivastava** and Roli Purwar, Green approach for fabrication of silver nanoparticles coated tasar silk fibroin nanofibrous mat for skin tissue regeneration*, Applied Materials and Interface*, Submitted.

8. **Chandra Mohan Srivastava** and Roli Purwar, Chitosan based *Antheraea assama* silk fibroin nonwoven composite constructs for wound dressing, *International Journal of Biological Macromolecules*, submitted.

Patent

Chandra Mohan Srivastava and Dr. Roli Purwar, "Silk Fibroin Flexible Films Prepared by Hydrogel Particles and Process There of" patent numbered 201711011922 dated 01-04-2017 by Delhi Technological University of Shahbad, Daulatpur, Bawana Road, Delhi-110042.

Conference Publications

1. **Chandra Mohan Srivastava** and Roli Purwar, Dextrose plasticized muga and tasar silk fibroin films for skin tissue engineering, BiTerm 2016, April 15-17 2016 at held at IIT Delhi.

2. **Chandra Mohan Srivastava** and Roli Purwar, Study on Structure and Properties of Non Mulberry Silk Cocoons, Chandra Mohan Srivastava and Roli Purwar, International Conference on Polymeric Biomaterials, Bioengineering and Biodiagnostics, 27-30 October 2014, Organized by APA and IIT Delhi, New Delhi, India

3. **Chandra Mohsn Srivastava** and RoliPurwar, **रेशमफ़ाइब्राइनप्रोटीनकाडेक्स्ट्रोस प्रेरितसमनुरूपणसंक्रमणकाअध्ययन**, National Conference on Biomedical Science and Technology, 21-22 Nov. 2013, at CSIR, National Physical Laboratory, Delhi. (**Awarded Best Poster**)

4. **Chandra Mohan Srivastava** and Roli Purwar, Preparation of Non-Woven Silk Fibroin Film Modified with Methyl Cellulose with Casting Method, Asian Workshop on Polymer Processing, 8-11 Dec. 2013.

5. **Chandra Mohan Srivastava** and Roli Purwar, Green fabrication of muga fibroin nanofibrous mat using ionic liquid for skin tissue engineering, International Conference on Nanomaterials and Nanotechnology a global platform for smart nanotechnology" held on 1-3 march 2017 at Allahabad, Organized by VinobaBhave Research Institute, Allahabad

6. **Chandra Mohan Srivastava** and Roli Purwar, Chitosan impregnated muga silk fibroin nonwoven composite constructs for wound dressing, national conference on " Clean and Green energy: Chemical and environmental aspects" held on 16-17 Feb 2017 at Delhi organized by Bhaskaracharya College of Applied Science, University of Delhi

CURRICULUM VITAE

CHANDRA MOHAN SRIVASTAVA

Research Scholar (CSIR-SRF)
Fiber Technology Research Lab
Department of Applied Chemistry
Delhi Technological University, Delhi-110 042
Email: cms.srivastava@gmail.com

Area of Research Interest

Fabrication of biomaterials based nanofibrous mat for wound dressing and regenerative medicine, hydrogel and composite dressings

Academic Qualifications

- ❖ **Ph.D. (Applied Chemistry)** in 2012- present, from Delhi Technological University, Delhi.

- ❖ **M. Tech (Plastic Engineering)** in 2011

- ❖ **M.Sc. (Chemistry)** in 2008 from University of Lucknow (U.P).

- ❖ **B.Sc. (Chemistry & Botany)** in 2006 from University of Lucknow (U.P).

- ❖ **Intermediate** in 2003 from U.P.Board Allahabad.

- ❖ **High School** in 2001 from U.P.Board Allahabad.

Teaching Experience

- ➢ Worked as **Lecturer** from September 2011 to August 2012 in **C.I.P.E.T High Learning Center, Ahmedabad (Gujarat).**

Research Experience

- ➢ Worked as **Junior Research Fellow** in DRDO sponsored project title **"Supercritical Carbon dioxide Assisted Synthesis of MWCNT Epoxy Composites"** at G. B. Pant University of Agriculture and Technology, Pant Nagar, Uttrakhand from Jan 2011-Sept 2011.

Scholarships and Awards

- **Senior Research Fellowship (SRF)** awarded by **CSIR-HRDG**, Delhi India at 1 October 2014.
- **Best poster** award in National Conference of Biomedical Science and Technology organized by **CSIR-NPL**, held on 21-22 November 2013 at NPL Delhi, India

Publications

- **Paper Published in Peer Reviewed Journals (SCI indexed)**   **- 09**
- **Publications in National Journals/Proceedings**   **- 05**
- **Conference Abstract**   **- 08**
- **Short Term Courses**   **- 02**
- **Workshop**   **- 03**
- **Reviewer of Journals** (Journal of Applied Polymer Science)   **- 01**
- **Book Chapter**   (Nova Science, USA)   **- 01**
- **Patent**   (Indian Patent Application Number- 201711911022)   - **01**